

GFZ

Helmholtz-Zentrum
P O T S D A M

HELMHOLTZ-ZENTRUM POTSDAM

**DEUTSCHES
GEOFORSCHUNGSZENTRUM**

Teti Zubaidah

Spatio-temporal characteristics of the geomagnetic field over the Lombok Island, the Lesser Sunda Islands region: New geological, tectonic, and seismo-electromagnetic insights along the Sunda-Banda Arcs transition

Scientific Technical Report STR10/07

Impressum

HELMHOLTZ-ZENTRUM POTSDAM

**DEUTSCHES
GEOFORSCHUNGSZENTRUM**

Telegrafenberg
D-14473 Potsdam

Gedruckt in Potsdam
April 2010

ISSN 1610-0956

Die vorliegende Arbeit
in der Schriftenreihe
Scientific Technical Report (STR) des GFZ
ist in elektronischer Form erhältlich unter
www.gfz-potsdam.de - Neuestes - Neue
Publikationen des GFZ

Teti Zubaidah

**Spatio-temporal characteristics
of the geomagnetic field over
the Lombok Island, the Lesser
Sunda Islands region:
New geological, tectonic, and
seismo-electromagnetic
insights along the Sunda-Banda
Arcs transition**

Dissertation

zur Erlangung des akademischen Grades

doctor rerum naturalium (Dr. rer. nat.)

in der Wissenschaftsdisziplin Geowissenschaften

eingereicht an der Mathematisch-Naturwissenschaftlichen Fakultät
der Universität Potsdam

März 2010

1. Gutachter: Prof. Dr. Michael Weber
2. Gutachter: Prof. Sri Widiyantoro PhD
3. Gutachter: Prof. Dr. Katsumi Hattori

Mitglieder der Kommission:

Prof. Dr. Frank Krueger
Prof. Dr. Patrick O'Brien
Prof. Dr. Romain Bousquet
Prof. Dr. Mioara Manda
Prof. Dr. Mohamed Hamoudi
Dr. Makky Sandra Jaya

Betreuerin des GFZ:

Dr. Monika Korte

Scientific Technical Report STR10/07

**Spatio-temporal characteristics of the geomagnetic field over
the Lombok Island, the Lesser Sunda Islands region:
New geological, tectonic, and seismo-electromagnetic insights
along the Sunda-Banda Arcs transition**

**Dissertation
zur Erlangung des akademischen Grades
"doctor rerum naturalium"
(Dr. rer. nat.)
in der Wissenschaftsdisziplin " Geowissenschaften"**

**eingereicht an der
Mathematisch-Naturwissenschaftlichen Fakultät
der Universität Potsdam**

**von
Teti Zubaidah**

Potsdam, den 29. März 2010

Abstract

The Lombok Island is part of the Lesser Sunda Islands (LSI) region – Indonesia, situated along the Sunda-Banda Arcs transition. It lies between zones characterized by the highest intensity geomagnetic anomalies of this region, remarkable as one of the eight most important features provided on the 1st edition of World Digital Magnetic Anomaly Map. The seismicity of this region during the last years is high, while the geological and tectonic structures of this region are still not known in detail. Some local magnetic surveys have been conducted previously during 2004–2005. However, due to the lower accuracy of the used equipment and a limited number of stations, the qualities of the previous measurements are questionable for more interpretations. Thus a more detailed study to better characterize the geomagnetic anomaly -spatially and temporally- over this region and to deeply explore the related regional geology, tectonic and seismicity is needed. The intriguing geomagnetic anomalies over this island region vis-à-vis the socio-cultural situations lead to a study with a special aim to contribute to the assessment of the potential of natural hazards (earthquakes) as well as a new natural resource of energy (geothermal potential).

This study is intended to discuss several crucial questions, including:

- i. The real values and the general pattern of magnetic anomalies over the island, as well as their relation to the regional one.
- ii. Any temporal changes of regional anomalies over the recent time.
- iii. The relationships between the anomalies and the geology and tectonic of this region, especially new insights that can be gained from the geomagnetic observations.
- iv. The relationships between the anomalies and the high seismicity of this region, especially some possible links between their variations to the earthquake occurrence.

First, all available geomagnetic data of this region and results of the previous measurements are evaluated. The new geomagnetic surveys carried out in 2006 and 2007/2008 are then presented in detail, followed by the general description of data processing and data quality evaluation. The new results show the general pattern of contiguous negative-positive anomalies, revealing an active arc related subduction region. They agree with earlier results obtained by satellite, aeromagnetic, and marine platforms; and provide a much more detailed picture of the strong anomalies on this island. The temporal characteristics of regional anomalies show a decreasing strength of the dipolar structure, where decreasing of the field intensities is faster than the regional secular variations as defined by the global model (the 10th generation of IGRF). However, some exceptions (increasing of anomalies) have to be noted and further analyzed for several locations.

Thereafter, simultaneous magnetic anomalies and gravity models are generated and interpreted in detail. Three profiles are investigated, providing new insights into the tectonics and geological evolution of the Lombok Island. Geological structure of this island can be divided as two main parts with different consecutive ages: an old part (from late Oligocene to late Miocene) in the South and a younger one (from Pliocene to Holocene) in the North. A new subduction in the back arc region (the Flores Thrust zone) is considered mature and active, showing a tendency of progressive subduction during 2005–2008. Geothermal potential in the northern part of this island can be

mapped in more detail using these geomagnetic regional survey data. The earlier estimates of reservoir depth can be confirmed further to a depth of about 800 m. Evaluation of temporal changes of the anomalies gives some possible explanations related to the evolution of the back arc region, large stress accumulations over the LSI region, a specific electrical characteristic of the crust of the Lombok Island region, and a structural discontinuity over this island.

Based on the results, several possible advanced studies involving geomagnetic data and anomaly investigations over the Lombok Island region can be suggested for the future:

- i. Monitoring the subduction activity of the back arc region (the Flores Thrust zone) and the accumulated stress over the LSI, that could contribute to middle term hazard assessment with a special attention to the earthquake occurrence in this region. Continuous geomagnetic field measurements from a geomagnetic observatory which can be established in the northern part of the Lombok Island and systematic measurements at several repeat stations can be useful in this regards.
- ii. Investigating the specific electrical characteristic (high conductivity) of the crust, that is probably related to some aquifer layers or metal mineralization. It needs other complementary geophysical methods, such as magnetotelluric (MT) or preferably DC resistivity measurements.
- iii. Determining the existence of an active structural fault over the Lombok Island, that could be related to long term hazard assessment over the LSI region. This needs an extension of geomagnetic investigations over the neighbouring islands (the Bali Island in the West and the Sumbawa Island in the East; probably also the Sumba and the Flores islands). This seems possible because the regional magnetic lineations might be used to delineate some structural discontinuities, based on the modelling of contrasts in crustal magnetizations.

Zusammenfassung

Die Insel Lombok, Teil der Lesser Sunda Islands (LSI) Region - Indonesien, befindet sich am Übergang zwischen Sunda und Banda Inselbogen. Sie liegt zwischen den Zonen der höchsten Intensität geomagnetische Anomalien dieser Region, welche als eines der acht wichtigsten Features in der 1. Auflage der globalen Karte magnetische Anomalien (World Digital Magnetic Anomaly Map) gekennzeichnet ist. Die Seismizität der Region in den letzten Jahren ist hoch, auf der anderen Seite sind die geologischen und tektonischen Strukturen dieser Region noch immer nicht im Detail bekannt. Einige lokale Magnetfeldmessungen wurden bereits in den Jahren 2004–2005 durchgeführt, aber aufgrund der geringeren Genauigkeit der verwendeten Geräte und der begrenzten Anzahl von Stationen, ist die Qualität der früheren Messungen für weitere Interpretationen fragwürdig. Daher ist eine eingehende Untersuchung zur besseren räumlichen und zeitlichen Charakterisierung der geomagnetischen Anomalien in dieser Region erforderlich, um die damit verbundenen Aspekte der regionalen Geologie, Tektonik und Seismizität zu untersuchen. Die außergewöhnlichen geomagnetischen Anomalien in dieser Insel Region gegenüber den sozio-kulturellen Gegebenheiten gab Anlaß zu einer Studie mit dem speziellen Ziel, einen Beitrag zur Abschätzung der Gefahr von Naturkatastrophen (Erdbeben) sowie neuer natürlicher Energievorräte (Geothermie) zu leisten.

Diese Studie soll mehrere entscheidende Fragen diskutieren, einschließlich der folgenden:

- i. Die tatsächlichen Werte und die allgemeinen Muster von magnetischen Anomalien auf der Insel, sowie deren Zusammenhang mit dem regionalen Muster.
- ii. Zeitliche Veränderungen der regionalen Anomalien im Laufe der letzten Zeit.
- iii. Die Beziehungen zwischen den Anomalien und der Geologie und Tektonik der Region, vor allem neue Erkenntnisse, die aus den geomagnetischen Beobachtungen gewonnen werden können.
- iv. Die Beziehungen zwischen den Anomalien und der hohen Seismizität dieser Region, vor allem einige mögliche Verbindungen zwischen ihren Variationen und Erdbeben Ereignissen.

Als erster wurden alle verfügbaren geomagnetischen Daten dieser Region und die Ergebnisse der früheren Messungen ausgewertet. Die neue geomagnetischen Messungen in den Jahren 2006 und 2007/2008 werden dann im Einzelnen dargestellt, gefolgt von der allgemeinen Beschreibung der Datenverarbeitung und der Bewertung der Datenqualität. Die neuen Ergebnisse zeigen die allgemeinen Muster von aufeinander folgenden negativen und positiven Anomalien, welche die aktive mit dem Inselbogen verbundene Subduktions-Region offenbart. Sie passen gut zu früheren Ergebnissen von Satellit, aeromagnetischen und marine Plattformen und bieten ein wesentlich genaueres Bild der starken Anomalien auf dieser Insel. Die zeitliche Besonderheiten der regionalen Anomalien zeigen eine abnehmende Stärke der dipolaren Struktur. Einige Ausnahmen (Erhöhung von Anomalien) für mehrere Standorte erfordern weitere Analysen.

Danach werden gleichzeitig Modelle der magnetischen Anomalien und des Schwerfelds generiert und im Detail interpretiert. Drei Profile werden untersucht und bieten neue Einblicke in die Tektonik und den geologischen Aufbau der Insel

Lombok. Die geologische Struktur der Insel kann in zwei Hauptteile aufgeteilt werden, mit verschiedenen aufeinander folgenden Zeiten: einen alten Teil (vom späten Oligozän bis zum späten Miozän) im Süden und einen jüngeren (aus dem Pliozän bis Holozän) im Norden. Eine neue Subduktion am Inselbogen-Rücken (Flores Thrust-Zone) gilt als ausgereift und ist aktiv, wie eine Tendenz der fortschreitenden Subduktion während der Jahre 2005–2008 zeigt. Das geothermie Potential im nördlichen Teil der Insel kann mit diesen geomagnetischen regionalen Messdaten im Detail abgebildet werden. Frühere Abschätzungen der Tiefe des geothermischen Reservoirs können bestätigt und auf eine Tiefe von ca. 800 m verbessert werden. Die Untersuchung der zeitlichen Veränderungen der Anomalien gibt einige mögliche Erklärungen zu der Entwicklung der Region des Inselbogen-Rückens, großen Druckansammlungen in der LSI Region, spezifischen elektrischen Merkmalen der Kruste der Insel Lombok Region, und einer strukturellen Diskontinuität über dieser Insel.

Die Ergebnisse geben Anregung zu mehreren möglichen zukünftigen Studien mit geomagnetischen Daten und Untersuchungen magnetischen Anomalien über die Insel Lombok und Umgebung:

- i. Die Überwachung der Tätigkeit der Subduktion in der Region des Inselbogen-Rückens (Flores Thrust-Zone) und den angesammelten Druck über den LSI, dass zur mittelfristigen Beurteilung der Erdbebengefährdung in dieser Region beitragen könnten. Kontinuierliche Messungen des Erdmagnetfeldes von einem geomagnetischen Observatorium, das im nördlichen Teil der Insel Lombok errichtet werden könnte, und systematische wiederholte Messungen an mehreren Stationen können dazu beitragen.
- ii. Die Untersuchung der spezifischen elektrischen Merkmale (hohe Leitfähigkeit) der Kruste, die vermutlich mit Aquiferschichten oder metallischer Mineralisierung in Zusammenhang steht. Es müssen weitere, ergänzende geophysikalische Methoden, wie magnetotellurische (MT) oder vorzugsweise DC-Widerstandsmessungen, durchgeführt werden.
- iii. Feststellung des Vorliegens einer aktiven Bruchzone über der Insel Lombok, die langfristig für die Beurteilung der Erdbebengefährdung für die LSI Region von Bedeutung ist. Dafür ist eine Auswertung der geomagnetischen Untersuchungen auf die benachbarten Inseln (die Insel Bali im Westen und der Insel Sumbawa im Osten, wahrscheinlich auch die Sumba und Flores Inseln) nötig. Dies scheint möglich, weil die regionalen magnetischen Lineaturen benutzt werden können, um strukturelle Brüche abzugrenzen, basierend auf der Modellierung von Gegensätzen in der Magnetisierung der Erdkruste.

Forewords

§ Praise be to Allah, to Whom belongs whatever is in the heavens and whatever is in the Earth, and to Him be praise in the Hereafter; and He is Full of Wisdom, acquainted with all things.

§ He knows that which goes down into the Earth and that which comes out of it, and that which comes down from the sky and that which goes up to it; and He is the Most Merciful, the Oft-Forgiving.

(Al-Qur'an, Surah Saba': 1-2)

When completing this work, the first thing that I want to say is thanks to Allah *SubhaanaHuu wa Ta'aala* that has allowed me to do that and made all the things easy for me. This work is really a small piece of efforts to understand His existence and His power, in the course of a study of mechanisms in the nature, particularly of the Earth, within the limitations of human logics and thoughts.

Complexities and unique characteristics of each Inch of the Earth's surface have given us such an enormous opportunity to deepen our knowledge and to sharpen our instinct. By investigating only about 15 ppm of the entire earth's surface, I must confess that the results of this study are still very far from the "true" knowledge. Nevertheless, I remain optimistic that this study will be able to enrich the treasury of human knowledge, which may open further geomagnetic studies in this studied area and nearby, as well as in other places. Also, hopefully, the results are really useful for development and social progress of the Lesser Sunda Islands region.

I will not forget to say many thanks for all parties which have supported and made possible this study to be well done. My formal thanks are as declared in the Acknowledgements, in which I should apologize if somebody had been forgotten to be mentioned.

But exclusively, here, I would like to express my deep gratitude to Monika Korte and Mioara Manda that have led me to better understand the "Geomagnetics", and who have sincerely and patiently conveyed each progress of this study. May Allah regard their efforts as good deeds and reward them well with multiply goodness.

To my family, especially my lovely husband and children, who have been *ikhlash* to accompany and help me in finishing this study, also my mother and my father who never stop in offering prays for their children; I address my deepest thanks. May Allah write all as charity records and reward them with much invaluable goodness from His side. Amien.

Telegrafenberg, 29th March 2010

Teti Zubaidah

Table of Contents

	Page
Abstract	iii
Zusammenfassung	v
Forewords	vii
Table of contents	viii
List of figures	x
List of tables	xiv
List of abbreviations	xv
1. Introduction	1
1.1 Geomagnetic field	1
1.1.1 Sources of the geomagnetic field	2
1.1.2 Geomagnetic components and units	3
1.1.3 Measuring instruments and methods	4
1.1.4 Geomagnetic variations and anomalies	5
1.2 The Lesser Sunda Islands (LSI)	7
1.2.1 General tectonic settings	8
1.2.2 Historical seismicity	9
1.2.3 Socio-cultural situations	10
1.2.4 The Lombok Island	11
1.3 Motivation, objective and synergy	12
2. Geomagnetic data	14
2.1 Related available data	14
2.1.1 The CHAMP satellite data over the Indonesian region	14
2.1.2 Marine and aeromagnetic data over the Sunda–Banda Arcs	16
2.1.3 Nearby observatory data	18
2.1.3.1 The Kupang (KPG) – MAGDAS observatory	18
2.1.3.2 The Tondano (TND) – BMG Indonesian observatory	20
2.1.3.3 The Kakadu (KDU) – Australian observatory	20
2.1.4 The BMG Indonesian repeat stations data	21
2.1.5 The IPS geophysical report and geomagnetic forecast data	22
2.2 Ground measurement campaign over the Lombok Island (2004–2008)	26
2.2.1 Previous surveys (2004–2005)	26
2.2.2 The 2006 survey	29
2.2.2.1 Survey areas and considerations	29
2.2.2.2 Calibration of equipment	29
2.2.2.3 Continuous measurement on the ‘Penyu’ Islet (PNY)	31
2.2.2.4 Base Station surveys	32
2.2.2.5 Southern and middle area surveys	35
2.2.2.6 Specific conclusions and remarks	36

2.2.3	The 2007/2008 survey	36
2.2.3.1	Survey areas and considerations	36
2.2.3.2	Southern, middle, and northern area surveys	37
2.2.3.3	Continuous measurement at 'Nurul Bayan' (NRB)	38
2.2.3.4	Calibration of equipment	39
2.2.3.5	Specific conclusions and remarks	39
3.	Lombok Island surveys: Data processing and visualization	41
3.1	Data processing and visualizations	41
3.1.1	Preliminary processing	41
3.1.2	Data reduction	43
3.1.3	Final processing	45
3.1.4	Visualization	46
3.2	Results	46
3.2.1	Results of the 2006 survey	46
3.2.2	Results of the 2007/2008 survey	48
3.2.3	Changes of geomagnetic field	51
4.	Modelling and interpretations	53
4.1	Some important constraints	53
4.2	Modelling over the most prominent dipolar structures	59
4.2.1	P1-06 model (the southern area using the 2006 survey results)	62
4.2.2	P1 model (the southern area using the 2007/2008 survey results)	65
4.2.3	P2 model (the northern area using the 2007/2008 survey results)	67
4.3	Modelling of the geomagnetic temporal characteristics	73
4.4	Geological and tectonic interpretations	75
4.4.1	Interpretation of P1-06/P1 model and its changes	75
4.4.2	Interpretation of P2 and P3 models	76
4.4.3	Interpretation of the overall model	77
4.5	Seismo-electromagnetic interpretations	89
4.5.1	Statistical reviews of past and present seismic activity	90
4.5.2	Geomagnetic changes over short time intervals at earthquake times	91
4.5.3	Interpretations of related seismo-electromagnetic mechanism	92
5.	Conclusions and outlooks	97
Appendixes		
A.	Final results of the 2006 and the 2007/2008 surveys	99
B.	The Talwani algorithm for 2D magnetic and gravity modellings	104
C.	Parameters of geological and tectonic modelling	108
References		
Acknowledgements		
Curriculum vitae		

List of figures

Figure		Page
1.1	A simple representation of the present day geomagnetic fields, as a dipole tilted about 11° with respect to the geographic coordinate system.	1
1.2	An artistic view of the magnetosphere, illustrating how the geomagnetic field is influenced by the solar radiation activities.	2
1.3	The geomagnetic coordinate system, showing the three orthogonal components, the horizontal component and the total field as well as the declination and the inclination.	3
1.4	Vector representation of total field anomalies.	7
1.5	The <i>Lesser Sunda Island</i> (LSI), including the islands of Bali, Lombok, Sumbawa, Flores, Solor, Lombok, Pantar, Alor, Kambing, and Wetar in the North; Sumba, Savu, Roti, and Timor in the South; and some other smaller islands around them, with the total area of 87,700 km ² .	7
1.6	The general tectonic settings of the Indonesian regions.	8
1.7	Daily working situations of traditional farmers in the LSI region.	10
1.8	General topography of the Lombok Island.	11
2.1	Physical layout of the CHAMP satellite (front view) with locations of the main instrumentations.	15
2.2	Map of the total component of the large-scale lithospheric anomaly field at geoid altitude for the Indonesian region obtained from the MF6 model.	16
2.3	Regional view of the geomagnetic anomaly over the Sunda-Banda arcs, resulting from all available marine and aeromagnetic data sources.	18
2.4	The location of the Lombok Island and the three nearby observatories, i.e. the Kupang (KPG) in Timor Island – Indonesia, the Tondano (TND) in Sulawesi Island – Indonesia, and the Kakadu (KDU) in Australia.	19
2.5	The geomagnetic field intensity at the Kupang (KPG)-MAGDAS observatory obtained during October 15 th – 27 th 2006 period.	19
2.6	The geomagnetic field intensity at the Tondano (TND) – BMG Indonesian observatory obtained during October 15 th – November 2 nd 2006 period.	20
2.7	The geomagnetic field intensity at the Kakadu (KDU) – Australian observatory obtained during October 15 th – November 2 nd 2006 period.	21
2.8	Regional view of geomagnetic anomaly over the Indonesian region for the epoch 2005.0, derived from the BMG Indonesian repeat stations total component field data.	23
2.9	Regional view of mean annual secular variation over the Indonesian region between the epochs 2000.0 – 2005.0, derived from the BMG Indonesian repeat stations annual secular variation data.	24
2.10	<i>K</i> -indices for the Australian region and <i>Kp</i> -index values during the survey days in 2006.	25
2.11	<i>K</i> -indices for the Australian region and <i>Kp</i> -index values during the survey days in 2007/2008.	25

2.12	The surveyed area of geomagnetic ground measurements over the Lombok Island in 2004, 2005, 2006, and 2007/2008.	27
2.13	Results of the 2005 survey (after applying re-processing procedures in 2008).	28
2.14	Station locations of the 2006 survey related to the 2005 survey and some additional important locations.	30
2.15	Results of two sequences of calibration between GSM-19 and ENVI PRO in 2006: (a) The actual and variation values of <i>the first</i> sequence of calibration; (b) The actual and the variation values of <i>the second</i> sequence of calibration.	31
2.16	Results of the continuous measurements on the 'Penyu' Islet (PNY) from October 15 th to November 2 nd 2006.	32
2.17	Locations of the three candidates of the South base station for the 2006 survey.	32
2.18	Diurnal variation obtained during two series of measurements (morning and afternoon) on three locations of the South base station candidates.	33
2.19	The total field intensity variations relative to the centres and the total geomagnetic anomaly profiles of the locations of (a) BS-1, (b) BS-2, (c) BS-3, and (d) BS-5; obtained from the most appropriate surveys.	34
2.20	Example of the 2006 survey at station M21, showing manually using of the ENVI PRO.	35
2.21	The total field intensity variations (in nT) relative to the centre [coordinate (5, 5)] and the total geomagnetic anomaly profile of the location of M13 (the maximum anomaly point of the 2005 survey).	35
2.22	Station locations of the 2007/2008 survey related to the 2006 survey, and several important locations.	37
2.23	Example of the 2007/2008 survey at station M21, exactly at the same location as in 2006, using the GSM-19T.	38
2.24	Continuous measurements of the geomagnetic field intensity at Nurul Bayan (NRB) obtained over several hours (mainly during night time) on February 16 th , 17 th and 19 th 2008.	39
2.25	Two sequences of calibration between GSM-19T and ENVI PRO in 2008: (a) The actual and variation values of <i>the first</i> sequence; (b) The actual and variation values of <i>the second</i> sequence.	40
3.1	The general algorithm of data processing and visualization.	42
3.2	Example of data pre-selection for a manually (using ENVI PRO) measured station (C39).	43
3.3	Example of a manual selection procedure for a manually (using ENVI PRO) measured station (C39).	43
3.4	Map of the geomagnetic total field anomaly obtained from measurements in 2006.	47
3.5	3D view of the geomagnetic total field anomaly map obtained from the measurements in 2006 for the same area as in Fig. 3.4 .	48
3.6	Map of the geomagnetic total field anomaly obtained from the measurements in 2007/2008, plotted over a regional topographical map of SRTM30 Plus v4.	49
3.7	3D view of the geomagnetic total field anomaly map obtained from measurements in 2007/2008 for the same area as in Fig. 3.6 .	50

3.8	Comparison of two regional views of geomagnetic anomaly over the Lombok Island and surroundings, generated from (a) all available marine and aeromagnetic data sources and (b) the similar data set combined with the most reliable data of the Lombok 2007/2008 survey.	51
3.9	Map of the geomagnetic changes obtained from the differences between the 2006 and the 2007/2008 measurements at 25 exact stations: (a) geomagnetic field intensity changes, and (b) geomagnetic anomaly changes.	52
4.1	The related parts of the Lombok geological map, used to determine the surficial rocks structures and their subsurface continuations for the models.	54
4.2	Plot of the earthquake epicentre data of Lombok–west Sumbawa segment and the adjacent segments of Bali in the West and Flores in the East, dated from January 1 st 1973 to September 8 th 2009 of all magnitudes and the depths up to 120 km.	55
4.3	The longitudinal cross sectional view of earthquake hypocentres for the Lombok–west Sumbawa segment (bounded by latitude -7°N to -12°N and longitude 115.5°E to 117.5°E).	56
4.4	Illustration of the applied isostasy principle of Airy’s model.	56
4.5	The regional gravity background for the Indonesian region derived from GGM02-GRACE Gravity Model 02.	57
4.6	The original Bouguer anomaly map of the Lombok Island.	58
4.7	The digitization results of the Bouguer anomaly map.	59
4.8	The background anomalies of the extracted profile of the 2006 survey (P1-06), showing the initial RMS error of the magnetic anomalies and the gravity models.	61
4.9	The background anomalies of two extracted profiles of the 2007/2008 survey (P1 and P2), passing through the most prominent negative anomaly in the east side.	61
4.10	The background anomalies of two extracted profiles of the 2007/2008 survey (P1 and P3), passing through the most prominent positive anomaly in the west side, showing the initial RMS error of the magnetic anomalies and the gravity models.	62
4.11	Comparison between modelled profile of P1-06 and the profile of observations, using magnetic data of the 2006 survey.	63
4.12	Comparison between modelled profile of P1 and the profile of observations, using magnetic data of the 2007/2008 survey.	66
4.13	Comparison between modelled profile of P2 and the profile of observations, using magnetic data of the 2007/2008 survey.	68
4.14	The detailed geological map of the Mount Rinjani range area.	70
4.15	The details of stratigraphy and geothermal reservoir of the P2 model, accompanied by the gravity and magnetic properties of each layer	71
4.16	The responses of magnetic and gravity models of P2 without Flores oceanic subducting crust contributions. The positive magnetic response is shifted to a lower level and the equilibrium of the gravity response is also disturbed.	72
4.17	Earthquake events around 300 km from the Lombok Island to the depth of 120 km in the time interval between the 2006 and the 2007/2008 surveys.	73
4.18	The model of geomagnetic changes for the P1-06 profile.	74

4.19	The overall model of the Lombok Island, compilation of P1 and P2 models, representing the present day tectonic settings of this region.	80
4.20	The tectonics and geological sequence of the Lombok Island in the Late Oligocene (28 Ma).	82
4.21	The tectonics and geological sequence of the Lombok Island between the Late Oligocene and Early Miocene (28–10 Ma).	82
4.22	The tectonics and geological sequence of the Lombok Island between the Early and Late Miocene (10–7 Ma).	83
4.23	The tectonics and geological sequence of the Lombok Island during the Late Miocene (7–5.33 Ma).	83
4.24	(a) The tectonics and geological sequence of the Lombok Island during early period of the Pliocene (5.33–3.6 Ma); (b) Enlargement view of the Lombok Island during the same period.	84
4.25	(a) The tectonics and geological sequence of the Lombok Island during middle period of the Pliocene (3.6–2 Ma); (b) Enlargement view of the Lombok Island during the same period.	85
4.26	(a) The tectonics and geological sequence of the Lombok Island during the latest period of the Pliocene (2–1.81 Ma); (b) Near surface structures of the Lombok Island during the same period.	86
4.27	(a) The tectonics and geological sequence of the Lombok Island during the Pleistocene (1.81–0.01 Ma); (b) Near surface structures of the Lombok Island during the same period.	87
4.28	(a) The polarity changes of the geomagnetic field during the last 120 Ma. (b) The polarity changed frequently during the Late Oligocene to the early periods of Holocene (28–10 Ma). (c) The polarity changed during the last 5 Ma, in compatibility with the modelled inclinations of rock and lavas in this study.	89
4.29	The earthquake distributions through time over the LSI region dated from January 1 st 1973 to September 8 th 2009.	91
4.30	Anomalously pertinent geomagnetic changes observed at three un-relocated stations in a short time interval, followed by four big earthquakes at the Sumbawa Island.	91
4.31	The longitudinal cross sectional view of earthquake hypocentres for (a) the Flores segment and (b) the Bali segment.	93
4.32	The stress map of the LSI region.	94
4.33	The schematic of anomaly field intensities due to piezomagnetically induced moment for a 100 km East-West fault, situated in the southern hemisphere.	94
4.34	The summary of all proposed structural boundaries crossing the LSI region.	96
B.1	Approximation of a 2D body by an N-sided polygon for gravity modelling	107
B.2	Approximation of horizontal ribbon for 2D magnetic modelling	107

List of tables

Table		Page
2.1	Number of BMG Indonesian repeat station surveyed by year.	22
3.1	The suitability evaluation of three nearby observatories.	44
3.2	Data quality evaluation for the 2006 and the 2007/2008 surveys.	46
3.3	Final results the 2006 survey.	100
3.4	Final results of the 2007/2008 survey.	101
4.1	Parameters of the P1-06 model	106
4.2	Parameters of the P1 model	107
4.3	Parameters of the P2 model	108
4.4	Summary of the modelled tectonics and geological sequence of the Lombok Island	81
4.5	The modelled inclinations and the proposed ages of the rocks and sediments	89
4.6	Limitation of earthquake grouping to the Java Trench and the Flores Thrust zones.	90

List of abbreviations

AIST	Agency of Industrial Science and Technology
BGR	<i>Die Bundesanstalt für Geowissenschaften und Rohstoffe</i>
BMG	<i>Badan Meteorologi dan Geofisika</i> , the Meteorological and Geophysical Agency of Indonesia
CCOP	The Coordinating Committee for Geoscience Programmes in East and Southeast Asia
CHAMP	The CHAllenging Mini-Satellite Payload
CPMN	Circum-pan Pacific Magnetometer Network
EC EF NEC	Earth-Centered, Earth-Fixed, North-East-Center
FGM	Fluxgate vector magnetometers
GEODAS	The GEOphysical DATA System
GFZ	Das GeoForschungsZentrum
GGM02	The GRACE Gravity Model 02
GPS	Global Positioning System
GRIMM	The GFZ Reference Internal Magnetic Model
IGA	The International Association of Geomagnetism and Aeronomy
IATME	The International Association for Terrestrial Magnetism and Electricity
ICS	The International Commission on Stratigraphy
IGRF	The International Geomagnetic Reference Field
INTERMAGNET	The International Real-time Magnetic Observatory Network
IPS	The Ionospheric Prediction Service
IUGS	The International Union of Geological Sciences
KDU	Kakadu geomagnetic observatory, Australia
LSI	The Lesser Sunda Islands
MAGDAS	The MAGnetic Data Acquisition System
MF6	The sixth-generation lithospheric magnetic field model (derived from CHAMP data)
NGK	The Adolf Schmidt Geomagnetic Observatory Niemegk
NRB	Nurul Bayan
OVM	Scalar Overhauser magnetometer
PDE	The Preliminary Determinations of Epicenters
PNY	<i>“Penyu”</i> Islet
SERC	The Space Environment Research Center
SINDBAD	The Seismic and Geoacoustic Investigations along the Sunda-Banda Arc Transition
SRTM	The Shuttle Radar Topography Mission
TND	Tondano geomagnetic observatory, Indonesia
USGS/NEIC	The U.S. Geological Survey/National Earthquake Information Center

Chapter 1

Introduction

The geomagnetic (Earth's magnetic) field studies, while one of the oldest geophysical sciences, are one of today's exciting themes, since they can provide information about the Earth and its surroundings, from the core to the space. The fundamental aspects of geomagnetic field studies are briefly described in this chapter, including the sources, the components and units, as well as the measurement methods. The specific topic of the geomagnetic variations and anomalies is discussed in more detail as a core of this study. The regional information of the studied area of the *Lesser Sunda Islands* (the *Sunda-Banda Arcs* transition), especially the Lombok Island, is described in terms of the general tectonic settings, historical seismicity and volcanism, and the socio-cultural situation. The motivations and objectives are formulated at the end of this chapter. These form the frame for the comprehensive study described in detail in the following chapters.

1.1 Geomagnetic field

The geomagnetic field refers to the magnetic fields associated with the Earth. The simplest approximation of the geomagnetic field is that of a hypothetical magnet (dipole) in the centre of the Earth, with its axis anti-parallel to the axis of rotation (geocentric axial dipole). A better approximation of the present day geomagnetic field, as depicted in **Fig. 1.1**, is that of a geocentric dipole, with the dipole axis tilted about 11° with respect to the geographic coordinate system (Glaßmeier et al, 2009).

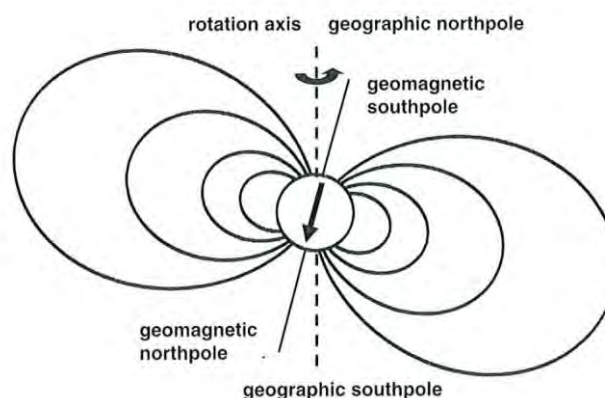


Figure 1.1 A simple representation of the present day geomagnetic fields, as a dipole tilted about 11° with respect to the geographic coordinate system (adopted from Glaßmeier et al, 2009). The field lines in the northern hemisphere are directed downward; conversely, upward in the southern hemisphere. In the polar region, they are vertical; but in the equatorial regions are horizontal.

A region in space around the Earth where the magnetic field is present is called the magnetosphere. Its shape is somewhat like a comet in response to the dynamic pressure of the solar wind. It is compressed on the side toward the sun to about 10 R_E (with R_E is the Earth's radii = 6371 km) and is extended tail-like on the side away from the sun to more than 100 R_E . **Figure 1.2** is an artistic view of the magnetosphere¹, illustrating how the geomagnetic field is influenced by the solar radiation activities.

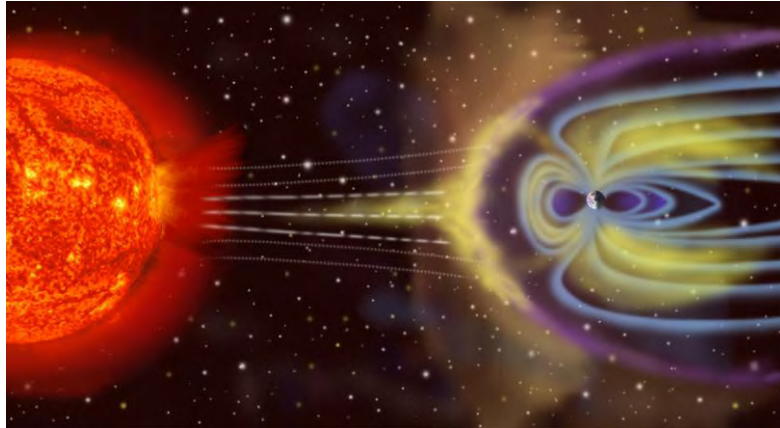


Figure 1.2 An artistic view of the magnetosphere, illustrating how the geomagnetic field is influenced by the solar radiation activities.

1.1.1 Sources of the geomagnetic field

Most of the geomagnetic field is ascribed to a self sustaining generation process. The most widely accepted theory is that of a dynamo process, proposed by Joseph Larmor in 1919, explaining that the field is most probably generated in the outer fluid core of the Earth (Glaßmeier et al, 2009). In such a dynamo process, kinetic energy is converted into magnetic energy, following the induction equation:

$$\frac{\partial B}{\partial t} = \nabla \times U \times B + \lambda \Delta B, \quad (1.1)$$

with B is the magnetic field, U the flow field, and λ the magnetic diffusivity, given by $\lambda = 1/\mu_0\sigma$, with σ the electric conductivity of the medium in which the dynamo is operating. Some conditions are needed to be fulfilled to operate a planetary dynamo: a rotational motion of planet, a fluid motion inside the core, a large electric conductivity, and a sufficiently large spatial scale. Earth's outer fluid core is such a regime and thus thought to be the region where the geomagnetic field is generated. However, scientists are still debating on the exact processes in the fluid outer core that produce the geomagnetic fields (Campbell, 2003).

The above described field is known as the core field or the main field. Together with the lithospheric field (which is produced by remanent and induced magnetized crustal rocks), they are the so-called internal parts of the geomagnetic field. Using spherical harmonic functions, in 1839, Gauss was able to show that the fields of internal origins are the strongest contribution of the geomagnetic total field intensities observed at the Earth's surface. It's known now that these contributions are about 90% of the total field intensity (Glaßmeier et al, 2009).

¹ <http://www.pieces-zine.com/200902magnet/images/magnetosphere.jpg>

The remaining 10% are the contributions of other fields, generated in the ionosphere and magnetosphere, the so-called external parts. These parts are simultaneously observed as some transient fields during the geomagnetic field measurements. They are mostly caused by influences of solar activity and variability, such as by coronal mass ejections, coronal hole streams, solar wind sector boundaries, and IMF (Interplanetary Magnetic Field) orientation changes, or by rather regular variations in atmospheric heating and ionospheric conductivity with solar irradiation (Lühr et al., 2009).

1.1.2 Geomagnetic components and units

The geomagnetic field is a vector field, which can be described in a cartesian coordinate system on the Earth's surface by its three orthogonal components or magnetic elements X (pointing in the geographic north direction), Y (pointing eastward), and Z (pointing downward). The geomagnetic intensity of the total field F can be obtained as $F = \sqrt{X^2 + Y^2 + Z^2}$. The declination D is defined as the angle between the horizontal component H (with $H = \sqrt{X^2 + Y^2}$) and the geographic north, while the inclination I is the angle between the horizontal plane and the field vector F . **Figure 1.3** illustrates the above relationships, with a set of names and symbols as used internationally (Campbell, 2003).

In practice, the magnetic declination at any point of the Earth's surface can be recognized as the angle between the direction of the north end of a compass needle and the true North. As a consensus, the declination is positive when the magnetic north is east of the true North. Meanwhile, positive values of inclination indicate that the field is pointing downward (into the Earth) at the point of measurement. Theoretically, using the geocentric dipole model, as depicted in **Fig. 1.1**, the inclination is $+90^\circ$ at the geomagnetic North pole, -90° at the geomagnetic South pole, and 0° at the geomagnetic equator.

The magnetic field strength is nowadays measured in the unit Tesla (T), with 1 T equal to 1 V.s.m^{-2} . In geomagnetism, a small subunit of $10^{-9} \text{ T} = 1 \text{ nT}$ is more convenient, because the strength of the geomagnetic field in mid latitude is about 50,000 nT (Glaßmeier et al, 2009). Moreover, the lithospheric and external fields are in the order of a few to a few thousand nT.

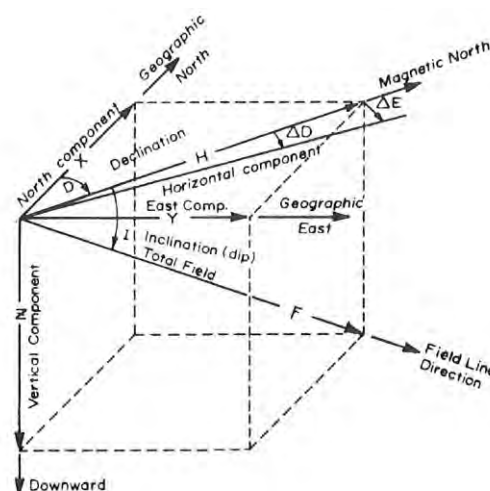


Figure 1.3 The geomagnetic coordinate system, showing the three orthogonal components X , Y , and Z ; the horizontal component H and the total field F as well as the declination D and the inclination I (adopted from Campbell, 2003).

1.1.3 Measuring instruments and methods

The instruments used for geomagnetic measurements are quite various; from the earliest field-sensing device of a lodestone magnetic compass to the most advanced one of a cryogenic superconductor magnetometer. Here, only two of them that have been used in this study (i.e. Proton Precession and Overhauser magnetometers) are described, referring to Campbell (2003) and the instruction manual of GSM-19 v7.0 (GEM System Inc.).

A proton is a hydrogen atom stripped of its orbital electron. In a hydrogen-rich liquid, the protons are not tied in place by a crystal lattice. The proton is considered as a spinning charged sphere having an inherent magnetic moment m_p , and an intrinsic spin angular momentum I_p . The ratio of these two vector quantities is called the scalar gyromagnetic ratio γ_p , with $\gamma_p = \frac{m_p}{I_p} (\gamma \text{ sec})^{-1}$, and generally adopted as $0.26751525 (\gamma \text{ sec})^{-1}$. An external magnetic field H exerts a torque on the spinning proton to align its magnetic moment and cause a precession of the spin axis. The angular frequency of the proton precession ω_p , called the Larmor frequency, is equal to the product of the gyromagnetic ratio and the magnitude of the total field (i.e. $\omega_p = 2\pi f_p = \gamma_p H$). Thus, knowing the gyromagnetic ratio, the local geomagnetic field intensity can be obtained by measuring the frequency of the precession.

In using a proton precession magnetometer, a single value of geomagnetic field measurements is obtained by the following steps of measuring process; including polarization, deflection, pause, counting, and storage. During polarization, a strong DC current is passed through the sensor, creating a polarization of the proton rich fluid in the sensor. A short pulse is then given, causing some deflections of the protons into the plane of precession. After that, a pause allows the electrical transients to die off, leaving a slowly decaying proton precession signal above the noise level. Now, the counting step is taking place, by measuring the proton precession frequency and converting it into magnetic field units. Finally, the results can be stored in memory, together with the time of the measurement.

An Overhauser magnetometer is a variant of the proton magnetometer. A selected chemical salt is added to the proton cell causing some of the orbital electron spin energy to be transferred to the protons in high-frequency fields. Beside a strong DC current, a strong RF (radio frequency) magnetic field is also used in the polarization stage to disturb the electron-proton coupling. By saturating free electron resonance lines, the polarization of protons in the sensor liquid is greatly increased. This allows the proton precessional frequency to be continuously measured, which enables faster sequential measurements. It is ideal for very high sensitivity total field measurements.

Measurements of the geomagnetic field (of local, regional, as well as global scale), have been carried out for a long time using various methods. Continued measurements of one-minute values are provided by the geomagnetic observatories; some 200 are operated world-wide today (Mandea, 2006). These values can be used as the references for other surveys, and are fundamental for knowing the geomagnetic changes locally as well as globally. Aeromagnetic surveys (conducted using an aeroplane, a helicopter or a balloon) are considered as an effective way to collect regional magnetic data rapidly and with low cost. However, a high quality aeromagnetic survey requires significant care, because it has to be conducted on magnetically quiet days and must avoid signal interferences during the survey, and moreover needs a proper levelling during the data processing. Other efforts are marine surveys, which are used to map the geomagnetic anomaly patterns over sea floors, mainly for structural studies and hydrocarbon explorations.

Among the geomagnetic satellite missions, the POGO satellites have provided the first global mapping of the geomagnetic intensities during 1967–1971, while MAGSAT is the first one that provides global geomagnetic vector data in 1979–1980. They have been followed by the Ørsted (since February 1999), CHAMP (since July 2000), and SAC-C (since November 2000) missions which are greatly improving corrections for external field influences, as well as main field and secular variation models. A new mission, a three-satellite constellation Swarm, scheduled for launch in the near future (2011), will optimize the separation of temporal and spatial variations of the fields, including the possibility to compile a global map of the lithospheric fields at scales ranging 5–3000 km (Mandea and Purucker, 2005). However, until nowadays, due to the flight altitude of satellites, only lithospheric anomalies of long wavelengths can be delineated. It is still impossible to resolve field structures of less than a few hundred kilometres from the available satellite data. Nevertheless, the interpretation and verification of geological provinces and tectonic boundaries could be provided by the high degree spherical harmonic models (Lühr et al., 2009).

Ground measurements can be used to resolve and understand short wavelength anomalies, locally and regionally. The quality of measurements can be guaranteed by choosing magnetically quiet locations and applying a proper data processing. Difficult topography can pose a problem, but otherwise the ground measurements need only low budgets. They also accommodate more flexibility to conduct measurements during the most favourable magnetic quietest time. To get the exact geomagnetic changes, one can relatively easy to go back to exactly the same locations to do repeat measurements. The repeat measurements are also a good option, if the previous results are considered as unsatisfying or unreliable; so that a higher degree of confidence can be maintained throughout a study of geomagnetic field anomalies.

1.1.4 Geomagnetic variations and anomalies

A standard mathematical representation of the core field and its long term variations is determined by international agreement. It is called the IGRF (International Geomagnetic Reference Field), which is the most widely known geomagnetic field model, used commonly for navigational purposes and as reference for determining regional anomalies. It is based on a classical spherical harmonic analysis, and it includes the main field and piecewise linear secular variation since 1900. A new IGRF model is adopted based on several candidate models every five years by a working group of the International Association of Geomagnetism and Aeronomy (IAGA). The latest version is the IGRF 10th generation (IAGA WG V-MOD, 2005; Maus et al., 2005), with a main field model for epoch 2005.0 and an extrapolated secular variation up to epoch 2010.0.

The geomagnetic field contributions are time varying fields, covering a broad range of timescales, from milliseconds to millennia. The geomagnetic secular variation refers to long period variations which arise primarily from the Earth's fluid outer core. A global investigation of the secular variation through the last 175 years shows that the dipole moment is decreasing at a rate of about 5% per century (Lühr et al., 2009), about five times faster than that expected for free decay of the dipole if the geodynamo process ceased operation. It probably indicates the early stages of geomagnetic reversal (Olson, 2002), since the last reversal occurred about 780,000 years ago. Meanwhile, the secular variation of nondipole fields shows an average characteristic of systematically westward drift of 0.2° per year, although this rate varies with latitude (Blakely, 1996).

The short period variations (from seconds to days), on the other hand, are primarily of external origins and mostly caused by the influences of solar activities. The Earth is continuously bathed by the solar wind, a stream of charged plasma emitted by the sun. A complex interaction between the internal part of the Earth's magnetic field and the solar wind, coupled with the Earth's rotation, tidal forces, and thermal effects, generates electrical currents in the ionosphere, which in turn produce magnetic fields that can reach magnitudes of up to 1000 nT at the Earth's surface (Blakely, 1996). Variations of the external parts also induce currents in the lithosphere and upper mantle resulting in induced secondary fields.

Concerning the external field variations, the K -indices and Kp -index are the specific terms officially adopted by the International Association for Terrestrial Magnetism and Electricity (IATME, which later became IAGA) in 1951, used to describe the degree of the external field disturbances. The Kp -index is a 3-hourly planetary geomagnetic index of activity based on the K -indices from 13 selected subauroral stations. The name Kp originates from the German words "planetarische Kennziffer" (= planetary index), that was introduced by Bartels in 1949 and has been derived since then at the Institut für Geophysik of Göttingen University, Germany. The K -indices, ranging from 0 to 9, are related to the maximum fluctuations of horizontal components observed on a magnetometer relative to a quiet day, during a three-hour interval. The Kp values of less than 3 mean a magnetically quiet condition, while the Kp values from 4 to 9 mean a calm, minor storm, moderate storm, strong storm, severe storm, and extreme storm condition; respectively. The conversion table from maximum fluctuation to K -indices varies from observatory to observatory in such a way that the historical rates of occurrence of certain levels of K are about the same at all observatories. In practice this means that observatories at higher geomagnetic latitude require higher levels of fluctuation for a given K -index. Siebert (1971) defined that "the K variations are all irregular disturbances of the geomagnetic field caused by solar particle radiation within the 3-h interval concerned. All other regular and irregular disturbances are non K variations. Geomagnetic activity is the occurrence of K variations." Since 1997 the Kp and related indices are derived at the Adolf Schmidt Geomagnetic Observatory Niemegk of the Helmholtz Centre Potsdam GFZ German Research Centre for Geosciences².

The term of geomagnetic anomalies refers to individual features, due to local and regional variability of crustal magnetization. Crustal magnetic anomalies are calculated by subtracting the core field from the measurements of the geomagnetic field intensities. If $|\mathbf{T}|$ represents the internal geomagnetic field intensity at any point, and $|\mathbf{F}|$ is the regional field intensity at the same point, then the total field anomaly ΔT is given by:

$$\Delta T = |\mathbf{T}| - |\mathbf{F}|. \quad (1.2)$$

Note that the total field anomaly is not equivalent to the magnitude of the anomalous field, but is a good approximation for it, since the anomalous field is usually small compared to the regional field. These mathematical relations can be graphically illustrated in **Fig. 1.4**.

Compared to the calculations of gravity anomalies that need some complex corrections of elevations and terrains, the calculation of magnetic anomalies is often treated in a less detailed way (Blakely, 1996). It usually consists of only two main steps: (i) data reduction which is an adjustment for daily variations and magnetic

² http://www-app3.gfz-potsdam.de/kp_index/index.html

disturbances; and (ii) the subtraction of suitable regional field, such as the IGRF model appropriate for the date of the survey. However, to ensure a high quality data processing, these two steps are crucial and need a very careful data selection, as described further in **Sec. 3.1**.

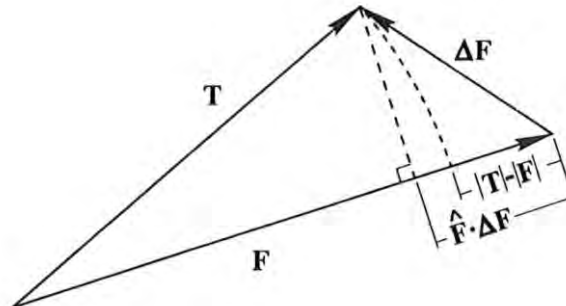


Figure 1.4 Vector representation of total field anomalies (adopted from Blakely, 1996). The geomagnetic field intensity T is the vector sum of the regional field F and the anomalous field ΔF . Length $|T-F|$ represent the total field anomaly, but length $\hat{F} \cdot \Delta F$ is a suitable approximation if $|F| \gg |\Delta F|$.

1.2 The Lesser Sunda Islands (LSI)

The Lesser Sunda Islands (LSI) region refers to a chain of medium to small islands, situated east of the Java Island in Indonesian region. Some references also call it Nusa Tenggara. From West to East, it consists of the islands of Bali, Lombok, Sumbawa, Flores, Solor, Lomblen, Pantar, Alor, Kambing, and Wetar in the North; Sumba, Savu, Roti, and Timor in the South; and some other smaller islands around them, with the total area of 87,700 km². Together with the Greater Sunda Islands (including the islands of Sumatra, Java, Borneo, and Celebes), these islands make up the Sunda Islands. With the exception of the Borneo Island and eastern Sumatra, the Sunda Islands belong to the zone of island arcs and submarine ridges, lying between Asia and Australia. **Figure 1.5** shows the locality of these islands.

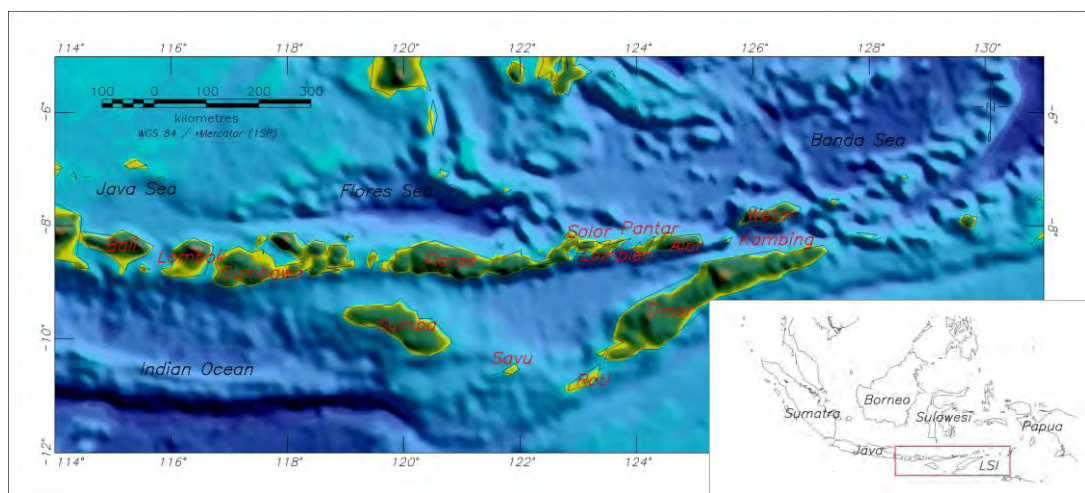


Figure 1.5 The Lesser Sunda Island (LSI), including the islands of Bali, Lombok, Sumbawa, Flores, Solor, Lomblen, Pantar, Alor, Kambing, and Wetar in the North; Sumba, Savu, Roti, and Timor in the South; and some other smaller islands around them, with the total area of 87,700 km². Inset is the Indonesian region, with the LSI shown in the red rectangular.

The LSI region differs from the Greater Sunda Islands of Java or Sumatra, containing many small islands as well as deep oceanic trenches. The landscapes of these islands are greatly various (i.e. from a lowland to mountainous, from a sandy beach to a humid tropical forest or contrarily to an arid savana), but naturally in a beautiful harmony. Flora and fauna immigration between these islands is restricted, leading to the evolution of a high rate of localized species. The well known Wallace Line (Wallace, 1869) passes through the islands between Bali and Lombok, along the deep waters of the Lombok Strait which formed a water barrier and maintains the biodiversity over these islands.

1.2.1 General tectonic settings

Figure 1.6 shows the main tectonic features over the Indonesian regions, including some active volcanoes, deep oceans, subduction zones and trenches. The Indonesian regions lay in a tectonic junction of the continental Eurasian – the oceanic Pacific/Philippine – the oceanic Indian – the continental Australian plates (Bird, 2003). For the Eastern-Indonesian regions, Hirschberger et al. (2005) indicated that this region clearly appears as a very active area where the deformation is widely distributed and rapidly evolving.

It is already well known that the Indonesian region is nearly perpendicularly subducted by the Indian oceanic plate along the Java Trench, as a continuation of an oblique subduction along north coast of Sumatra Island (Hamilton, 1979). Two continental arcs were formed due to this active subduction, namely the Sunda and the Banda arcs, as shown by shadowed areas with light green and light blue in **Fig. 1.6**, respectively. The LSI is depicted in the red polygon and lies over the transitional regions between the two arcs.

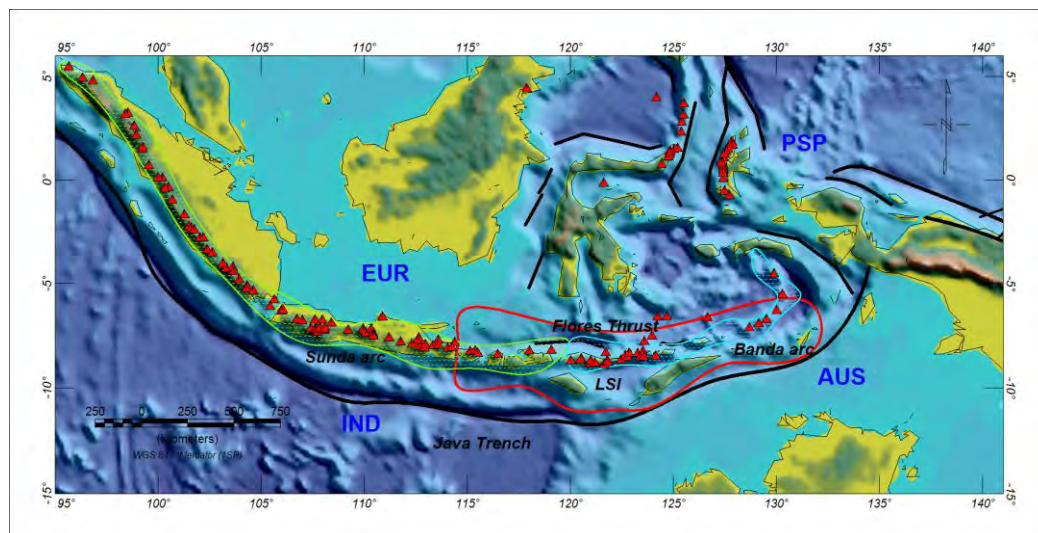


Figure 1.6 The general tectonic settings of the Indonesian regions, which lie in a junction of the continental Eurasian (EUR)–the oceanic Pacific Sea/Philippine (PSP)–the oceanic Indian (IND)–the continental Australia (AUS) plates (Bird, 2003). The Indian oceanic plate is subducting beneath the Eurasian plate along the Java Trench. The LSI is situated along the transitional regions between the *Sunda-Banda Arcs* (Hall and Smyth, 2008), flanked by the Java Trench and the Flores Thrust (Hamilton, 1979), the morphologies of which are not completely known (Silver et al., 1983; Silver et al., 1986). The topography and bathymetry are from the SRTM 30 Plus v4 data (Becker et al., 2009), generated using Oasis Montaj (Geosoft software). The volcano data are from the Smithsonian Institution, Global Volcanism Program³.

³ <http://www.volcano.si.edu>

The LSI consists of two geologically distinct archipelagos. The northern archipelago (including the islands of Bali, Lombok, Sumbawa, Flores and Wetar) is volcanic in origin, whereas the southern one (including the islands of Sumba, Savu, Roti, and Timor) is non-volcanic and appear to belong to the Australian plate. There is a long history of geological and tectonic study of the LSI; however, the detail of geological formations is not fully understood, and theories of the tectonic evolution of these islands changed extensively during the last decades of the 20th century.

Thus, beside the above well known settings, some other aspects of this regional tectonics still need more explanations. Here, the existence and extension of the Flores Thrust zone is highlighted. For the first time, Hamilton (1979) has proposed its existence in the back arc region of the LSI. The extension of this thrust zone onto north off the Bali Island was introduced later by Silver et al. (1983, 1986). Their study is based on a seismic multibeam survey, conducted using the R/V Thomas Washington during April 1981. Later on, the existence of two flanking slabs around the LSI is supported by an independent new seismic tomography study (Fig. 6 of Hafkenscheid et al., 2001). Results of the new study show the possible existence of a slab subducting in the north off the Bali Island, which could not be recognized before from the previous tomography study (Fig. 3B of Widiyantoro and van der Hilst, 1996). However, the trace of the subducting slab in the back arc region of the Sunda-Banda arcs is not as clear as of the Molucca region (Fig. 8 of Hafkenscheid et al., 2001). It is probably due to relatively young age of this subduction, as proposed about 3 Ma by Silver et al. (1983), while the crusts in the Indonesian region is also very thin (Hall and Smyth, 2008).

1.2.2 Historical seismicity

Lying at the collision of three tectonic plates, the LSI comprises one of the most geologically complex and active regions in the world. Despite many earthquake occurrences (see **Sec. 4.1** and **4.5.1** for the detailed data) and many volcanoes in this region, the historical seismicity of this region is poorly understood, due to a limited available data (from 1963 only). The situation is better for the western part of Indonesia (i.e. the Sumatra Island, see inset of **Fig. 1.5** for location), since the regional earthquake history can be traced since 1797.

In the subduction zones, it is common that the periodicity of giant earthquake recurrence is some 300 to 500 years (Satake and Atwater, 2007). After about 300 years of moment accumulations, a giant and devastating earthquake in the Sumatra regions occurred in December 2004. Triyoso has suggested that following this biggest one in Sumatra, the stresses will be transferred to the neighbouring area following the paths of clustered faults⁴. Some big earthquakes that happened recently (from end of March 2005 to end of September 2009) in the western Sumatra regions could be related to the locked strain releases, as suggested by Natawidjaja and Triyoso (2007).

Based on the shallow large earthquakes of Eastern-Indonesian data, Triyoso has identified a possibility of having large shallow earthquakes with an occurrence probability of 100 years return period over the LSI regions⁵. Moreover, Soloviev and Ismail-Zadeh (2003) have generated non-linear dynamic numerical models for long term earthquake predictions, based on the global movement data of HS2-NUVEL1 model. They have predicted that for observed seismicity of $M > 6$ and $M > 7$, there are two main clusters over the Indonesian regions. One cluster is over the Northwest end of the Sumatera Island and the other greatest one is over the LSI region. Therefore,

⁴ http://www.emsc-csem.org/Doc/SUMATRA_280305/EffectOnStaticStrainCh.pdf

⁵ http://www.hrdp-network.com/pirba/content/e5781/e5795/e5809/e15439/eventReport15468/PSHA_Wahyu2009.pdf

studies related to the earthquake occurrence probability over this region are urgently needed.

1.2.3 Socio-cultural situations

Having a total area as wide as the Java Island (87,700 km²), the LSI is inhabited by more than 12 millions people of a great variety of ethnic groups with at least 33 different languages. Most of the LSI people work as traditional farmers, cultivating rice, maize, coconut, coffee, cacao and some vegetables. Others work as fishermen, merchants, or in some other informal sectors, while only a small portion of people work formally. **Figure 1.7** illustrates daily working situations of traditional farmers in the LSI region.



Figure 1.7 Daily working situations of traditional farmers in the LSI region (taken during geomagnetic survey over the Lombok Island region in 2007). Physical powers of man and animal are used intensively to cultivate rice.

Since the availability of electrical power in the LSI is still of a big deficit, physical powers of man and animal are used intensively there. Horses are also still used as one of the main locomotion of public transportations, especially in some remote areas. Only around big cities, the houses are furnished with electrical and communication equipment. In some villages, people have to pay too much for electricity which is generated with diesel machines, provided by private companies. Finding new energy resource is needed to develop the LSI, which should be a resource with a low environmental impact to maintain the natural beauty of this region.

Most of the LSI people do not have a proper opportunity to get formal educations, mainly because some economical reasons (i.e. poverty). Due to this situation, the community knowledge about natural disasters (especially earthquakes and tsunamis) as well as their knowledges to react in such situations are somehow limited. This has been inferred from a direct investigation that has been conducted during field measurements in the northern part of the Lombok Island. It took place on a junior and senior high school situated several hundred metres from the coast. Two simple questions needed to be answered: *the first* about the mechanism of tectonic earthquake and tsunami generation, and *the second* on how to behave if an earthquake or a tsunami hit their boarding school. This investigation showed that

only about 6% of the students can answer well, while another 19% have insufficient knowledge, whereas 75% of them know nothing (or their answers showed clear misconceptions).

Compared to the Western-Indonesian region where a better situation of economy and education exists, a regular teaching and training on disaster preparedness in schools and communities have been initiated there since 2005. A non governmental organization called the Tsunami Alert Community (Kogami⁶) has introduced an active work for it, including mapping out the evacuation routes and training the community how to apply it.

1.2.4 The Lombok Island

The Lombok Island is where the transition towards Eastern-Indonesia begins, both naturally and culturally. The flora and fauna there are of intermediate zone between Asia and Australia. The western part of this Island is the greenest and most humid. As one moves East, the dry season becomes more pronounced. An old mountainous chain with some steep canyons facing to the Indian Ocean is the general view of the southern part of this Island. Facing to the North, one finds a new mountainous range and very fertile area with tall trees and vegetations covering the land. The principal mountain is the Mt. Rinjani (3726 m), the second-highest active volcano in Indonesia, fascinating with abundant fresh water infill and its newest cone on its caldera. **Figure 1.8** shows the general topography of the Lombok Island, surrounded with arrays of beautiful beaches and many arising islets (with total number of 72) close to its south- and north- coastal areas.

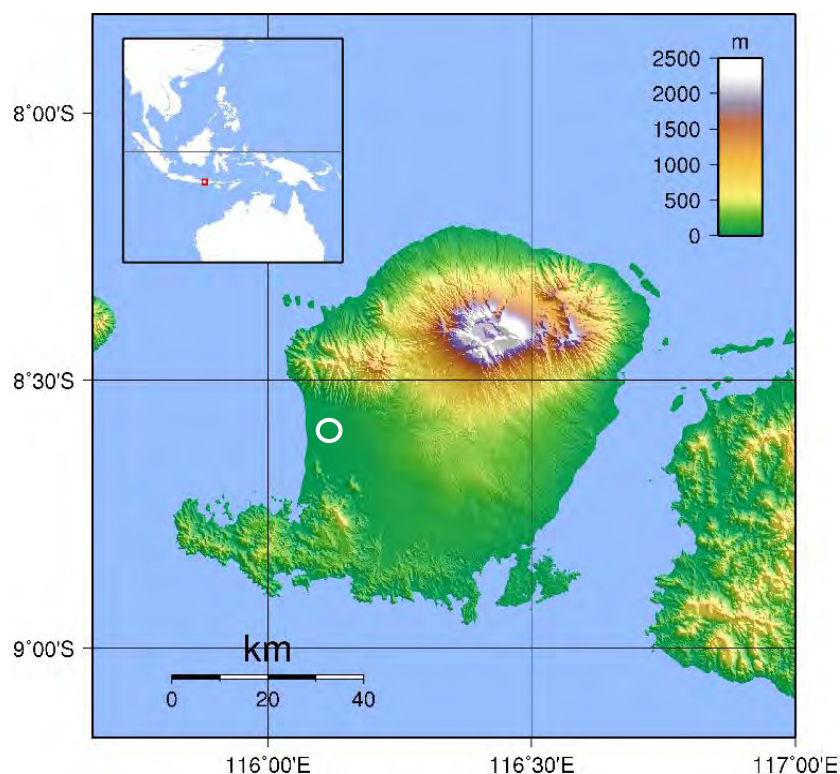


Figure 1.8 General topography of the Lombok Island⁷. In Mataram City (white circle), the density of populations in 2007 is more than that of the Berlin City in June 2008.

⁶ <http://kogami.or.id/>

⁷ modified from http://upload.wikimedia.org/wikipedia/commons/b/bb/Lombok_Topography.png

In the middle part of this Island, more than 3 million peoples⁸ (most of them are children and adolescents) are concentrated, resulting in rather dense area with the average density of more than 600 persons/km². In Mataram City (the capital city of West Nusa Tenggara province, depicted as a white circle of **Fig. 1.8**), the density of populations in 2007 reached 5810 persons/km²; much denser than the Berlin City (3830 persons/km² in June 2008⁹). This number will be very likely increased, due to more and more migrated people from other nearby islands (such as Java and Sulawesi). The reason for this migration is mainly of economical interest, since an increasing rate of tourists visiting this Island is predicted, especially when a new international airport will be fully operated (scheduled in 2012).

1.3 Motivation, objective and synergy

Investigations of geomagnetic anomaly over the Lombok Island have been conducted since 2004, firstly, covering surrounding areas of the Mataram City (depicted as a white circle of **Fig. 1.8**). At this city, the Electrical Engineering Department of Mataram University has established a new Basic Electrical laboratory. During calibration procedures of new magnetic measuring instruments in this laboratory (i.e. Tesla meter and Flux meter), difficulties in zero adjustment (to cancel the influence of the external ambient fields, including Earth's magnetic field) have been experienced. Moreover the readings were almost always getting "out of range" of the available scales.

Several physical phenomena that could be related to the extreme magnetic induction are also daily observable in the Mataram City. The most clear one is prominent shortening of the life time of batteries which are used in the "classical magnetically induced" clocks. These clocks need battery replacements every two months for continuous operations (i.e. too often, compared to a normal condition which needs only one year replacement). Another phenomenon is intensive destructions of the data recorded on the magnetic floppy disks. Since there are no suspected man made sources of these strong inductions over this city, the possibility of the nature (e.g. the Earth's magnetic field) as the responsible source has to be investigated.

As described in **Chap. 2**, the earlier results of global data from satellite measurements and regional data from marine and aeromagnetic surveys indicate that the Lombok Island lies between zones characterized by the highest intensity geomagnetic anomalies of this region. Manda and Thébault (2007) remark it as one of the eight most important features provided on the 1st edition of World Digital Magnetic Anomaly Map. Although some preliminary studies were conducted (Zubaidah et al., 2005), however no high qualities of geomagnetic data were available for this Island. Due to the lower accuracy of the used equipment and a limited number of stations, the quality of the previous measurements is questionable for more interpretations. Thus a more detailed study to better characterize the geomagnetic anomaly over this Island region was needed.

This study is intended to answer several crucial questions:

1. Which are the real values of anomalies over this region? Which is the general pattern? How well the regional pattern fit to the global one?
2. Have the geomagnetic anomalies changed over the recent time? How have they changed? Are there any specific regional characteristics of the changes, compared to the global one?

⁸ <http://ntb.go.id/bankdata/>

⁹ <http://www.berlin.de/>

3. Which are the relationships between these geomagnetic anomalies to the geology and tectonics of this region? What new insights can be gained from the geomagnetic observations?
4. Which are the relationships between these anomalies and the high seismicity of this region? Is it possible to link the geomagnetic anomaly variations to the earthquake occurrence?

Since the forth set of questions is the most crucial one and might trigger some socio-cultural impacts, a short clarification concerning this specific point related to the objective of this study is given in the following:

There are many different personal viewpoints in relating the geomagnetic anomalies and their variations to the (possibility of) earthquake occurrences, which basically can be classified to three different groups. Some authors view the efforts of short term predictions of earthquakes using precursory anomalous signals with strong scepticism. Johnston et al. (2006), based on the absence of electric and magnetic field precursors in the San Andreas fault system, concluded that useful prediction of damaging earthquakes seems unlikely using these electromagnetic data. Campbell (2003) even called such efforts as a magnetic fraud. Contrarily, several authors believe that someday people will be able to predict the earthquake occurrences in only a short range of days. They argued that it is just like people being able to fly with aeroplanes today, which was still a dream before the 19th century. This group then has actively proposed new methods, called seismo-electromagnetic, to detect some low- and high- frequency anomalous signals related to earthquakes. Among this “optimistic” group members are Uyeda (2009), Hayakawa (2009), Hattori et al. (2004a, 2004b), and Molchanov (2003). The rest part is ones that perform a moderate view and are waiting for more intensive study results. They also suggest to use an integrated geophysical observations rather than a single one, as seismo-electromagnetic observations, in order to process all available precursory data (Eftaxias et al., 2009). Moreover, some authors have proposed a global data resource to allow more proper statistical approaches (Balasis and Manda, 2007).

Here, it should be emphasized that this study is not to make an alignment either to the skeptic or the optimistic groups. It is intended to provide a proponent data and analysis of seismo-electromagnetic phenomena from a particular high seismicity region characterized with high geomagnetic anomaly.

The intriguing geomagnetic anomalies over the Lombok Island region vis-à-vis the above described socio-cultural situations lead to a study with a special aim to assess the potential of natural hazards (especially earthquakes) as well as natural resources (especially new sources of energy).

Chapter 2

Geomagnetic data

The geomagnetic data from different platforms (satellites, marine campaign, aeromagnetic surveys, observatories, and repeat stations) are firstly presented, giving an overall view of data availability and how they can support in describing the geomagnetic anomaly over the Lombok Island. Thereafter, the ground measurements taken during scientific fields campaigns are in focus. Results of the previous surveys (2004–2005) are also included to give the actual stand before the recent campaigns. As a core of this chapter, ground measurements that have been conducted consecutively in 2006 and 2007/2008 are highlighted, including the descriptions of surveyed area, as well each important step during the campaign. The specific conclusions of each survey are also documented, which could be used as ready references for planning the next surveys.

2.1 Related available data

2.1.1 The CHAMP satellite data over the Indonesian region

The CHALLENGING Mini-Satellite Payload (CHAMP) is a satellite used for scientific objectives in geophysical research and application, including Earth's gravity field, Earth's magnetic and electric fields investigations, as well as sounding of atmospheric limb and ionosphere. It was launched on July 15th 2000, managed by Helmholtz Centre Potsdam Deutsches GeoForschungsZentrum (GFZ). The physical dimensions of the CHAMP satellite are 522 kg of total mass, 750 mm of height, 8333 mm (with 4044mm Boom) of length, and 1621 mm of width. A deployable boom mounted at the front end of the satellite (see **Fig. 2.1**) consists of three segments: the outer part which is carrying an absolute scalar Overhauser magnetometer (OVM), the middle segment with the optical bench on which two star sensor heads and two Fluxgate vector magnetometers (FGM) are mounted, and the inner segment with the deployable part of the hinge.

The position of the OVM at the tip of the boom ensures magnetic cleanliness, so that the magnetic stray is less than 0.5 nT there. Both Compact Spherical Coil (CSC) sensors of the FGMs are mounted together with the star cameras on a common optical bench, providing a mechanical stability between these systems of better than 10 arcsec. The optical bench is placed about halfway between the satellite body and the OVM to avoid magnetic interference from the spacecraft as well as cross-talk between the FGMs and the OVM.

The OVM, which is regarded as the reference instrument for the magnetic field measurements, directly gives the magnetic field sampled at 1 Hz with a resolution of 0.01 nT. Additionally, the FGMs measure three components of the magnetic field vector, sampled at a high rate of 50 Hz that are averaged to 1 Hz for the Level 2 or 5

Hz for the Level 3 products. The important instrument parameters for the FGM (scale factor, bias and misalignment) are determined regularly with the help of an OVM/FGM in-flight calibration procedure.

A processed OVM data set contains the GPS universal time and its offset in 0.1 ms, satellite position (latitude and longitude, geocentric geographic, in degree), altitude above reference sphere (in km), data quality, and scalar magnetic field value. A processed FGM data set contains information like the OVM data set, except that the scalar magnetic field values are replaced by calibrated B-Field-Vectors in FGM-1 sensor or EC EF NEC (Earth-Centered, Earth-Fixed, North-East-Center) System.

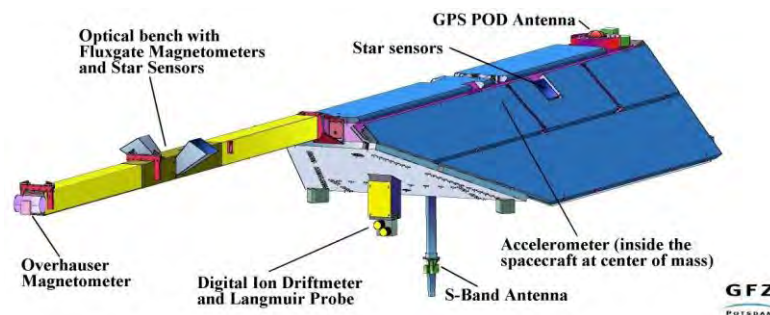


Figure 2.1 Physical layout of the CHAMP satellite (front view) with locations of the main instrumentations¹⁰.

With its high inclination (87°), CHAMP covers all local times, and with its long active life-time (now, more than 9 years in orbit) it also allows the study of the secular variation. Due to its low circular orbit (starting at 454 km altitude and decaying at some 300 km) and its high-resolution instrumentation, CHAMP promises an improvement in accuracy by an order of magnitude compared to the MAGSAT or Ørsted missions, and is particularly well suited to advance crustal field studies from space.

The magnetic CHAMP data have been used to generate several models, for example the GRIMM-GFZ Reference Internal Magnetic Model- (Lesur et al., 2008) and the MF's series (Maus et al., 2006; Maus et al., 2007; Maus et al., 2008). The GRIMM model, which is a core field and secular variation model, has been derived from nearly 6 years of CHAMP satellite data and 5 years of observatory hourly means. The sixth-generation lithospheric magnetic field model (MF6), which is used as a reference in this study, is the first satellite-based magnetic model to resolve the direction of oceanic magnetic lineations, revealing the age structure of oceanic crust. This model was produced using a new scalar data set product from 4 years (2004–2007) of the FGM measurements, resolves the crustal magnetic field to spherical harmonic degree 120, corresponding to length scales down to 333 km (Maus et al., 2008). The procedures used in the data selection and processing sequence remain unchanged from the previous MF4 (Maus et al., 2006) and MF5 (Maus et al., 2007) models, with significant changes in using an improved scalar data product and expansion to a higher spherical harmonic degree that became possible by the cleaner input data and the lower altitude of the CHAMP satellite.

¹⁰ http://op.gfz-potsdam.de/champ/systems/index_SYSTEMS.html

Figure 2.2 shows the total component of the magnetic anomaly over the Indonesian region using the magnetic field model MF6 at geoid altitude. This figure clearly shows that the subduction zone along the Sunda-Banda arcs mainly coincides with negative anomaly bands. It also indicates that the Lombok Island lies between extremes of geomagnetic anomaly in this region, which leads to a high interest in understanding their sources as well as geological and tectonic implications. Consequently, a more detailed geomagnetic anomaly map is needed for sharpening these views, which can be provided by combining all available marine and aeromagnetic data over the Sunda-Banda Arcs.

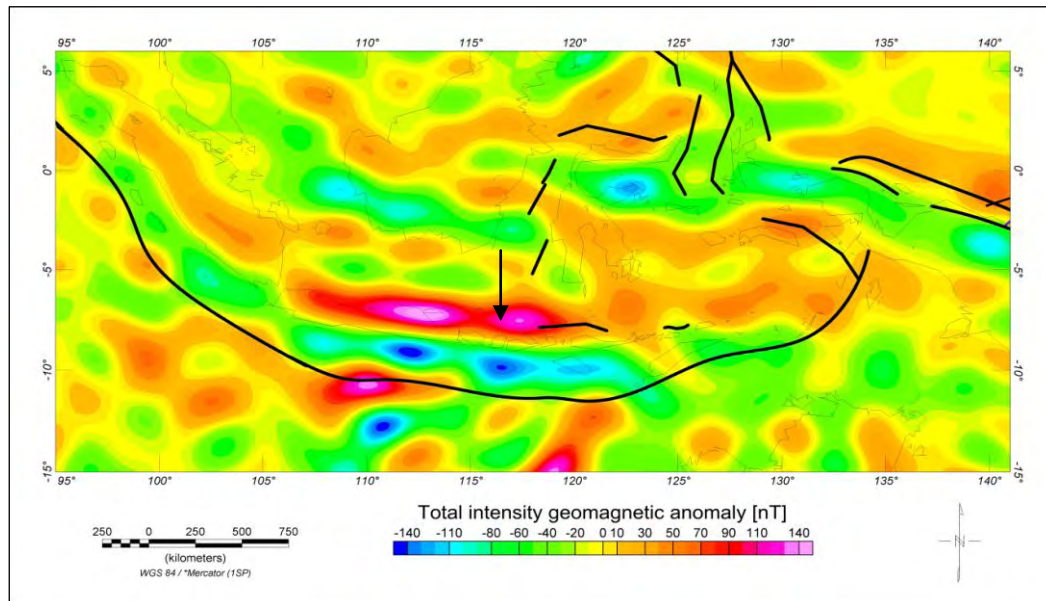


Figure 2.2 Map of the total component of the large-scale lithospheric anomaly field at geoid altitude for the Indonesian region obtained from the MF6 model (Maus et al., 2008). Plate boundaries and subduction zones are indicated as black lines. The Lombok Island (pointed out by a black arrow) lies between the extremities of geomagnetic anomalies in this region.

2.1.2 Marine and aeromagnetic data over the Sunda-Banda Arcs

To produce a more detailed geomagnetic anomaly map that can be used for sharpening the satellite data view and getting a more regional one, all available marine and aeromagnetic data over the Sunda-Banda Arcs (ranged from 105°E to 127°E and from -5°N to -15°N) have been collected. Here, the sources of these data and how they have been processed are briefly described.

The data set of Quesnel et al. (2009) has been used as the main part of the marine magnetic data sources. These authors have revised the GEOPHYSICAL DATA SYSTEM (GEODAS)¹¹ data set by cleaning and leveling the initial data set, which consists of 20,241,539 worldwide marine data, including 2411 cruises during the period 1953–2004. They have firstly applied the CM4 model (Sabaka et al., 2004) to properly remove the core and external field contributions from measurements, then carried out cleaning phases and leveling procedure by adjustment to NGDC-720 (Maus, 2008). As a result, a first coherent marine magnetic global dataset at short- and long-wavelengths could be provided.

¹¹ www.ngdc.noaa.gov/mgg/geodas/

A second part of marine data has been obtained from a data exchange with the Bundesanstalt für Geowissenschaften und Rohstoffe (BGR). The SINDBAD (Seismic and Geoacoustic Investigations along the Sunda-Banda Arc Transition) data have been provided, corresponding to a marine survey of the RV SONNE from October 9th to November 9th 2006. This data set consists of 4933 km profiles, divided in three sectors (i.e. East Java, Lombok Basin, Roti Basin/Savu Basin), ranging from 110°E to 123°E (Müller et al., 2006). The data from two Overhauser magnetometer sensors, two towed Fluxgate magnetometer sensors, and the ship GPS recording have been processed over the following steps: (i) interpolating all data gaps, (ii) subtracting the ambient core field using the 10th generation of IGRF (Maus et al., 2005), (iii) band pass filtering in time domain (i.e. based on spectral analysis, the signals with wavelengths shorter than 6 km or longer than 250 km are removed), and (iv) summing up the total field differences between both Overhauser sensors or other arbitrary sensor pairs.

Additionally, five aeromagnetic data sets (i.e. I1 (1967), I2 (1971), I3 (1973), I4 (1978), and I5 (1978–79)) have been extracted from the 2nd edition of the Magnetic anomaly map of East Asia (Ishihara et al., 2002). The data sets originally come from the Geological Research and Development Centre Indonesia and have been compiled by the Geological Survey of Japan (AIST) and The Coordinating Committee for Geoscience Programmes in East and Southeast Asia (CCOP). These aeromagnetic data sets have been used to fill in the areas where no marine data are available: over the northern part of and north off the Java Island and north off the Lesser Sunda Islands.

All three available data sources have been combined to get a single data set as well as single grid using the Kriging method, provided in the Oasis Montaj version 6.4 (Geosoft software). This method is a local estimation technique by determining the most probable value at each grid node using a statistical analysis of the entire dataset, so that it can provide the best linear unbiased estimate of an unknown characteristic being studied. To determine a value at each grid node, it first calculates a variogram of the data to show the correlation of the data as a function of distance. This method has also the capability to blank un-sampled areas (or areas with too few sample data) and is able to produce an error grid that gives an indication of the degree of confidence at each grid node.

Figure 2.3 shows a regional view of geomagnetic anomaly over the Sunda-Banda Arcs resulting from all available marine and aeromagnetic data sources. Some main geological features (e.g. subduction zone, volcanic islands belt and magmatic arcs) are clearly reflected in this map.

Since marine and aeromagnetic data contain both long- and short-wavelengths of magnetic anomalies, they can represent not only deep but also shallower (e.g. lithospheric) sources of anomaly. Moreover, knowing the more detailed boundaries between negative and positive part of anomalies (magnetic lineations) is useful to describe more localized tectonic or geological features. We should be aware of such specific features, since they also probably indicate high seismological risks or hazardous volcanic areas. A recent example are the “LUSI mud volcano” phenomena (Mazzini et al., 2007), located exactly in the extremity of geomagnetic anomaly on the Java Island, depicted as black triangle of **Fig. 2.3**. It has swamped 12 villages, killing 13 people and requiring the evacuation of about 36,000 people since its first eruption on May 29th 2006 (Source: the AFP, on December 4th 2008).

One should notice that the marine and aeromagnetic data coverage over the Java Island supports the determination of clear boundaries between negative and positive part of anomalies, while large data gaps exist in the Lesser Sunda Islands

region. Over the latest mentioned region, the available data are inadequate to determine such specific tectonic and geological features with a high degree of confidence. Adding magnetic data from un-covered regions, especially from the Lombok Island which lies between the extremes of the anomaly, is urgently needed to fill in the gaps.

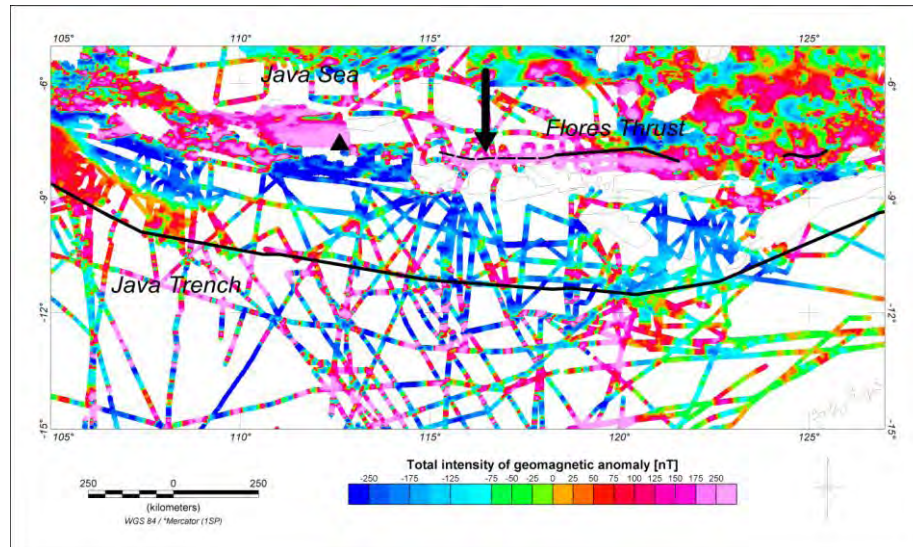


Figure 2.3 Regional view of the geomagnetic anomaly over the Sunda-Banda arcs, resulting from all available marine and aeromagnetic data sources. Plate boundaries and subduction zones are indicated as black solid lines, while the dashed one indicates its presumed extension. The white areas over oceans or islands indicate that no data are available. The data coverage over the Java Island allows the determination of clear magnetic lineations, while significant data gaps exist over the Lesser Sunda Islands (including the Lombok Island: pointed out by dotted black arrow). The “LUSI mud volcano” location on the Java Island is depicted as a black triangle.

2.1.3 Nearby observatory data

Additional magnetic data used in this study are available from three nearby observatories: Kupang (KPG) in Timor Island – Indonesia, Tondano (TND) in Sulawesi Island – Indonesia, and Kakadu (KDU) in Australia. **Figure 2.4** shows the locations of these observatories related to the Lombok Island (represented by the “Penyu” islet (PNY)).

Continuous magnetic recordings are necessary to eliminate the external field contributions from any measurement in magnetic anomaly studies. In general, a local Base Station is set up for that purpose, but if such local data are not available (see **Sec. 2.2**), the data from nearby observatories can be used to approximate the external variations. In the following, further information about these observatories are given, including information of the available data and how data have been obtained.

2.1.3.1 The Kupang (KPG) – MAGDAS observatory

The MAGDAS (MAGnetic Data Acquisition System) is a real time magnetometer network for space weather research applications deployed in the CPMN (Circum-pan Pacific Magnetometer Network) region by the Space Environment Research Center (SERC) Kyushu University, Japan. Fifty fluxgate-type magnetometers and their data acquisition systems transfer the averaged digital data from overseas sites to Fukuoka Japan, in nearly real time. Three components of the ambient magnetic field are obtained at the sampling rate of 1/16 seconds and digitized

by using the field-canceling coils for the dynamic range of $\pm 64,000$ nT/16bit. The total field is then estimated from the three components. The data resolution ranges are 0.061 nT/LSB (Least Significant Bit), 0.031 nT/LSB, and 0.0091 nT/LSB for ± 2000 nT, ± 1000 nT, and ± 300 nT range (at high-, middle-, and low-latitude stations), respectively. The estimated noise level of the MAGDAS magnetometers is 0.02 nT peak to peak (Yumoto and the MAGDAS Group, 2006).

The Kupang (KPG) station, located on $(-10.2^\circ\text{N}, 123.4^\circ\text{E})$ is the nearest MAGDAS station (about 850 km east of the Lombok Island, see **Fig. 2.4** for an estimated location). Over the period of interest in this study, the one-minute data of three components and the total field from KPG are available from July 22nd to October 27th 2006, only. The data for October 28th 2006 and later on are strange and should not be considered as geomagnetic data, probably due to an incidence of a burned cable. **Figure 2.5** shows the geomagnetic field intensity obtained from KPG during the survey days of the Lombok Island (continuous measurements on the ‘Penyu’ Islet) in 2006. The night time mean value is 45613.6 nT.

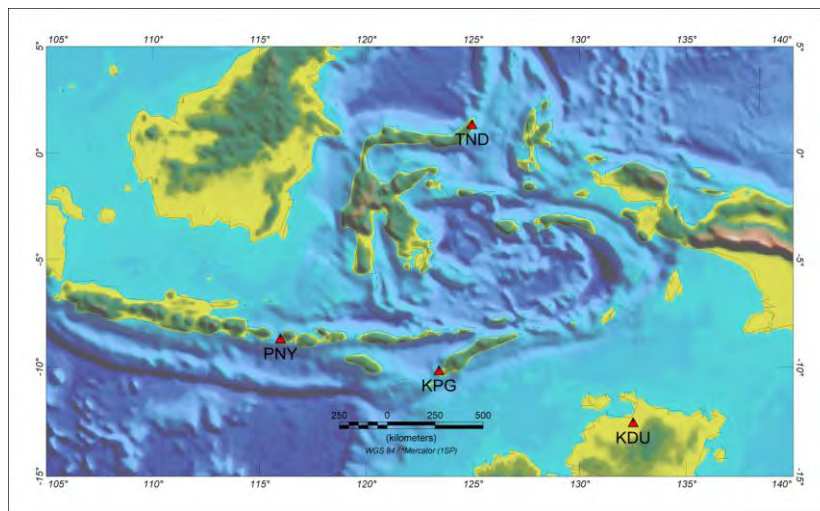


Figure 2.4 The location of the Lombok Island (represented by the “Penyu” islet, PNY) and the three nearby observatories, i.e. the Kupang (KPG) in Timor Island – Indonesia, the Tondano (TND) in Sulawesi Island – Indonesia, and the Kakadu (KDU) in Australia.

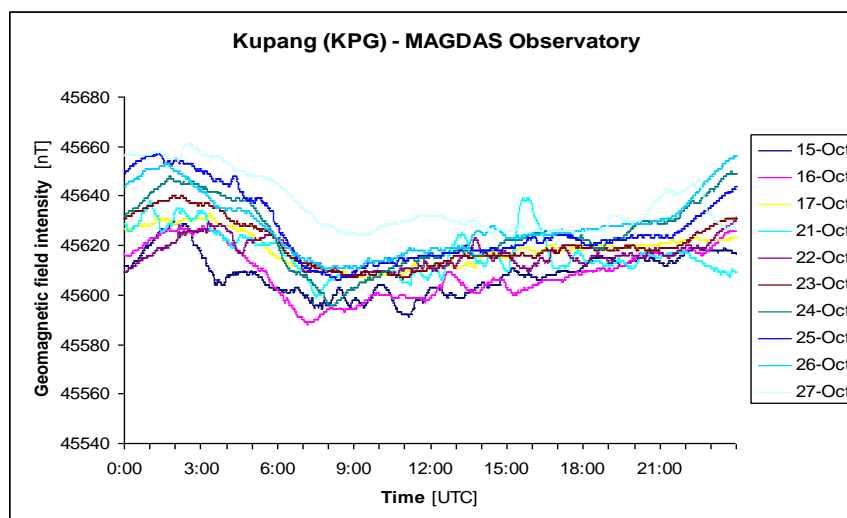


Figure 2.5 The geomagnetic field intensity at the Kupang (KPG)-MAGDAS observatory obtained during October 15th – 27th 2006 period. The night time mean value is 45613.6 nT.

2.1.3.2 The Tondano (TND) – BMG Indonesian observatory

Tondano (TND) is one of three Indonesian observatories operated by the Meteorological and Geophysical Agency (*Badan Meteorologi dan Geofisika*, BMG). It is located on (1.29°N, 124.95°E), near Manado in Sulawesi Island, about 1500 km northeast of the Lombok Island (see **Fig. 2.4** for an estimated location). TND has operated since 1991, the installing funding being provided by Australian Government Overseas Aid Program (AusAID). The first instruments, a Digital Fluxgate Magnetometer (FM100C) and a Proton Magnetometer (Scintrex-MP3), have provided a poor data quality. They have been upgraded and replaced with a DMI Three Axis Fluxgate Magnetometer and a Proton Precession Magnetometer (GSM-90), by the Geoscience Australia (GA) during 1998–2001.

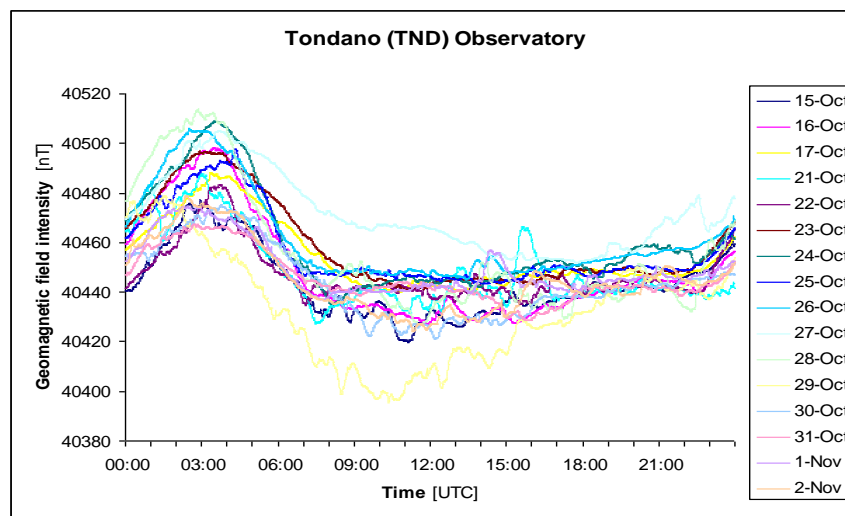


Figure 2.6 The geomagnetic field intensity at the Tondano (TND) – BMG Indonesian observatory obtained during October 15th – November 2nd 2006 period. The night time mean value is 40442.7 nT.

As a result, it is now possible to transmit absolute observations as well as variometer data to the GA from this observatory for routine processing¹². However, the data used in this work still have to be obtained directly from the BMG, since there are no on-line data available for this observatory on the GA website so far. **Figure 2.6** shows the one-minute values of the field intensity obtained from the TND during the survey period of the Lombok Island (continuous measurements on the ‘Penyu’ Islet) in 2006. The night time mean value is 40442.7 nT.

2.1.3.3 The Kakadu (KDU) – Australian Observatory

Kakadu (KDU) is an Australian observatory operated by the Geoscience Australia (GA), located on (-12.6°N, 132.5°E), about 2250 km southeast of the Lombok Island, 210 km East of Darwin (see **Fig. 2.4** for an estimated location). Continuous magnetic field recording began there in March 1995. They consist of three component measurements using a suspended linear Fluxgate Variometer (DMI FGE) and total field measurements using an Overhauser magnetometer (GSM-90). The KDU data are sent to the International Real-time Magnetic Observatory Network (INTERMAGNET), the IPS Radio and Space Services, and the Ørsted Satellite Project.

¹² www.ga.gov.au/geomag/data_reports/geomag_report.jsp

The data used in this study related to the 2006 survey were obtained from the INTERMAGNET website¹³. Meanwhile, related to the 2007/2008 survey, the data were obtained from the GA website¹⁴, since there are no 2008 definitive data available for this observatory on the INTERMAGNET website at time of writing. **Figure 2.6** shows one-minute values of the geomagnetic field intensity obtained from KDU during the survey days of the Lombok Island (continuous measurements on the 'Penyu' Islet) in 2006. The night time mean value is 46357.1 nT.

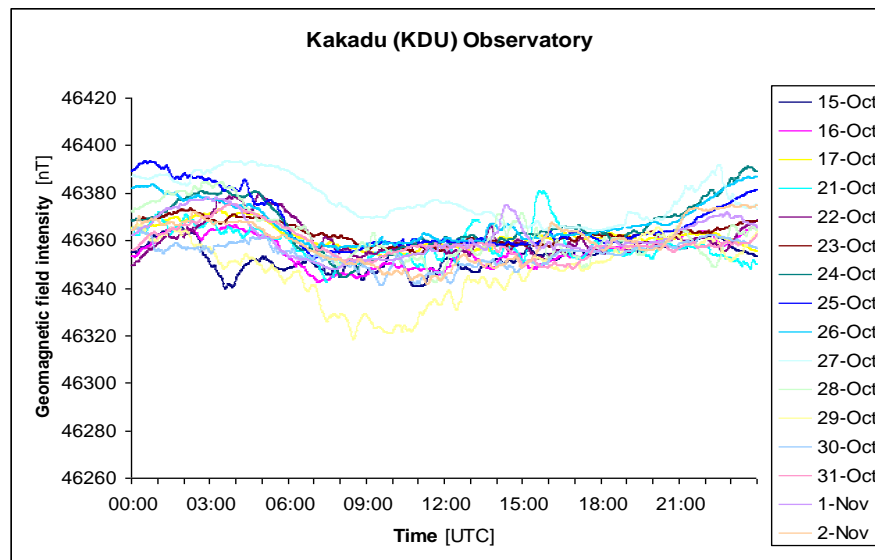


Figure 2.7 The geomagnetic field intensity at the Kakadu (KDU) – Australian observatory obtained during October 15th – November 2nd 2006 period. The night time mean value is 46357.1 nT.

2.1.4 The BMG Indonesian repeat stations data

As an official Indonesian government agency, the Meteorological and Geophysical Agency (*Badan Meteorologi dan Geofisika*, BMG) has issued a geophysical technical report containing information of an Indonesian geomagnetic repeat stations survey for the epoch 2005.0 (Harijono, 2006). This contains the results of the seventh regional survey. Earlier surveys have been periodically conducted by the BMG since 1960. **Table 2.1** shows the number of repeat stations that have been surveyed by year. From this overview, we can infer that the number of repeat stations is too few in comparison with the large area of the Indonesian region, not dense enough to underline such specific features like regional anomalies. Despite this limitation, the data still could be used to get a general overview of geomagnetic field in Indonesia, especially to monitor secular variation over this region.

In the latest regional survey, the declination, inclination and the total field intensity have been measured on each repeat station using two Declination Inclination Magnetometers (DIM-100 EDA and DIM Yomthree) and a Proton Magnetometer (G-816 Geometrics). The horizontal and vertical components have then been derived mathematically. On the latest report of BMG, the measurements were reduced to the same epoch by means of the Tondano (TND) observatory data. **Figure 2.8** shows the total geomagnetic anomaly over the Indonesian region, which has been derived from the BMG Indonesian repeat stations total component field data, from

¹³ http://ottawa.intermagnet.org/apps/dl_data_prel_e.php

¹⁴ <http://www.ga.gov.au/oracle/geomag/minute.jsp>

which the 10th generation IGRF values (IAGA WG V-MOD, 2005; Maus et al., 2005) have been subtracted. **Figure 2.9** shows the corresponding average annual secular variation between the epochs 2000.0 – 2005.0.

Table 2.1 Number of BMG Indonesian repeat station surveyed by year.

Region	1960-1962	1970-1974	1985	1990	1995	2000-2001	2005
Sumatera	4	10	15	15	15	13	12
Jawa	7	7	8	8	8	9	8
Kalimantan	3	4	8	9	9	9	10
Sulawesi	0	4	9	7	7	7	8
Nusa Tenggara	1	1	5	6	6	5	5
Maluku	0	1	4	2	2	3	4
Papua	0	5	10	6	6	7	7
Total	15	32	59	53	53	53	53

2.1.5 The IPS geophysical report and geomagnetic forecast data

The IPS (Ionospheric Prediction Service) acts as the Australian Space Weather Agency, providing the Australian national radio propagation and space weather services. Systems and technologies affected by space weather, including (i) HF radio systems, such as communications and surveillance systems; (ii) Geophysical exploration, power systems protection and the cathodic protection of long-distance pipelines; and (iii) Satellite and spacecraft operations, are supported by IPS.

The archive of IPS Daily Solar and Geophysical Report is available from October 2000 on, via the website¹⁵. The information can be sorted by date, thread, subject or author. The actual IPS reports can also be accessed directly by subscription to the IPS Mailing List (provided as daily report or weekly digest issued every Thursday) or even through the SMS services. The issued data on these reports are basically monitoring results on eight stations (Darwin, Townsville, Learmonth, Culgoora, Camden, Canberra, Hobart, and Casey (Antarctic)), summarized in the form of K -, A - and $Pc3$ -indices (see **Sec. 1.1.4** for definitions). The forecast for the next days is also given; thereby it is possible to use it to schedule the geomagnetic surveys for the most favourable geomagnetic conditions (i.e. only on the quietest periods to ensure the best results).

Figure 2.10 and **2.11** show the related K -indices for the Australian region during the survey days in 2006 and 2007/2008, respectively, in comparison with the Kp -index (see **Sec. 1.1.4** for definition) values provided on-line by Helmholtz Centre Potsdam Deutsches GeoForschungsZentrum – GFZ Potsdam¹⁶. Both figures indicate that the surveys have been conducted mainly during magnetically quiet periods (i.e. K and $Kp < 3$).

¹⁵ www.ips.gov.au/pipermail/ips-dsgr/

¹⁶ http://www-app3.gfz-potsdam.de/kp_index/index.html

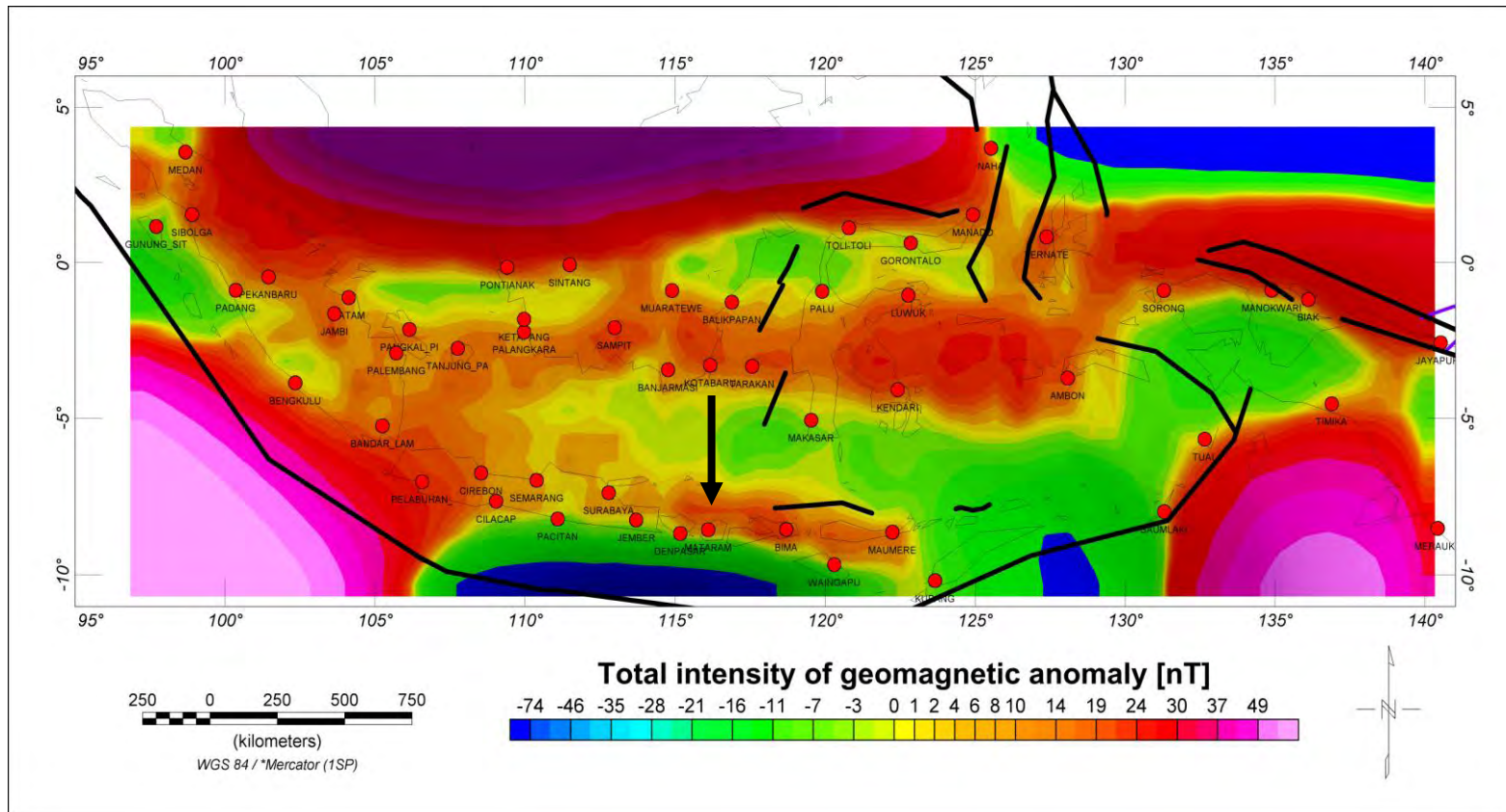


Figure 2.8 Regional view of geomagnetic anomaly over the Indonesian region for the epoch 2005.0. This map has been derived from the BMG Indonesian repeat stations total component field data (Table 6 of Harijono, 2006), from which the 10th generation IGRF values (IAGA WG V-MOD, 2005; Maus et al., 2005) have been subtracted. The data have been gridded using the Kriging method (spherical model) in the Oasis Montaj 6.4. Plate boundaries and subduction zones are indicated as black lines. The repeat station locations are shown as red dots, while the Lombok Island is pointed out by a black arrow.

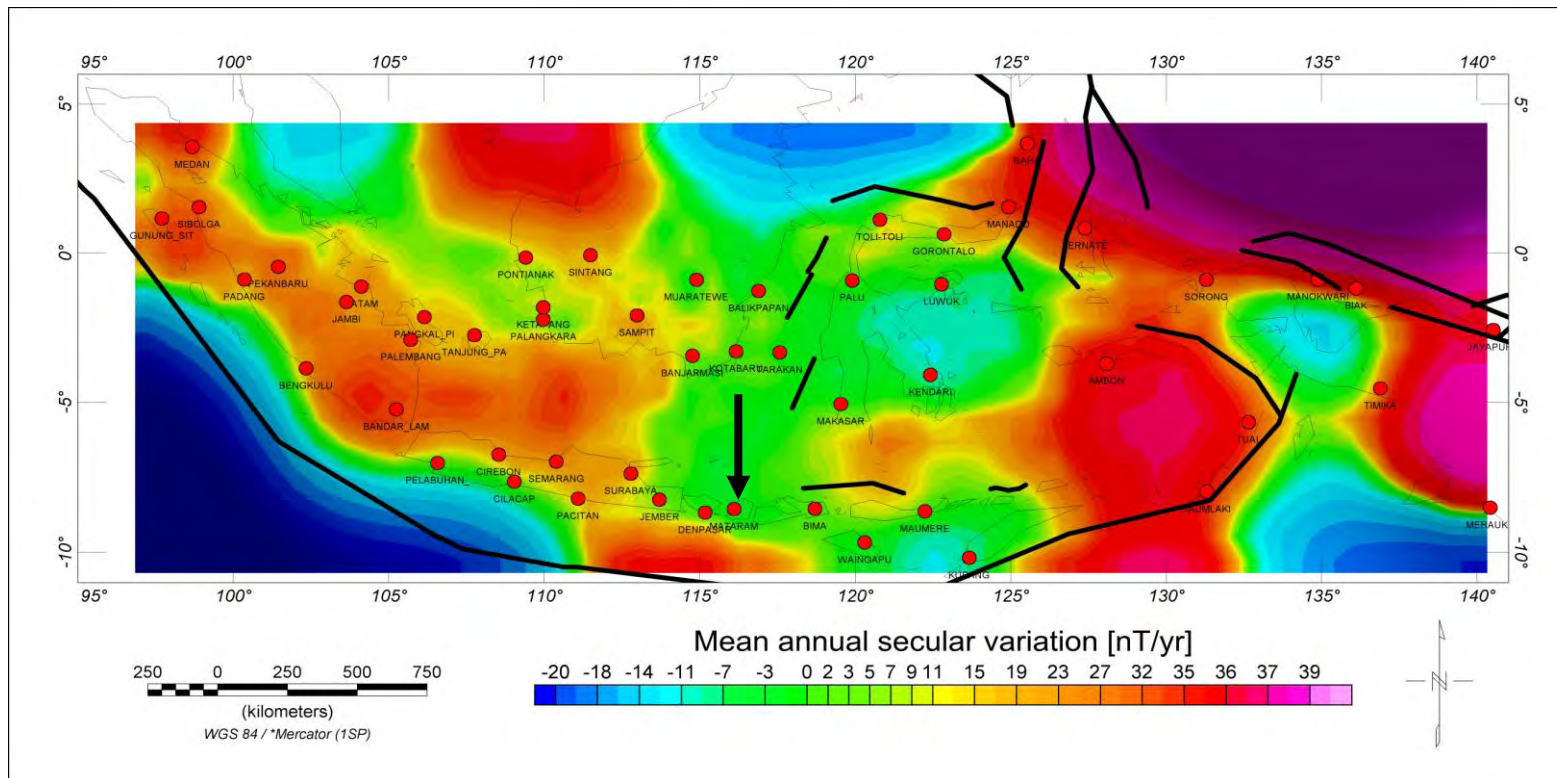


Figure 2.9 Regional view of mean annual secular variation over the Indonesian region between the epochs 2000.0 – 2005.0. This map has been derived from the BMG Indonesian repeat stations annual secular variation data (Harijono, 2006). The data have been gridded using the Kriging method (spherical model) in the Oasis Montaj 6.4. Plate boundaries and subduction zones are indicated as black lines. The repeat station locations are shown as red dots, while the Lombok Island is pointed out by a black arrow.

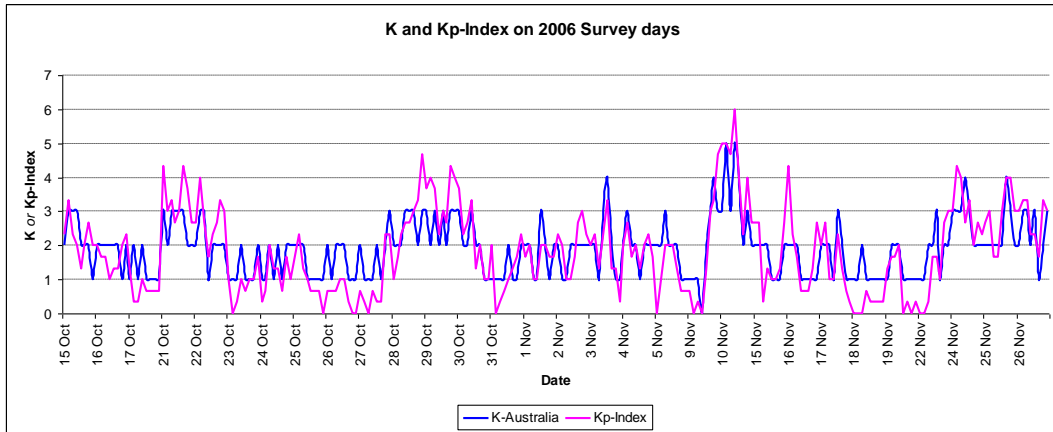


Figure 2.10 K -indices for the Australian region and Kp -index values during the survey days in 2006, indicating that the survey has been conducted mainly during magnetically quiet periods (i.e. K and $Kp < 3$).

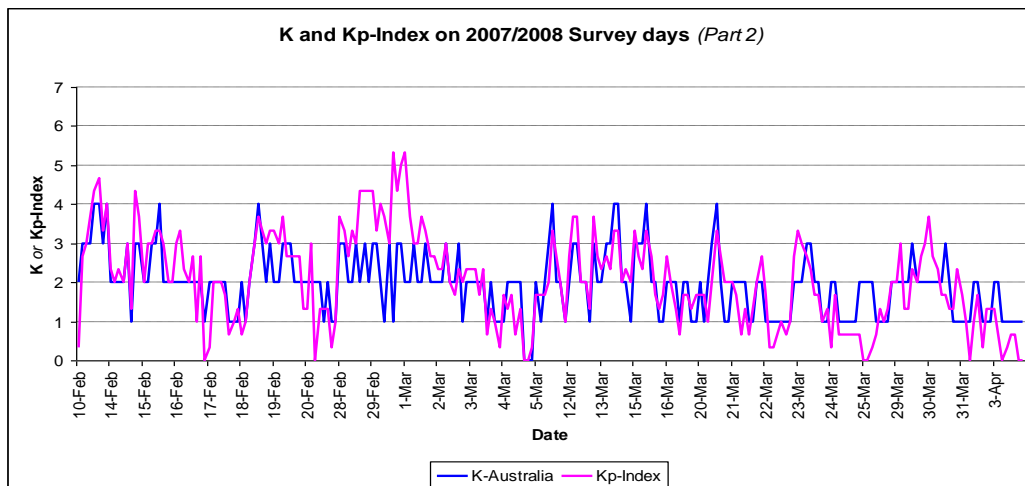
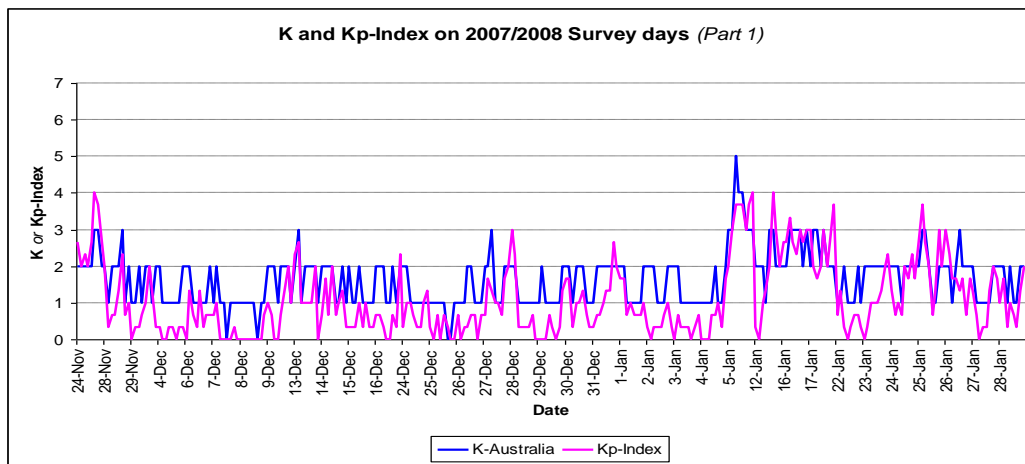


Figure 2.11 K -indices for the Australian region and Kp -index values during the survey days in 2007/2008, indicating that the survey has been conducted mainly during magnetically quiet periods (i.e. K and $Kp < 3$).

2.2 Ground measurement campaign over the Lombok Island (2004–2008)

2.2.1 Previous surveys (2004–2005)

During July–August 2004, the first ground measurements over the Lombok Island have been intuitively initiated by Zubaidah et al. (2005) around the location of the Basic Electrical laboratory of Mataram University (marked as red plus encircled symbol of **Fig. 2.12**). It covered the surrounding $5 \times 5 \text{ km}^2$ area with regular grid of $1 \times 1 \text{ km}^2$ (depicted as pink polygon of the same figure). Several reasons to decide this selected area have been discussed in **Sec. 1.3**. This survey has only used the available equipment in the laboratory (an analog Flux meter and a digital Gauss/Tesla meter with resolution of 0.01 mT (equal to 10,000 nT) and accuracy of $\pm 2\%$ of reading for ± 3 counts in DC mode). They are clearly not a proper equipment to be used for geomagnetic measurements. The accuracy of these measurements, limited by the instrument resolutions, is much too low to use them for describing detailed features of the geomagnetic anomalies over this Island, and the investigated area was very narrow. Therefore, the results of the 2004 survey (showing a maximum anomaly of 76,000 nT) could be used only to confirm extreme high values of the geomagnetic field in this area.

After analyzing and noting several factors that make the results of 2004 survey unsatisfactory, a further survey has been conducted on 59 stations during July–August 2005, covering a broader area of about $25 \times 30 \text{ km}^2$ in the middle part of the Lombok Island (depicted as blue polygon of **Fig. 2.12**). A proper measuring equipment (ENVI PRO Proton Magnetic System - Scintrex) has been used, measuring the total magnetic fields ranged 23,000–100,000 nT, with a resolution of 0.1 nT and an accuracy of $\pm 1 \text{ nT}$ (Scintrex Ltd., 1997). The looping method has been used to overcome the problem of using only one single instrument (without Base station), where measurements at the first site on a day are repeated at the end of that day, then a linear trend between the first and the last measurements are applied for data reduction.

The results of the 2005 survey (after applying re-processing procedures in 2008) are shown as 2D geomagnetic total field intensity anomaly map on **Fig. 2.13**. This map has been generated using only relatively good quality data, which have been classified based on the minimum standard deviation ($StDev < 100 \text{ nT}$) and relatively low value of anomaly (i.e. the anomaly value should be less than 4000 nT; after subtracting the 10th generation IGRF values (IAGA WG V-MOD, 2005; Maus et al., 2005)). To obtain it, Kriging method in the Oasis montaj 6.4 (Geosoft software) has been applied, using simple linear power model with a blanking radius of 0.0527° (equal to 5.85 km) and pre-filtering with low-pass desampling factor of 3 to interpolate the available data and to show the empty spaces for the parts without data.

Initially, by applying the looping method for data reduction, a maximum anomaly of about 11,000 nT has been found, which still amounts to about 3725 nT after applying re-processing procedures (i.e. data selection and a proper data reduction using KDU observatory) in 2008. Such an extreme value of anomaly and the fact that no dipolar structure (i.e. only positive anomalies have been found) over such a broad region is, certainly, uncommon and unreasonable. Therefore, these results could not be used for further interpretations. However, they are still valuable in providing the first impressions of extreme geomagnetic anomaly over the Lombok Island, even the real values of the anomalies have not been estimated.

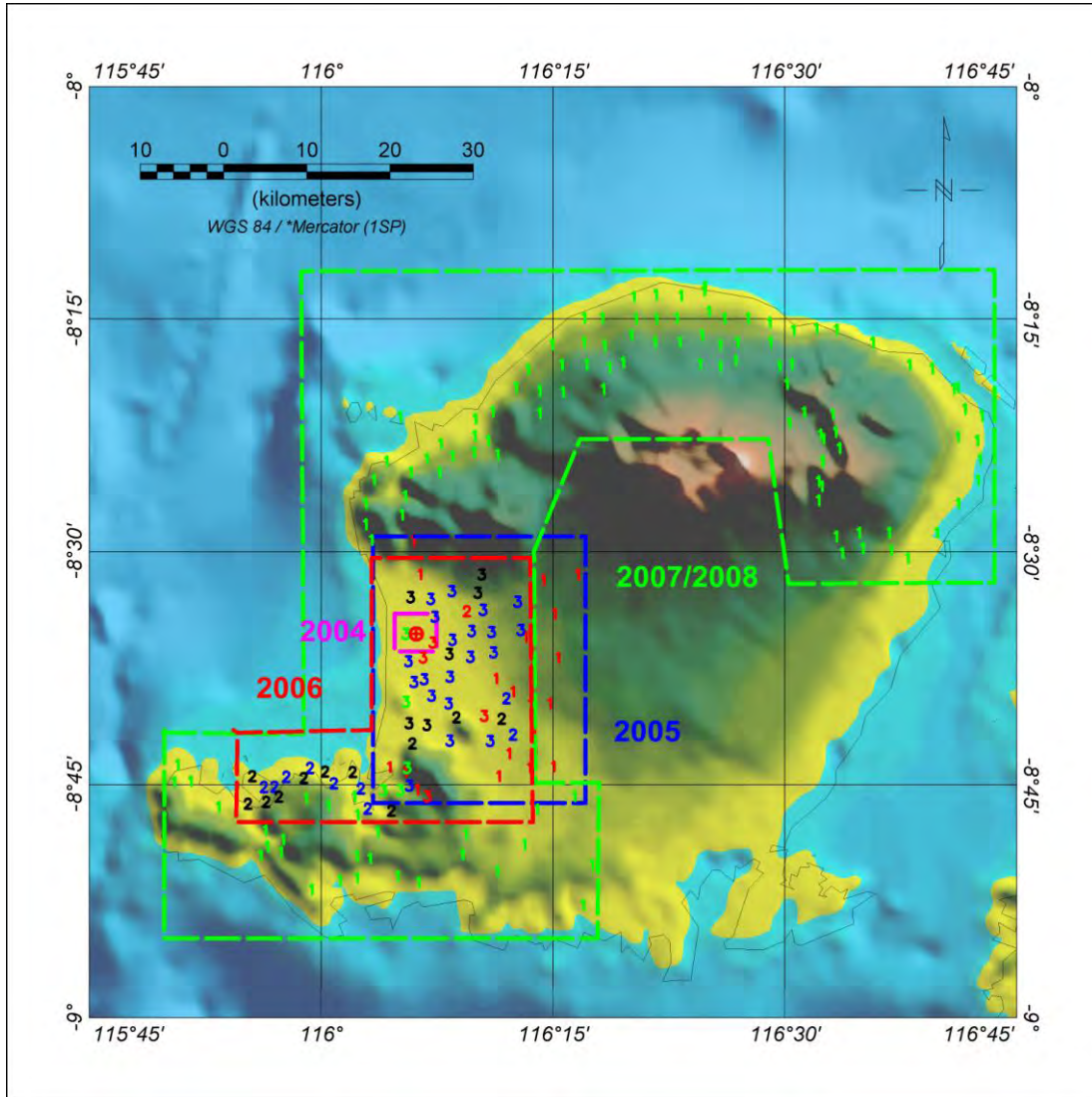


Figure 2.12 The surveyed area of geomagnetic ground measurements over the Lombok Island, depicted as polygonal dashed coloured lines showing the surveyed areas in 2004 (pink), 2005 (blue), 2006 (red), and 2007/2008 (green). The numbers of occupied stations in each year are 36, 59, 56 and 177, respectively. Different symbols indicate:

- ⊕ The Basic Electrical laboratory of Mataram University
- 1 Once surveyed station in 2005
- 1 Once surveyed station in 2007/2008
- 2 Twice surveyed station in 2005 and 2006, relocated in 2006
- 2 Twice surveyed station in 2006 and 2007/2008, without relocation
- 2 Twice surveyed station in 2006 and 2007/2008, relocated in 2007
- 3 Three times surveyed station, without relocations
- 3 Three times surveyed station, relocated in 2006
- 3 Three times surveyed station, relocated in 2007/2008
- 3 Three times surveyed station, relocated in 2006 and 2007/2008

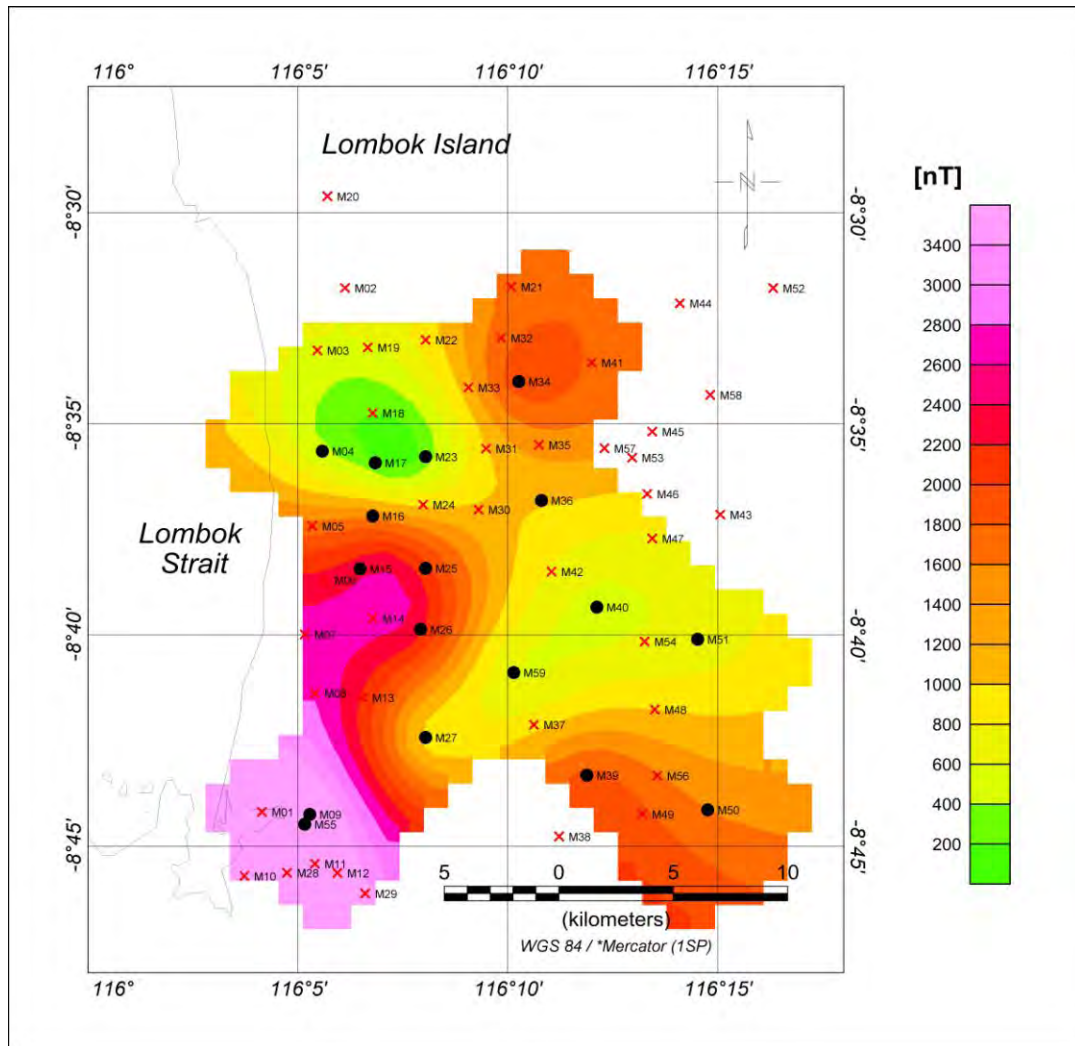


Figure 2.13 Results of the 2005 survey (after applying re-processing procedures in 2008). The geomagnetic survey stations and their names are shown, providing relatively good quality (black points) and relatively low quality (red crosses) data (see text for more details). Only data with relatively good quality are used, interpolated over the surveyed area on the middle part of the Lombok Island. Note the rather uncommon extreme values (the maximum value of about 3,725 nT) and the fact that only positive anomaly values are found.

Besides, several conclusions to get improvements in conducting the next surveys have been gained as follows:

1. Choosing appropriate locations of stations (e.g. as magnetically quiet as possible) is critical in minimizing the noise and improving the quality of data. Therefore, relocation of disturbed stations to the more magnetically quiet locations is strongly recommended.
2. Considering large diurnal variations in the equatorial regions, such as the Lombok Island; however, we can not take a simple assumption that the measured geomagnetic values have always linear trends of increment (or decrement) along the survey time. In this region, using the looping method is not applicable for long (more than two) hour surveys, especially when measurements are conducted during mid-days (11.00–13.00 of local time). Hence, using the data from the Base station or the nearby observatories for proper data reduction is very important to minimize the influence of external field variations.

3. Before conducting a geomagnetic survey, calibration of the used measuring equipment (to any standard equipment) is necessary. Otherwise, large uncertainties might be found in results, and then the reliability of the results could not be fully guaranteed.
4. The mode of survey, available as several options on the equipment, has to be appropriately chosen. In our case, using ENVI PRO in the “*base mode*” is recommended, because using it in the “*search mode*” might give several minutes of initial unstable readings and very noisy data (reaching 200% of the nominal values), following the ON/OFF states.

2.2.2 The 2006 Survey

2.2.2.1 Survey areas and considerations

The next geomagnetic field measurements on the Lombok Island have been done in the time span October–November 2006 (Zubaidah et al., 2009), covering a broader area of about 20 x 30 km² in the middle part and 20 x 10 km² in the southern part of the Lombok Island (depicted as red polygon of **Fig. 2.12**). An improved ground-based magnetic survey of total field intensity has been conducted at 56 stations, with an average distance between adjacent stations around 2.5 km. This survey included measurements at 36 “old” stations (occupied in 2005), to make possible a directly check of the reliability of 2005 survey results. Additionally, several stations had to be re-located to magnetically more quiet neighbouring places, in order to ensure a higher quality of these measurements, considering *the first* conclusion from the 2005 survey. These relocations have involved various distances between the old positions and the new ones, ranging from several tens of meters to one kilometre.

Since no dipolar structure has been found from the 2005 survey, an additional survey at 15 new stations has also been conducted in the more southern area to deeply explore the presumed lower (and even negative) anomaly region. This presumption is based on the regional scale geomagnetic anomaly maps, as depicted on **Fig. 2.2, 2.3** and **2.8**. Other 5 new stations have also been inserted in the middle of the surveyed area, to get a more regular grid and enhance the resolution. Since no significant anomalies have been presumed over the most eastern part of the 2005 survey area, several old stations in this part have not been considered to be re-surveyed in 2006. **Figure 2.14** shows locations and names of 2006 survey stations related to the 2005 survey, as well as several important locations that are explained in the following.

2.2.2.2 Calibration of equipment

Considering *the second* and *the third* conclusions from the 2005 survey, two equipments were used for this survey, and of course they have been calibrated. *The first* equipment is an Overhauser magnetometer (GSM-19 v7.0, GEM System), measuring the total magnetic field in the range 15,000–120,000 nT with a resolution of 0.01 nT and an accuracy of ± 0.1 nT, planned to be installed on the Base station. *The second* one is an ENVI PRO Proton Magnetic System (Scintrex) that was used during the 2005 survey), measuring the total magnetic fields in the range 23,000–100,000 nT, with a resolution of 0.1 nT and an accuracy of ± 1 nT. It has been planned to be used as a rover magnetometer to get the data from all stations. Since *the first* one has been verified before the survey, using the standard magnetometer at the Niemeck geomagnetic observatory (NGK) in Germany, it is considered as the standard equipment in the following calibration.

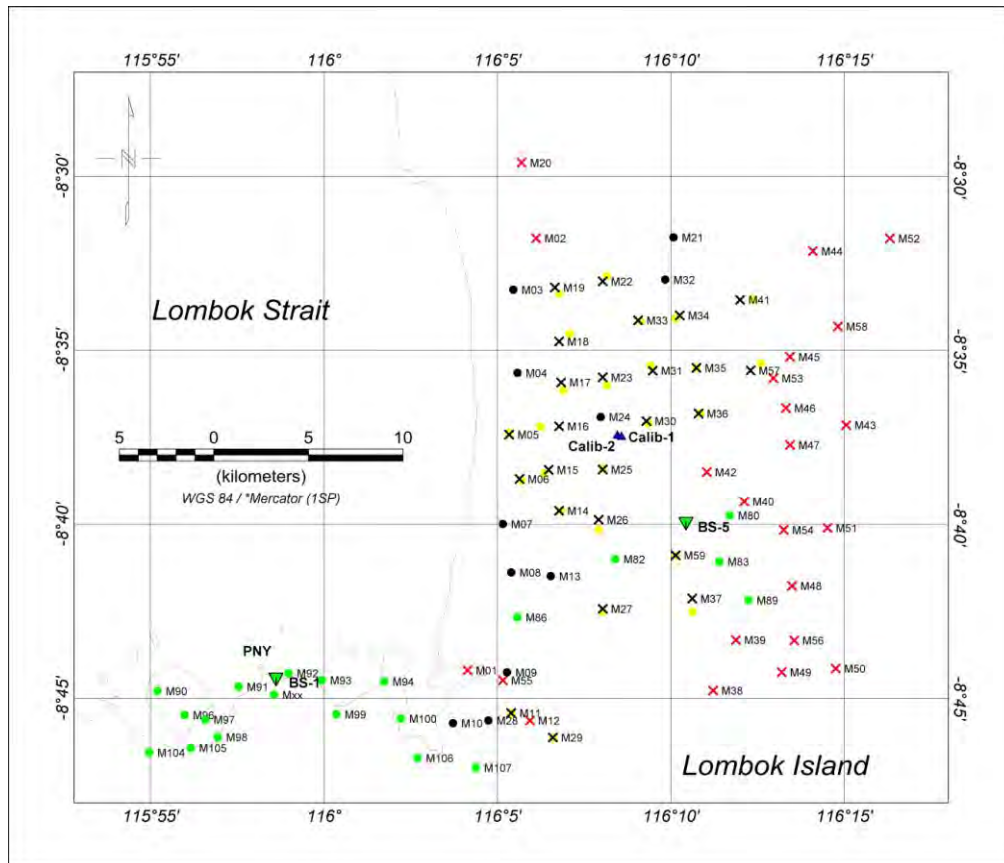


Figure 2.14 Station locations of the 2006 survey related to the 2005 survey and some additional important locations, are shown with several different symbols:

- X 2005 station not re-surveyed during 2006 survey
- 2005 station relocated during 2006 survey
- 2006 station without relocation of 2005 survey
- 2006 station actual position after relocation
- ▼ New 2006 station
- ▼ Base station
- ▲ Calibration location

The calibration procedure has been conducted on October 14th 2006 via cross-readings at two locations (marked as **Calib-1** and **Calib-2** of Fig. 2.14), which are separated about 250 meter from each other, in two sequences following IAGA procedure (Newitt et al., 1996). **Figure 2.15** shows the results of two sequences of calibrations, indicating a very good correlation between the GSM-19 and the ENVI PRO. However, the ENVI PRO shows much lower resolutions as well as lower accuracy than the GSM-19. Additionally, as has been mentioned in *the fourth* conclusions from the 2005 survey, the ENVI PRO measurements are unstable during a few minutes at the beginning of measurements (following the ON/OFF state). One has to note, that differences in the measured geomagnetic field intensity are in fact due to the differences of geomagnetic values between two locations. By applying statistical procedures and calculations of IAGA, it can be concluded that the measurements given by ENVI PRO are 4.1 nT lower than those of GSM-19. After providing a proper calibration of the equipment, both instruments are reliable and the results could be guaranteed.

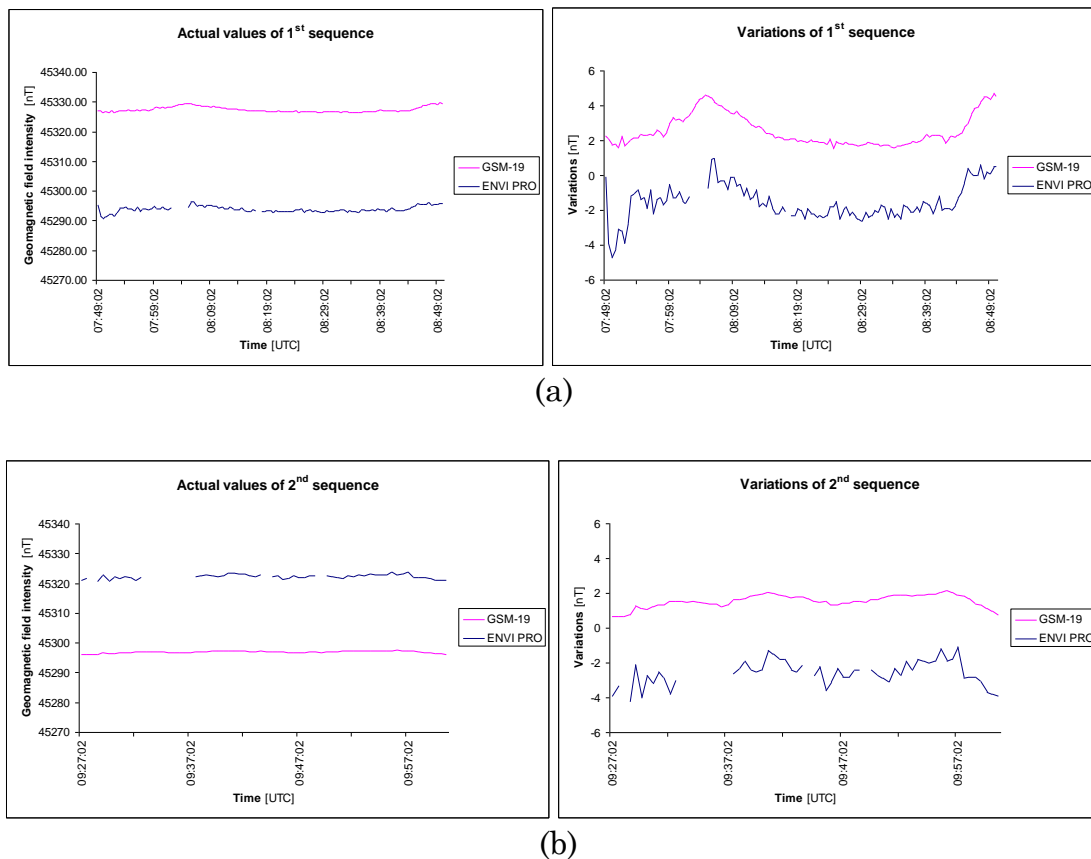


Figure 2.15 Results of two sequences of calibration between GSM-19 and ENVI PRO in 2006: (a) The actual and variation values of *the first* sequence of calibration (GSM-19 on Calib-1 and ENVI PRO on Calib-2); (b) The actual and variation values of *the second* sequence of calibration (GSM-19 on Calib-2 and ENVI PRO on Calib-1). Measurements using ENVI PRO are 4.1 nT lower than those of GSM-19.

2.2.2.3 Continuous measurement on the ‘Penyu’ Islet (PNY)

Before starting the survey on a wider area, it is useful to conduct continuous measurement over several days at a permanent place to get the information about diurnal variation characteristics and geomagnetic night time mean value of this region, which are used further in the data reduction processing. Sixteen days of continuous measurements have been obtained during October 15th – 31st 2006 on the ‘Penyu’ Islet (marked as PNY of **Fig. 2.14**), a tiny and magnetically quiet island located in the southern part of the Lombok Island, about 1.5 km from the location of the South Base station (marked as BS-1 of **Fig. 2.14**).

Figure 2.16 shows the one-minute values of the geomagnetic field intensity obtained from PNY, with a night time mean value of 45382.1 nT. It can be concluded that the maximum diurnal variations usually occur at 02:30 UTC or 10:30 local time, with the discrepancy between the day- and night- time mean value of about 13.1 nT. Compared to the nearby observatory data (KPG, TND, and KDU, see **Sec. 2.1.3** for more details), it could be shown that the daily variations on the Lombok Island have the same trend. It means that there are no artificial sources that could generate some additional local variations, saying some pseudo geomagnetic anomalies. In other words, the extreme geomagnetic anomalies on the Lombok Island should be generated by some intrinsic sources related to the local Earth’s characteristics.

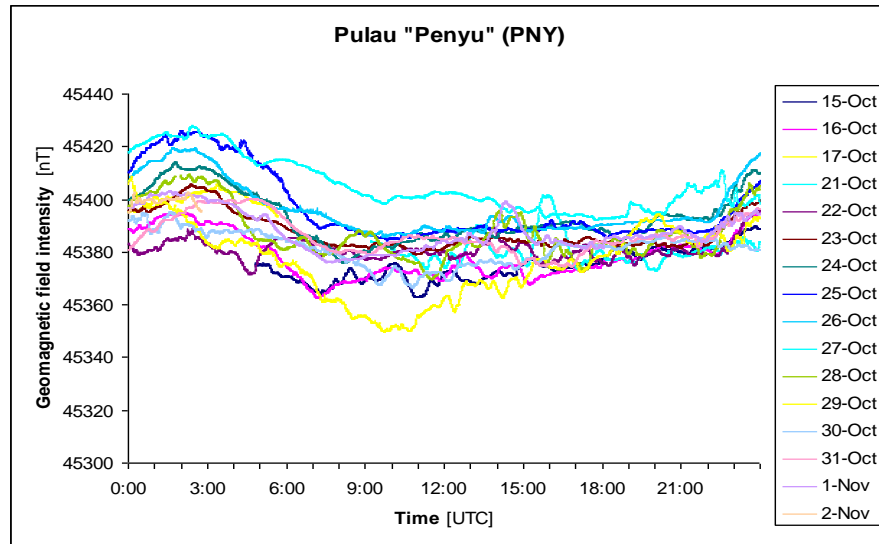


Figure 2.16 Results of the continuous measurements on the ‘Penyu’ Islet (PNY): the geomagnetic field intensity measured from October 15th to November 2nd 2006. The night time mean value is 45382.1 nT.

2.2.2.4 Base station surveys

Considering *the first* and *the second* conclusions of the 2005 survey, with the aim of finding the most appropriate location of the South base station, three locations on magnetically quiet area have been selected as candidates (namely as BS-1, BS-2, and BS-3; depicted as 1, 2, and 3 on **Fig. 2.17**).

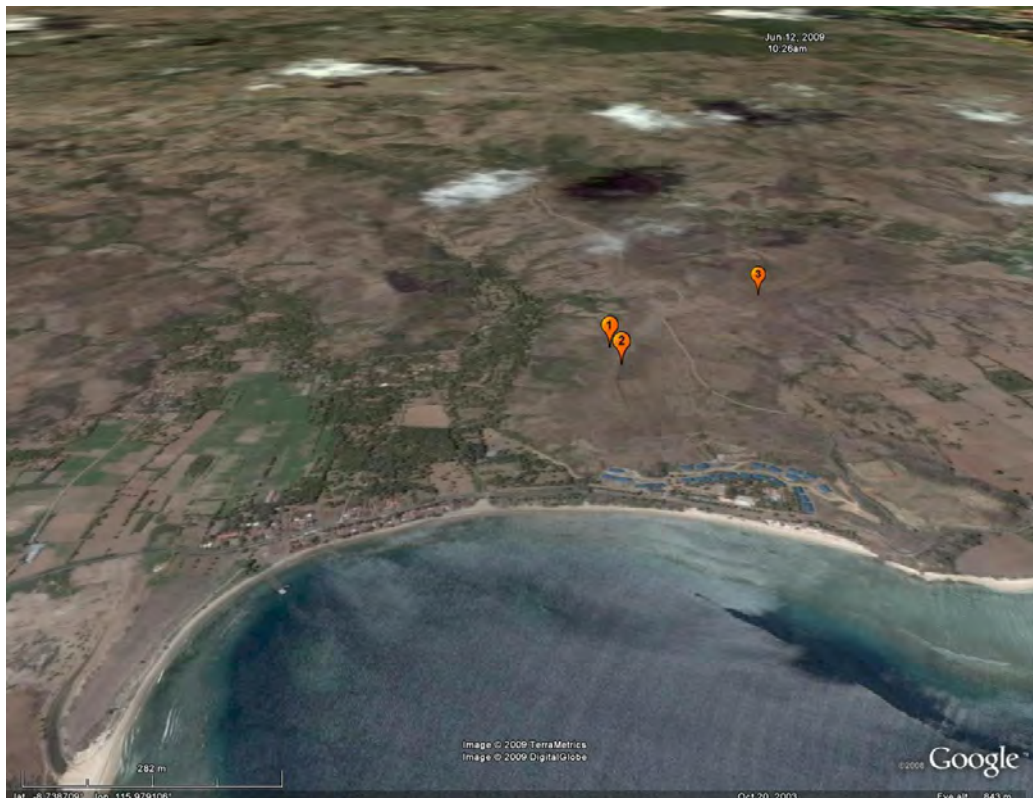


Figure 2.17 Locations of the three candidates of the South base station for the 2006 survey (namely as BS-1, BS-2, and BS-3), depicted as 1, 2 and 3, respectively.

The total field gradient surveys have been conducted on these locations during August 11th–13th 2006, covering the surrounding 10 x 10 m² area with a regular grid of 1 x 1 m², following IAGA procedure (Newitt et al., 1996). A standard proton magnetometer Type G-856 (Geometrics) has been used manually, measuring the total magnetic fields ranged 20,000–90,000 nT with a resolution of 0.1 nT and an accuracy of ±0.5 nT. Regarding the unknown diurnal variation characterizing this area for the time of surveys, two series of measurements (morning and afternoon) have been conducted on each location, to obtain the most appropriate estimates.

Figure 2.18 shows the diurnal variation obtained at the basis coordinate ($x = 0, y = 0$) of each location, which have been measured repetitively after finishing the measurements of all grid points in one direction. It can be concluded that the most appropriate surveys have been obtained in the afternoon for BS-1 and BS-2, but in the morning for BS-3.

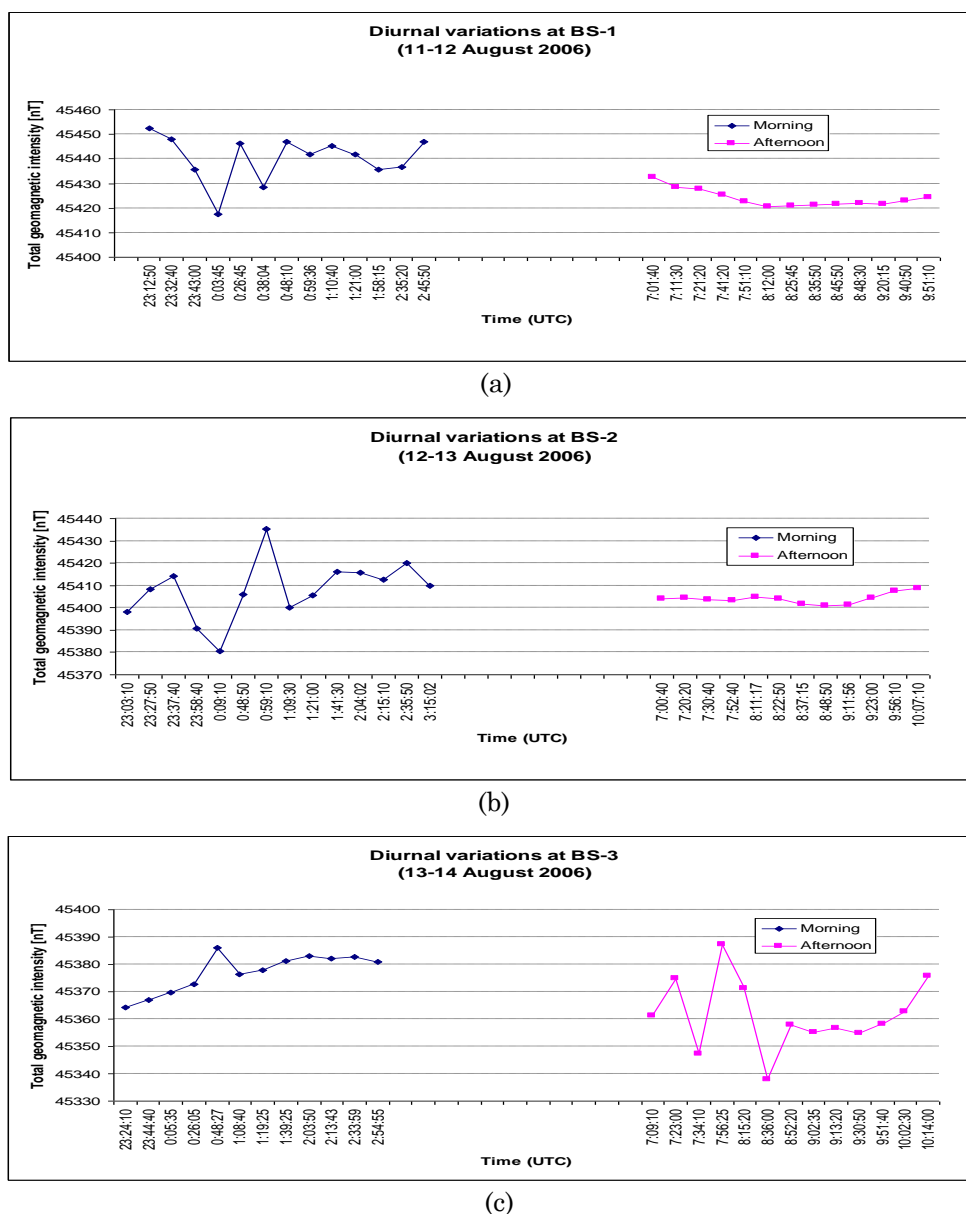


Figure 2.18 Diurnal variation obtained during two series of measurements (morning and afternoon) on three locations of the South base station candidates: (a) BS-1, (b) BS-2 and (c) BS-3. The best estimates for the diurnal variation in the afternoon for BS-1 and BS-2, and in the morning for BS-3.

Figure 2.19 (a) to (c) show the field variations along the main axis relative to the centres [coordinate (5, 5)]. The total geomagnetic anomaly profiles of each location are also indicated for the times with less important diurnal variation. It could be concluded that the location of BS-1 is the best candidate, due to its minimum horizontal gradient and non-existence of such very localized anomalies.

A total field gradient survey has also been conducted on November 7th 2006 to find a suitable location for the North base station (depicted as BS-5 in **Fig. 2.14**). **Figure 2.19** (d) shows the field variations along the main axis relative to the centres [coordinate (5,5)] and the interpolated total geomagnetic anomaly profile. Considering the IAGA criteria for a good station location (Newitt et al., 1996), it could be concluded that this location is suitable, since the field varies by no more than some ± 50 nT within a radius of 10 m, except at one grid point in the southern direction that exceeding this limit by 2.5 nT.

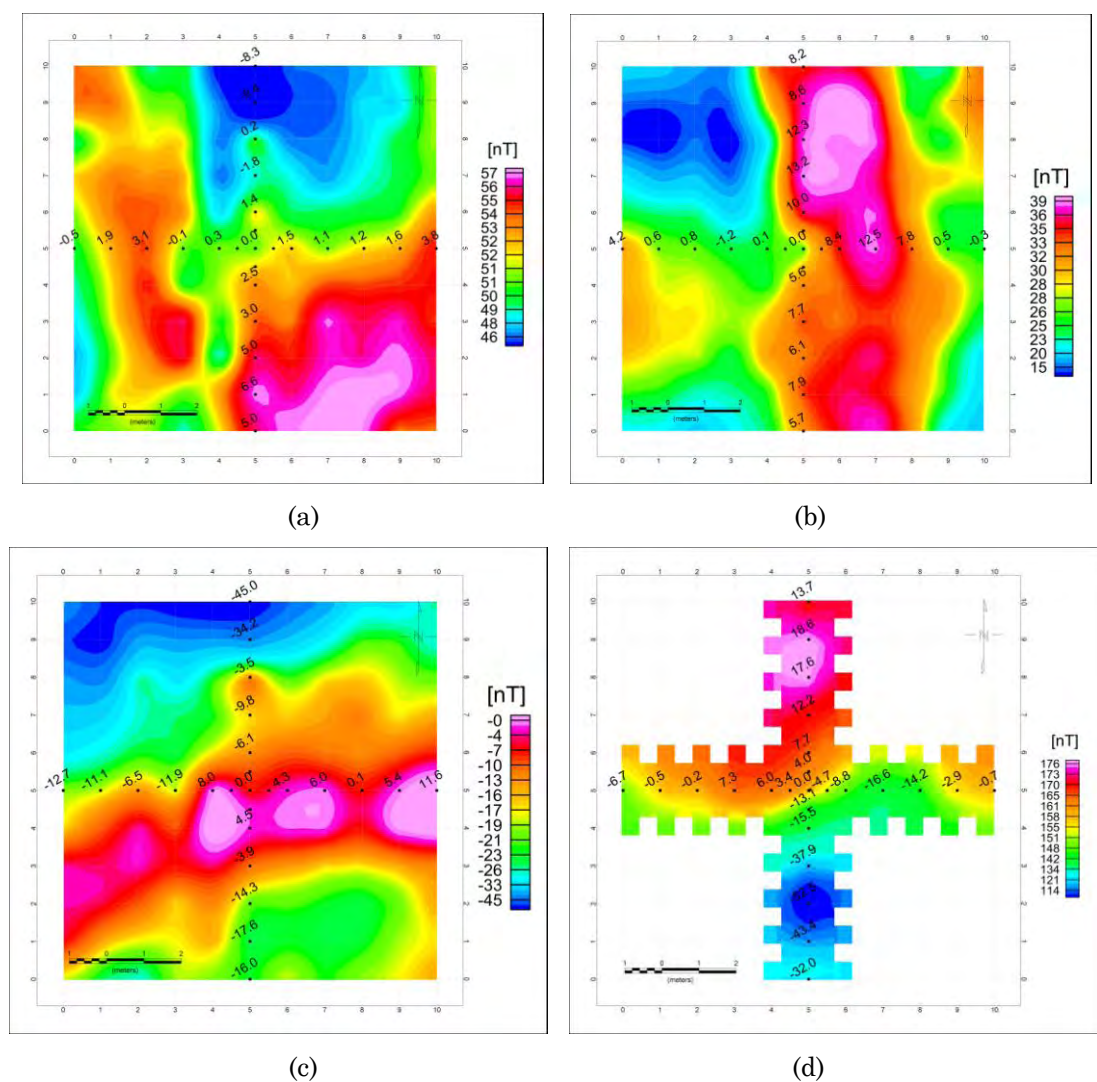


Figure 2.19 The total field intensity variations (in nT) relative to the centres [coordinate (5, 5)] and the total geomagnetic anomaly profiles of the locations of (a) BS-1, (b) BS-2, (c) BS-3, and (d) BS-5; obtained from the most appropriate surveys. The local xy coordinate system is used. These results indicate BS-1 as the best location for the South base station and the BS-5 as a suitable location for the North base station, due to non-existence of very localized anomalies.

2.2.2.5 Southern and middle area surveys

The survey on the southern area has been carried out in two parts, during November 3rd – 5th 2006 (15 new stations) and on November 18th 2006 (5 old stations), while the survey on the middle area has been carried out on several days during November 9th – 26th 2006, including 5 new and 32 old stations. The total geomagnetic field intensity was measured using the ENVI PRO in the “*base mode*”, providing more stable readings, considering *the fourth* conclusion of the 2005 survey. The measurements have been obtained manually every 30 seconds during 30–60 minutes, including the geomagnetic field intensity and the percentage of the noise level, as well as the time when each individual value has been acquired. **Figure 2.20** shows how the survey has been held at a station (M21).



Figure 2.20 Example of the 2006 survey at station M21, showing manually using of the ENVI PRO. One operator has to handle the equipment (hold the sensor and carry the console) and read the measured values, while the other has to write the readings on the data sheet, immediately. These data then have to be inputted to the computer manually for data processing.

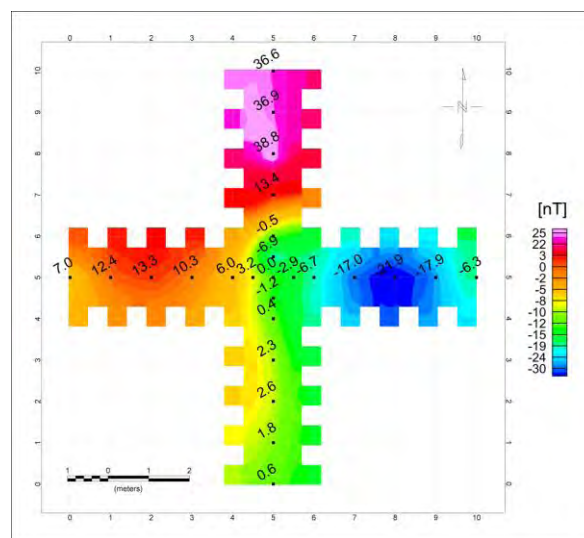


Figure 2.21 The total field intensity variations (in nT) relative to the centre [coordinate (5, 5)] and the total geomagnetic anomaly profile of the location of M13 (the maximum anomaly point of the 2005 survey), shown in the local xy coordinate system. These results confirm that large geomagnetic anomalies on the Lombok Island are linked to a regional feature.

Additionally, a gradient survey has been carried out on the maximum anomaly point of the 2005 survey (depicted as M13 in **Fig. 2.13** and **2.14**). The results of this survey (as could be shown in **Fig. 2.21**) are needed to confirm whether the extreme anomalies on the Lombok Island are not only isolated values of 2005 survey stations (e.g. due to very local variations on a certain points on the Lombok Island); but they are a regional feature of this island.

2.2.2.6 Specific conclusions and remarks

To get improvements in conducting the next surveys, some specific conclusions and remarks of 2006 survey could be given as follow:

1. Conducting surveys on the magnetically quietest periods is necessary to minimize the effects of large external variations linked to geomagnetic storms, especially when a base station is not available. Otherwise, it is very difficult to reduce data and to get the desirable quality in applying statistical approach (using criteria of $StDev < 2$ nT), although many outliers (based on the noise level) have been cancelled in the pre-selection of the measured data. Using the geomagnetic forecast information is considered to properly schedule the next surveys.
2. In this survey, two base stations have been set up consecutively for data reduction purpose, one for the southern area and one for the northern/middle area (depicted as BS-1 and BS-5, respectively, in **Fig. 2.14**). Unfortunately, the North base station was irresponsibly destroyed by some local people on the second day of the second part of the survey. To overcome this problem, data from the nearby observatories are used for the transient corrections. To avoid the next similar problems, communication to the local communities (i.e. to socialize the purposes of geomagnetic measurements for our daily live and particularly the urgency of this research) should be developed intensively.

2.2.3 The 2007/2008 survey

2.2.3.1 Survey areas and considerations

After finishing the data processing of the 2006 survey (as described in detail in **Chap. 3**), the 2007/2008 survey has been conducted during November 2007–April 2008 over a broader area of the Lombok Island (depicted as green polygon of **Fig. 2.12**). It covers not only the subduction zone in the South (the Java Trench), but also the volcanic area (Mount Rinjani) and the zone of possible subduction extension and reactivation in the North (the Flores Thrust zone). The aim is to connect the ground measurements to the existing eastern Asian anomaly map of **Fig. 2.3**, as well as to find possible relations to the main concerned geological and tectonic settings of this region.

An advanced ground-based magnetic survey of total field intensity has been conducted at 177 stations, including measurements at 55 old stations (all except one station, i.e. M33), previously occupied in 2006. Several stations had to be further re-located to magnetically more quiet neighbouring places, mainly due to rapid changes of land utilizations by the local communities, which potentially generate man made noise and disturb measurements. To get a better understanding about geomagnetic anomaly patterns in the boundary or transitional region between the negative and positive part of anomaly, 31 new stations have been added in the most southern part of the Lombok Island. It is considered that some specific geological features could be found related to geomagnetic anomalies on such transitional regions. Other 91 new stations have been added in the northern part of the Lombok Island, regarding the presumed maximum positive anomaly (as depicted on the regional scale geomagnetic

anomaly maps of **Fig. 2.2, 2.3** and **2.8**) and the recent volcanic and seismic activities on this area. **Figure 2.22** shows the locations of the 2007/2008 survey stations related to the 2006 survey, as well as the name of several important locations that will be explained in the following.

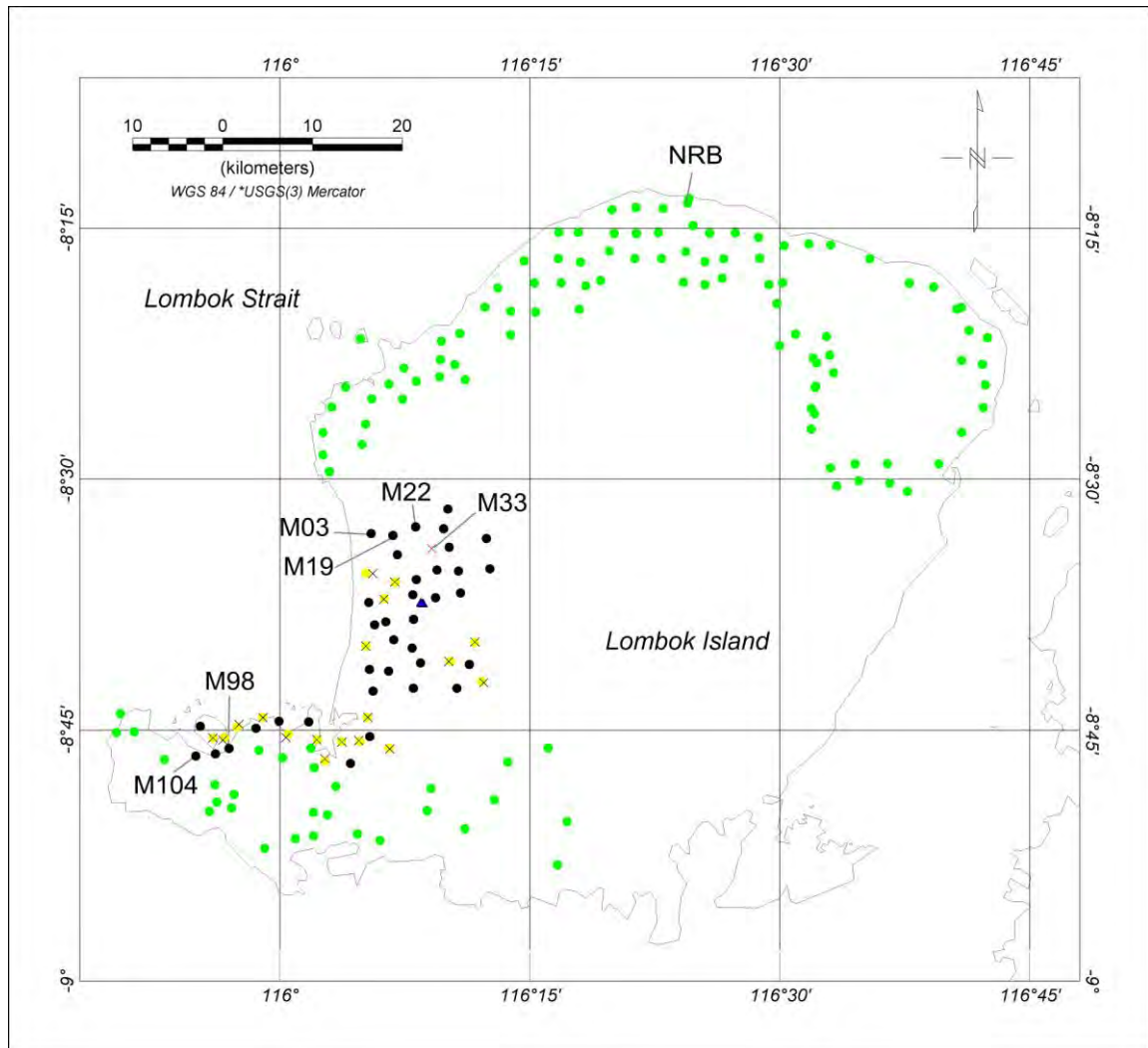


Figure 2.22 Station locations of the 2007/2008 survey related to the 2006 survey, and several important locations, are shown in different symbols as follow:

- X 2006 station not re-surveyed during 2007/2008 survey
- X 2006 station relocated during 2007/2008 survey
- 2007/2008 station without relocation of 2006 survey
- 2007/2008 station actual position after relocation
- New 2007/2008 station
- ▲ Calibration location

2.2.3.2 Southern, middle, and northern area surveys

The data processing results of the 2006 survey (see **Sec. 3.1.3**) suggest that it is more important to use the higher resolution and accuracy equipment at all stations and reduce the measurements by means of neighbouring observatory data, instead of using the one available high resolution and accuracy equipment as base station and the lower resolution and accuracy equipment for all stations. Regarding the 2006 calibration results, a standard proton precession magnetometer (GSM-19T v6.0, GEM

System) has been used at all stations, replacing the old manually operated one (ENVI PRO Proton Magnetic System, Scintrex). It measures the total magnetic fields ranged 10,000–120,000 nT with a higher resolution of 0.01 nT (compared to the ENVI PRO with only 0.1 nT resolution) and an accuracy of ± 1 nT. Using this equipment helps in minimizing local noises generated by operators as well as the human error (during writing the values on the data sheets or during the data entry procedures to the computer), since measurements have not to be conducted in a manual mode as with the ENVI PRO. Nevertheless, the ENVI PRO has been used over three-day measurements (including 10 stations) in the northern area, because the GSM-19T failed after operating in excessive rainy conditions.

Figure 2.23 shows how measurements have been conducted at station M21, exactly at the same location as in 2006. Note some changes of local situation, and the applied survey methodology on this location, comparing to those of one year earlier as shown in **Fig. 2.20**. Since no base station has been established during the 2007/2008 survey, the measurements have been obtained every 60 seconds during 30–60 minutes, considering the simplest way to compare and reduce these data using one-minute values of observatories.



Figure 2.23 Example of the 2007/2008 survey at station M21, exactly at the same location as in 2006, using the GSM-19T. The operators have only to set up the equipment at the beginning, while the measurements can be automatically recorded in the memory. The stored measurements then can be loaded to the computer for data processing.

2.2.3.3 Continuous measurement at “Nurul Bayan” (NRB)

Regarding the aim to establish a geomagnetic observatory on the Lombok Island, it is important to conduct continuous measurements over several days at a prospective place to get information about the ambient noise level of that location. The continuous measurements have been carried out for several hours (mainly during night time) on February 16th, 17th and 19th 2008 at Nurul Bayan station (marked as NRB of **Fig. 2.22**), located in the most northern part of the Lombok Island.

Figure 2.24 shows variations of the geomagnetic field intensity (one-minute values) obtained at NRB, showing good agreement to the KDU data over the same time interval. Although there are some differences due to the larger diurnal variation at NRB (compared to KDU), signals show that there are no significant local induction sources that could influence the geomagnetic field measurements on this location and that the location is free of artificial disturbances. It can be concluded that this location is suitable as a candidate for a geomagnetic observatory.

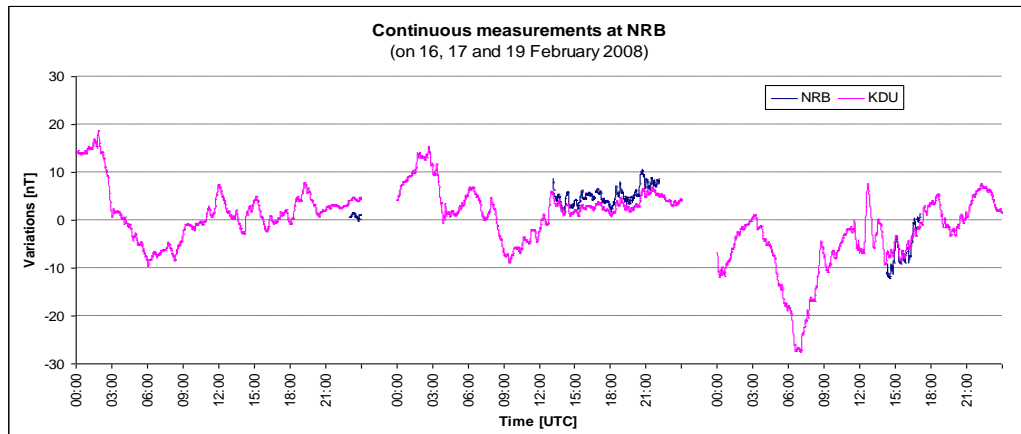


Figure 2.24 Continuous measurements of the geomagnetic field intensity at Nurul Bayan (NRB) obtained over several hours (mainly during night time) on February 16th, 17th and 19th 2008. These data show good agreement to the KDU data got over the same time interval, ensuring the suitability of NRB location as a candidate for geomagnetic observatory.

2.2.3.4 Calibration of equipment

The calibration procedure between the GSM-19T and the ENVI PRO has been conducted on April 3rd 2008 via cross-readings at exactly the same locations as in 2006 (depicted as a blue triangle of **Fig. 2.22**). **Figure 2.25** shows the results of two sequences of calibrations, indicating very good correlations between both equipments. Comparing to the previous calibration in 2006, the relation between the measured geomagnetic values on two locations has changed (i.e. values for **Calib-2** are higher than that of **Calib-1** in 2006). This also shows more variations in ENVI PRO readings, probably due to the rainy conditions at the time of measurements. Nevertheless, by applying statistical procedures and IAGA calculations (Newitt et al., 1996), the same conclusion could be drawn, getting a difference of 6.2 nT.

2.2.3.5 Specific conclusions and remarks

1. The survey time span coincides with the peak of wet season in the Indonesian region, so that excessive rainy conditions dominated the survey days. Such conditions are really not favourable for conducting geomagnetic ground surveys, because of several reasons:
 - a. Extreme precipitation can make the gasket sealing of the equipment leak, resulting in short circuits in the electronic components and leading to resetting the memory and erasing the data storage.
 - b. Heavy lightning can generate electrostatic discharge effects and cause ionization of the proton rich fluid in the sensor of the equipment. The effects on the polarization processes result in very low signal strength and very inferior values of field readings (about 30% as normally). If this problem occurs, the sensor needs about two days to recover before the next measurements could be conducted properly.
 - c. Heavy wind influences the sensitivity of the sensor, resulting low signal conditions and noisy readings.
 - d. Difficulties arose to reach the exact locations of old stations, due to very slick soil (that contains much clay) or even floods.
 - e. Finally, the survey team has been drastically decreased of their stamina, because of spreading of epidemic diseases.

In general, the survey in this region could be conducted in more proper way, if it is not during the rainy season (from October of the year to April of the following year).

2. Eight large earthquakes ($M > 5.0$) occurred in the 300 km radius around the Lombok Island during the time interval between the 2006 and the 2007/2008 surveys. Four of them happened during the beginning of the 2007/2008 survey days. These are opportunities to investigate the possible correlation of the geomagnetic ground-measurements with seismic events, and to analyze the seismo-electromagnetic phenomena.

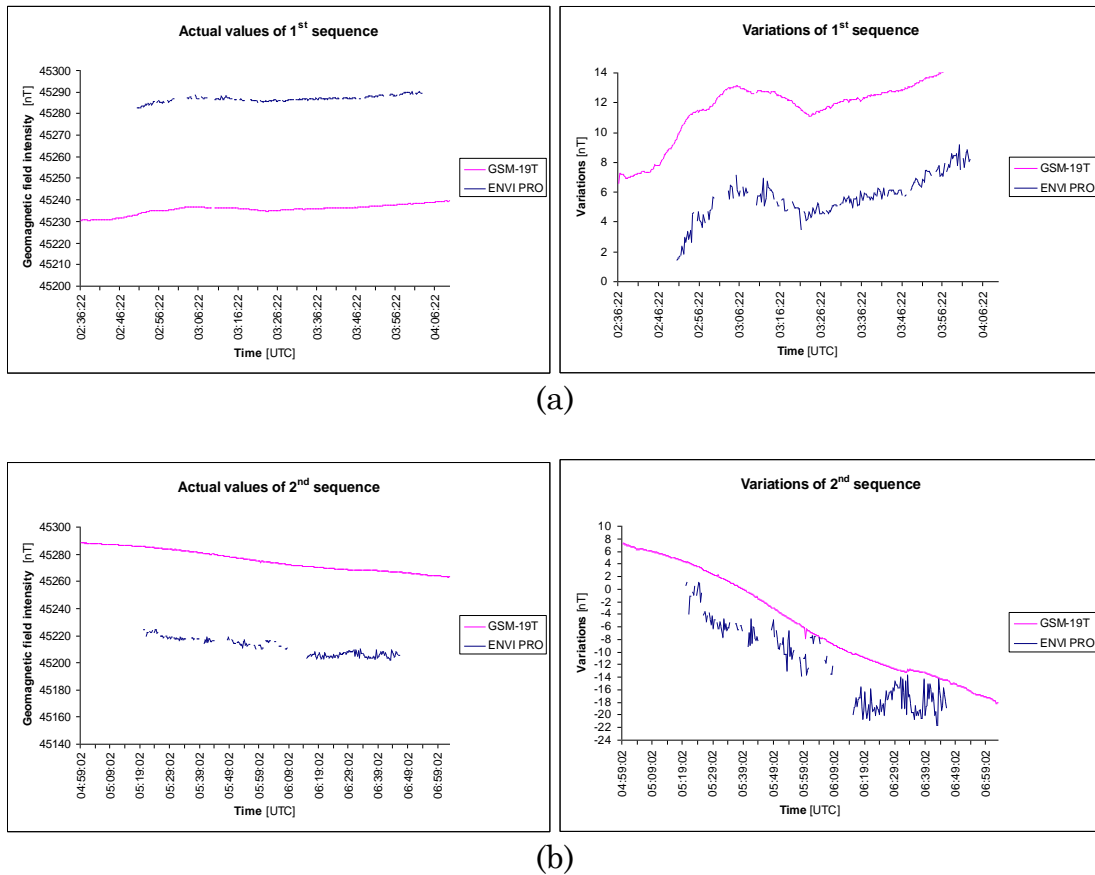


Figure 2.25 Two sequences of calibration between GSM-19T and ENVI PRO in 2008: (a) The actual and variation values of *the first* sequence (GSM-19T on Calib-1 and ENVI PRO on Calib-2); (b) The actual and variation values of *the second* sequence (GSM-19T on Calib-2 and ENVI PRO on Calib-1). The measurements using ENVI PRO are 6.2 nT lower than those of GSM-19T.

Chapter 3

Lombok Island surveys: Data processing and visualization

Following the conducted surveys, a well structured data processing steps is a fundamental prerequisite in achieving high quality results. Through the first part of this chapter, the data processing is described comprehensively, and then applied step by step to facilitate the quality evaluation of results. Proper visualizations of results are then presented as 2D and 3D maps. At the end, the geomagnetic changes noted between both surveys are presented, as an important clue in understanding the possible related mechanisms. The results presented here are the basics for all generated models and their interpretations studied in **Chap. 4**.

3.1 Data processing and visualizations

To get a comprehensive picture in understanding the data processing and visualization procedures, a schematic diagram showing the general algorithm could be drawn, as in **Fig. 3.1**. The complete algorithm consists of several consecutive steps, including preliminary processing, data reduction, IGRF subtraction, calibration adjustment, statistical evaluation, magnetic quietest period selection, gridding and interpolation. Details of each step are described in the following sections.

3.1.1 Preliminary processing

Before a further processing of the original data, several preliminary steps have to be conducted to get more reliable data inputs, including pre-selection of the measured values and comparison of their variation trends to the observatory data.

The noise level in the ENVI PRO readings is based on the noisiness of the individual periods of the precession signal, given as percentages of the measured total field values. The signal quality indicator in the GSM-19 or GSM-19T is a number presented in the form xy , where x and y are between 0 and 9. The value of x is associated with the measurement time and is a kind of gradient indicator (i.e. $x = 9$ means maximum measurement time was accomplished, while $x = 0$ means measurement was too short). The value of y indicates if the signal amplitude coincide with the time of measurement (i.e. $y = 9$ means optimal conditions, while $y = 0$ means unacceptable reading). In the pre-selection procedure, only data with a noise level $< 20\%$ (for manual measurements using ENVI PRO) or data with a signal quality indicator $x = 9$ and $y \geq 6$ (for automatic measurements using GSM-19 or GSM-19T) are kept. **Figure 3.2** shows one example of the pre-selection results (i.e. for C39 station that has been measured manually using ENVI PRO).

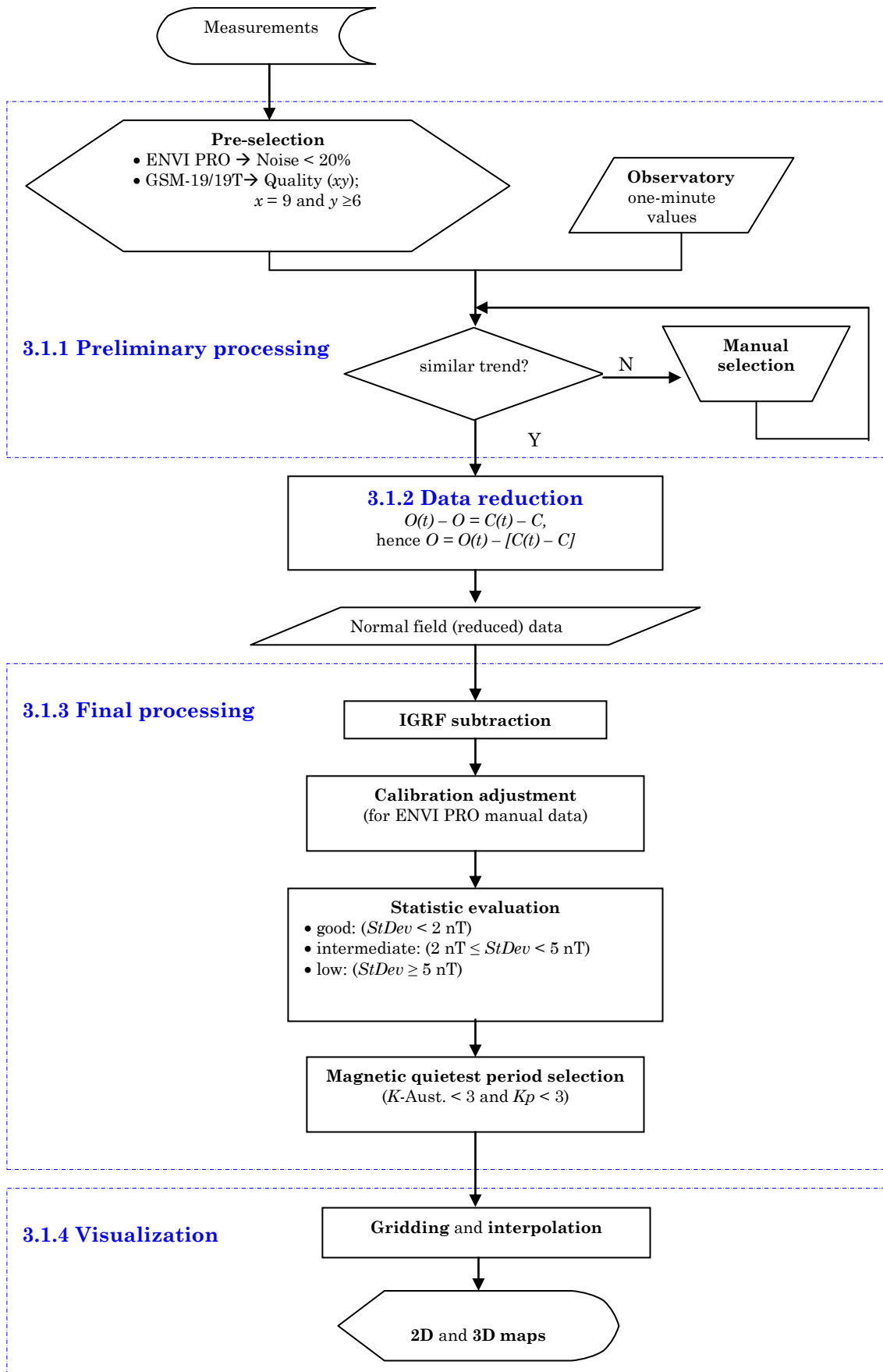


Figure 3.1 The general algorithm of data processing and visualization.

After pre-selecting of the input data, comparison of the variation trends to the observatory data are done by plotting the measurements together with the observatory one-minute values for the same time interval. The aim is to get selected data which have similar trend as the observatory one, assuming that the diurnal variation of both locations is similar. This procedure can be done by scanning (removing the outliers from) the station data manually and iteratively, until a maximum fluctuation (in comparison to the instantaneous observatory data) of ± 2 nT has been obtained. **Figure 3.3** shows the results of this procedure for the same station of **Fig. 3.2** (C39 station), with KDU data as the reference.

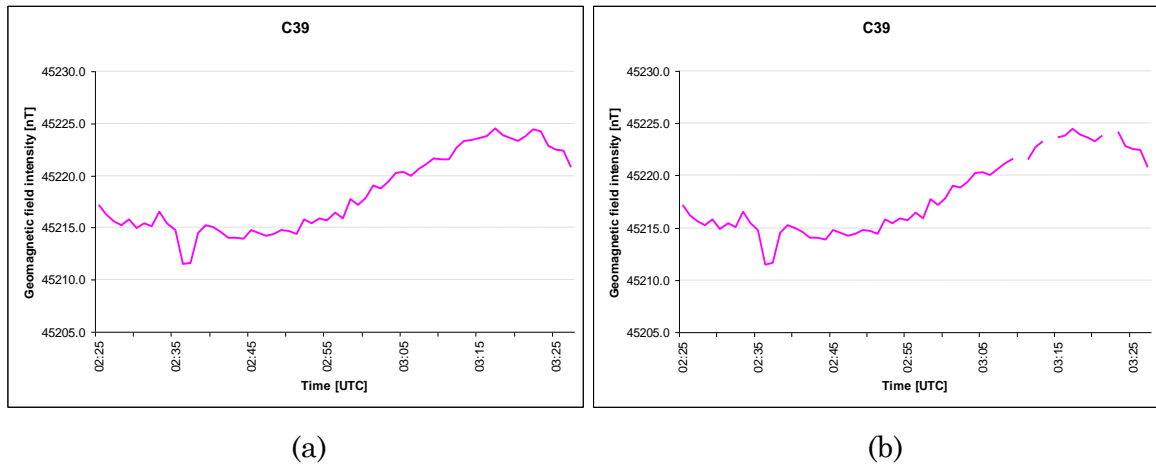


Figure 3.2 Example of data pre-selection for a manually (using ENVI PRO) measured station (C39): (a) initial data and (b) pre-selected data.

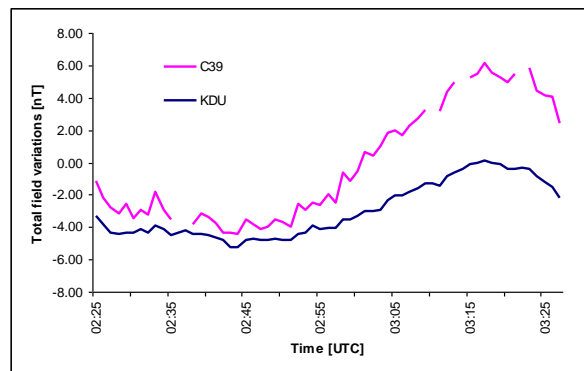


Figure 3.3 Example of a manual selection procedure for a manually (using ENVI PRO) measured station (C39). A trend of diurnal variation similar to the reference observatory (KDU) has been obtained.

3.1.2 Data reduction

Based on the assumption that transient variations of the geomagnetic field are identical at both the observed stations and the reference station, a simple formulation (Newitt et al., 1996) can be applied to minimize the external field contributions from the measured values (i.e. in order to obtain mean internal field values for the observed stations), as follows:

$$O(t) - O = C(t) - C,$$

hence

$$O = O(t) - [C(t) - C] \tag{3.1}$$

where O is the geomagnetic mean value of the observed station (valid over the survey time); $O(t)$, the instantaneous geomagnetic value measured at the observed station; $C(t)$, the instantaneous geomagnetic value measured at the reference station; and C , the geomagnetic mean value of the reference station.

Following the above formulation, continuous field readings from a nearby reference station are necessary for this data processing. Two base stations have been set up consecutively during the 2006 survey for this purpose, one for the southern area (BS-1) and one for the middle area (BS-5); see **Sec. 2.2.2.4** for more detailed information. Unfortunately, the second base station was destroyed on the second day of the second part of the survey. Therefore, for the middle area, the available one-minute values provided by one of the three nearby geomagnetic observatories (see **Sec. 2.1.3**) had to be chosen as the reference station for data reduction processing.

The evaluation of the suitability of the data provided by the three nearby geomagnetic observatories has been done by comparing them with corresponding variations recorded continuously during 16 days in the Penyu Island – PNY (see **Sec. 2.2.2.3**), in the following manner. Firstly, the night time mean values of PNY and three observatories have been calculated by averaging the total field values on undisturbed survey days (when $Kp < 3$) in the time interval of 06.30–22.00 UTC (14.30–06.00 -in the next day- of local time). The diurnal variation for each location can be calculated by subtracting their night time mean values from their instantaneous one-minute values. In this case, the most similar diurnal variation to that of PNY is considered as the most suitable one. It could be evaluated by taking the average of the (absolute values of) instantaneous differences between the diurnal variation of the observatory and that of PNY. The summary of this evaluation is given in **Table 3.1**.

Table 3.1 The suitability evaluation of three nearby observatories.

Name	Location		Dist. from Lombok [km]	Mean value [nT]			Avg. diff. to PNY [nT]
	Geographic	Geomagnetic		Night	Day	Discrep.	
Penyu (PNY)	-8.73°N, 115.97°E	-18.89°N, 188.10°E	1.5	45382.06	45395.13	13.06	0
Kupang (KPG)	-10.2°N, 123.4°E	-20.08°N, 195.93°E	850	45613.59	45629.50	15.92	3.83
Tondano (TND)	1.29°N, 124.95°E	-8.53°N, 196.92°E	1500	40442.70	40463.70	21.00	7.44
Kakadu (KDU)	-12.6°N, 132.5°E	-21.90°N, 205.63°E	2250	46357.08	46364.74	7.66	4.02

As can be inferred from **Table 3.1**, data provided by TND turned out not to be suitable, because of their large average differences to PNY and significantly larger discrepancy of diurnal variation (about 21 nT between day and night time), probably due to its location closer to the magnetic equator. Data provided by KPG, which is the nearest observatory (about 850 km east of the Lombok Island), are actually the most suitable, giving the lowest average differences to PNY and nearly the same discrepancy between night and day time values as that of PNY. Unfortunately, because of some technical problems, KPG data are not available for some days of the 2006 survey. Consequently, the KDU data have been chosen to minimize the external field contributions in survey measurements. These data are also in good agreement with PNY, because KDU is located nearly at the same geomagnetic latitude, despite its relative far geographical distance (about 2250 km southeast of the Lombok Island). Based on these evaluation results, the KDU data have also been chosen to reduce the measurements in 2007/2008, while no base station data were available.

All measurements have been reduced to a middle epoch, a date near the middle of the survey time-span. The data reduction for measurements in 2006 (that have been conducted from October 15th 2006 to November 26th 2006) is for epoch 2006.84, which is November 1st 2006. Whereas epoch 2008.08 (January 29th 2008) has been chosen to reduce measurements in 2007/2008 (that have been conducted from November 24th 2007 to April 3rd 2008). The mean values of KDU for both epochs are 46358.3 nT and 46324.1 nT, respectively. These values are in a good agreement with the annual mean values of KDU obtained from the British Geological Survey website¹⁷, which are 46370 nT in 2006.5 and 46339 nT in 2007.5. After successful data reduction, the mean values for each station (valid over the survey time span) can be determined by averaging the instantaneous reduced data.

3.1.3 Final processing

The final steps in the data processing are the IGRF subtraction, calibration adjustment (for the manual measurements), statistical evaluation and magnetic quietest period selection. All related steps are explained in the following.

The IGRF subtraction implies that the 10th generation of IGRF values (IAGA WG V-MOD, 2005; Maus et al., 2005) for the respective epoch are subtracted from the station mean values to eliminate the core field. The resulting values can be considered as lithospheric geomagnetic anomaly values. The exact IGRF values of each station on a certain survey day can be obtained from the on-line calculator at the Internet site¹⁸.

The GRIMM (Lesur et al., 2008) and its improvement, GRIMM-2 (Lesur et al., 2009), are actually a better constrained core models. These models pay special attention to the years 2002–2005, a period with remarkable geomagnetic jerks. At mid and low latitudes only night time data and at high latitudes (for all local times) vector data are used in these models. However, the GRIMM and the GRIMM-2 are not used in this study to eliminate the core field contributions, because the models were not available at the time of the data processing.

Calibration adjustment has been applied to measurements in 2006 on all stations by adding a fixed value of 4.1 nT. Whereas a fixed value of 6.2 nT has to be added to the manual measurements in 2007/2008 on 10 stations (i.e. C44, C43, C42, C45, C39, C35, C36, C59, C51, and CSN); see **Sec. 2.2.2.2** and **2.2.3.4** for calibration factors determination.

Statistical evaluation means that after data reduction, the quality of instantaneous data from all stations can be classified by using the standard deviation (*StDev*) values, following the criteria: good quality ($StDev < 2$ nT), intermediate ($2 \text{ nT} \leq StDev < 5$ nT), and low quality ($StDev \geq 5$ nT) data. This classification ensures the quality of data used further in visualizing the results; thereby also ensuring the reliability of the generated models and their interpretations. **Table 3.2** shows the results of data quality evaluations of measurements in 2006 and 2007/2008. It can be inferred that measurements in 2006, when the manual instrument (i.e. ENVI PRO) was used on all stations, are acceptable, while the measurements in 2007/2008 when the automatic instrument with better resolution (i.e. GSM 19T) was used on almost all stations (except on 10 stations) are of a better quality.

The last step in the data processing is the magnetic quietest period selection. This has been done to choose the more reliable data when there were redundant measurements at the same station on different days. In this case, the observations

¹⁷ http://www.geomag.bgs.ac.uk/gifs/annual_means.shtml

¹⁸ <http://ngdc.noaa.gov/geomagmodels/IGRFWMM.jsp>

made during the more magnetically quiet days, i.e. on the day when the K -indices for the Australian observatories¹⁹ and the Kp -index²⁰ are smaller than 3, have been kept.

The final results of data processing, including the remarks on data quality evaluation, are given in **Table 3.3** (for measurements in 2006) and **Table 3.4** (for measurements in 2007/2008), and can be found in **Appendix A**.

Table 3.2 Data quality evaluation for the 2006 and the 2007/2008 surveys.

Criteria of quality	2006		2007/2008	
	No. of Station	%	No. of Station	%
Good ($StDev < 2$ nT)	42	75	175	99
Intermediate ($2 \text{ nT} \leq StDev < 5$ nT)	12	21	2	1
Low ($StDev \geq 5$ nT)	2	4	0	0
Total number of stations	56		177	

3.1.4 Visualization

By using only the most reliable data, geomagnetic anomaly maps in two and three dimensional format have been generated using Oasis montaj 6.4 (Geosoft software). The most reliable data means they are of good quality (marked as Class 1 in **Table 3.3** and **3.4**) and obtained during quietest period. Additionally, for measurements in 2007/2008, if a station has not been further relocated, then the difference of anomaly values obtained in 2006 and in 2007/2008 should be less than 100 nT. In **Table 3.3** and **3.4**, the most reliable data could be inferred from the Station (*the first*) column, where the names are marked in black.

To obtain 2D geomagnetic anomaly maps, the Kriging method has been applied, using a linear power model. A blanking radius of 0.0527° (equal to 5.85 km) has been chosen to interpolate the available data in 2006 and to show the empty spaces for the parts without data. In the same manner, a blanking radius of 0.09° (equal to 10 km) has been chosen in interpolating 2007/2008 data. These blanking radii generate the most appropriate views over the survey area.

Other attributes that have to be chosen properly in generating a good map are datum and projection. Since the GPS (Global Positioning System) has been used to determine the exact location of stations, the World Geodetic System 1984 (WGS 84) datum has been considered for coordinate transformation, as recommended by IAGA²¹. Additionally, the Mercator projection has been used to show grids over maps, considering its capability in pointing accurate directions and showing proper shapes. Moreover, no size distortions (known as the main disadvantage of this kind of projection) should occur on the equatorial regions such as over the Lombok Island.

3.2 Results

3.2.1 Results of the 2006 survey

The results of measurements in 2006 are shown in **Fig. 3.4**, depicting a strong dipolar magnetic anomaly in the southern part of the surveyed area, with the minimum point located on (-8.76°N , 116.03°E) and the maximum point on (-8.73°N , 116.09°E). The new values of the geomagnetic anomaly are lower compared to the 2004–2005 survey results with differences ranging from -239.3 to -2941.8 nT. These

¹⁹ <http://www.ips.gov.au>

²⁰ http://www.gfzpotdam.de/pb2/pb23/GeoMag/niemegk/kp_index/index.html

²¹ <http://www.ngdc.noaa.gov/IAGA/vmod/igrf.html>

differences are larger than a normal decrease of an induced anomaly due to the main field in this region, characterized by a secular variation of some -13 nT/year. However, the previous measurements have to be taken with care because of the large uncertainties in the observations. Therefore, these differences are not discussed further here, but the annual changes are investigated in comparison with data from 2007/2008 survey, as described in **Sec. 3.2.3**.

Furthermore, by generating a 3D view as shown in **Fig. 3.5**, the horizontal gradient as well as geomagnetic anomaly pattern in the Lombok Island could be described as repeated contiguous negative-positive anomalies: a low anomaly in the northern part of the surveyed area, a high positive anomaly in the middle, and a negative anomaly in the southern part of the surveyed area. If the negative anomaly extends southward, then it matches the general geomagnetic anomaly pattern along the Java Trench (see **Fig. 2.3**). This ensures its reliability and promises a smooth transition to the global geomagnetic view, given by models (see **Fig. 2.2**).

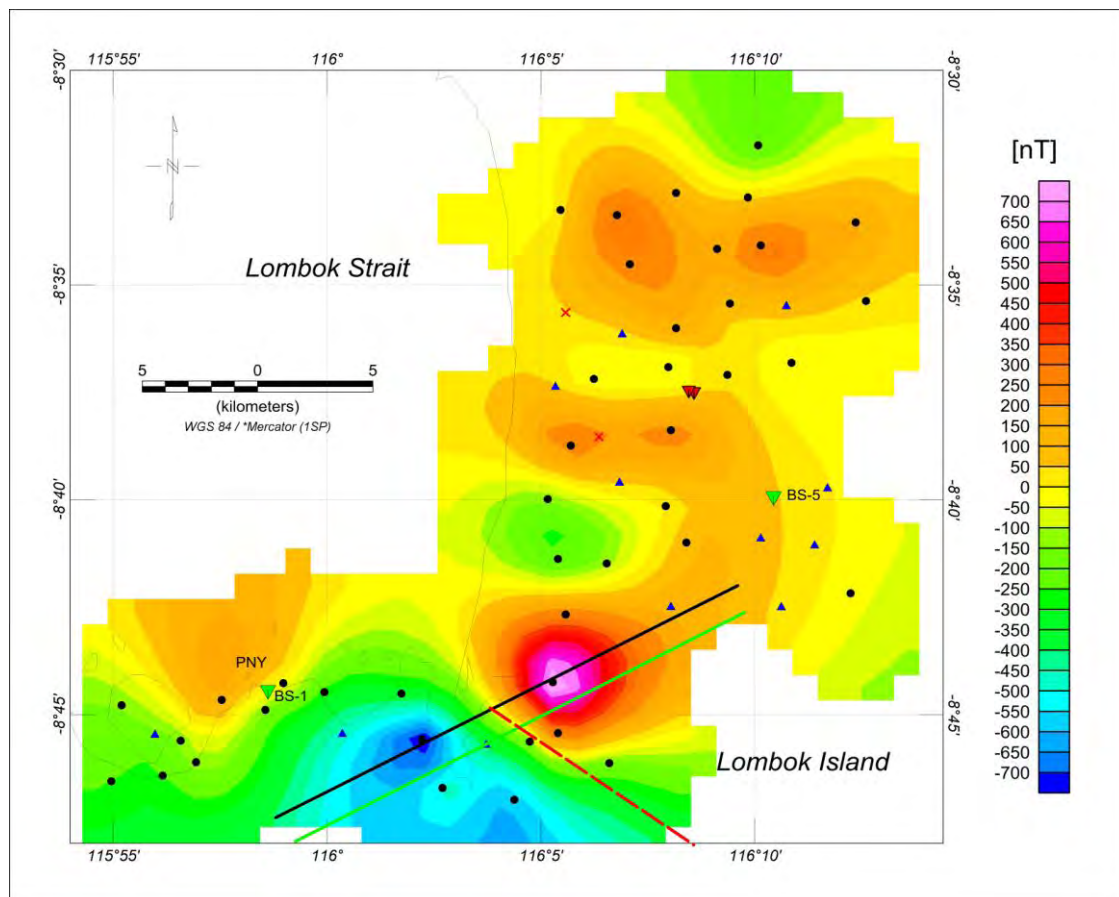


Figure 3.4 Map of the geomagnetic total field anomaly obtained from measurements in 2006. Only the most reliable data are used and interpolated over the surveyed area on the Lombok Island. The two base station locations are shown as green inverted triangles, while the calibration stations are depicted as red inverted triangles. The exact location of the Penyu Island is marked with PNY. The geomagnetic survey stations are also shown, providing good quality (black points), intermediate (blue triangles) and low quality (red crosses) data (see **Sec. 3.1.3** for more details). The black line represents the trace of the magnetic profile (P1-06) studied in **Chap. 4**, which connects two peaks of a strongest apparent dipolar magnetic anomaly. The green line represents the trace of the geological profile used in the corresponding model, while the red dashed one represents the modelled strike direction.

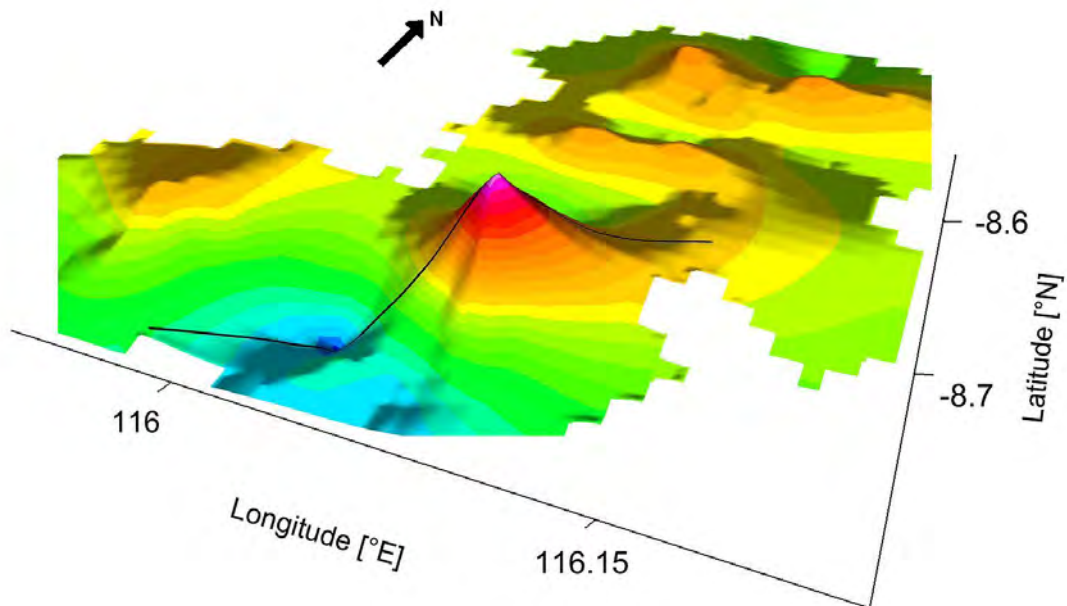


Figure 3.5 3D view of the geomagnetic total field anomaly map obtained from the measurements in 2006 for the same area as in **Fig. 3.4**, underlining the repeated contiguous negative-positive anomalies. The intensities of the geomagnetic anomalies are contoured in the form of elevations and levelled with colour scale exactly as in **Fig. 3.4**. The black curve represents the trace of the magnetic profile (P1-06) studied in **Chap. 4**, which connects two peaks of a strongest apparent dipolar magnetic anomaly structure.

3.2.2 Results of the 2007/2008 survey

The results of measurements in 2007/2008 are shown in **Fig. 3.6**, depicting three strong dipolar magnetic anomaly structures, one in the southern part, and two in the northern part of the surveyed area. The southern dipolar structure, with the minimum point located on $(-8.81^{\circ}\text{N}, 115.96^{\circ}\text{E})$ and the maximum point on $(-8.72^{\circ}\text{N}, 116.13^{\circ}\text{E})$, is very close to the dipolar structure inferred from measurements in 2006. This is the strongest dipolar structure in the southern part of the Lombok Island, undoubtedly, since a broader area with much better distribution of stations has been covered by the measurements in 2007/2008.

However, the other two dipolar structures in the northern part of the Lombok Island are even stronger. One of them is at the east side, showing the most prominent negative anomaly, with the minimum point located on $(-8.44^{\circ}\text{N}, 116.53^{\circ}\text{E})$ and the maximum point on $(-8.36^{\circ}\text{N}, 116.54^{\circ}\text{E})$. The other one is at the west side, showing the most prominent positive anomaly, with the minimum and maximum points located on $(-8.41^{\circ}\text{N}, 116.17^{\circ}\text{E})$ and $(-8.30^{\circ}\text{N}, 116.32^{\circ}\text{E})$, respectively.

By generating a 3D view as shown in **Fig. 3.7**, the horizontal gradient and the geomagnetic anomaly patterns on the Lombok Island can be more accurately described. This figure is still underlining repeated contiguous negative-positive anomalies, of shorter wavelengths in the south and longer wavelengths in the north, separated by low positive anomaly ripples in the middle. As has been expected, the negative anomaly extends southward, matching with the general geomagnetic anomaly pattern along the Java Trench. Additionally, the contiguous positive

anomaly peaks over the northern end of the Lombok Island also suits the general geomagnetic anomaly pattern along the Flores Thrust zone. These ensure their reliability and promise a smooth transition to the regional and global geomagnetic data (see Fig. 2.2 and 2.3).

Re-evaluation of the used core model, regarding the GRIMM (Lesur et al., 2008) and the GRIMM-2 (Lesur et al., 2009), confirms the same anomaly patterns over the Lombok Island. However, using these core models result a higher values of positive anomalies as well a lower values of negative ones.

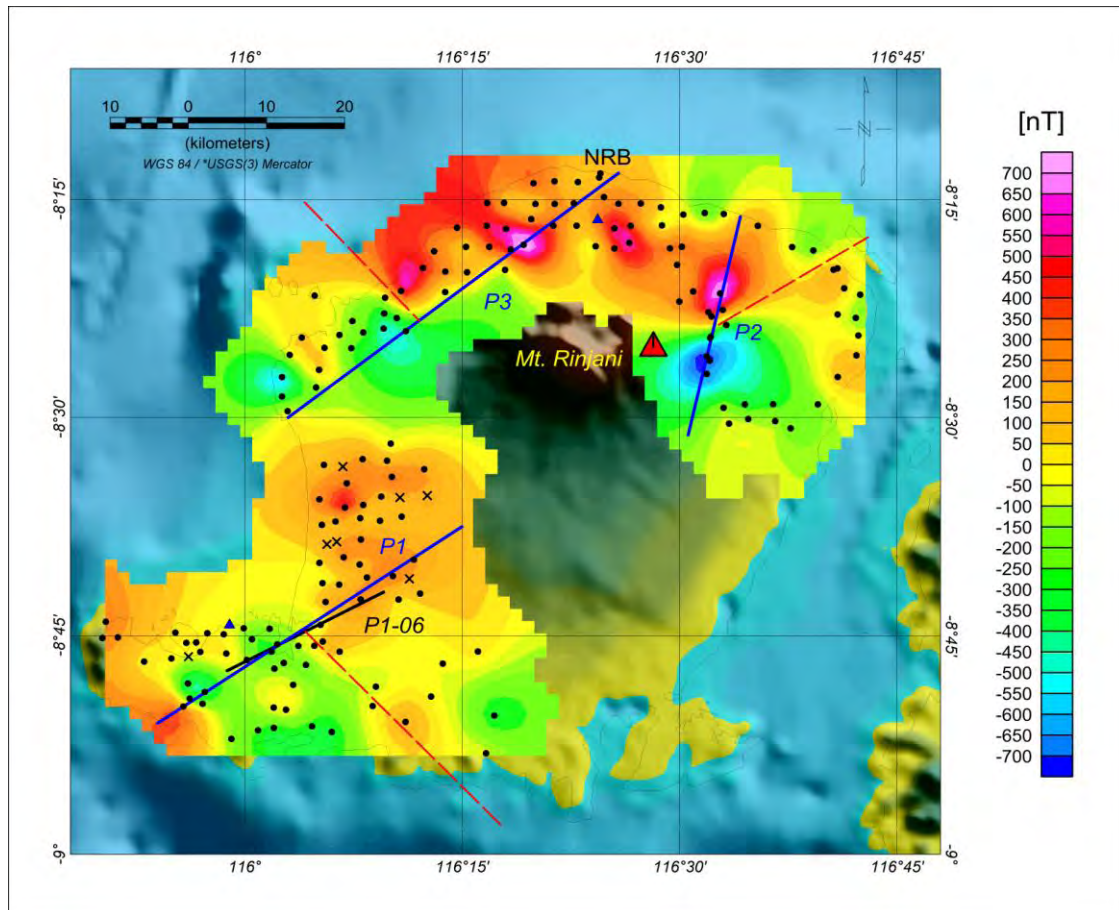


Figure 3.6 Map of the geomagnetic total field anomaly obtained from the measurements in 2007/2008, plotted over a regional topographical map of SRTM30 Plus v4 (Becker et al., 2009). Only the most reliable data are used and interpolated over the surveyed area on the Lombok Island. The geomagnetic survey stations are shown, providing good quality (black points) and intermediate quality (blue triangles), while the black crosses represent the stations with large difference in anomaly value compared to that in 2006 (Diff. > 100 nT). The blue line represents the traces of the magnetic profiles (P1, P2, and P3) studied in Chap. 4, which connects the peaks of dipole magnetic anomalies, while the black line represents the trace of the magnetic profile (P1-06) that has been inferred from measurements in 2006. The red dashed lines are the modelled strike directions of the related profiles. The position of the summit of Mount Rinjani is depicted with a red triangle, while NRB label is the location of “Nurul Bayan” station.

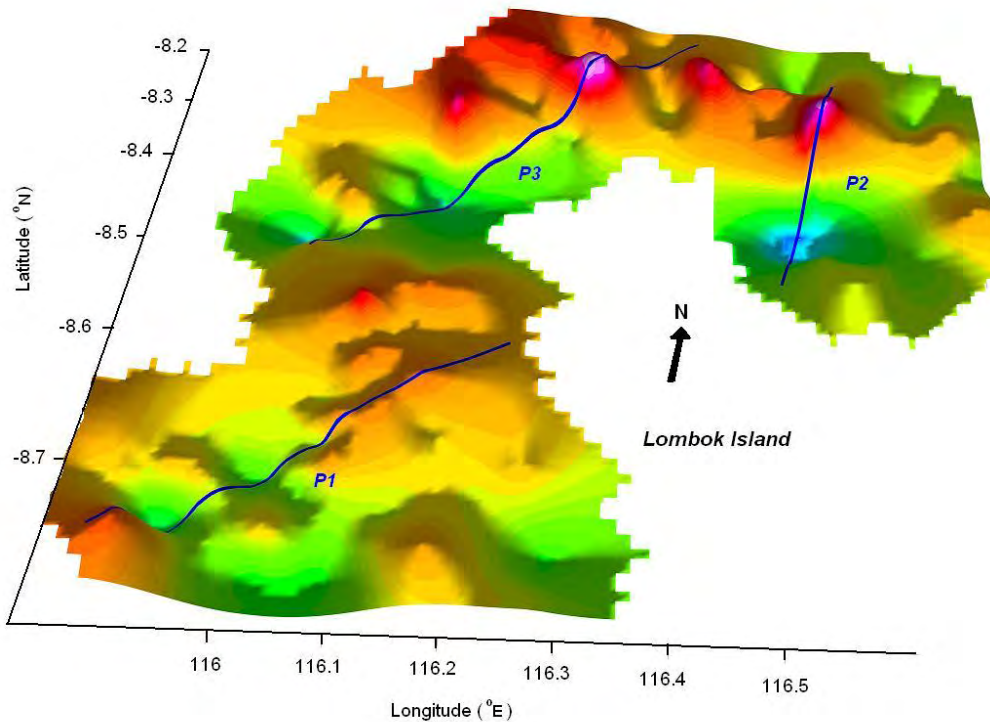


Figure 3.7 3D view of the geomagnetic total field anomaly map obtained from measurements in 2007/2008 for the same area as in **Fig. 3.6**, underlining the repeated contiguous negative-positive anomalies of shorter wavelengths in the South and longer wavelengths in the North, separated by low positive anomaly ripples in the middle. The intensities of the geomagnetic anomalies are contoured in the form of elevations and levelled with colour scale exactly as in **Fig. 3.6**. The blue curves represent the traces of the magnetic profiles (P1, P2 and P3) studied in **Chap. 4**, connecting the peaks of dipolar magnetic anomaly structures.

To demonstrate the reliability of the Lombok 2007/2008 ground measurements in generating a smooth transition to the regional and global geomagnetic data and the capability to underline the most active tectonic elements on this region, **Fig. 3.8** shows a clear comparison of two regional views of geomagnetic anomaly over the Lombok Island and surroundings, before and after taking into account the contribution of the new ground measurements. The view (a) has been generated by using only all available marine and aeromagnetic data sources (see **Sec. 2.1.2**), while for view (b) the same data set combined with the most reliable data of the Lombok 2007/2008 ground measurements have been used.

There are still very large uncertainties to directly delineate the transition between the large-scale negative part of anomaly in the south and the positive part of anomaly in the north of view (a), whereas some prominent magnetic lineations over the Lombok Island could be gently deduced from view (b). These lineations underline the most active tectonic elements on this region (i.e. the Java Trench, the Flores Thrust zone and its presumed extension, and the Mt. Rinjani). The links between the geomagnetic data and these tectonic elements have been modelled, interpreted, and are discussed in **Chap. 4**.

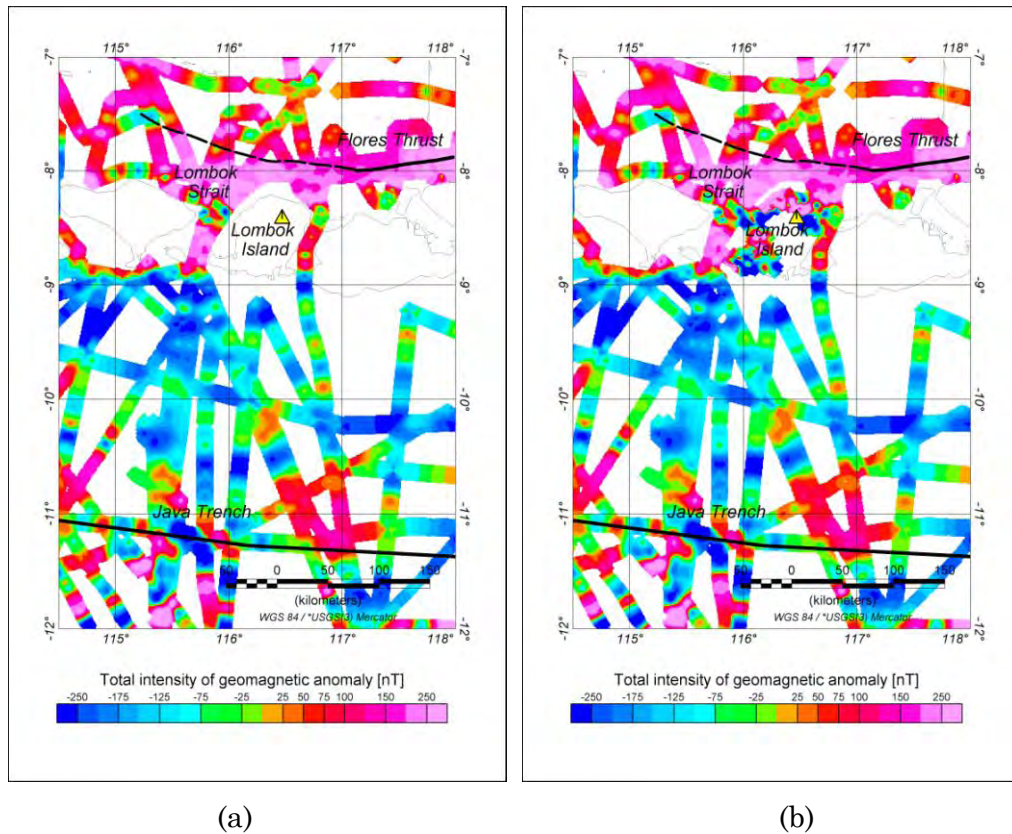


Figure 3.8 Comparison of two regional views of geomagnetic anomaly over the Lombok Island and surroundings, generated from (a) all available marine and aeromagnetic data sources (see **Sec. 2.1.2**) and (b) the similar data set combined with the most reliable data of the Lombok 2007/2008 survey. The white areas over oceans or islands indicate that no data are available. Very large uncertainties in view (a) restrict to deduce a direct delineation between the large-scale negative part of anomaly in the South and the positive one in the North, whereas some prominent magnetic lineations could be gently deduced from view (b). The latest view also demonstrates the capability of ground measurements to underline the most active tectonic elements on this region [i.e. The Java Trench (black solid line in the South), The Flores Thrust zone and its presumed extension (black solid and dashed lines in the North), and the Mount Rinjani (yellow triangle)].

3.2.3 Changes of geomagnetic field

As discussed in **Sec. 3.2.1**, the new values of the geomagnetic anomaly in 2006 are much lower compared to the 2004–2005 survey results, with values larger than the normal decrease of an induced anomaly due to the main field variations in this region. Therefore, only changes between 2006 and 2007/2008 are described and discussed in more detail.

The changes are calculated by subtracting the 2006 values from that of the 2007/2008 obtained at 25 exact stations. These stations have been surveyed at exactly the same locations (i.e. no further relocation in 2007/2008) and providing the most reliable data in both surveys. Two different approaches are used in representing the changes of geomagnetic field over southern and middle part of the Lombok Island. The *first* approach has been done by evaluating the changes of the geomagnetic field intensity, while the *second* one has been done by evaluating the changes of the geomagnetic anomaly values.

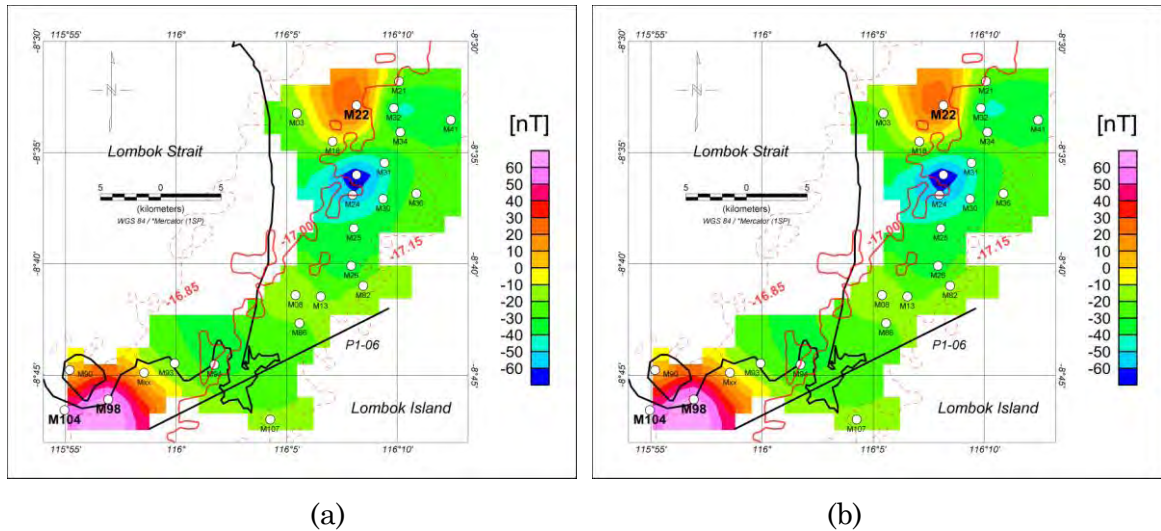


Figure 3.9 Map of the geomagnetic changes obtained from the differences between the 2006 and the 2007/2008 measurements at 25 exact stations: (a) geomagnetic field intensity changes, and (b) geomagnetic anomaly changes. Contours are the core field variations as given by the IGRF (IAGA WG V-MOD, 2005; Maus et al., 2005). Both figures provide anomalous changes (increasing of geomagnetic field intensities and anomaly values) at stations M22, M98, and M104. The location of P1-06 profile, along which the geomagnetic changes are modelled in **Chap. 4**, is shown as a black line.

Figure 3.9 (a) and (b) shows the corresponding maps of two approaches. Generally, both figures suggest nearly the same conclusion about the regional geomagnetic anomaly changes. The differences of field intensity or anomaly values ranged from -100 to +80 nT, which are still large compared to the effects of an induced anomaly due to the core field variations in this region.

Furthermore, the core field variations in this area between two consecutive surveys, as given by the 10th generation of IGRF values (IAGA WG V-MOD, 2005; Maus et al., 2005), are only over a narrow range of negative differences (from -16.85 to -17.15 nT). Meanwhile, if the GRIMM (Lesur et al., 2008), a better constrained core model which estimate more secular variations over this region, is used, the differences should also be in a negative range (from -42.0 to -42.4 nT). Therefore both approaches indicate some anomalous changes in the most northern and the most southern of investigated area, where the positive differences occur. Increasing of geomagnetic field intensities as well as anomaly values are observed at stations M22, M98, and M104.

These anomalously changes, therefore, could be investigated as possibly linked to some local tectonic, geological or seismic changes of this region, as explored in more detail in **Chap. 4**.

Chapter 4

Modelling and interpretations

In order to understand the causal relationship between the predicted sources of geomagnetic anomalies and their attributed phenomena, forward modelling has been applied, followed by comprehensive interpretations. A simultaneous modelling of magnetic anomalies and gravity followed by two kinds of interpretations are presented in this chapter. The geological and tectonic interpretations are directed to resolve some uncertainties in the past and present tectonics as well as geology of the Lombok Island and nearby regions. The suggested interpretation might support some new hypotheses and answer crucial questions, and still keep the compatibilities with the well-known accepted backgrounds (see again **Sec. 1.2.1** and **1.2.2**). As an inherent debate, the seismo-electromagnetic interpretations describe and propose some possible mechanisms accompanying the geological and tectonic processes. Thus the interpretations corroborate each other in sharpening and supporting a hypothesis from different point of views.

4.1 Some important constraints

Realizing that there is no unique solution in modelling, some constraints have to be consistently defined before generating models. The well defined constraints help in minimizing the range of possible solutions, then guiding the generated model to be the most realistic one. In this kind of modelling, the most important constraints are the surficial geological conditions and the known regional tectonic settings as well as the historical seismicity of the region. The local conditions mean the specific conditions of the Lombok Island, while the regional settings mean the background conditions of the surroundings (i.e. the region of the Lesser Sunda Islands or the Sunda-Banda arcs transition).

Firstly, the local Earth's surface shape is derived from the topography grid of SRTM30 Plus v4 (Becker et al., 2009), obtained from the Geosoft DAP server²². The SRTM (Shuttle Radar Topography Mission) data set are elevation data obtained by a radar system that flew onboard the Space Shuttle Endeavour during an 11-day mission in February of 2000 (Farr et al., 2007). The SRTM was carried out by the National Geospatial-Intelligence Agency (NGA) and the National Aeronautics and Space Administration (NASA).

The structures of surficial rocks as well as their subsurface continuations are determined from the local geological map (Mangga et al., 1994). The geology was mapped in 1988 during October–December by Geological Research and Development Centre Indonesia using aerial photographs with scale 1:100,000. The related parts of

²² <http://dap.geosoft.com/geodap/home/default.aspx>

the map can be seen in **Fig. 4.1**, showing also the locations of the extracted profiles (P1-06, P1, P2 and P3) and some important rocks and sedimentary structures discussed through this Chapter.

The regional tectonic settings as well as the deeper geological structures are estimated based on the seismic and geoaoustic investigations over the closest areas of the Java Trench (the 116°E Corridor of Kopp and Flueh, 2007) and of the Flores Thrust zone (the profile 63 of Fig. 16 of Silver et al., 1983; the decollement model of Fig. 6a of McCaffrey and Nabelek, 1984). Two subducting slabs are modelled below the Lombok Island, one with the dip angle of about 30° coming from the South (representing the “definitive” Indian oceanic slab) and the other of about 6° coming from the North (representing the “hypothetical” Flores oceanic slab).

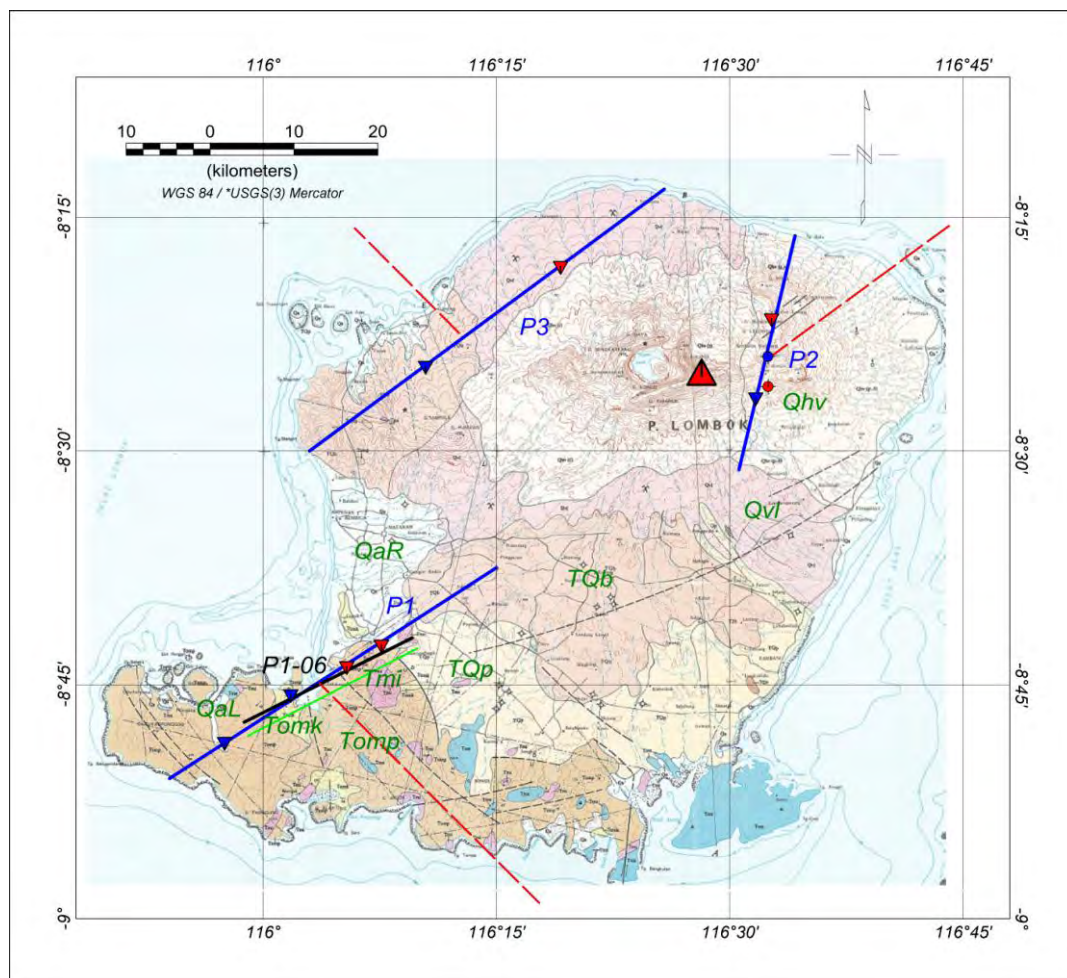


Figure 4.1 The related parts of the Lombok geological map (Mangga et al., 1994), used to determine the surficial rocks structures and their subsurface continuations for the models. The extracted profiles are depicted as a bold black line (P1-06) and three bold blue lines (P1, P2 and P3), while the red dashed lines are their modelled strike directions. The red and blue inverted triangles are the maxima and the minima of geomagnetic anomalies on each profile, respectively. The position of the summit of Mount Rinjani (3726 m, the second highest active volcano in the Indonesian region) is depicted with a red triangle, whereas the locations of cold and hot springs (Sundhoro et al., 2000) are depicted as a blue and a red circle symbols, respectively. The main geological structures mentioned in the modelling are labelled in green letters.

To properly position these two subducting slabs, the historical seismicity data obtained from Engdahl catalogues (Engdahl et al., 1998; Engdahl et al., 2007) are used. These catalogues are hypocentres relocated data, based on the Preliminary Determinations of Epicenters (PDE) catalogues of the U.S. Geological Survey/National Earthquake Information Center (USGS/NEIC). The PDE catalogues are the most complete computations of hypocenters and magnitudes, which are monthly listings and are normally produced a few months after the events occur, that can be accessed on-line through the web site²³. The relocated earthquake data from February 16th 1963 to October 24th 2009 for the latitude -7°N to -12°N and longitude 114.5°E to 121.5°E with the depths up to 120 km of all magnitudes are included.

However, for studying the Lombok Island, the earthquake data should be bounded only to the longitude 115.5°E to 117.5°E . This bounding is chosen regarding the proposed plate boundary segments in the Banda Arc region revealed from the newest high resolution GPS measurements over the Sunda-Banda arcs transition region (Segment 2 of Nugroho et al., 2009). The earthquake data of the Lombok–west Sumbawa and the adjacent segments (Bali in the West, and Flores in the East) are plotted in **Fig. 4.2**. This figure shows the location of the epicentres in sized circles related to the magnitudes and in different colours related to the depths. **Figure 4.3** then provides the longitudinal cross sectional view of these earthquakes for the Lombok–west Sumbawa segment and the positions of the “definitive” Indian oceanic slab as well as the “hypothetical” Flores oceanic slab, inferred from the most possible Wadati-Benioff zones.

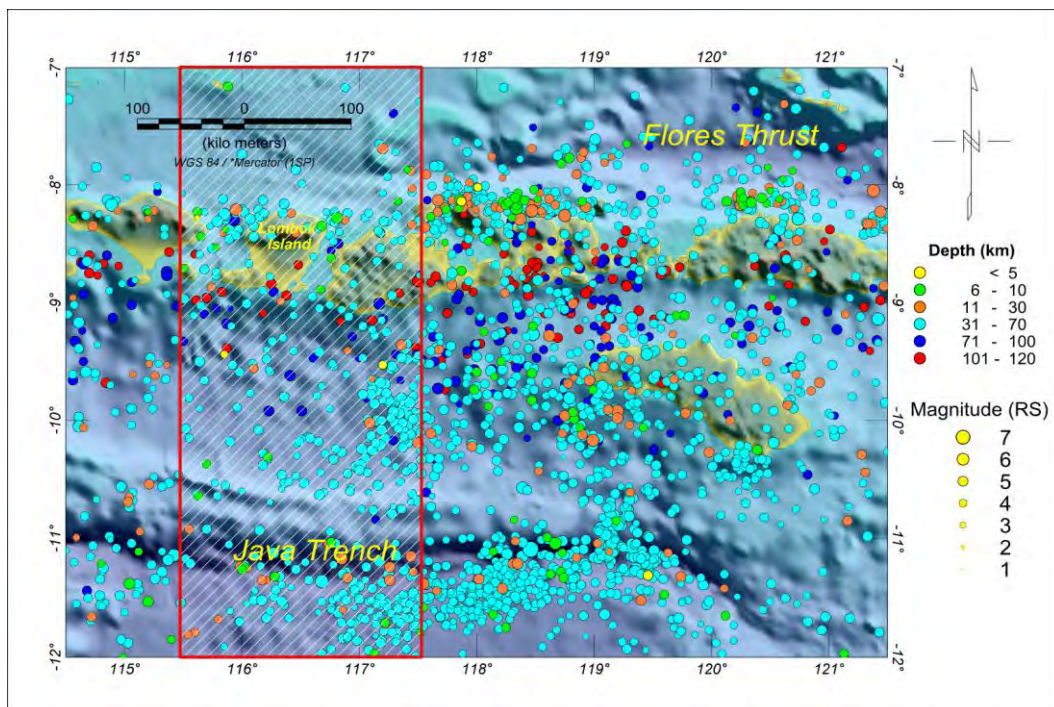


Figure 4.2 Plot of the earthquake epicentre data of Lombok–west Sumbawa segment (in the red shaded box) and the adjacent segments of Bali in the West and Flores in the East, dated from February 16th 1963 to October 24th 2009 of all magnitudes and the depths up to 120 km. The sizes of the circles represent the magnitudes, while the colours are related to the depths (see the legends on the right side). The bounding of Lombok–west Sumbawa segment is chosen regarding the proposed plate boundary segmentations (Segment 2 of Nugroho et al., 2009).

²³ <http://neic.usgs.gov/neis/epic/>

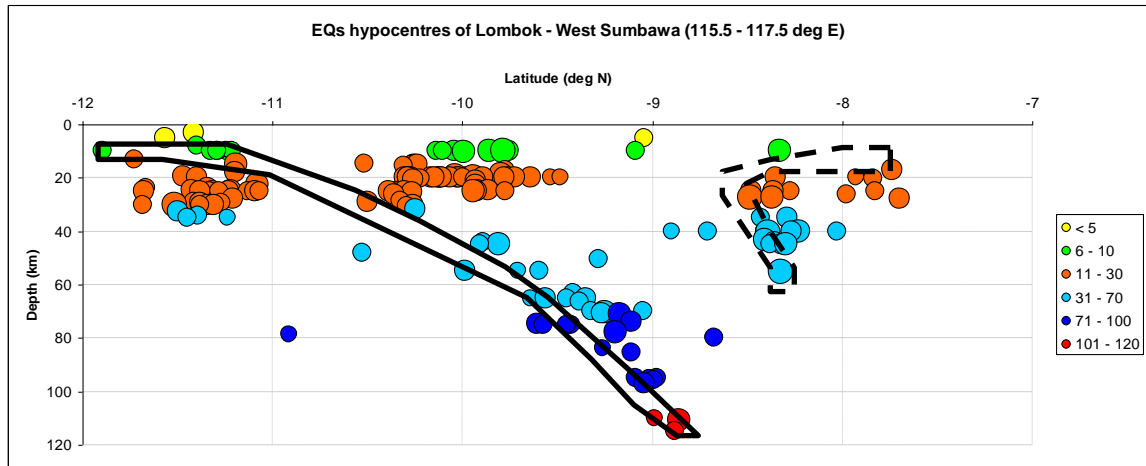


Figure 4.3 The longitudinal cross sectional view of earthquake hypocentres for the Lombok–west Sumbawa segment (bounded by latitude -7°N to -12°N and longitude 115.5°E to 117.5°E , as depicted in the red shaded box of **Fig. 4.2**). The positions of the “definitive” Indian oceanic slab and the “hypothetical” Flores oceanic slab are inferred from the most possible Wadati-Benioff zones, showing a “post-mature” subduction in the South and possibility of a “mature” subduction in the North. The sizes of the circles represent the magnitudes and the colours are related to the depths. The horizontal axis is the latitude ($^{\circ}\text{N}$) and the vertical axis is the altitude (in km), with a vertical exaggeration of 2.0.

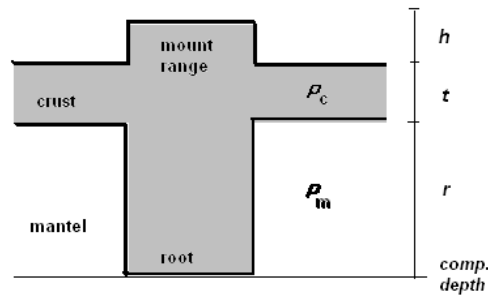


Figure 4.4 Illustration of the applied isostasy principle of Airy’s model (see the text for complete explanations of the used symbols). Following the calculation of **Eqn. (4.1)**, the northern part of the Lombok Island is compensated to 24–28.5 km depth.

Another complementary constraint for the regional tectonic settings is the depth of the ‘root’ of the Lombok Island below the Mount Rinjani range (with the summit of 3726 m height). This has been manually calculated considering the isostasy principle of Airy’s hypothesis (Sec. 5.5.2 of Fowler, 2005), as illustrated in **Fig. 4.4** and using the following formulations:

$$t\rho_c + r\rho_m = (h+t+r)\rho_c,$$

hence

$$r\rho_m = h\rho_c + r\rho_c,$$

and

$$r = h \frac{\rho_c}{(\rho_m - \rho_c)}, \quad (4.1)$$

where h is the height of the mountainous range; t , the average crustal thickness of the region; r , the thickness of the root; ρ_c , the average density of the crust of the region; and ρ_m , the average density of the mantle of the region. For the Lombok Island region, as a volcanic Island, the average density of the crust can be estimated as 2700 kg.m^{-3} (Hunt et al., 1995). The average density of mantle is given as 3300 kg.m^{-3} (Blakely, 2005). By assuming the average height of the northern mountainous range is in the range of 2–3 km and the average regional crustal thickness is 15 km, then the calculated root is 9–13.5 km thick. One can also say that the northern part of the Lombok Island is compensated to 24–28.5 km depth. In the models, the maximum compensation depth (i.e. 28.5 km) is chosen.

Since the aim is to obtain an integrated model of magnetic anomalies and gravity, the regional and local gravity anomaly data are also significant constraints. The GGM02-GRACE Gravity Model 02 (Tapley et al., 2005), obtained from the Geosoft DAP server²⁴, is used to describe the regional gravity background as can be seen in **Fig. 4.5**. The global gravity data of GGM02 show that the Lombok Island as well as the other Lesser Sunda islands could be considered to lie between two basin ranges, with the southern basin range being wider and deeper than the northern one. The lands with their elevated mountainous ranges are characterized by continuous positive anomalies. Some important tectonic features of this region are well defined, but the global data are not suitable to be used in the local gravity modelling due to the resolution limited to about 300 km.

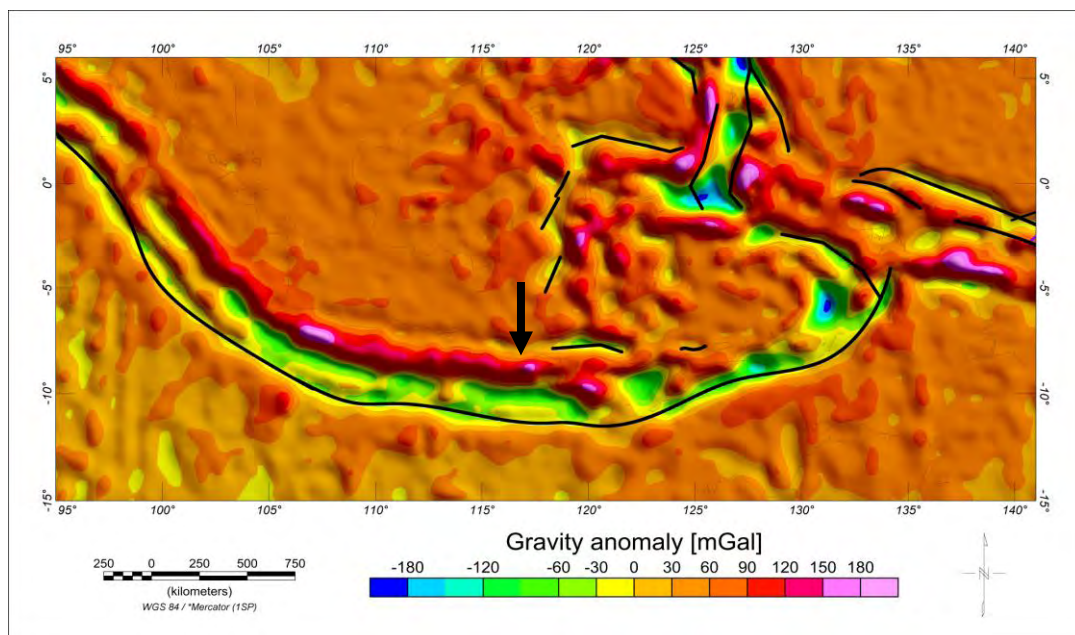


Figure 4.5 The regional gravity background for the Indonesian region derived from GGM02-GRACE Gravity Model 02 (Tapley et al., 2005). Plate boundaries and subduction zones are indicated as black lines. This map underlines some basins with prominent negative gravity anomaly values while contrasting the elevated terrains with positive anomalies. The Lombok Island (pointed out by a black arrow) as well as the other Lesser Sunda islands lie between two negative anomalies and are showing continuous positive anomalies over the lands.

²⁴ <http://dap.geosoft.com/geodap/home/default.aspx>

For higher resolution modelling, the local gravity anomaly data over the Lombok Island should be used. Since no local gravity data are available directly, the data have been obtained by digitization from the available Bouguer anomaly map (Sukardi, 1979) depicted in **Fig. 4.6**. This map was issued by the Geological Survey of Indonesia, as a result of gravity measurements in 246 stations and 2 base stations that have been conducted during 5 months in the years 1974–1975. The accuracy of the used altimeter is better than 5 meters, except for the mountainous area such as Mount Rinjani where the errors could reach up to 10 meters. The data reductions are based on the Potsdam value using a Bouguer density of 2670 kg.m^{-3} . Digitisations of this map are done by interpolating the original 5 mGal contours to one mGal intervals, then estimating the gravity anomaly values of each station using the nearest contours and generating the grid based on these estimated values. As shown in **Fig. 4.7**, the results of these processes could successfully reconstruct the main features of the original gravity data of **Fig. 4.6**.

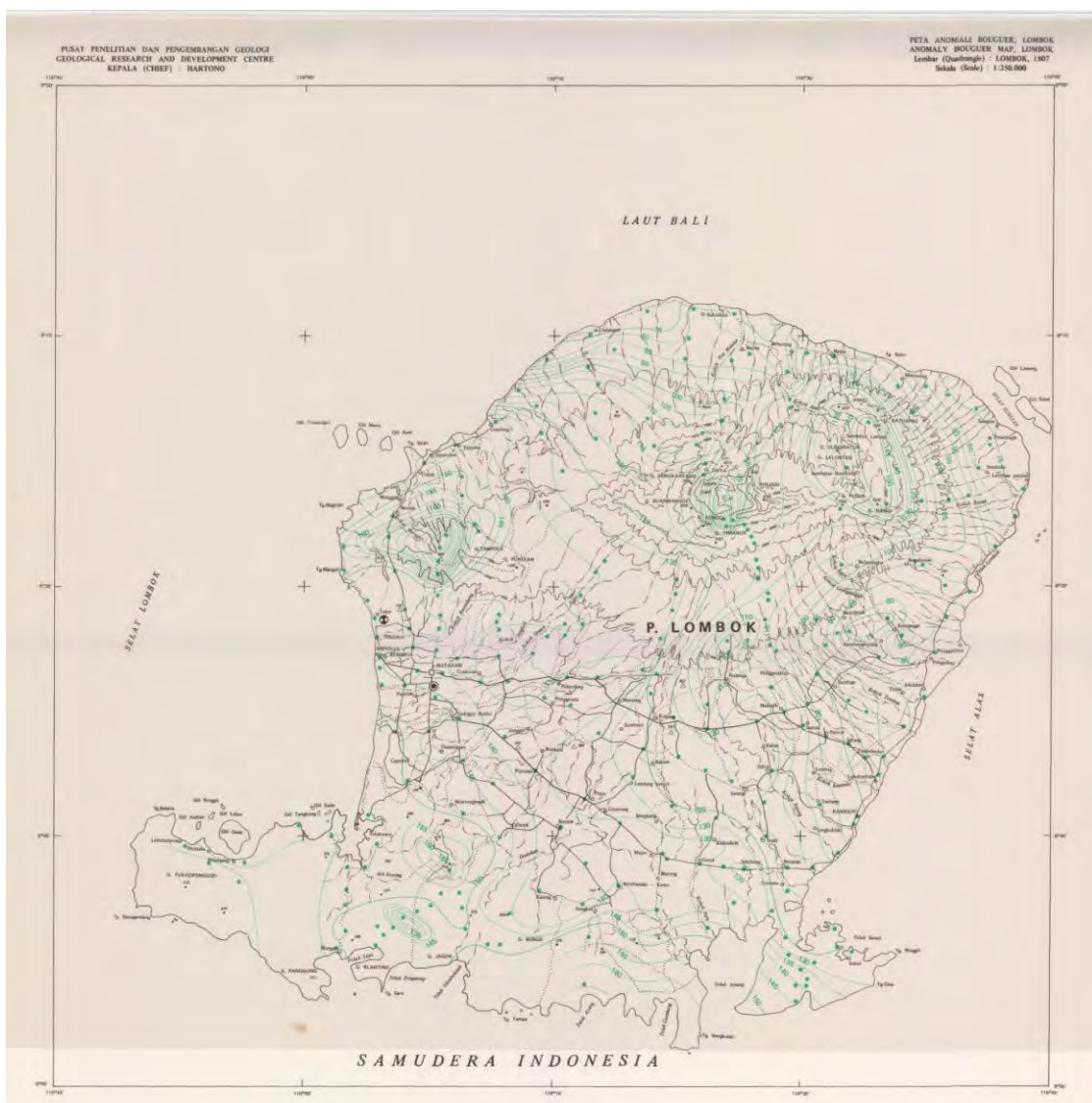


Figure 4.6 The original Bouguer anomaly map of the Lombok Island (Sukardi, 1979). The contours are 5 mGal intervals, with the major high anomaly concentrated in the northern part and some minor ones in the southern part. Green points are the locations of the gravity stations. A Bouguer density of 2670 kg.m^{-3} was used for the data reductions, based on the Potsdam value.

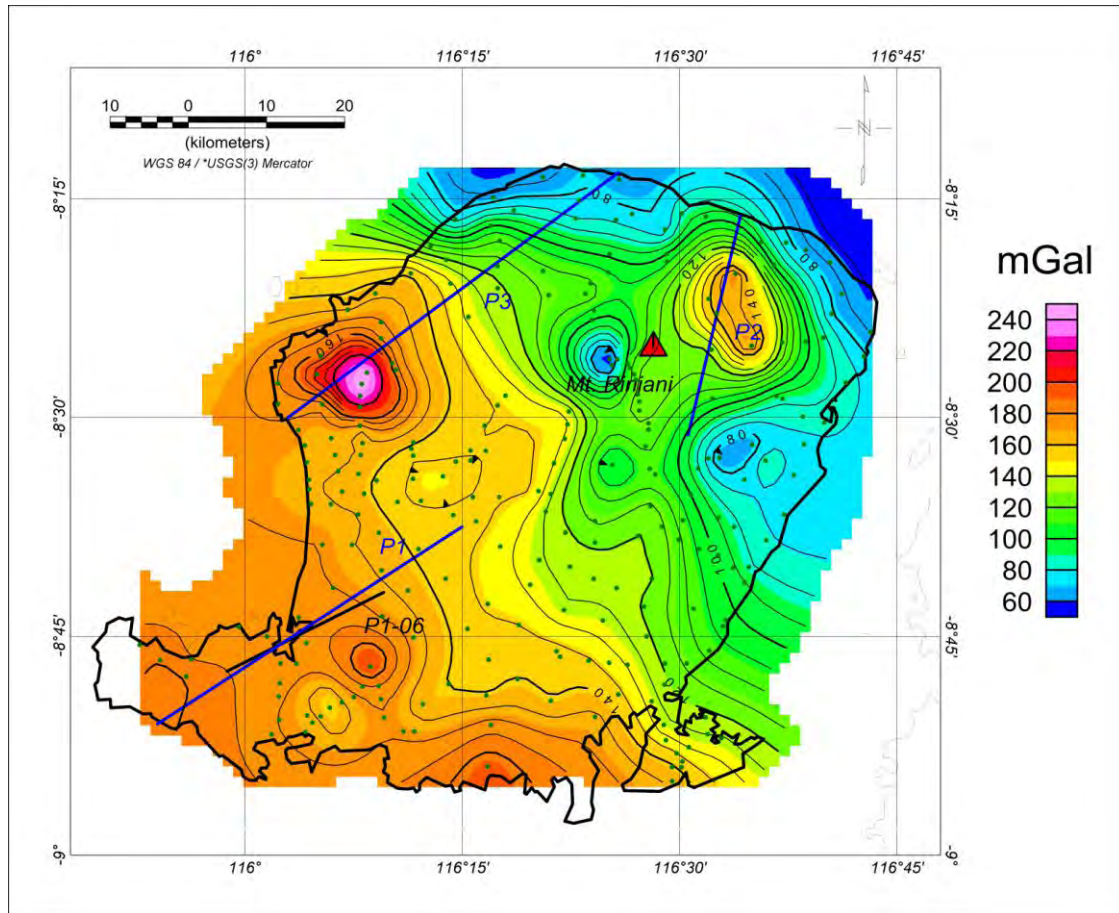


Figure 4.7 The digitization results of the Bouguer anomaly map (Sukardi, 1979), used in the gravity modelling. Green points are the locations of the gravity stations. The contours are of 5 mGal intervals, reconstructing the major high anomaly concentrated in the northern part and some minor ones in the southern part, as of the original map (see **Fig. 4.6**). The position of the summit of Mount Rinjani is depicted with a red triangle, while its active crater is characterized by low gravity anomaly. The extracted profiles for the modelling are depicted as a bold black line (P1-06) and three bold blue lines (P1, P2 and P3), mainly coinciding with the concentrations of high gravity anomalies.

4.2 Modelling over the most prominent dipolar structures

The models are obtained using the GM-SYS Profile Modeling (an extension to Oasis montaj, Geosoft software), which can generate models from magnetic and gravity data simultaneously as an integrated model. In practice, interdependency between magnetic anomalies and gravity modelling will substantially reduce the range of possible solutions and provide the most reasonable and reliable model. The GM-SYS modelling uses Talwani's algorithm in providing forward modelling of magnetic and gravity data. The complete algorithm is described in more detail in **Appendix B**.

The magnetic anomalies model assumes surficial rocks and lavas as well as deeper structures, as several blocks having different susceptibilities and remanent magnetizations, as the sources of magnetic anomalies. In this modelling method, the general shapes of the magnetic anomaly signals are determined primarily by location and shape of each block, whereas detailed curvatures and their amplitudes are influenced by the susceptibilities and the remanence parameters (magnetization

intensity, inclination, and declination) of each block. Complementary, the gravity model considers the contrasts of the rock densities as the source of gravity anomalies. By defining the proper parameters for magnetic and gravity modelling, as well as applying the known tectonic and geological settings consistently, the models could be adjusted to get the minimum RMS errors between models and observations. For ensuring the reliability of the generated models, both magnetic and gravity responses have to be adjusted until the limiting factor could be reached. The limiting factor means the maximum tolerable RMS errors, which are set to 10% peak to peak modelled anomalies.

To start the models, the observed magnetic and gravity anomaly signals are directly imported from the concerned grids by digitizing the desired profile on the 2D anomaly maps (**Fig. 3.2** and **3.4**), taking some number of points with 250 m intervals. These intervals are chosen to have about ten points between two adjacent stations (which are separated by around 2.5 km). **Figure 4.8** shows the extracted profile of the 2006 survey (P1-06), connecting the strongest apparent dipolar magnetic anomaly from the negative part on (-8.79°N, 115.98°E) to the positive part on (-8.70°N, 116.16°E). **Figure 4.9** shows two extracted profiles of the 2007/2008 survey (P1 and P2). The first profile connects the strongest apparent dipolar magnetic anomaly in the southern part from the negative part on (-8.85°N, 115.90°E) to the positive part on (-8.63°N, 116.25°E). The second one connects the negative part on (-8.52°N, 116.51°E) to the positive part on (-8.27°N, 116.57°E) which passes through the most prominent negative anomaly in the east side. **Figure 4.10** also shows two extracted profiles of the 2007/2008 survey (P1 and P3). The latest profile connects the negative part on (-8.50°N, 116.05°E) to the positive part on (-8.22°N, 116.43°E) which passes through the most prominent positive anomaly in the west side.

Initially, several parameters of the ambient core magnetic field have to be given, including its magnitude (H), inclination (FI), and declination (FD); additionally the profile azimuth and the relative strike angle have also to be set. All initial magnetic parameters are determined from the 10th generation of IGRF (IAGA WG V-MOD, 2005; Maus et al., 2005), at the location of the South base station (BS-1 of **Fig. 3.2**) for P1-06 and P1; but at “Nurul Bayan” station (NRB of **Fig. 3.4**) for P2 and P3. These values can be accessed from an online calculator²⁵. The profile azimuths are determined from the direction of the extracted profiles counted clockwise from the true North, while the strike angles are set by considering the magnetic lineations as well as the known nearest surface lineaments on the geological map (Mangga et al., 1994). The modelled strike directions of each profile are depicted as red dashed lines in **Fig. 3.2, 3.4** and **4.1**.

At these initial steps, only a continuous structure (having a density of 2670 kg.m⁻³) with topography has been modelled for each profile, in order to recognize the background anomalies and the initial RMS errors. The other magnetic and gravity parameters are determined later, when the formations of rocks and sediments of each profile have been postulated from the specific geological structures. **Figures 4.8, 4.9** and **4.10** show the background anomalies of P1-06, P1 and P2, and P1 and P3 profiles; respectively. Note that the twisted lines in the observed anomaly signals as well as the topography between P1 and P3 in **Fig. 4.10** are due to the latitude/longitude offset between both profiles.

²⁵ <http://ngdc.noaa.gov/geomagmodels/IGRFWMM.jsp>

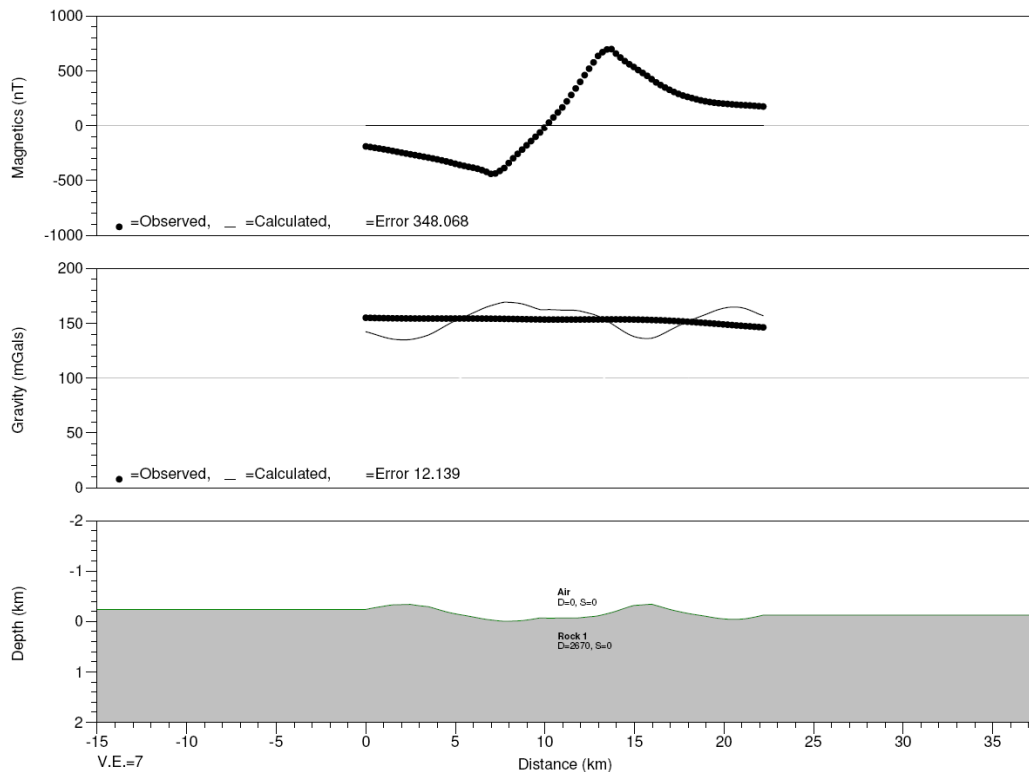


Figure 4.8 The background anomalies of the extracted profile of the 2006 survey (P1-06), showing the initial RMS error of about 348 nT for magnetic anomalies model and about 12.2 mGal for gravity model.

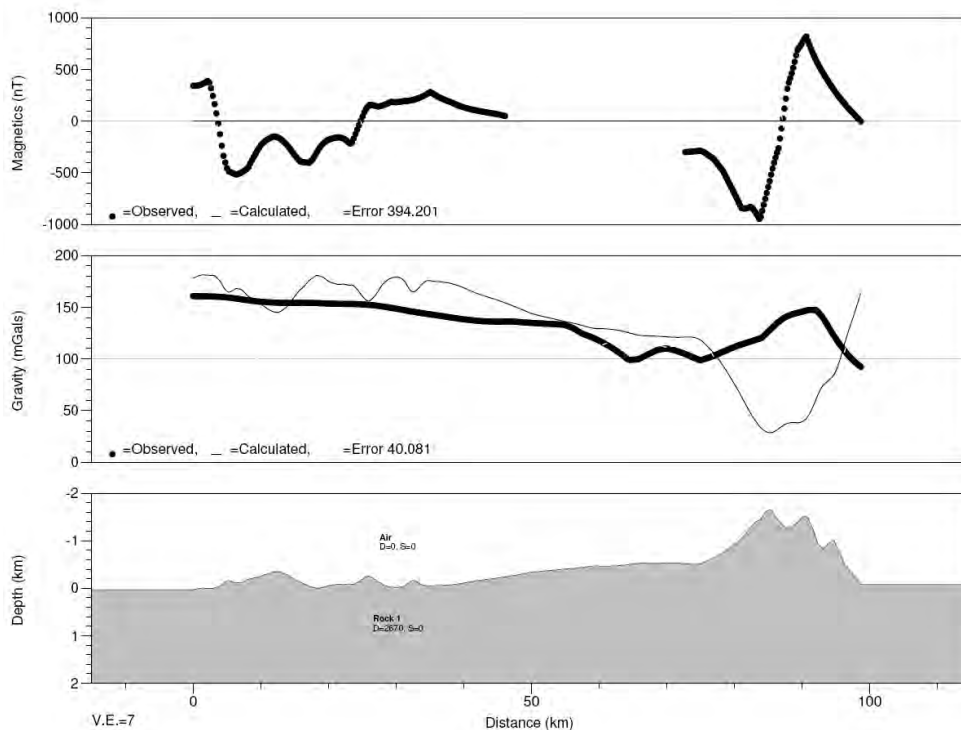


Figure 4.9 The background anomalies of two extracted profiles of the 2007/2008 survey (P1 and P2), passing through the most prominent negative anomaly in the east side, showing the initial RMS error of about 394 nT for the magnetic anomalies model and about 40.1 mGal for the gravity model.

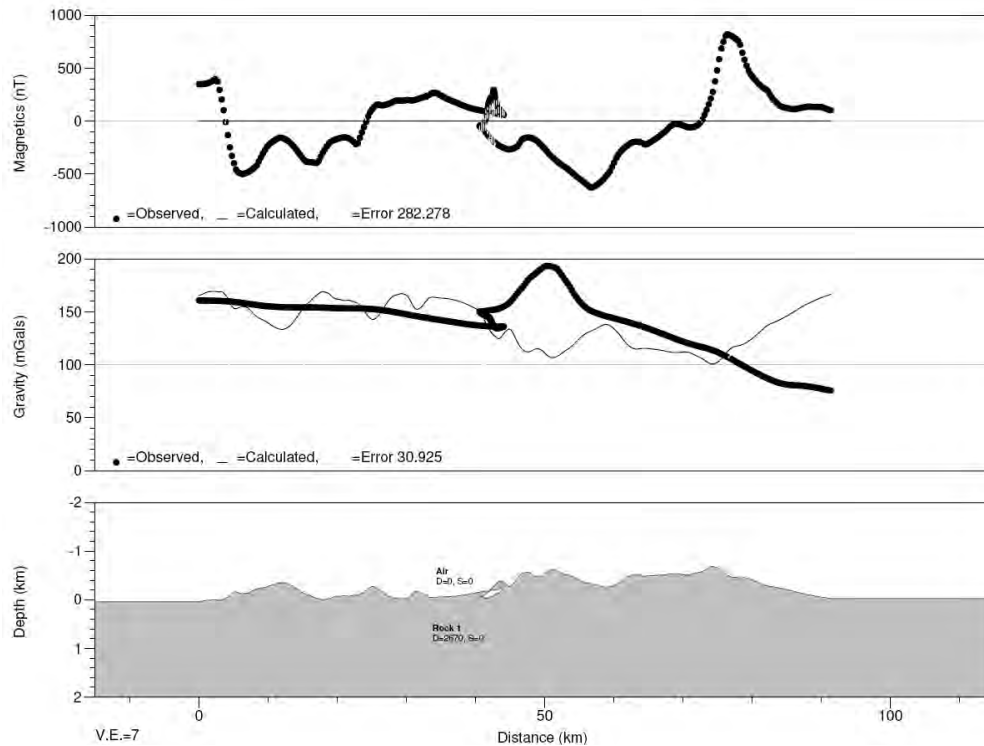


Figure 4.10 The background anomalies of two extracted profiles of the 2007/2008 survey (P1 and P3), passing through the most prominent positive anomaly in the west side, showing the initial RMS error of about 282 nT for the magnetic anomalies model and about 30.9 mGal for the gravity model. The twisted lines in the observed anomaly signals as well as the topography are due to the latitude/longitude offset between both profiles.

In the following, each profile is modelled and resolved separately for simplicity, but later the individual results are combined. By combining all results, it makes possible to get the overall view of the Lombok Island; hence the single grand design of related processes could also be better understood.

4.2.1 P1-06 model (the southern area using the 2006 survey results)

In postulating the formations of rocks for P1-06, the geological profile (green lines of **Fig. 3.2** and **4.1**) has been shifted about 1.5 km landward from the anomaly profile (blue lines of the same figures) to resolve uncertainties of geological structures across the coastal area. Firstly, an intrusive igneous rock (labelled as *Tmi* on **Fig. 4.1** and **4.11**), has been assumed as the main source of magnetic anomalies, due to its extremely high susceptibility. The model has been started by taking a simple subsurface continuation of this block (directed straight downward to the basement rocks), also by simply determining its inclination and declination initially in line with the ambient magnetic field. Based on the local geological map, it has been considered that this intrusion is composed by Dacites and Basalts. To produce such a huge anomaly, the initial susceptibility should be close to the maximum value of basaltic rocks (ranged 250–180,000 $\times 10^{-6}$ SI (Table 1 of Hunt et al., 1995)), while the remanent magnetization has to be relatively low and in the permissible range of Koenigsberger ratio (Qn) of intrusive rocks (ranged 0.1–20 (Table 6 of Hunt et al., 1995)).

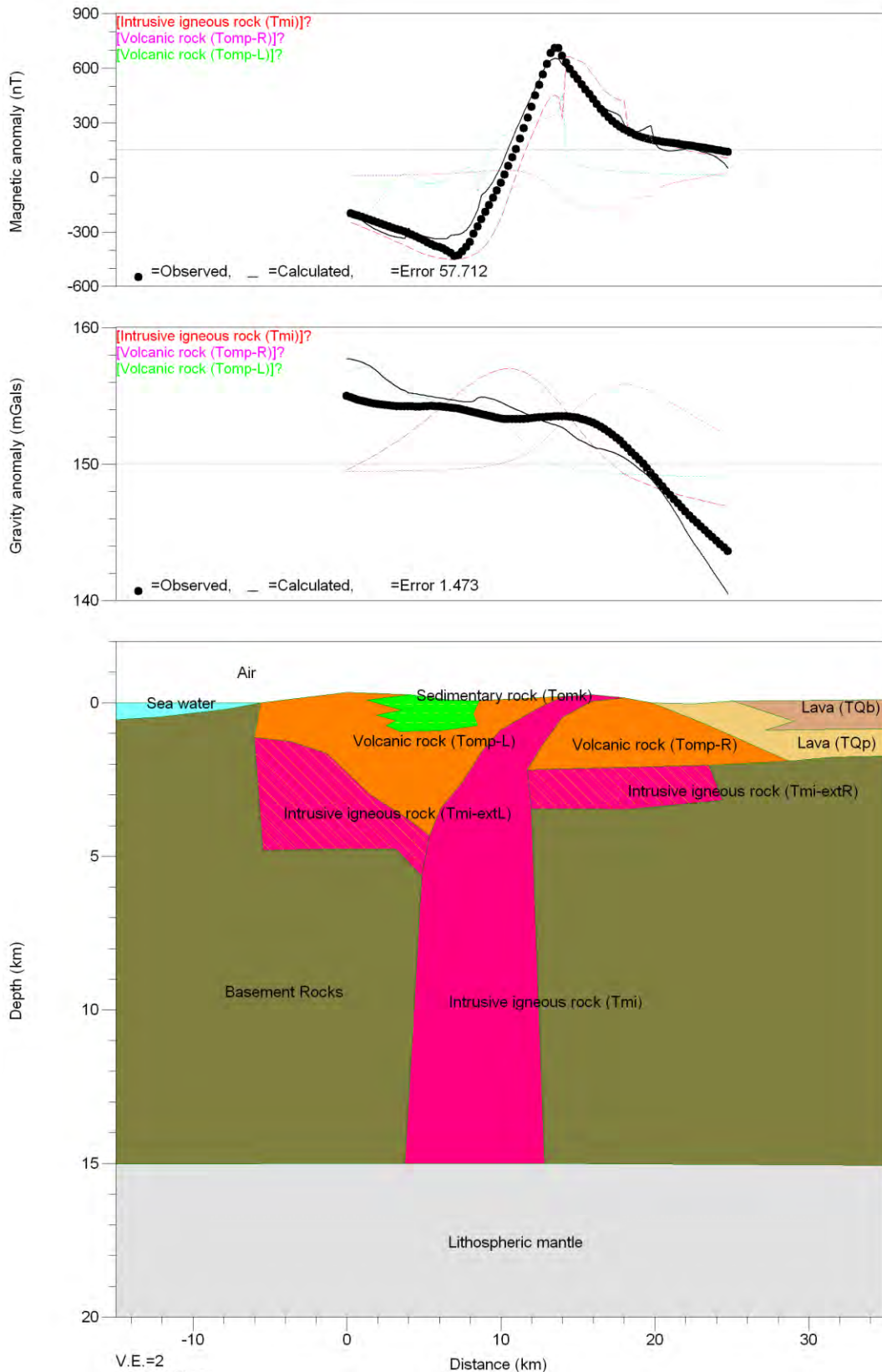


Figure 4.11 Comparison between modelled profile of P1-06 (black lines on top panels) and the profile of observations (black dots on top panels), using magnetic data of the 2006 survey and gravity data of Sukardi (1979). The individual responses of the blocks can be seen as the coloured lines, explained by the legend on the left top of top panels. This model assumes intrusive igneous rock (*Tmi*) and volcanic rocks (*Tomp-R* and *Tomp-L*) as the main sources of magnetic and gravity anomalies in the southern area.

The inclination and declination values then have to be adjusted, in combination with magnetization intensity, to get the desired responses. Changes of the declination only affect the anomaly amplitudes and have no effects on the shape of the response signal. Therefore the initial value of declination will always be kept in all of the magnetic models. Changes in the inclination of the magnetization only affect the response signal on the right side of the block. In other words, the negative part of the anomaly signal could only be fit by shifting the block to the left (as seen in the dashed red curve of **Fig. 4.11**), and getting a significant decrease of the RMS error (from initially 348 nT down to about 150 nT).

To improve the fit to the anomaly signal, contributions of other nearby rocks have to be taken into account. Volcanic rocks typically have strong remanent magnetization. After considering the geological map, two blocks of volcanic rocks have been modelled on both sides of the intrusive rocks, labelled as *Tomp-R* and *Tomp-L* on **Fig. 4.11**, representative of surrounding volcanic rocks (labelled as *Tomp* on the geological map of **Fig. 4.1**). For these blocks, some low values of susceptibility (i.e. $1,000 \times 10^{-6}$ SI) and relatively high values of remanent magnetization intensity have been taken, but still the relationship between both values in the permissible range of Koenigsberger ratio (Qn) of volcanic rocks (ranged 30–50 (Table 6 of Hunt et al., 1995)) has to be kept. Their inclinations then have to be adjusted to a value which provides the lowest error; note that both inclinations must be equal, regarding the same age of their geological formations.

With the above described approaches, the total response shape (black curve of **Fig. 4.11**) already agrees with the observed curvature (black points of **Fig. 4.11**). At this step, the RMS error has been reduced to about 130 nT, without reaching yet the expected limitation of misfit (the RMS error should be less than 10% of the peak to peak anomaly, i.e. about 120 nT). Then, adjustments of the lowest ends of both volcanic blocks (their lowest boundaries to the basement rocks) lead to significantly reduced errors. Further decreasing of errors could be reached by introducing lateral extensions of the intrusive rock, representing the sills on the right and left sides (labelled as *Tmi-extR* and *Tmi-extL* on **Fig. 4.11**). The possible occurrence of such sills is supported by the geological map of **Fig. 4.1**, regarding the occurrence of many small intrusions in the surroundings.

After applying those approaches, the RMS error has been reduced to about 80 nT (better than the expectation, actually), but with still considerably bothersome ripples at both peaks of negative and positive anomalies. Although they are below the possible resolution given by the magnetic station density, a smoother response of the negative anomaly is aimed for. Therefore the contribution of a surficial sedimentary rock (labelled as *Tomk* on **Fig. 4.1** and **4.11**) is considered, which was underestimated before. This block, as described by the geological map, could be considered as Sandstone with mean susceptibility value of about $10,000 \times 10^{-6}$ SI (Table 1 of Hunt et al., 1995). Its inclination and declination is assumed to be the same as those of volcanic rocks (*TompL* and *TompR*), due to the same age of their geological formations. By adjusting its remanent magnetization intensity in the permissible range of Koenigsberger ratio (Qn) of average sedimentary rocks (ranged 0.02–10 (Table 6 of Hunt et al., 1995)), a smooth negative anomaly peak has been achieved.

In fact, the magnetic anomalies model, although reaching such a very low RMS error, as a stand alone one is not enough to ensure the reliability for a more complex model. Therefore, the gravity modelling is expected to be the suitable complement. In the gravity modelling, the density of each block has to be determined in order to match the observed gravity signal. Several references composed based on on-site measurements are used in determining the suitable ranges of rock densities, then the

buoyancy principle is followed to determine the exact density of each block. It means that only lighter masses can well up and intrude the denser masses.

Since the Bouguer gravity anomaly is used (instead of free air gravity anomaly), according to the user's guide of the GM-SYS gravity modelling, the density of the air has to be set to the same value as the applied Bouguer correction of the used data. It is set to 2670 kg.m^{-3} (Sukardi, 1979). Then the density of the lithospheric mantle is chosen as the high value of 3300 kg.m^{-3} , in contrast to the sea water with a lower value of 1030 kg.m^{-3} (Table 1 of Blakely, 2005). The basement rocks are assumed to be metamorphic rocks which have the average value of 2760 kg.m^{-3} (Table 1 of Hunt et al., 1995); while the volcanic rocks are of some lower density (2750 kg.m^{-3}) but they are still denser compared to the normal crust (2670 kg.m^{-3}). The sedimentary rock, as a product of decomposition and sedimentation processes of the volcanic rocks, should have a lower density than its basic materials (i.e. the density of the sedimentary rock should be less than that of the volcanic rocks, given as 2700 kg.m^{-3}). Finally, the intrusive bodies have to be lighter than the mantle and the basement rocks, but having not too much contrast with the older volcanic rocks. This is the reason that not all intrusions could reach the surface but also intrude laterally and appear as some sills. These intrusive bodies are considered as porphyry (based on on-site drilling²⁶) and having a density of about 2740 kg.m^{-3} (Table 1 of Hunt et al., 1995).

Carefully adjusting the detailed shapes of intrusive rock and its bounding to the volcanic rocks both on the right and on the left leads to a smoother positive magnetic anomaly peak, hence minimizing the RMS error to the very low value of about 57.7 nT (less than 5% of the peak to peak anomaly) for the magnetic anomalies model and 1.5 mGal (about 10% of the peak to peak anomaly) for the gravity model.

All initial parameters for the P1-06 model and its magnetic as well as gravity properties are given in **Table 4.1** of **Appendix C**. Some lavas appear in the most right side of this profile (following the geological map), but actually they do not influence both magnetic and gravity responses. For this reason, their parameters are not included in **Table 4.1**. In a different manner, the Eclogite crust of the deeper structure (100 km below P1-06) is considered as of very high density (Anderson, 2007; Fowler, 2005; Blakely, 2005) and influences the gravity response a little. However, it does not influence the magnetic response due to its non magnetic materials.

4.2.2 P1 model (the southern area using the 2007/2008 survey results)

Principally, the modelling steps are the same for the P1 model as for the P1-06 model. The main structures are also similar and have identical magnetic and gravity parameters, considering continuity in geological settings of both profiles (see **Fig. 4.1**). In comparison to the P1-06 profile, the magnetic profile of P1 has nearly the same direction (azimuth) and shares the same strike. It has double the length and crosses P1-06 profile about its middle. Whereas the geological profile for the P1-06 model has been shifted landward, that of the P1 model is settled to accommodate the more complex structures on the most southern-end (left side) of the profile. All initial parameters for P1 model and its magnetic as well as gravity properties are given in **Table 4.2** of **Appendix C**. Below are some considerations in determining several parameters of the new blocks (which are not included in the P1-06 model).

²⁶ http://www.southernarcminerals.com/projects/lombok/west_lombok/geology/

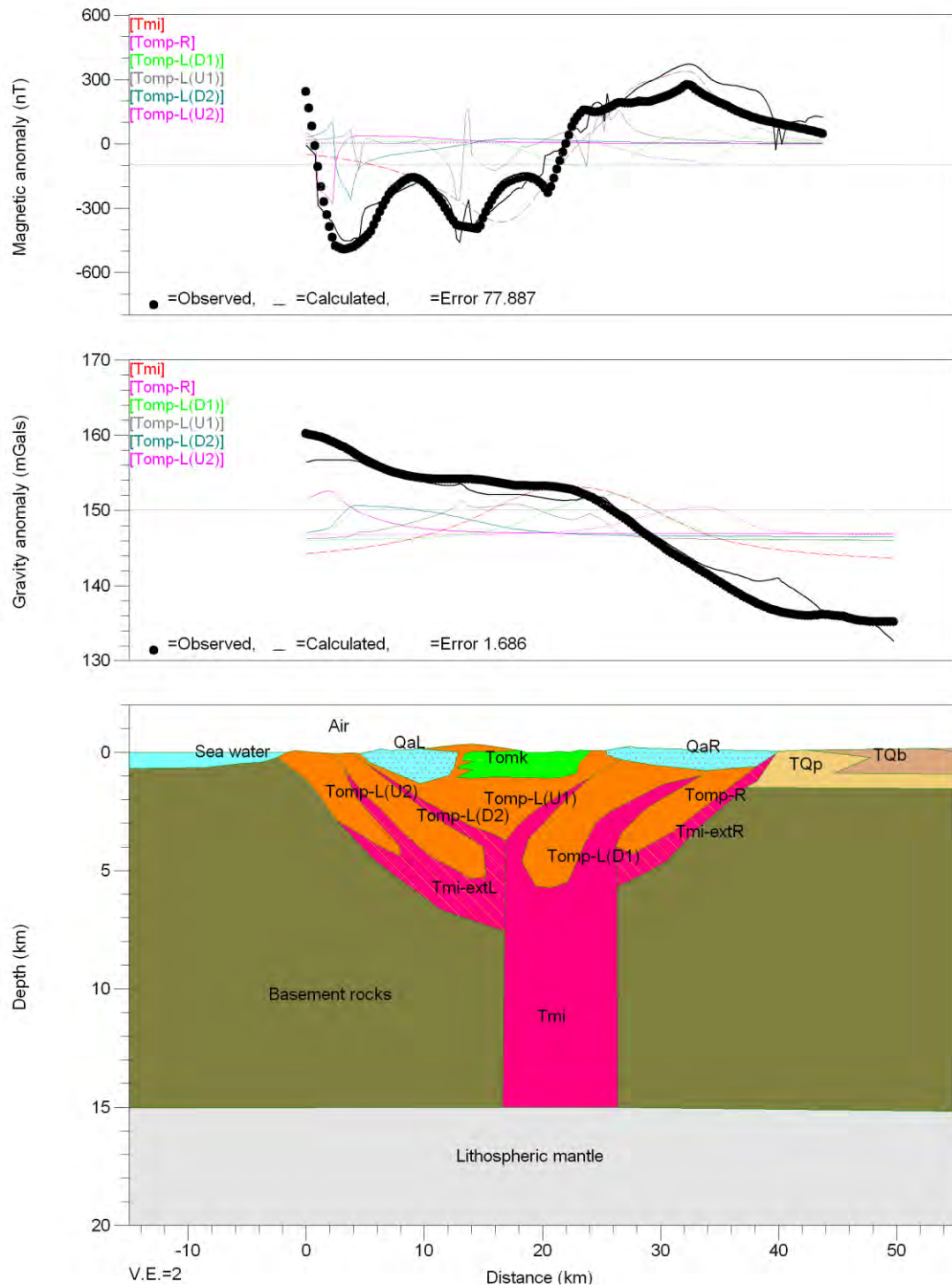


Figure 4.12 Comparison between modelled profile of P1 (black lines on top panels) and the profile of observations (black dots on top panels), using magnetic data of the 2007/2008 survey and gravity data of Sukardi (1979). The individual responses of the blocks can be seen as coloured lines, described by the legend on the left top of top panels. This model assumes intrusive igneous rock (*Tmi*) and volcanic rocks (*Tomp-R* and *Tomp-Ls*) as the main sources of magnetic and gravity anomalies in the southern area. The intrusive bodies appeared more intense than that of P1-06 (see Fig. 4.11 for comparison), splitting the left volcanic rocks (*Tomp-L*) into four separate structures.

Two alluvial structures (labelled as *QaR* and *QaL* on **Fig. 4.1** and **4.12**) are of un-cemented particles thus having no remanent magnetization. Both are also of low densities, having bulk densities ranging from 1500 to 2750 kg.m⁻³ (Brye et al., 2004). The alluvium on the left side (*QaL*) is denser and has slightly higher susceptibility than that of the right side (*QaR*), as the on-site samples indicate that it is very fine sand with dark colour which probably contains some iron ores. Contrarily, the alluvium on the right side (*QaR*) is coarse sands of normal coastal sediments which have been deposited due to wind blows and oceanic waves from the Lombok Strait. Its low density is therefore responsible for the low gravity on the right side of the profile.

Two lavas involved in P1 model (labelled as *TQp* and *TQb* on **Fig. 4.1** and **4.12**) are Tertiary lavas of Mount Rinjani, which were sequentially deposited. This fact is accommodated in the model by giving different inclinations (the specific reason will be discussed later in **Sec. 4.4.3**). The lavas are supposed to have moderate susceptibilities but high remanent magnetizations, in comparison to the lavas of other active volcanoes (Negro et al., 2002). *TQp* are calcareous breccias and lava, considered as common rocks with density of 2670 kg.m⁻³; while *TQb* are breccias and lava of denser materials than *TQp*.

The most noticeable difference between P1-06 and P1 models is that the intrusive bodies now break the volcanic rocks more intensively, especially in the left side. The sills come into several smaller intrusions which have upward shapes, possibly representing some minor intrusions over the surroundings. Many of them do not come up to the surface, but the most right intrusion (*Tmi-extR* of **Fig. 4.12**) is splitting the volcanic rocks from the basement rocks and the lava (*TQp*). The proper magnetic model could be achieved only by carefully adjusting the detailed shapes of intrusive bodies and their bounding to the volcanic rocks along the profile. The significant known lineaments on the geological map, which cross over this profile (see **Fig. 4.1**), have been used to guide in placing the proposed intrusions. It leads to a much better fit of the model by following some ripples in the magnetic observations, especially in the negative part of anomaly. Finally, the RMS error can be minimized to the very low value of about 78 nT for the magnetic anomalies model and 1.7 mGal for the gravity model (i.e. both are less than 10% of the peak to peak anomalies).

4.2.3 P2 model (the northern area using the 2007/2008 survey results)

The modelling steps of the P2 profile are slightly different from the former ones, since the strategy was to firstly resolve the gravity model before the magnetic one. This strategy has been proven as the more effective way in modelling some complex structures, as suggested by Anand et al. (2008). The known regional tectonic settings are the main constraints for the gravity modelling. Moreover, the reasonable geological chronology and related geomechanical tendencies (that will be discussed later in **Sec. 4.4.3**) should be considered to construct a reliable stratigraphy. Another constraint is the compatibility to the former models. For example, two Tertiary lava structures of the P1-06 and P1 models (*TQp* and *TQb*) have to be continued through this model (see the geological map of **Fig. 4.1**); thus they should have identical magnetic and gravity parameters as the former ones. However, new layers of one km thick lower sedimentary rocks have been proposed to be involved in this model. They are supposed to be deposited (above the basement rocks) before the formations of *TQps* and *TQbs*. The time of their deposition was just after the termination of active magmatic Tertiary intrusions in the South (i.e. at the same time as the formation of intrusive rocks -*Tmis*- in the P1-06 and P1 model). These deposition activities have precisely filled the time gap in the geological sequences (as will be discussed later in **Sec. 4.4.3**).

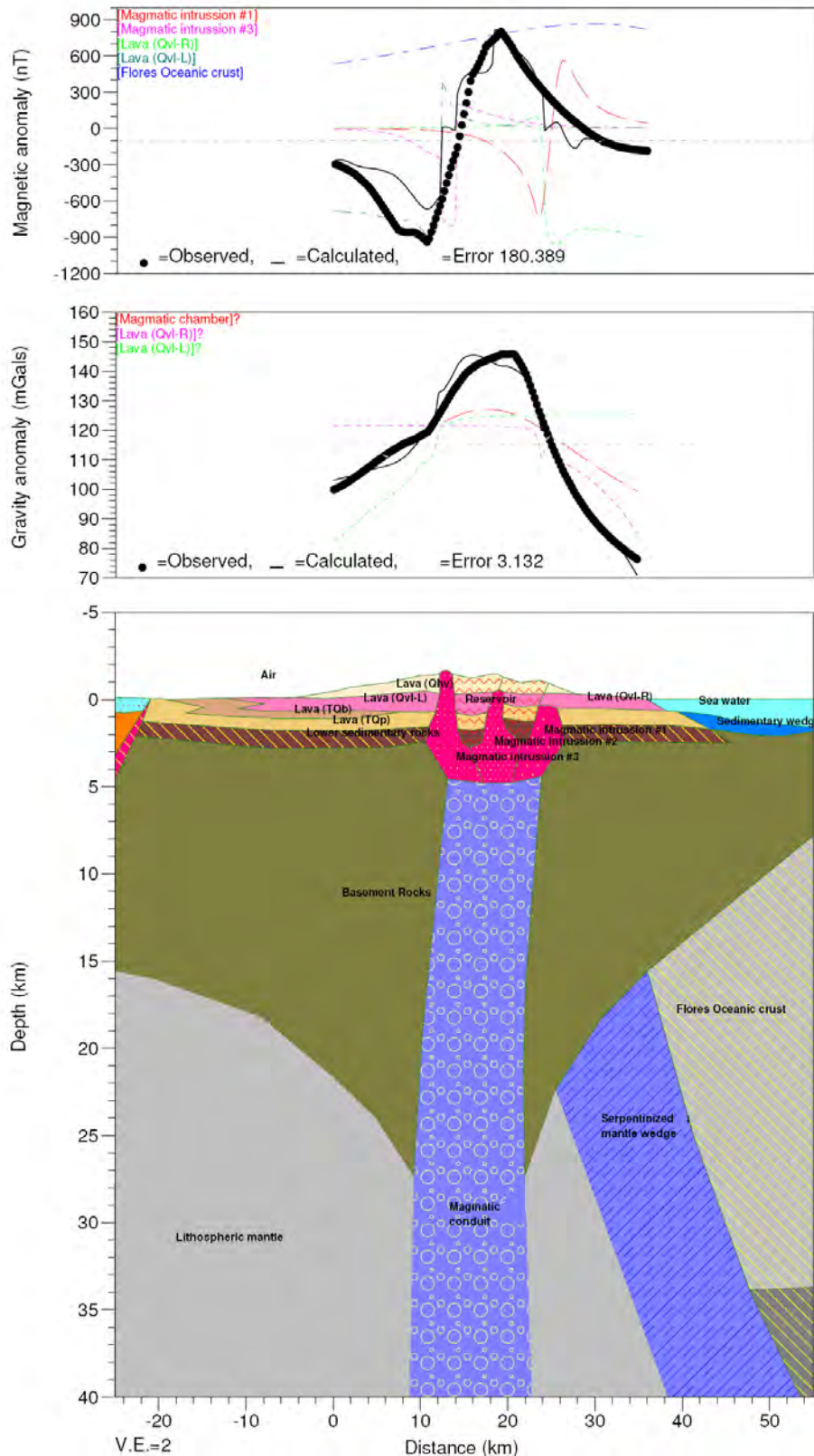


Figure 4.13 Comparison between modelled profile of P2 (black lines on top panels) and the profile of observations (black dots on top panels), using magnetic data of the 2007/2008 survey and gravity data of Sukardi (1979). The individual responses of the blocks can be seen as coloured lines, described by the legend on the left top of top panels. This model assumes magmatic intrusions (#1 and #3) and the pumiceous lavas (*Qvl-L* and *Qvl-R*) as the main sources of magnetic anomalies in the northern area, whereas the magmatic conduit and the pumiceous lavas are the main sources of gravity anomalies.

Other younger lavas of Mount Rinjani which were sequentially deposited in the Quaternary (labelled as *Qvl* (*-L* and *-R*) and *Qhv* on **Fig. 4.1** and **4.13**) are then modelled above the Tertiary lavas (*TQp* and *TQb*). Three magmatic intrusions are proposed as the driving mechanisms of accompanying lava depositions. A magmatic conduit is modelled directly below these intrusions until 90–180 km depth, considering the low *b-value* anomaly which indicates partial melting of the mantle just beneath the Mount Rinjani (Wandonu et al., 2004).

The *b-value* can be determined from the ‘Gutenberg-Richter law’ of magnitude-frequency relationship (Gutenberg and Richter, 1945), where a large value indicates that small earthquakes occur frequently, whereas a small value indicates that small earthquakes are not so frequent and the large earthquakes are more likely to occur (Fowler, 2005). A large *b-value* is typical of volcanic regions (Fowler, 2005) and could be associated with the zone of partially melted mantle and active magmatic conduits (Lin et al., 2008; Bridges and Gao, 2006; Sanchez et al., 2004; Wiemer and McNutt, 1997; Wyss et al., 2001; Murru et al., 1999).

Flores oceanic crust as well as its advanced eclogite and the corresponding serpentized mantle wedge are also modelled, but their contributions to the gravity and magnetic responses will be evaluated later. The convergence velocity along the Flores Thrust zone, revealed from the newest high resolution GPS measurements (Nugroho et al., 2009), is about 22 mm.yr⁻¹ relative to the back arc or the stable Sunda Shelf (Harris, 2009). If this velocity is considered constant through the time, then the north subducting slab (that has been initiated at 3 Ma) should be 66 km long nowadays. In the models, this fact is accommodated by the depth of the “hypothetical” Flores oceanic slab of 56 km, with some 10 km bending to the Lombok Island.

All initial parameters for P2 model and its gravity as well as magnetic properties are given in **Table 4.3** of **Appendix C**. Below are specific characteristics of the new structures.

Due to their old ages, the proposed lower sedimentary rocks are considered as compacted sediments with density of 2500 kg.m⁻³, a slightly higher density than the average sedimentary rocks (Table 1 of Hunt et al., 1995). *Qvl-L* and *Qvl-R* are pumiceous tuffs, laharic breccias and lavas that could be considered as Dacitic mixed pumices (Mangga et al., 1994) which are supposed to have very low density of about 750 kg.m⁻³ (Hahn et al., 1979 in Whitham and Sparks, 1986). On the other hand, *Qhv* is lava, breccias and tuff, which could be considered as the normal rocks with the average density of 2670 kg.m⁻³.

In modelling the deeper structures, the densities of each block regard the buoyancy principle as well as all related physical processes in a volcanic arc. Since the lithospheric mantle and the basement rocks beneath the Lombok Island should be considered as continuous structures, the same parameters as for the former models are used. The partially melted mantle and magmatic conduit are modelled with some lower (but still high) density than the original mantle. Three accompanying magmatic intrusions should have the same density as the intrusive igneous bodies of the former models (*Tmis* on **Fig. 4.11** and **4.12**). The Flores oceanic crust is modelled as a denser material than the basement rocks which enable the initiation of subduction processes. The advanced ongoing subduction is then represented by the eclogite crust, modelled at 35 km depth as a very dense material. The corresponding serpentized mantle wedge is water rich lithospheric mantle which is overlying the eclogite crust that can be modelled as material with slightly lower density (Blakely, 2005). By applying all above parameters, the shape of the high gravity anomaly response can be reconstructed, mainly from the contributions of the high density magmatic conduit and the very low density pumiceous lavas.

Now, the modelling of magnetic anomalies is started. As in the previous models, both Quaternary lavas have moderate susceptibilities, but their remanent magnetizations should be less than that of the Tertiary ones (TQp and TQb). Here, Qhv is considered of the lowest magnetization, due to its young age. On the other hand, the susceptibility and magnetization of the partially melted mantle are set to zero, considering its magnetic instability in high thermal conditions above the Currie temperature. Two of magmatic intrusions (numbered as #1 and #3 on **Fig. 4.13**) are of the same magnetization as, but of lower susceptibility than, the Tertiary intrusions ($Tmis$ in the former models). Contrarily, the middle magmatic intrusion (numbered as #2 on **Fig. 4.13**), is of very low susceptibility and very low remanent magnetization. It is considered as an active (present day) geothermal conduit.

The geothermal activities in this location are moderate (Sundhoro et al., 2000; Hadi et al., 2007a; Hadi et al., 2007b; Johnstone, 2005), manifested by hot and cold springs (see geological map of **Fig. 4.1** for the locations). In this model, the geothermal fields are accommodated as reservoirs of some lava structures (streaked with undulated red lines and marked as *Reservoir* on **Fig. 4.13**). Over this reservoir, the lavas should have higher densities (compared to the equivalent lavas of surroundings) due to saturated water infiltrations. The topmost lava (Qhv) is an exception, since it has been considered as the overburden layers (Fig. 4 and 5 of Sundhoro et al., 2000; Fig. 11 of Hadi et al., 2007a). It means that Qhv is considered as a 'waste' layer, containing soil and ancillary material which lies above the area of economic or scientific interest.

Demagnetization processes normally occur on a geothermal reservoir (Hochstein et al., 1997) and significantly reduce the susceptibilities and magnetizations to very low values. Following the classification of Hochstein et al. (1997), the geothermal fields of Mount Rinjani are considered as the complex patterns of Type C, so that the low resistivity anomaly data (obtained from the compilation map of Fig. 14 of Hadi et al. (2007a)) can be used to localize the demagnetization areas. By modelling this reservoir, the RMS error of gravity model could be reduced significantly, but the magnetic responses are still not satisfying.

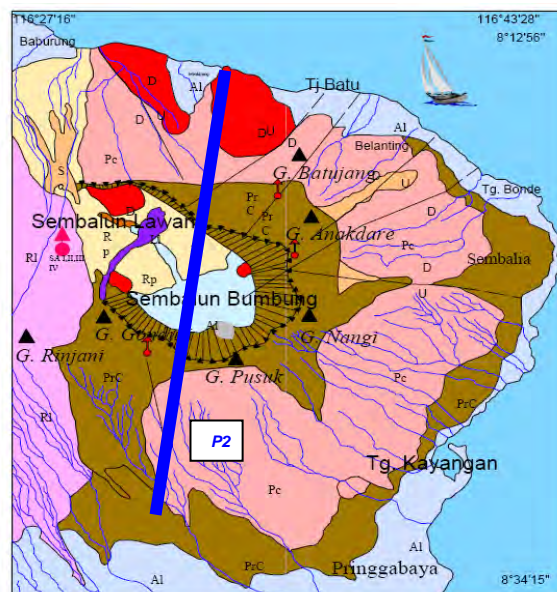


Figure 4.14 The detailed geological map of the Mount Rinjani range area (adapted from Fig. 2 of Sundhoro et al., 2000). The significant known faults are used to guide up- and down-layering of the proposed stratigraphy. The P2 profile is shown as blue line.

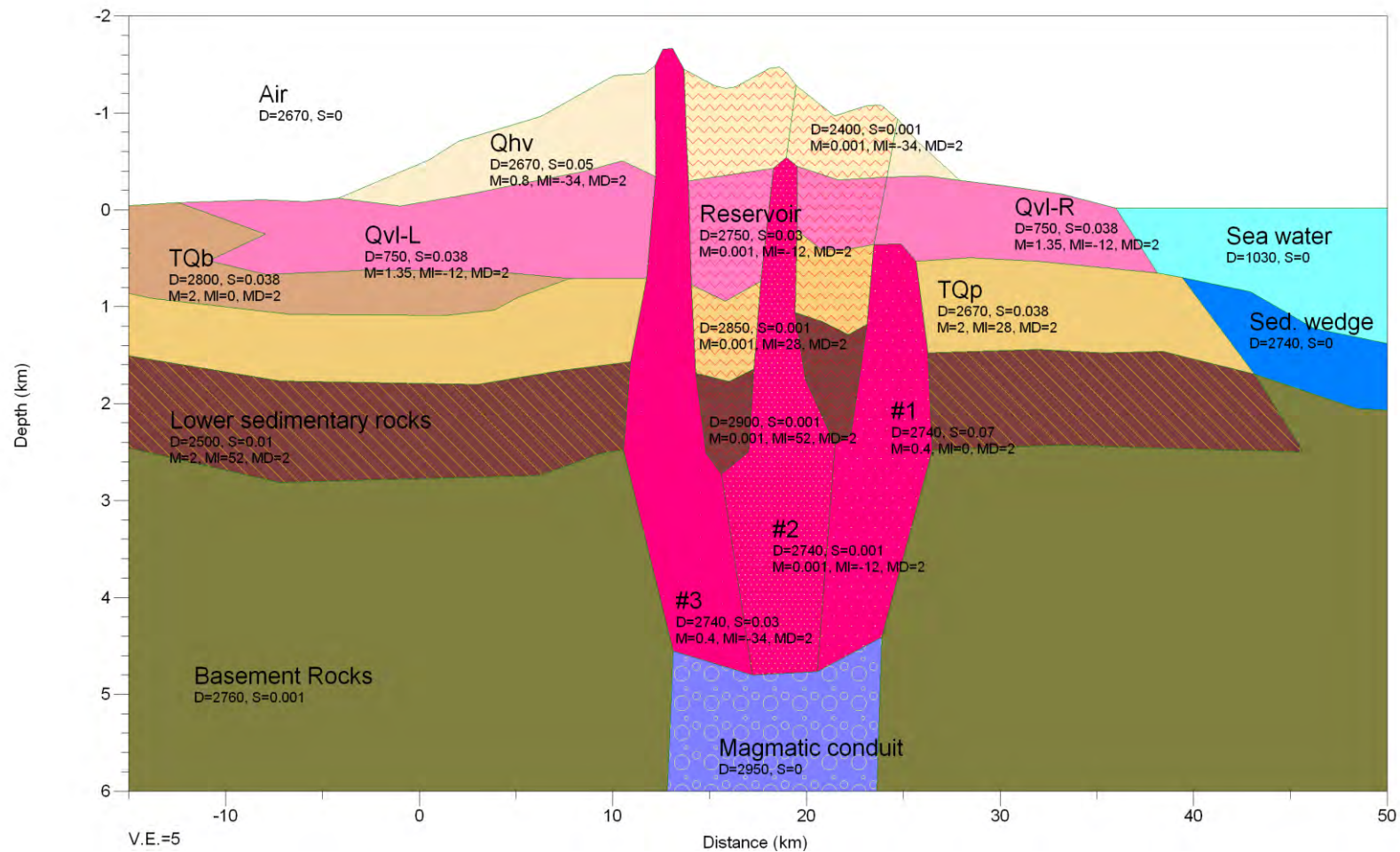


Figure 4.15 The details of stratigraphy and geothermal reservoir of the P2 model, accompanied by the gravity and magnetic properties of each layer.

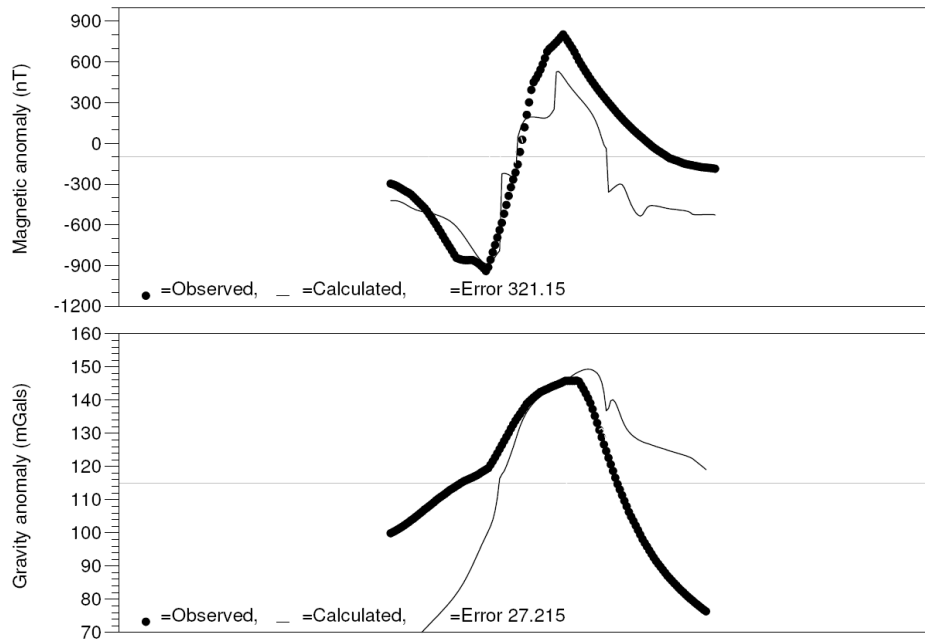


Figure 4.16 The responses of magnetic and gravity models of P2 without Flores oceanic subducting crust contributions. The positive magnetic response is shifted to a lower level and the equilibrium of the gravity response is also disturbed.

The proper magnetic anomalies model can be achieved only by carefully adjusting the detailed shapes of magmatic intrusions and precisely evaluating the layering scheme of the lavas. The significant known faults on the detailed geological map of this area (**Fig. 4.14**, adapted from Figure 2 of Sundhoro et al., 2000) have been used to guide in placing up- and down layering of the proposed stratigraphy. The compatibility between this stratigraphy and related geological sequence (discussed later in **Sec. 4.4.3**) is therefore aimed for. All efforts lead to much better fits of the gravity and magnetic models, especially in the positive part of anomaly. **Figure 4.15** shows the details of stratigraphy and the reservoir model, accompanied by the gravity and magnetic properties of each layer. Finally, the RMS error can be minimized to the very low value of about 180 nT (about 10% of the peak to peak anomaly) for the magnetic anomalies model and 3.13 mGal (less than 5% of the peak to peak anomaly) for the gravity model.

As stated before, the contributions of Flores oceanic crust as well as its advanced eclogite and the corresponding serpentized mantle wedge will also be evaluated. In the above magnetic model, the Flores oceanic crust and the serpentized mantle have been included and considered as two materials with high magnetizations but very different inclinations, in contrast to the eclogite crust which is a non-magnetic material. If the subduction process of the Flores oceanic crust is excluded from this model, then the positive magnetic response is shifted lower. The magnetic model can not fit the observation anymore, and the RMS error is larger (about 321 nT, i.e. 18% of peak to peak anomaly). Moreover, the equilibrium of the gravity response is also disturbed, since the very dense mantle has to take over the emptied spaces left by the oceanic crust, resulting in a very high gravity anomaly on the right side of the profile. Without the contributions of Flores subducting oceanic crust, the RMS error of the gravity model reaches about 40% of peak to peak anomaly, as depicted in **Fig. 4.16**.

4.3 Modelling of the geomagnetic temporal characteristics

The geomagnetic changes are modelled by taking the geological structures of the P1-06 profile (as of **Fig. 4.11**), but using the 2007/2008 survey data (as of **Fig. 3.4**). Along this profile, as depicted in **Fig. 3.7**, the secular variations between two consecutive surveys, as given by the 10th generation of IGRF values (IAGA WG V-MOD, 2005; Maus et al., 2005), are only over a narrow range of -17.00 to -17.15 nT. Since it is impossible that the magnetic as well as gravity parameters have altered significantly during a one year interval, little distortions in the block shapes are the most reasonable source for the observed changes. Some earthquakes which happened during the time interval between the 2006 and the 2007/2008 surveys (dated November 26th 2006–March 31st 2008) could be the reasons for this option.

One hundred earthquake events (eight of them with magnitudes more than 5 RS) occurred around 300 km from the Lombok Island to the depth of 120 km, as plotted on **Figure 4.17**. The most significant earthquakes (M 5.5–6.5) are shallow earthquakes over the north of Sumbawa Island. These earthquakes were close and strong enough to trigger some displacements in the brittle soil structures, including the rocks and sediments of the modelled P1-06 profile (red line of **Fig. 4.17**). Moreover, four of these earthquakes happened during the beginning of the 2007/2008 survey days. As reported by USGS²⁷, the historic moment tensor solutions of these events are of normal faulting.

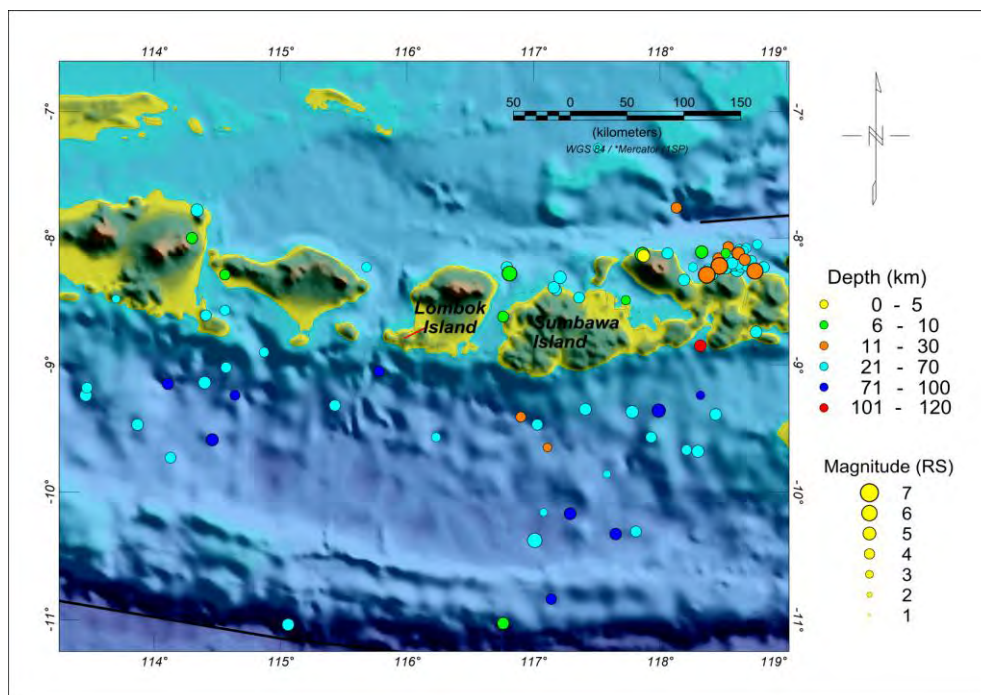
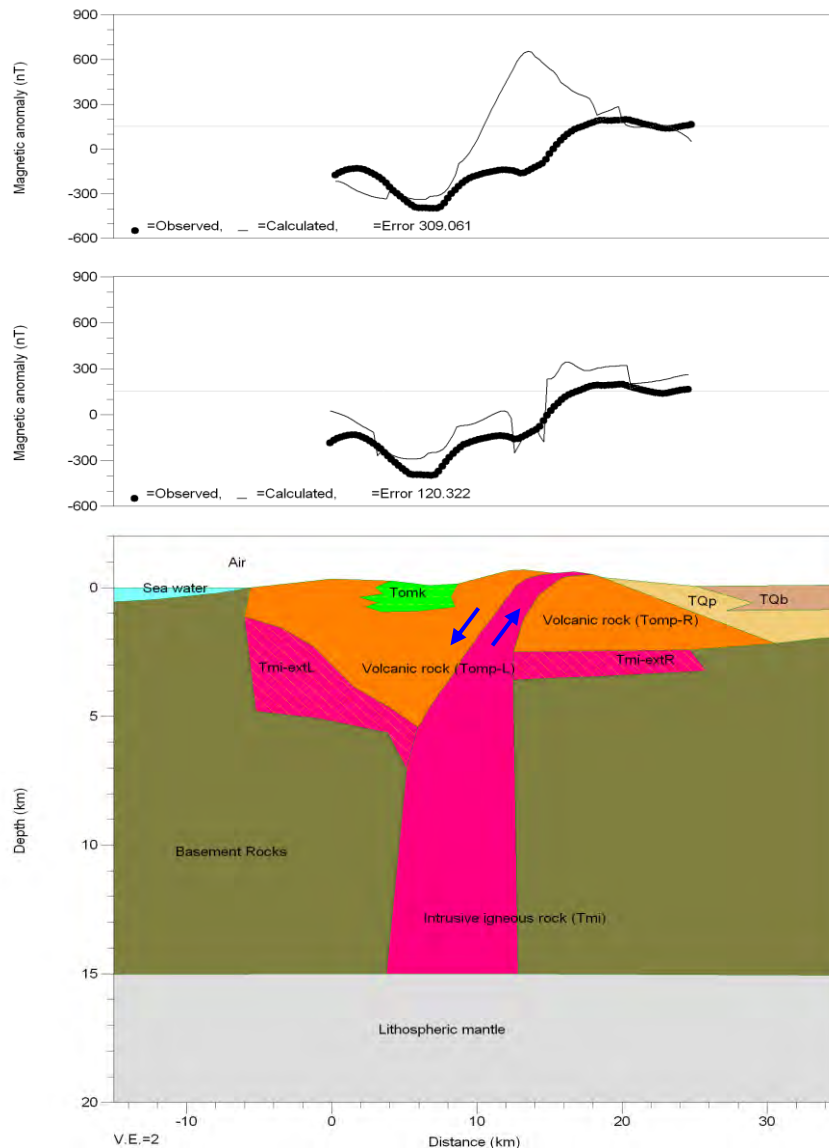


Figure 4.17 Earthquake events around 300 km from the Lombok Island to the depth of 120 km in the time interval between the 2006 and the 2007/2008 surveys (dated from November 26th 2006 to March 31st 2008). There were 100 events; eight of them are with magnitudes more than 5 RS. The modelled P1-06 profile is depicted as a red line. The most significant (M 5.5–6.5) are shallow earthquakes over the north of Sumbawa Island (on the upper middle right of this Figure); four of them happened during the beginning of the 2007/2008 survey days.

²⁷ http://neic.usgs.gov/neis/eq_depot/2007/eq_071125_kda6/neic_kda6_m.html

The model then accommodates the above facts by assuming that the energy was radiated to the location of P1-06 profile, causing upwards movement of the blocks on the right side (north part) in contrast with downward movements of the left side (south part) of the profile. The modelled strike is along the bounding between the left volcanic rock (*Tomp-L*) and the main intrusive body (*Tmi*). However, these movements should not drastically change the surficial structures, since no significant damages have been reported for the area along this profile.

Figure 4.18 shows the resolved model of the geomagnetic changes for the P1-06 profile. Since only the principal driving mechanism is desired to be known, in resolving this model, only the similarities in trend should be fit and short wavelength anomalies do not all have to be resolved. The final proper response can be achieved only by adjusting the left volcanic rock about 500 m downward and the igneous intrusive rock about 50 m upward. The achieved model, regardless of the unresolved short wavelength anomalies, is indeed not satisfying, because such large quantities of down- and up-ward movements have to be applied, while no noticeable surficial deformations are indicated at that location. Therefore, other mechanisms are expected to be the complements to explain these changes.



(Figure 4.18)

(Figure on the previous page)

Figure 4.18 The model of geomagnetic changes for the P1-06 profile. The profiles of observations are shown as black dots on two top panels, while the black lines on the first and the second top panel show the magnetic response signals before and after modelling, respectively. This model uses magnetic data of the 2007/2008 survey and gravity data of Sukardi (1979). The fits could be achieved by carefully adjusting up- and down ward movements of the blocks at the middle part of the profile, considering radiated energy from the significant earthquake happened during the beginning of the 2007/2008 survey days. The directions of the movements are symbolized with two blue arrows (see also **Fig. 4.11** for comparison to this model).

4.4 Geological and tectonic interpretations

After resolving all significant profiles as well as the changes of the southern one, a possible interpretation in terms of geology and tectonics can be suggested. In the followings, each profile will be separately interpreted -firstly- for simplicity and clearance, but finally the overall model will be discussed in understanding the Lombok Island region comprehensively.

4.4.1 Interpretation of P1-06/P1 model and its changes

In the P1-06 and P1 models, the intrusive rock formations (*Tmi* blocks) in combination with Tertiary volcanic rocks (*Tomp* blocks) are considered as the main sources of the magnetic anomaly in the southern area of the Lombok Island. These intrusions might be related to the subduction processes on the Java Trench; about 315 km south of the centre of intrusions (Kopp and Flueh, 2007). On this convergent margin, the Australian plate subducts beneath the Eurasian plate, resulting in compressional faults with directions normal to the Java Trench (Kopp et al., 2006). Moreover, from the best documented tectonic regime for the Lombok Island and circumference regions (segment 3 in Fig. 7 of Špičák et al., 2007), all 19 earthquake events in 1977 show normal faulting (no strike-slip) with very homogeneous positions of nodal planes parallel to the trench.

In the P1-06 model, a possible tectonic interpretation can be inferred from the differences of the depth extensions of the volcanic rocks, with the left block reaching about 0.5 km deeper than the right one. The volcanic rocks (i.e. the oldest formation on the Lombok Island, which formed in the Late Oligocene to Early Miocene) can be assumed to be a direct product of the Java Trench subduction, and therefore initially a single continuous structure. Discontinuities in the local geological structures occurred later, by intruded igneous rock in the Middle Miocene, as a result of a continued subduction on this region. A subsurface normal faulting could then be assumed, regarding the relationship between volcanic rocks on the left side (*Tomp-L* of **Fig. 4.11**) and the volcanic rocks on the right side (*Tomp-R* of the same figures), corresponding to the hanging wall and the footwall (i.e. *Tomp-L* moves downward relative to *Tomp-R*).

In the advanced P1 model, more complex up and down normal faults (like graben and horst structures) are considered for the intrusion. All of these faults follow some certain paths which are the bounding of the intrusive rock to the volcanic rocks, but the most intense one occurs exactly in line with the inferred fault of P1-06 profile. Another fact that should be considered is the magnetic ripples in the most southern end of P1 profile which tend to some higher positive anomaly value. This is also consistent with the positive anomaly values of adjacent measurement stations over the south-western end of the overall volcanic rocks (see **Fig. 3.4**), opening a possibility to consider this part as a distinct volcanic structure. It means that a secondary subsurface normal fault might be found there.

It can be summarized that the P1-06 and P1 models, both of them, suggest the possible existence of the main subsurface normal faulting in the southern area of the Lombok Island. Moreover, the P1 model underlines a possible secondary subsurface normal fault. These faults might also be considered as a potential trigger for local tectonic earthquakes in this region. As has been discussed through analyzing the geomagnetic changes over this region (see **Sec. 4.3**), a remote strong earthquake could disturb the stability of the brittle structures of these profiles, hence accumulating more stress and leading to the ruptures. This interpretation agrees well with the known regional geological and tectonic structures. Note that the boundary between the negative and positive part of geomagnetic anomalies (red dashed lines next to the P1-06 and P1 profiles in **Fig. 3.2** and **3.4**), considered also as the strike directions of the suspected fault lines in the P1-06 and P1 models, are parallel to the known nearest surface lineament (red dashed line next to the P1-06/P1 profile in **Fig. 4.1**)

4.4.2 Interpretation of P2 and P3 models

In the P2 model, two magmatic intrusions (labelled as #1 and #3) can be assumed as the main sources of magnetic anomaly in the northern area of the Lombok Island, because of their high susceptibilities. The Tertiary and Quaternary lava layers (*TQp*, *TQb*, and *Qvl*) also contribute to this anomaly due to high remanent magnetizations and the inclination contrasts to the youngest lava (*Qhv*). On the other hand, the gravity anomaly along this profile could point out the existence of an active magmatic conduit below these intrusions due to its high density, in contrast with lower densities of the host rocks and very low density of the pumiceous lavas (*Qvl*).

The geothermal potential of this area that has been previously investigated (Sundhoro et al., 2000; Hadi et al., 2007a; Hadi et al., 2007b; Johnstone, 2005) is fully supported by the P2 model, by involving demagnetization processes for the presumed reservoir. This model can help in guiding the determination of geothermal reservoir depth, which could only roughly be estimated by the previous investigations (as deeper than 700 m, with about 1 km thickness). Getting the certain depth of the reservoir is very important, particularly when the geothermal potential is aimed to be explored intensively. If the magmatic intrusion #2 is considered as the geothermal conduit, the depth of reservoir is certainly about 800 m, with 2 km thickness (up to 2800 m depth).

Although the P3 profile is not modelled in detail, it could be deduced that up to 3 km depth the model should be similar with the P2 model, considering the similarity in the surficial structures (see the geological map of **Fig. 4.1**). However, for the deeper structures, both models should be different, since **Fig 4.9** and **4.10** show that the relationships between magnetic and gravity anomalies of the models are contradictive. The main difference is that the high gravity in the P3 profile is shifted rather to the South and followed by low gravity in the North. It probably indicates the shifting of the magmatic conduit to the South, but without accompanying demagnetization processes, since there is no evidence of geothermal activity on this area. On the other hand, the most prominent positive magnetic anomaly coinciding with low gravity in the North probably indicates the more extensive surficial distributions of pumiceous lavas (*Qvl*) in this area.

Over a regional scale, the P2 and P3 models could support the existence of the Flores oceanic subducting crust in the north of the Lombok Island, as well as its ongoing activities. However, the front of the subduction probably differs; reaching further South in the P3 profile (i.e. the Flores Thrust zone comes nearer to the west side of the Lombok Island).

4.4.3 Interpretation of the overall model

The overall model of the Lombok Island is constructed by combining the southern profiles with the northern ones. Here, the P1 and P2 models are considered as the most representative models of both areas. **Figure 4.19** shows the model, relating the Java Trench and the Flores Thrust zone, described as two oceanic subducting crusts flanking the Lombok Island in opposite directions. This figure is the present day tectonic setting of this region, which still leaves some questions about what happened in the past. To answer them, the tectonics and geological sequences of this Island from the Late Oligocene to the early periods of Holocene (28–0.01 Ma) are given chronologically through **Fig. 4.20** to **4.27**.

The tectonics and geological sequences of **Fig. 4.20** to **4.27** are reconstructed based on the regional tectonic evolution of South East Asia by Hall (2002) and the local geological map (Mangga et al., 1994). The global positioning system velocities of Nugroho et al. (2009) that have been accommodated in Fig.2 of Harris et al. (2009) are used to estimate the temporal positions of the subducting slabs (i.e. the depths and the distances of their past fronts to the present location of the Lombok Island). On those figures, the horizontal distances are the relative positions to the southern end of the P2 profile, refers about the middle of the present location of the Lombok Island. **Table 4.4** summarizes the sequential processes depicted on each figure.

In determining the time boundaries between two consecutive sequences, the geological time scale of Ogg et al. (2008) is applied. This time scale represents the decisions and recommendations of the International Commission on Stratigraphy (ICS), as ratified by the International Union of Geological Sciences (IUGS) through March 2008. The newest geological time scale which has been officially ratified by the IUGS on June 30th 2009²⁸ is not used in this study, to maintain terms equality with the used local geological map (Mangga et al., 1994). A critical difference between the two ratifications is about the exact limit between the Tertiary and the Quaternary periods, that is formerly established in 1983 as the base of the Calabrian stage (1.81 Ma), but currently is shifted to the base of the Gelasian stage (2.59 Ma). In this study, following the 'old' terms, the Pliocene still represents the ages of 5.33–1.81 Ma, and the Pleistocene of 1.81–0.01 Ma.

The events related to the sequences depicted on those figures are explained in the following.

The first sequence (depicted on **Fig. 4.20**) happened in the Late Oligocene (28 Ma), when a continuous basement rock was developed under shallow sea water. This thin basement rock is considered as an extensional part of the stable Sunda Shelf to the West, separating the Indian oceanic crust from the Flores oceanic crust by a distance of about 150 km. No magnetic and gravity anomalies existed at this early stage, due to its non-magnetic materials and considered flat surface (without reliefs).

Volcanic activity in this region started later, between the Late Oligocene and Early Miocene (28–10 Ma), as depicted in **Fig. 4.21**. The initiation of the Indian oceanic crust subduction in the South is considered as the driving mechanism of this volcanism. It happened at the beginning of this period, with its front located at about 60 km south of the activated volcanism. Whereas the Bali Island in the West has been completely formed at 15 Ma, at the present location of the Lombok Island there was still a continuous Tertiary volcanic rock (*Tomp*) interfingering with sedimentary quartz sandstone (*Tomk*). These rocks were built on an older arc crust under shallow sea water (less than 1 km depth). The first detected magnetic anomaly signal was

²⁸ <http://www.stratigraphy.org/view.php?id=23>

produced by these volcanic and sedimentary structures, given in the P1-06 and P1 models by their remanent magnetizations with inclinations of 17°.

While the paper of Hall (2002) has underlined the most dramatic events which occurred at the eastern end of the Java Trench at about 10 Ma, the geological sequences of the presented models underline the initiation of dacitic and basaltic intrusion (*Tmi*) in the Middle Miocene (between 10–7 Ma), as depicted in **Fig. 4.22**. The main normal fault of the southern area was then formed due to this intrusion, splitting the volcanic structure into two main parts (*Tomp-R* and *Tomp-L* of P1-06 model). These events resulted from a continuous subduction of the Indian oceanic crust in the South that had reached 87 km depth by that time. When this subduction reached 40 km depth, the advanced eclogite crust and its accompanying serpentinized mantle wedge began to form. Due to the lateral extension of the Sunda Shelf (including the Basement rock), the subduction front has been shifted 105 km away to the South, keeping a relatively steep angle due to its old age which is dated as old as Cretaceous (Hall, 2002). The volcanic and sedimentary rocks were for the first time raised above the sea level, while some part of the basement rocks in the Indian Ocean (that was formerly exposed) was then covered by the sedimentary wedge.

Since the subduction in the South still continued, reaching 145 km depth during the Late Miocene (7–5.33 Ma), more extensive dacitic and basaltic intrusions (*Tmi*) resulted in the southwest of the initial intrusion, as depicted in **Fig. 4.23**. The advanced up and down normal faulting as modelled in the P1 profile were seen. The subducting slab was elongated, forming more serpentinized mantle wedge and more melange.

As depicted in **Fig. 4.24**, during early period of the Pliocene (5.33–3.6 Ma), due to the deeper subduction in the South, the alluviums (*QaR* and *QaL*) were deposited as the “proto” Lombok Island was raised to higher altitude. Meanwhile, the partially melted mantle that had been raised to shallower depth in the previous sequence of **Fig. 4.23** (probably as a consequence of the ongoing subduction in the South), during this sequence was also shifted to the North, due to the compressional force of the Indian oceanic slab. Following the shifting of the partially melted mantle to the North, the volcanic and intrusion activities in the southern area then ceased. This event is recorded as the observed magnetic anomaly signal in the P1-06 and P1 models, given by the remanent magnetizations of intrusive igneous rock (*Tmi*) with inclination of 52°.

The above event was directly followed by the initiation of the Flores oceanic crust subduction in the North, dated around 3 Ma (Silver et al., 1983; Harris et al., 2009). This is a newly formed back arc trench, that probably resulted from the Indian oceanic slab break-off/roll back (Price and Audley-Charles, 1983), as a consequence of the ongoing continental collision between the eastern side of the Eurasian and the Australian continental crusts. The Flores Thrust (together with the Wetar Thrust in the East) then acts as the new boundary between the South East Asian and the Australian plates (Hall, 2002). This new subduction zone in the North (working together with the old one in the South) results in upwelling of partially melted mantle and generating new magmatic intrusions. The oldest lava was deposited over the Mount Rinjani range, filling the time gap on the geological sequences (before the depositions of exposed Tertiary and Quaternary lavas) precisely. This lava layer is characterized in the P2 model by the same inclination as the intrusive igneous rock (*Tmi* blocks) of 52°, due to the overlapping of their formation ages. Due to very intensive weathering processes through about a 1.5 Ma time interval in such tropical region, the oldest deposited lava layer was completely transformed to be a sedimentary rocks layer (labelled as *Lower sedimentary rocks* in the P2 model).

During middle period of the Pliocene (3.6–2 Ma), as depicted in **Fig. 4.25**, the north slab was further subducting to about 20 km depth. Due to the deeper and simultaneous subductions from both sides, the magma was again welling up, depositing the first Tertiary lava (*TQp*) with inclination 28° , covering the formerly deposited lava layer (which had been transformed to be *the Lower sedimentary rocks*). Immediately before the cessation of magmatic intrusion #1, a normal fault was formed in the north end of the lava structures (see the inset in **Fig. 4.25** (b) for clearer views of the near-surface structures).

Through the proposed tectonics and geological sequences, the process of lava depositions was followed by the formation of the ‘root’ in the bottom part of the basement rocks to maintain the isostasy. This root got deeper as the lava structures built a higher mountainous range above the Lombok Island. Notice also that the magmatic conduit shape was modelled not straight upward, but somehow deflected, considering the working geodynamical forces.

During the latest period of the Pliocene (2–1.81 Ma), deeper and simultaneous subductions were still working from both sides, accompanied with a bending of the north slab and the formation of its advanced eclogite crust as well as the associated serpentized mantle wedge. The north slab reached about 55 km depth and was bent due to the high solidity of the basement rocks. New upwelling of the magma then produced the second Tertiary lava (*TQb*), flowing only westward and southward (due to the local temporal terrains), as depicted in **Fig. 4.26**. Immediately after the deposition of this lava, the magmatic intrusion #1 ceased, recording the same inclination as the latest deposited lava layer (*TQb*) of 0° .

During the Pleistocene (1.81–0.01 Ma), the subductions from both sides simultaneously advanced, while sedimentary wedge and melange were intensively formed in the north coast of the Lombok Island. A new magmatic intrusion #2 was initiated, producing the first Quaternary lava of pumice (*Qvl*), flowing to all directions, as depicted in **Fig. 4.27**. The second normal fault was formed in the middle of the lava structures following this intrusion, with the down part in the South. After a complete lava deposition, this magmatic intrusion ceased, recording the same inclination as the last deposited lava layer (*Qvl*) of -12° . This is the first negative inclination that has been recorded through the proposed tectonics and geological sequences of the Lombok Island.

The last geological sequence happened in the Holocene (after 0.01 Ma), as depicted in **Fig. 4.19** and its enlargement of near surface structures in **Fig. 4.14**. The magmatic intrusion #3 was initiated, producing the second Quaternary lava (*Qhv*), flowing to all directions. After the last deposition of the lava layers, the third normal fault was formed in these lava structures (south of the previous ones). The magmatic intrusions over this area then ceased, recording the present day inclination of the Lombok Island region of -33.75° . The volcanic activity complex under the northern part of the Lombok Island was then shifted westward (to around the present location of the summit of Mount Rinjani) after this latest geological sequence. The shifting of the active part of this volcanic complex still took place during the last 10,000 years before the present caldera formation (Takada et al., 2003; Nasution et al., 2003). Geomechanical tendency of magma in intruding the weakest parts of the crust is the possible mechanism of this shifting (Nasution, *pers. communication*). The modelled area now becomes the oldest crater of the Mount Rinjani range.

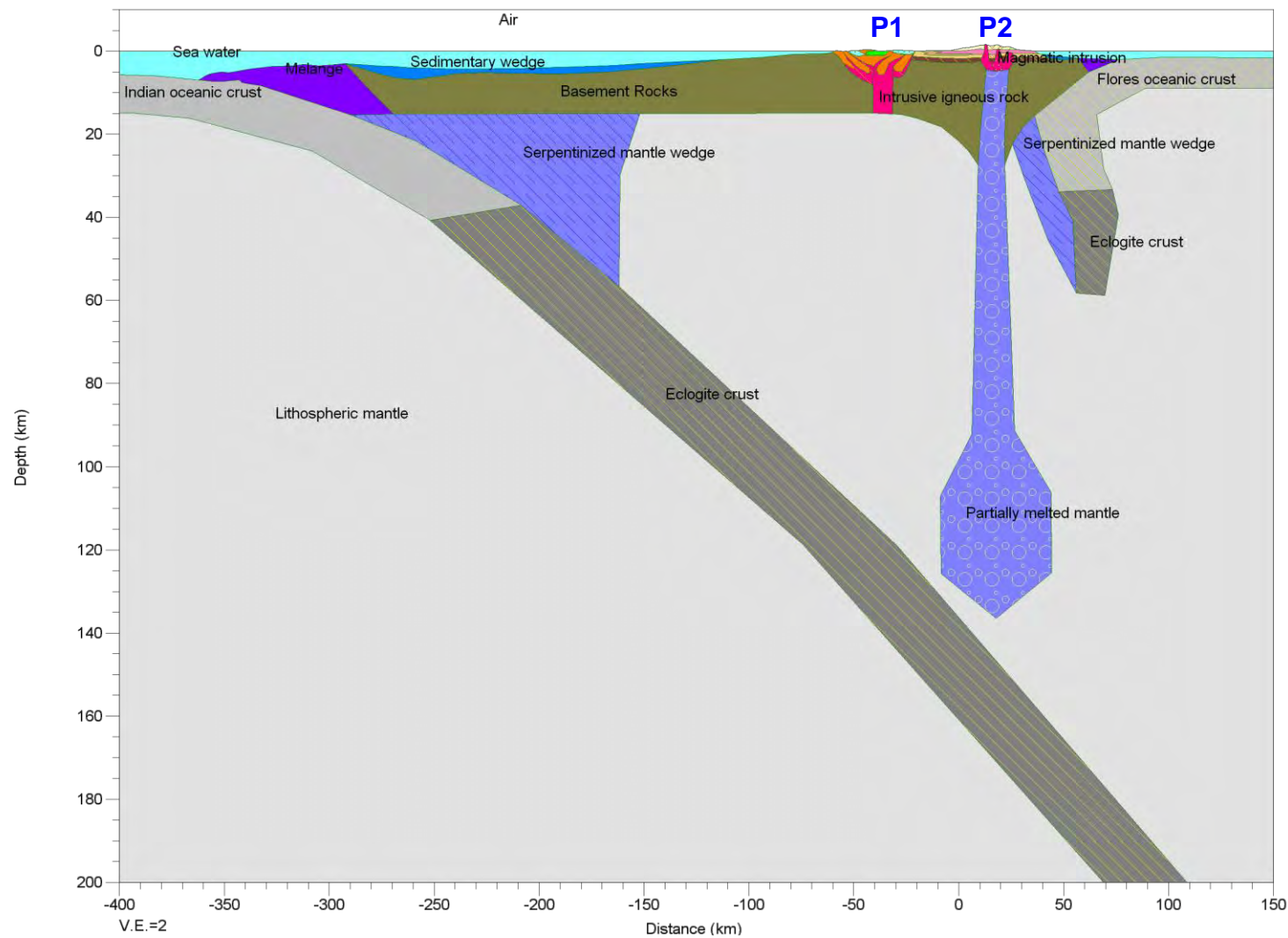


(Figure 4.19)

(Figure on the previous page)

Figure 4.19 The overall model of the Lombok Island, compilation of P1 and P2 models (Fig. 4.12 and 4.13), representing the present day tectonic settings of this region. The magnetic and gravity anomalies over the southern area are caused by the Indian oceanic crust which is subducting at the Java Trench (315 km south of the main intrusion of P1) and leading to the formation of volcanic rocks as well as intrusions of igneous rock structures. From the opposite direction, the Flores oceanic crust is subducting at the Flores Thrust zone (about 60 km north of the main intrusion of P2). The two simultaneous opposite subductions cause the magnetic and gravity anomalies over the northern area by upwelling of partially melted mantle and forming some lava structures.

Table 4.4 Summary of the modelled tectonics and geological sequence of the Lombok Island

Sequence	Time (Ma)	Events	Figure
Late Oligocene	28	Development of basement under shallow sea water	4.20
Late Oligocene– Early Miocene	28–10	Initiation of subduction and starting of volcanic activity in the South	4.21
Early Miocene– Late Miocene	10–7	Raising above sea level, dacitic/basaltic intrusion and the main normal faulting in the South	4.22
Late Miocene	7–5.33	Advanced dacitic/basaltic intrusion and formation of up and down normal faulting in the South	4.23
Early period of Pliocene	5.33–3.6	- Deposition of alluviums, ceasing of volcanism in the South - Initiation of subduction in the North, followed by first magmatic intrusion and lava deposition (later become <i>the lower sedimentary rocks</i>)	4.24
Middle period of Pliocene	3.6–2	Deeper subductions, deposition of the first Tertiary lava (<i>TQp</i>) and first normal faulting in the North	4.25
Latest period of Pliocene	2–1.81	Deeper subductions, deposition of the second Tertiary lava (<i>TQb</i>), transformation oceanic slab to eclogite and formation of serpentinized mantle wedge in the North	4.26
Pleistocene	1.81–0.01	Advanced simultaneous subductions from both sides, deposition of first Quaternary lava (<i>Qv</i>), second normal faulting in the North	4.27
Holocene	0.01–0.00	Active subductions from both sides, deposition of second Quaternary lava (<i>Qhv</i>), third normal faulting in the North. Active volcanic (new crater) and geothermal manifestation (old crater) in the North.	4.19

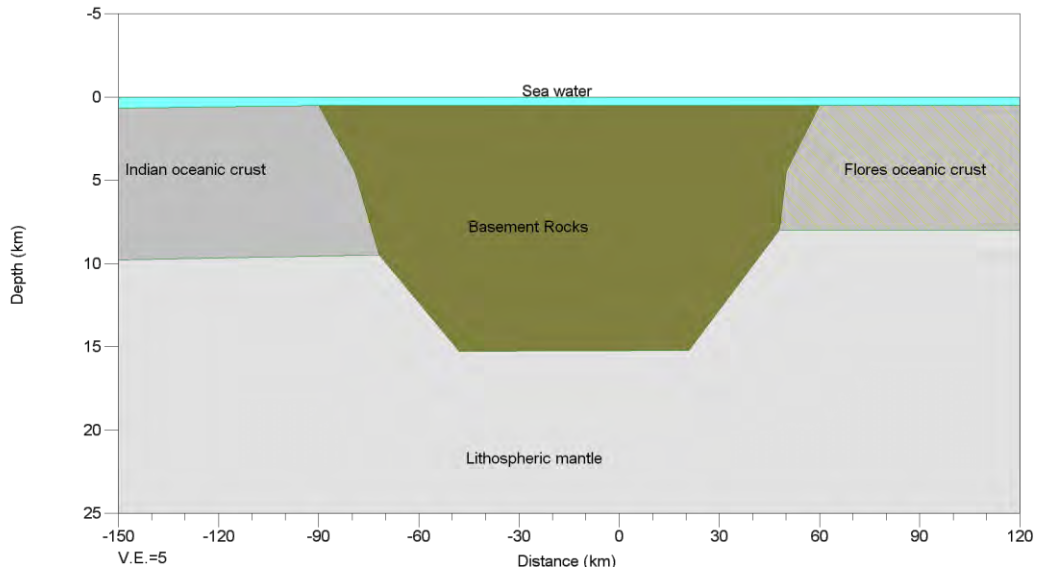


Figure 4.20 The tectonics and geological sequence of the Lombok Island in the Late Oligocene (28 Ma). A continuous basement rock was developed under shallow sea water. No magnetic and gravity anomalies are produced by geological structure at this early stage.

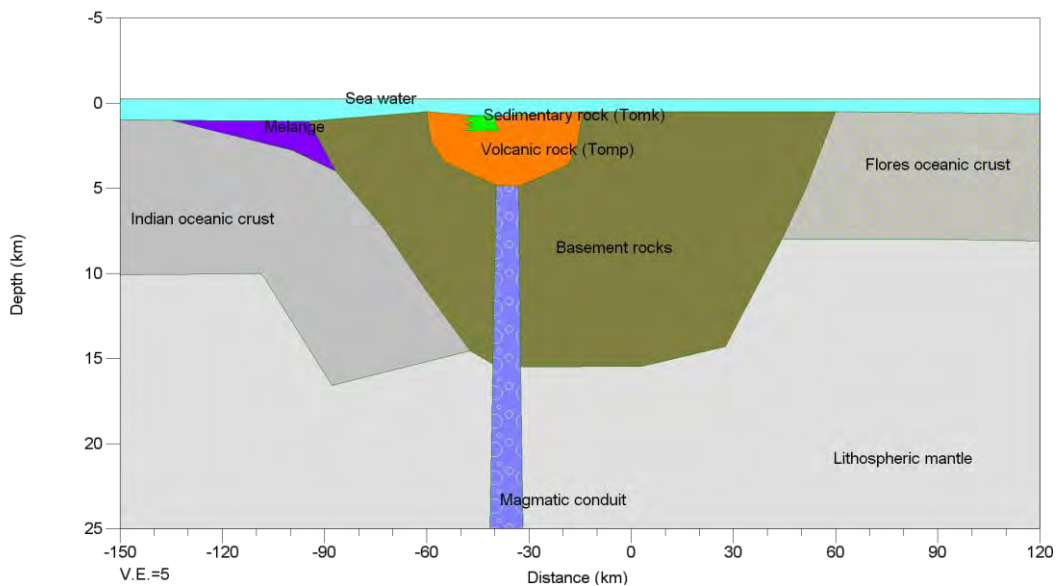


Figure 4.21 The tectonics and geological sequence of the Lombok Island between the Late Oligocene and Early Miocene (28–10 Ma). Volcanic activity was started, as the subduction of the Indian oceanic crust in the South was initiated. A continuous volcanic rock (*Tomp*) interfingered with quartz sandstone (*Tomk*) was built on an older arc crust under shallow sea water. The magnetic anomaly signal produced by these volcanic and sedimentary structures, is given in the P1-06 and P1 models, characterized by remanent magnetizations with inclinations of 17° .

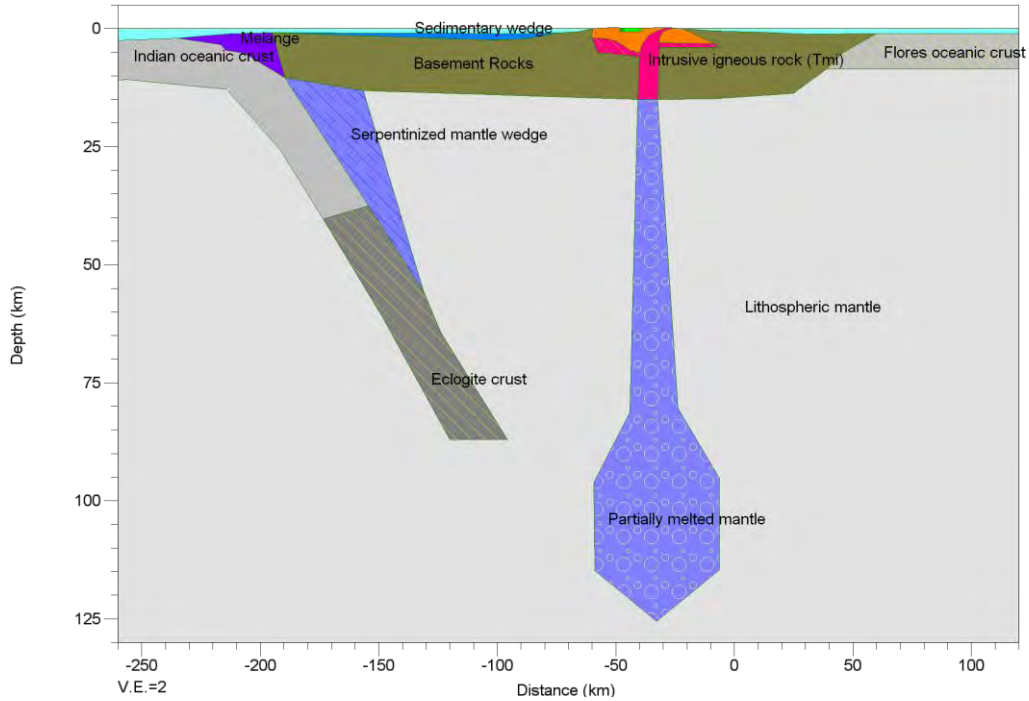


Figure 4.22 The tectonics and geological sequence of the Lombok Island between the Early and Late Miocene (10–7 Ma). Initiation of dacitic and basaltic intrusion (*Tmi*) resulted from a continuous subduction of the Indian oceanic crust in the South, while the volcanic and accompanying intrusion were for the first time raised above the sea level, and the main normal fault was formed, as seen along the P1-06 profile.

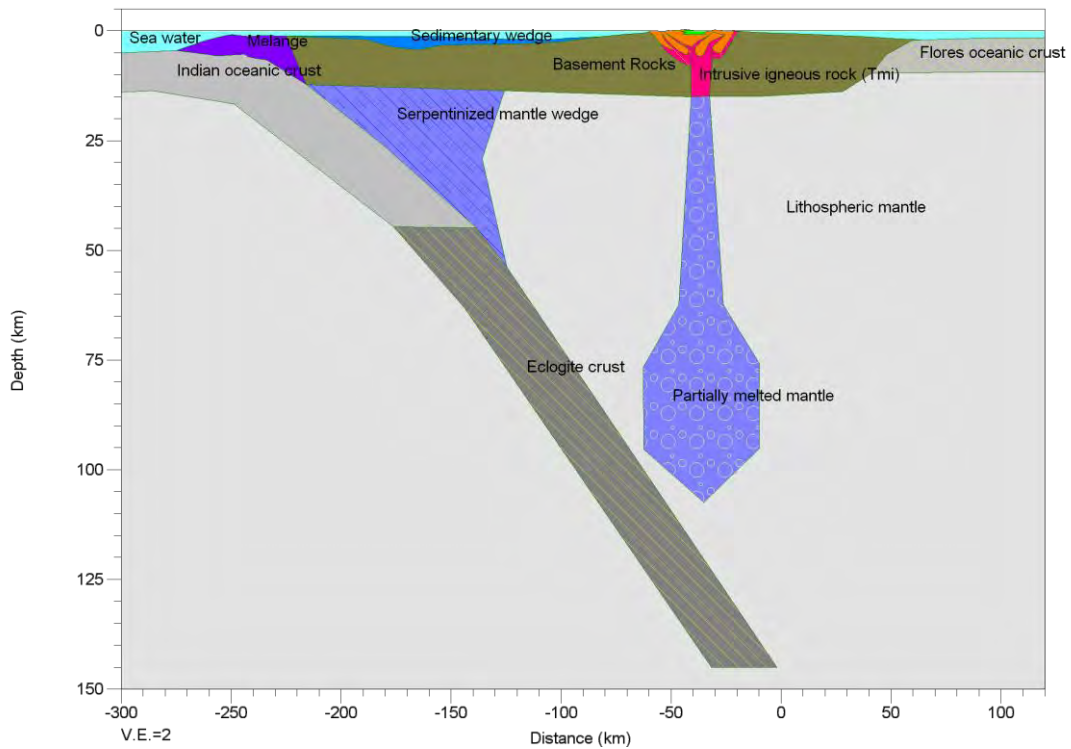
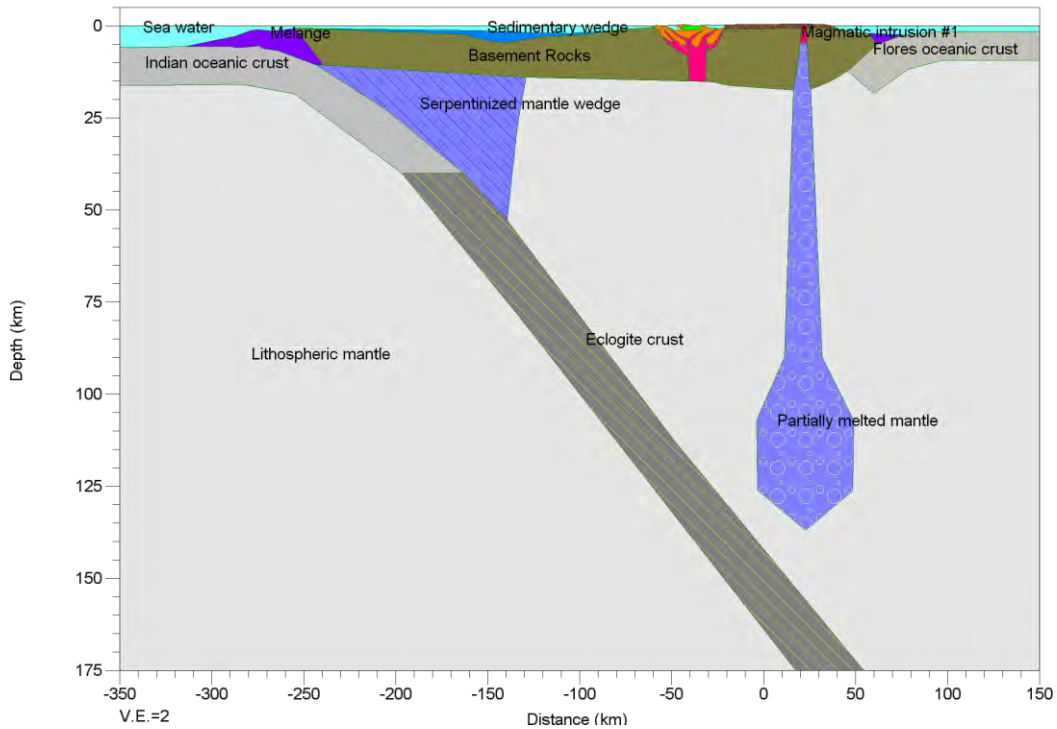
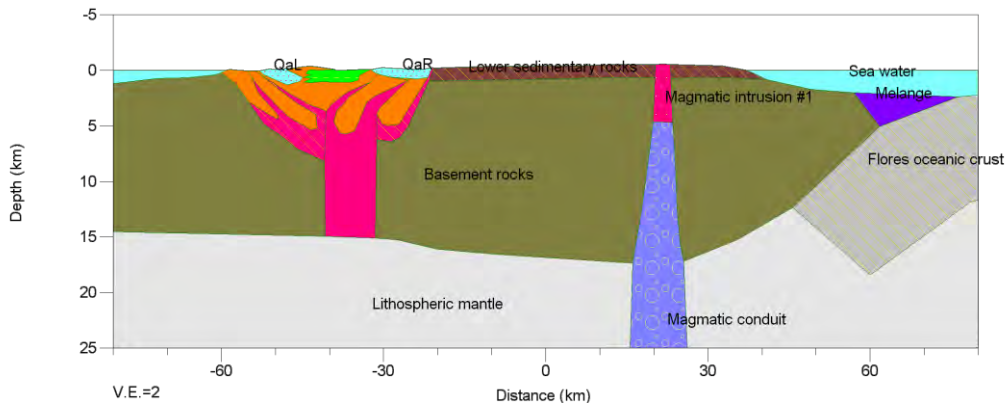


Figure 4.23 The tectonics and geological sequence of the Lombok Island during the Late Miocene (7–5.33 Ma). More extensive dacitic and basaltic intrusions (*Tmi*) resulted from a continuous subduction in the South, forming up and down faulting, as seen along the P1 profile.

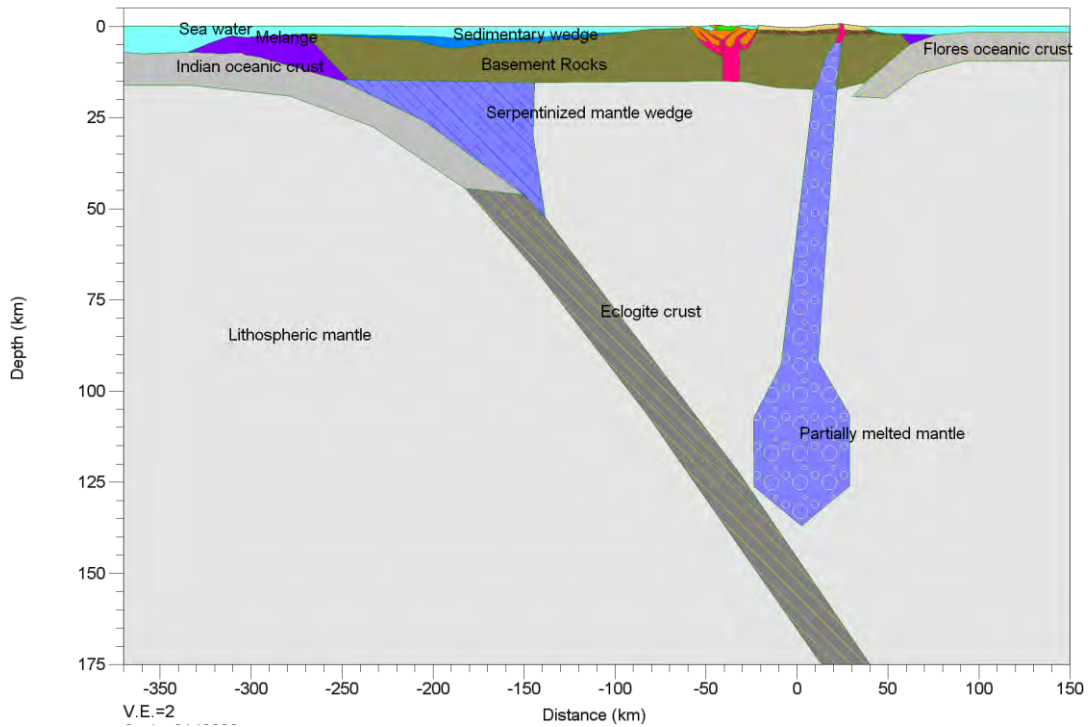


(a)

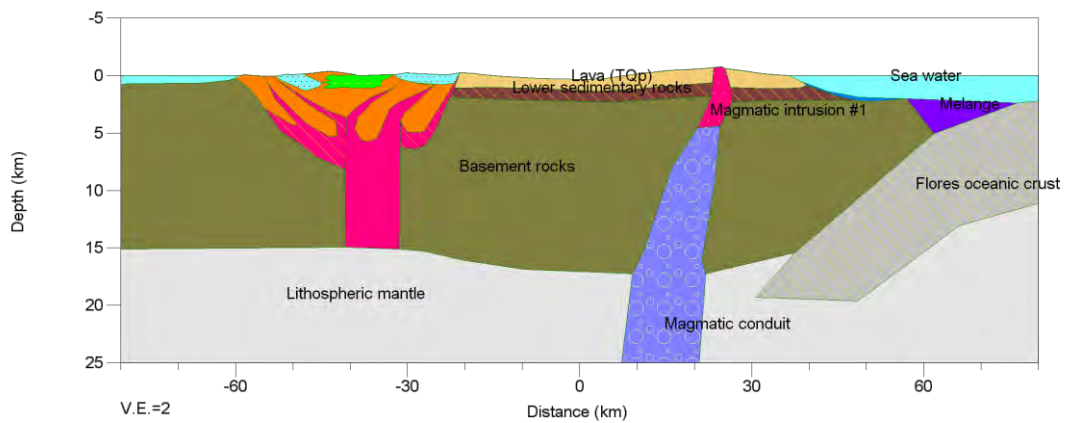


(b)

Figure 4.24 (a) The tectonics and geological sequence of the Lombok Island during early period of the Pliocene (5.33–3.6 Ma). Due to the deeper subduction in the South, the alluviums (*QaR* and *QaL*) were deposited as the Island was raised to higher altitude. The intrusion in the southern area then ceased, resulting in the observed magnetic anomaly signal given in the P1-06 and P1 models by remanent magnetization with inclination of 52°. At the same time, the shifting of partially melted mantle to the North took place, followed by the initiation of the Flores oceanic crust subduction in the North, generating new magmatic intrusions and forming the first lava deposition. (b) Enlargement view of the Lombok Island during early period of the Pliocene (5.33–3.6 Ma).

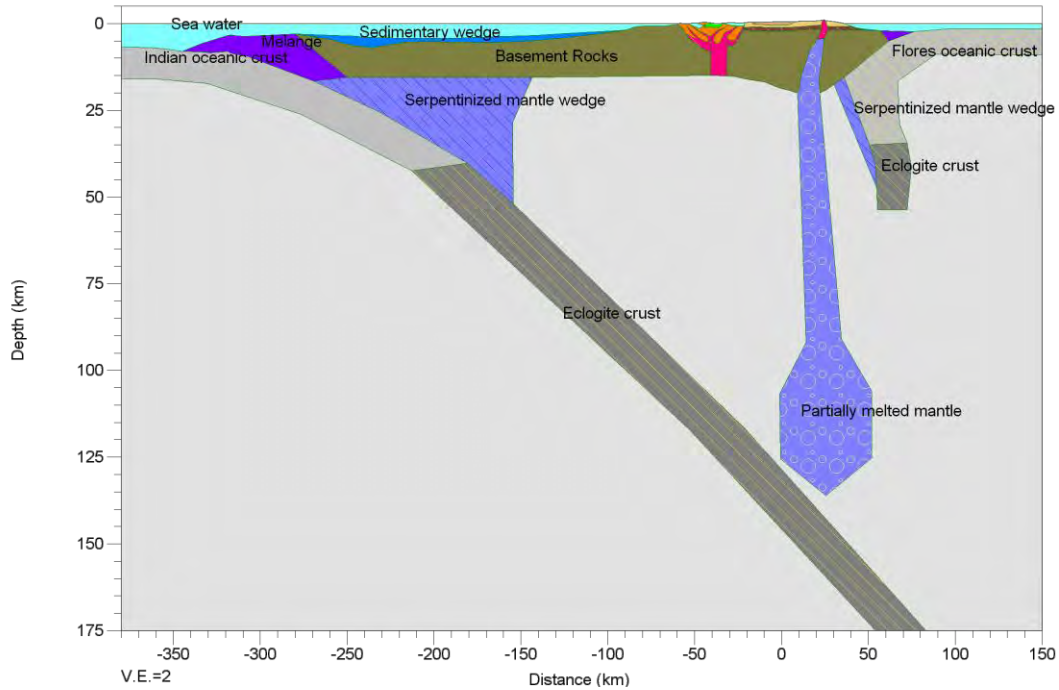


(a)

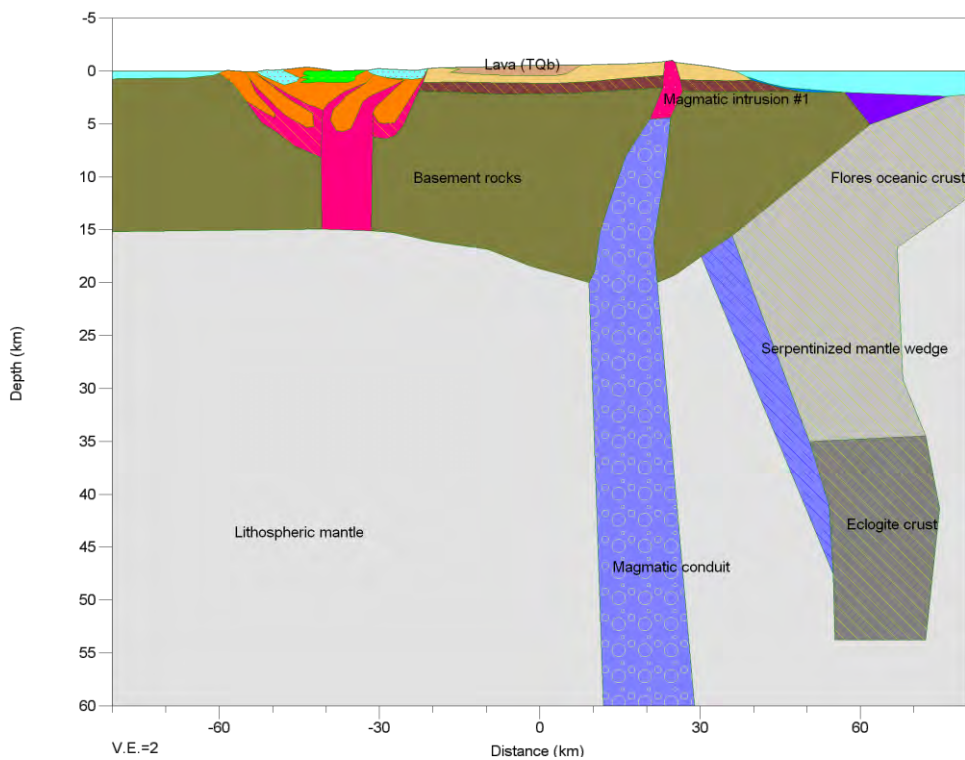


(b)

Figure 4.25 (a) The tectonics and geological sequence of the Lombok Island during middle period of the Pliocene (3.6–2 Ma). Due to the deeper and simultaneously subductions from both sides, the magmatic intrusion #1 was initially formed, producing the first Tertiary lava (*TQp*) with inclination 28°. The former lava (which had been transformed to be *the Lower sedimentary rocks*) was then buried. A normal fault was formed in the north end of the lava structures following this intrusion. (b) Enlargement view of the Lombok Island during middle period of the Pliocene (3.6–2 Ma).

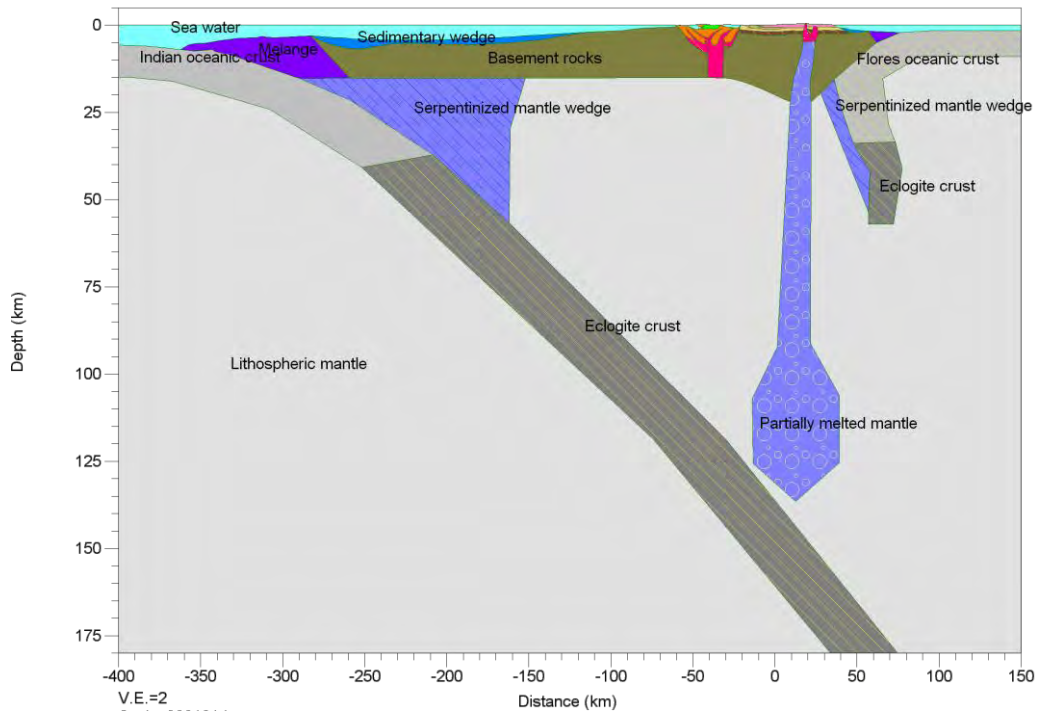


(a)

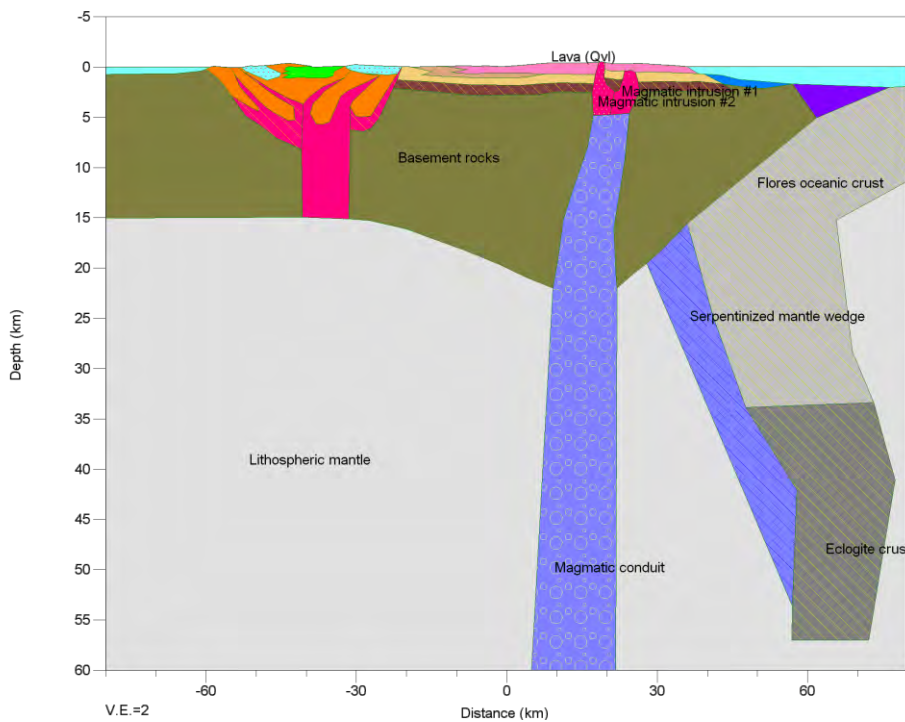


(b)

Figure 4.26 (a) The tectonics and geological sequence of the Lombok Island during the latest period of the Pliocene (2–1.81 Ma). Deeper and simultaneous subductions were still working, transforming the deeper part of the north oceanic crust to Eclogite and forming the serpentinized mantle wedge above it. The second Tertiary lava (*TQb*) flowed; only westward and southward due to the local temporal terrains. The magmatic intrusion #1 then ceased, recording the same inclination as the last deposited lava layer (*TQb*) of 0°. (b) Near surface structures of the Lombok Island during the latest period of the Pliocene (2–1.81 Ma).



(a)



(b)

Figure 4.27 (a) The tectonics and geological sequence of the Lombok Island during the Pleistocene (1.81–0.01 Ma). The simultaneous subductions from both sides advanced, while sedimentary wedge and melange were intensively formed in the north coastal area of the Lombok Island. The magmatic intrusion #2 was initiated, producing the first Quaternary lava of pumice (*Qvl*), flowing to all directions. The second normal fault was formed in the middle of lava structures following this intrusion. The intrusion then ceased, recording the same inclination as the last deposited lava layer (*Qvl*) of -12° . (b) Near surface structures of the Lombok Island during the Pleistocene (1.81–0.01 Ma).

Below are some important aspects taking into account and reflected from the proposed models.

As Kim et al. (2009) classify the maturity of subductions based on some morphological characteristics (i.e. the development of active magmatic arc-related volcanism, the existence of Wadati-Benioff zone to more than 50 km deep, and a wide trench–arc distance), they then used the existence of serpentized mantle wedge as one of four possible explanations for a broad and large low gravity anomalies which characterize a “mature” subduction zone. Meanwhile, Hacker et al. (2003) used the serpentized mantle in describing a seismically active subduction. Using the proposed models, this study suggests that the new subduction in the back arc region (the Flores Thrust zone) is a “mature” subduction, characterized by large high magnetic anomalies which are contributed by the generated serpentized materials. As has been analyzed before, without the contributions of the mature Flores Thrust subduction, the RMS errors are larger (about 18% in magnetic anomalies model and about 40% in gravity model), because the magnetic response is shifted to a much lower level and the gravity equilibrium is disturbed (see **Fig. 4.15**). Whether the north subduction is active up to the present is discussed later in **Sec. 4.5**.

Moreover, including a serpentized mantle wedge above the north eclogite crust in the models probably could answer the question about the origin of the ankaramitic arc magma in the Lombok Island, as asked by Elburg et al. (2007): why the measured water contents in the primitive lava structures over the most northern part of the Lombok Island are very low for an arc-related magma. The water contents of these lavas are only about a tenth of the other normal (non-ankaramitic) lavas over the whole parts of this island and other normal arc islands. Since the age of this ankaramitic lava was not well dated, the modelled first Tertiary lava (*TQp*) then could be associated with this questionable ‘dry’ lava. In the proposed models, this lava has been deposited prior to the formation of the north serpentized mantle wedge (which is rich of water contents). The other modelled younger lavas were deposited after serpentized mantle wedge formation, thus considered as the normal ones.

The inclination changes through the geological sequences are another important fact reflected in the models. **Table 4.5** shows the modelled inclinations and the proposed ages of each block. It can be used to evaluate the compatibility between the modelled inclinations and the global geomagnetic field polarity changes that has been widely accepted (Cande and Kent, 1995). **Figure 4.28** (a) shows the polarity changes of the geomagnetic field during the last 120 Ma, depicting frequent polarity changes during the Late Oligocene to the early periods of Holocene (28–0.01 Ma). These changes are compatible with the modelled inclinations described in the followings.

During the long earlier time interval when the volcanic and sedimentary rocks-*Tomp/Tomk* formed (28–10 Ma), as shown with a red line of **Fig. 4.28** (b), reverse and normal polarities occurred for nearly equal shares of time; so that assuming reverse polarities for these rocks is quite reasonable. During the formation times of the intrusive bodies-*Tmi* and the deposition times of the *Lower sedimentary rocks* (5.33–3.6 Ma) and the first Tertiary lava-*TQp* (2.6–2 Ma) were dominated with reverse polarities, as shown with red lines of **Fig. 4.28** (c). In this study, a zero inclination has been proposed at the latest period of Pliocene at about 1.81 Ma, marked with a blue line of **Fig. 4.28** (c). This could be in relation with the polarity reversal which occurred between Gelasian and Calabrian stages in the geological time scale of Ogg et al. (2008), following the end of the Olduvai normal subchron (Glaßmeier et al, 2009). After the above transitional stages, in 0.01 Ma, the proposed magnetic models recover the present day’s normal polarity, marked with a green line of **Fig. 4.28** (c), in the Quaternary lavas-*Qvll/Qhv* and the latest two magmatic intrusions (#2 and #3).

Table 4.5 The modelled inclinations and the proposed ages of the rocks and sediments

Block's names (labels)	Proposed age [Ma]	Modelled Inclination [deg]	Polarity
Volcanic rock (<i>Tomp-R</i>), Volcanic rock (<i>Tomp-L</i>), Sedimentary rock (<i>Tomk</i>)	28–10	17	Reverse
Intrusive igneous rock (<i>Tmi</i>), Intrusive igneous rock (<i>Tmi-extR</i>), Intrusive igneous rock (<i>Tmi-extL</i>), Lower sedimentary rocks	5.33–3.6	52	Reverse
First Tertiary lava (<i>TQp</i>)	2.6–2	28	Reverse
Second Tertiary lava (<i>TQb</i>), Magmatic intrusion (#1)	1.81	0	-
Magmatic intrusion (#2), First Quaternary lava (<i>Qvl-R</i>), First Quaternary lava (<i>Qvl-L</i>)	0.01	-12	Normal
Magmatic intrusion (#3), Second Quaternary lava (<i>Qhv</i>)	< 0.01	-33.75	Normal

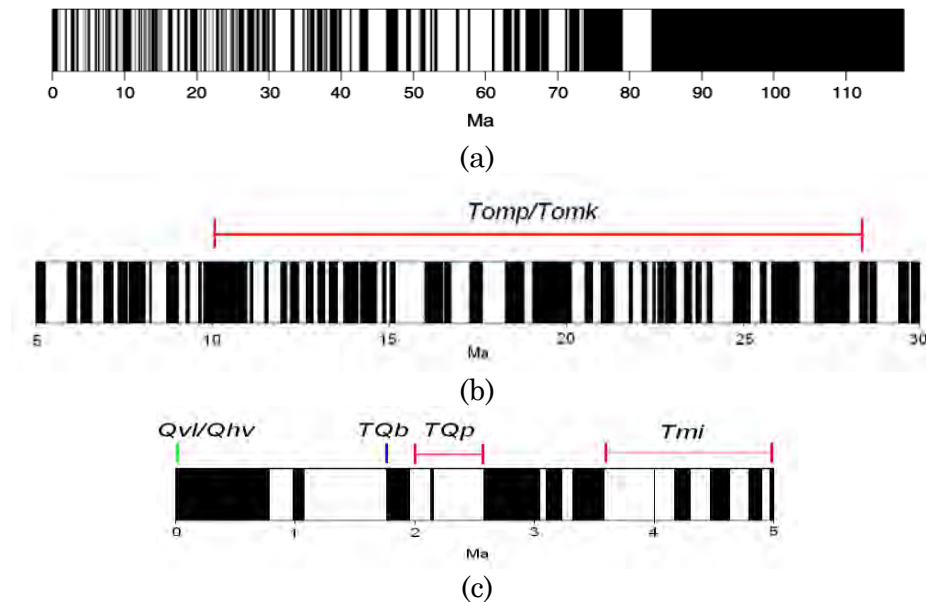


Figure 4.28 (a) The polarity changes of the geomagnetic field during the last 120 Ma, according to Cande and Kent (1995). The black parts represent normal polarities (as of present days), while the white ones represent reverse polarities. (b) The polarity changed frequently during the Late Oligocene to the early periods of Holocene (28–10 Ma), making the assumption of reverse polarities for the volcanic and sedimentary rocks quite reasonable. (c) The polarity changed during the last 5 Ma, in compatibility with the modelled inclinations of rock and lavas in this study. The ranges of proposed ages of each rock/lava are marked with red for reverse, blue for zero, and green for normal polarities.

4.5 Seismo-electromagnetic interpretations

Whereas the resolved models have been interpreted tectonically and geologically, the large geomagnetic changes that have been observed in a one year interval could not be explained satisfactorily (see **Sec. 4.3**). Some complementary interpretations are therefore needed to find other possible mechanisms that could be related to these changes. Seismo-electromagnetic interpretation, especially based on the piezomagnetic field effects study (Sasai, 1994), probably could help to explain the changes. This kind of study considers that the geomagnetic changes originate from stress-induced tectonomagnetic effects.

Nishida et al. (2004) have reported the anomalously large secular changes (lasting at least for about 3 to 30 years), based on the continuous and repeated geomagnetic observations that have been performed at 8 stations in the eastern part of Hokkaido, Japan. This region is situated in the southwestern end of the Kuril Arc where a collision of the North American plate with the Eurasia plate took place. The piezomagnetic modelling could explain well the changes by assuming large stress sensitivity of the order of 10^{-2} MPa⁻¹, which is one order larger than the common value. In the second part of this study, Nishida et al. (2007) have explored the piezomagnetic effects to analyze geomagnetic changes as precursory and co-seismic signals. Although they could not detect significant signals for the two recent Japanese earthquakes (the 2003 Tokachi-oki of M 8.0 and the 2004 Kushiro-oki of M 7.1, in Hokkaido), they can predict effects of several nT for strong earthquakes expected along the Kurile Trench, a region which is also characterized by large amplitudes of geomagnetic anomalies.

In the Lombok Island, besides large changes of geomagnetic anomaly during one year interval, significant changes over a short time interval -before and after two big earthquake occurrences close to this Island- are also observed. Some possible seismo-electromagnetic interpretations related to these events are given through the following sections.

4.5.1 Statistical reviews of past and present seismic activity

Before the seismo-electromagnetic interpretations, it is necessary to evaluate the seismicity of this region in terms of the time of earthquake occurrences. The earthquake data that have been used to generate **Fig. 4.2** are evaluated. Since the evaluation should help in determining whether some earthquakes reflect the activity of the Indian oceanic crust or the Flores oceanic crust, the earthquake zones have to be grouped. **Table 4.6** provides the limitations used in grouping the earthquakes to two different zones (i.e. the Java Trench and the Flores Thrust), considering the proposed slabs geometries in **Fig. 4.3**. A summary of the evaluation results can be visualized in **Fig. 4.29**, showing the subduction activities of both slabs.

One could infer that the subduction activities of the Indian oceanic crust at the Java Trench zone are about two times, but mainly show similar trend to those of the Flores oceanic crust at the Flores Thrust zone. The relationship between them is somehow like actions and reactions. However, there were some exceptional cases during the time interval of 1976–1978 and 2004, when the Java Trench zone was much more active than the Flores Thrust zone. They are in contrast with the time interval of 2005–2008, when the Flores Thrust zone shows more activities. In 2009 (until September 8th), both zones are not so active. The active parts of the Indian oceanic crust probably have migrated far to the west; reactivating the oblique subduction and releasing the rest of the locked stresses in the west off the Sumatra Island (see the historical seismicity in **Sec 1.2.2**).

Table 4.6 Limitation of earthquake grouping to the Java Trench and the Flores Thrust zones.

Depth (km)	The Java Trench	The Flores Thrust
0–5	-11 °N – -12 °N	-7 N° – -8.5 N°
6–10	-10 °N – -12 °N	-7 N° – -9.0 N°
11–30	-9.5 °N – -12 °N	-7 N° – -8.75 N°
31–70	-9.0 °N – -11°N	-7 N° – -8.75 N°
71–100	-8.5 °N – -11 °N	Unrecognized
101–120	-8.0 °N – -10 °N	Unrecognized

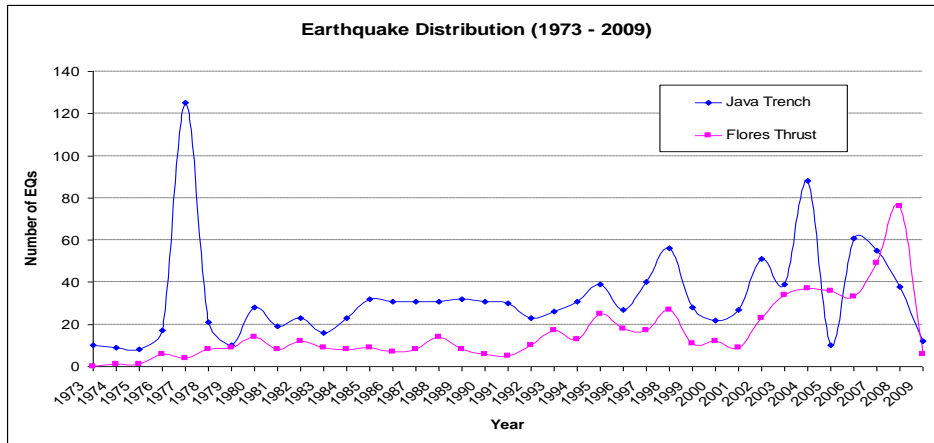


Figure 4.29 The earthquake distributions through time over the LSI region dated from January 1st 1973 to September 8th 2009. The subduction activities in the Java Trench are about two times but mainly with similar trend to those in the Flores Thrust. The exceptional cases are: during the time interval of 1976–1978 and 2004 in which the Java Trench was much more active than the Flores Thrust; in contrast with the time interval of 2005–2008 in which the Flores Thrust shows more activities.

4.5.2 Geomagnetic changes over short time intervals at earthquake times

As described in **Sec 4.3**, four big earthquakes (M 5.5–6.5) occurred during the beginning of the 2007/2008 survey days at the Sumbawa Island (about 275 km from the Lombok Island), on November 25th and 26th 2007. Pertinent short time changes of the geomagnetic anomalies were observed around the times of these earthquakes (H-1 to H+2) at three un-relocated stations (i.e. M19, M22 and M03; see **Fig. 2.22** and **3.7** for the locations), as shown in **Fig. 4.30**.

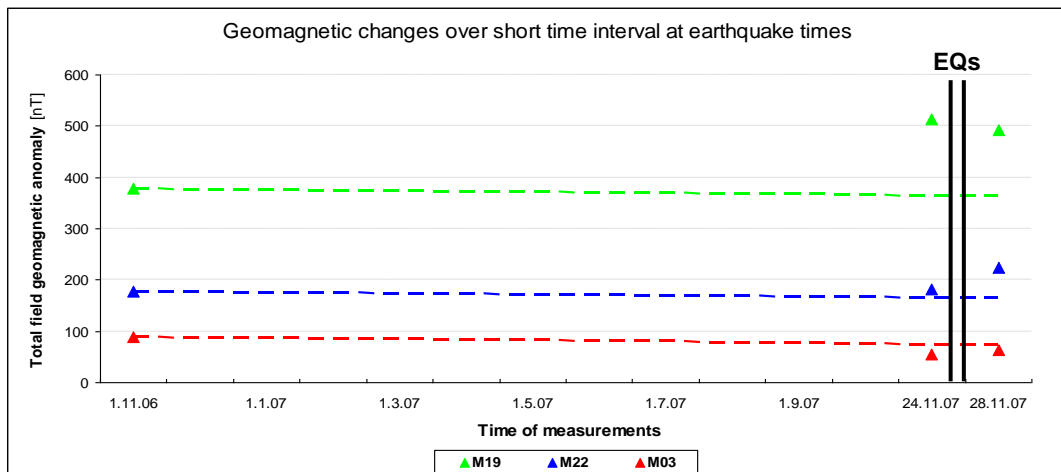


Figure 4.30 Anomalously pertinent geomagnetic changes observed at three un-relocated stations in a short time interval, followed by four big earthquakes (M 5.5–6.5) which occurred on November 25th and 26th 2007 (two black lines) at the Sumbawa Island (about 275 km from the Lombok Island). The dashed lines are linear changes over the time for related stations, assumed by using the secular variations given by the 10th generation of IGRF values (IAGA WG V-MOD, 2005; Maus et al., 2005). The horizontal axis is scaled to one month intervals, except for the latest interval which is only 4 days. As calculated, the scalar magnitudes of the changes are 20.48 nT for M19, 42.50 nT for M22, and 7.84 nT for M03.

On this figure, if the changes could be assumed linearly over the time, by using the secular variations as given by the 10th generation of IGRF values (IAGA WG V-MOD, 2005; Maus et al., 2005), the geomagnetic anomalies at the three stations should follow the related dashed lines. However, by comparing the geomagnetic anomaly values from the field measurements taken on one day before and two days after the earthquakes (i.e. on November 24th and 28th 2007), the short time interval changes are considerably large. Since the time interval between the last two measurements is very short in comparison to one year time interval, the value of anomalously sudden changes could be calculated directly from the differences between the latest two measurements. As calculated, the scalar magnitudes of the changes are 20.48 nT for M19, 42.50 nT for M22, and 7.84 nT for M03. Note that on both and in between days of measurements, the K_p of Australian region and K_p - values are ≤ 3 (see **Fig. 2.11**), therefore these short time interval changes are not related to the disturbances due to the external field variations.

4.5.3 Interpretations of related seismo-electromagnetic mechanism

As has been reviewed in **Sec. 4.5.1**, the seismic activities during 2005–2008 in the LSI region are quite high, especially for the Flores Thrust zone. In terms of seismo-electromagnetic mechanism, the large changes of geomagnetic anomaly field observed during the same time interval and during a short time interval around some big earthquake occurrences (H-1 to H+2) might be linked to the following circumstances.

a. Progressive subduction of the Back arc region

During 2005–2008, the Flores Thrust might progressively grow from the East to the West; with the mature subduction fronts just reaching the West end of (North off) the Lombok Island. This growth is considered progressive for a relatively young age subduction, which was initiated about 3 Ma (Silver et al., 1983), to reach a mature stage of subduction. In a common subduction zone, Stern (2004) has suggested that the infant arc phase may continue for 5 or 10 million years after the initiation of subduction, before an immature subduction reached the threshold depth (60–135 km) for mature arc magmagenesis. Meanwhile, Gurnis et al. (2004) come to a conclusion in evaluating the geological evolution of the Izu-Bonin-Mariana trenches, that these trenches (which were potentially formed as early as 49–48 Ma) needed some 10–15 million years to become a mature subduction; a rather longer period of time as infant subduction zones.

However, a progressive growth of the Flores Thrust zone during the latest decade seems plausible, since generally the Indonesian arcs are different from other common ones. Instead of performing continuous developments; they perform a staccato subsequent Cenozoic growth (Hall and Smyth, 2008). The Sunda arc is a good example, where subduction over the Java Trench had ceased in the late Cretaceous and was resumed in the Eocene. Over the Flores Thrust zone, a staccato development might be manifested by its progressive growth during the latest decade, which could be inferred from the significant changes of geomagnetic anomaly over the Lombok Island within 2005–2008. The abundant energy released from the Sumatra mega thrust earthquake ($M 9.2$) at the end of 2004 probably triggered this growth.

The growth could also be traced by comparing the most possible Wadati-Benioff zones of the Flores and the Bali segments (**Fig. 4.31** (a) and (b)) to that of the Lombok-west Sumbawa segment (**Fig. 4.3**). Whereas the south subductions along the three segments are all “post-mature”, the maturities of the north subductions along these segments are gradually different (i.e. are “post-mature” along the Flores

segment, are “mature” along the Lombok-west Sumbawa segment, and are “immature” along the Bali segment).

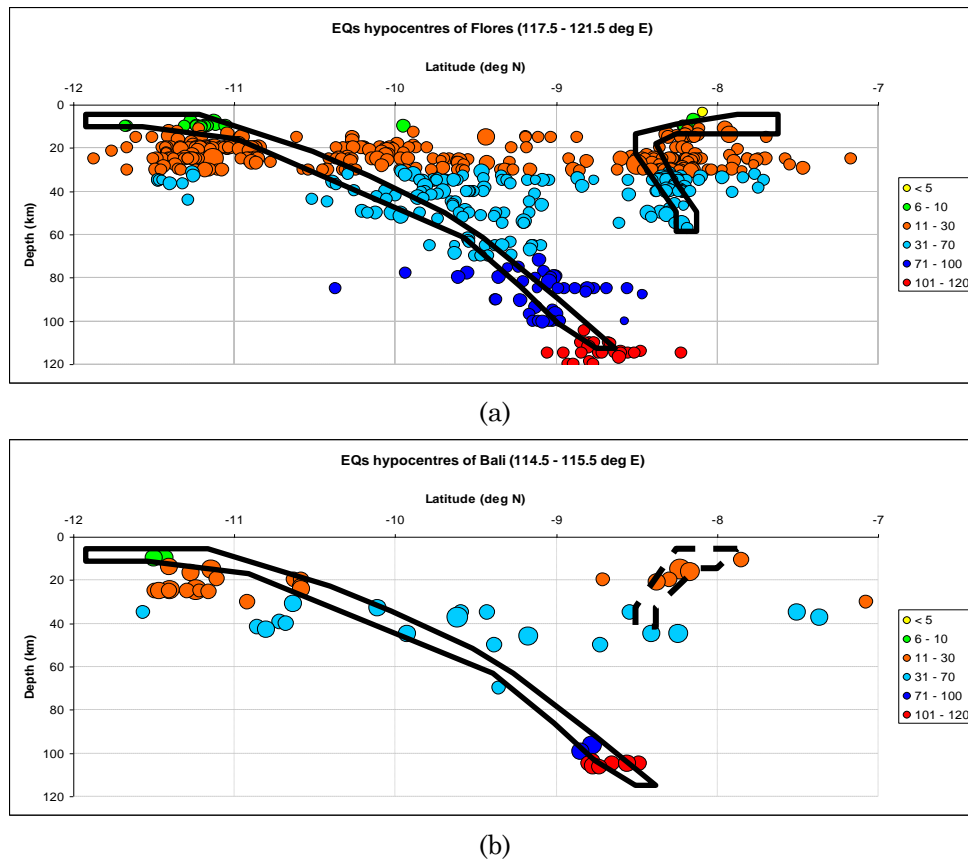


Figure 4.31 The longitudinal cross sectional view of earthquake hypocentres for (a) the Flores segment (bounded by longitude 117.5°E to 121.5°E) and (b) the Bali segment (bounded by longitude 114.5°E to 115.5°E), related to the Earthquake’s epicentres of **Fig. 4.2**. The positions of the “definitive” Indian oceanic slab and the “hypothetical” Flores oceanic slab are inferred from the most possible Wadati-Benioff zones, showing the “post-mature” subductions in the South. The subductions in the North are considered as a “mature” subduction for the Flores segment and an “immature” subduction for the Bali one. The sizes of the circles represent the magnitudes and the colours are related to the depths. The horizontal axis is the latitude (°N) and the vertical axis is the altitude (in km), with vertical exaggeration of 2.0.

b. Stress accumulations over the LSI region

While a large stress sensitivity of one order larger than the common has to be assumed to produce geomagnetic changes of some 1–2 nTyr⁻¹ (Nishida et al., 2004), seismo-magnetic effects of several tens of nT, as observed in the Lombok Island, require a combination of the most favourable circumstances, with very strongly magnetic rocks and high stresses (Stacey, 1964). From the newest available global stress data, Heidbach et al. (2009) have concluded that the Indonesian region is one of some specific regions, characterized with short wavelength stress patterns (<200 km). It could be implied that local stress sources such as density contrasts and active fault systems in this area have high impact in comparison to plate boundary forces and control the regional stress pattern.

Using the stress data of Heidbach et al. (2008) which can be accessed online²⁹, it could be inferred from **Fig. 4.32** that the LSI (especially the Lombok and the Sumbawa islands) is flanked by three stress regimes. Two of these regimes (of normal

²⁹ http://dc-app3-14.gfz-potsdam.de/pub/casmo/casmo_frame.html

faults in the South and of thrust faults in the North) are intense, with the stresses over the thrust regime being the most intense. Concerning the intense stress from the north thrust regime, if the strike direction is East-West (parallel to the Flores Thrust zone), decreasing of total geomagnetic field anomaly at the location of the Lombok Island is expected due to piezomagnetic effects (Stacey, 1964; see the related schema in Fig. 4.33).

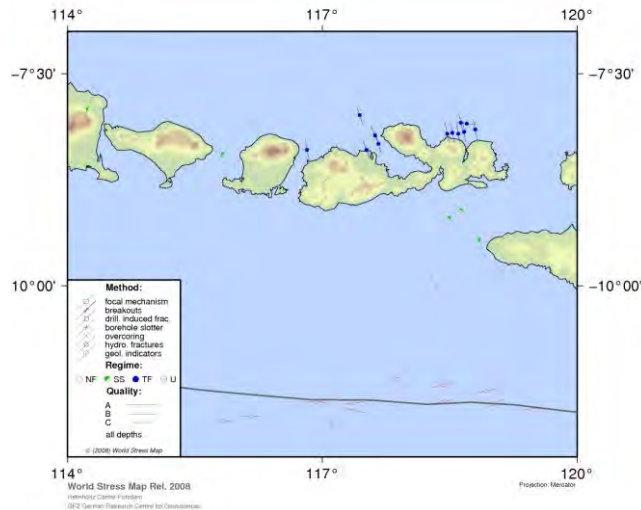


Figure 4.32 The stress map of the LSI region, showing that the Lombok Island is flanked by three stress regimes: of normal faults in the South, of thrust faults in the North and of strike slip fault in the West. The stresses over the north thrust regime are more intense and might generate piezomagnetic effects, resulting in negative changes of geomagnetic anomaly field intensities over the Lombok Island.

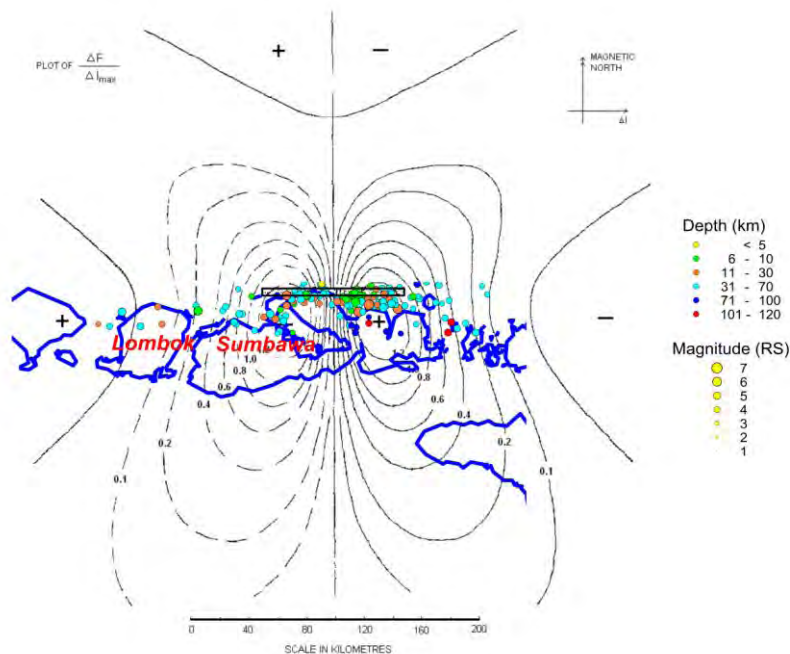


Figure 4.33 The schematic of anomaly field intensities ΔF due to piezomagnetically induced moment ΔI_{max} for a 100 km East-West fault, situated in the southern hemisphere (modified from Fig 6 (c) of Stacey, 1964). If the stressed zone of the Flores Thrust lies along this fault, decreasing of geomagnetic anomalies is expected due to piezomagnetic effects at the location of the Lombok Island. The earthquake data are from the PDE catalogue of the USGS/NEIC, dated from November 19th 1999 to September 8th 2009 of all magnitudes and the depths up to 120 km.

The maximum magnitude of the piezomagnetically induced moment ΔI_{max} could be roughly estimated by assuming a 100 km fault length (approximated from the stressed zone in **Fig. 4.32** and the earthquake data from the PDE catalogue of the USGS/NEIC during the latest decade) and taking the maximum modelled magnetizations I_{max} of the common lavas in this study of 36.7 Am^{-1} (see **Table 4.3** in **Appendix C** for the used parameters). These magnetizations are including the induced part I_{ind} of 34.7 Am^{-1} and the remanent part I_{rem} of 2 Am^{-1} . The induced part is calculated as $I_{ind} = F/(x+1)$, with x is the susceptibility of the lavas (0.038 in SI), situated in the middle part of the Lombok Island with ambient magnetic field F of 36 Am^{-1} (equal to $45,257 \text{ nT}$).

Following Stacey's calculation, corresponding to a peak stress of 100 kg.cm^{-2} , the maximum magnetic anomaly due to seismo magnetic effects can be calculated as $\Delta F_{max} = 4I_{max}$ (in the SI unit) = 146.8 nT . Using graphical method of **Fig. 4.33**, the decreasing of anomaly at the location of the Lombok Island is expected in the order of $0.1 \Delta F_{max} = -14.68 \text{ nT}$. The decreasing of geomagnetic anomaly values over the Lombok Island during 2005–2008, therefore (at least a small fraction of them) could be associated with these effects.

c. Specific crustal electrical characteristics of the Lombok Island

During the last decade, several research groups have proposed that large earthquakes may generate some observable co-seismic Ultra Low Frequency (ULF) signals (Hayakawa, 2009; Uyeda, 2009; Hattori et al., 2004a; Molchanov, 2003). These signals are in a frequency range around 0.01–0.05 Hz, which could be detected as significant changes in geomagnetic field intensity over short time intervals around earthquakes (Hattori et al., 2004a). Since the geomagnetic field in the Lombok Island have been measured in 60 sec intervals (i.e. equal to the sampling frequency of 0.017 Hz), it is possible to consider the short time interval changes discussed in **Sec. 4.5.2** as the co-seismic ULF signals.

Some empirical data show that the relationship between the magnitudes and the observable radii (measured from the epicentres) is linear (Hattori et al., 2004a; Hattori, 2004b). For earthquakes with M 5.5–6.5 (such as the Sumbawa earthquakes, discussed in **Sec. 4.5.2**), the co-seismic ULF signals should be observable in the radii of 40 km (for M 5.5) to 80 km (for M 6.5) only. Because these signals are transmitted only through conductive channels, a long distance transmission is very difficult for a homogeneous or a simple layered Earth (Bernard, 1992). However, long distance transmissions of the ULF signals could be possible due to inhomogeneities in the subterranean electrical structures (Uyeda et al., 2009). Thus if the Sumbawa earthquakes are considered in generating some co-seismic ULF signals that observable throughout a quite far distance (about 275 km), it suggests that some parts in the crustal structures of the Lombok Island region have some specific electrical characteristics (i.e. a high conductivity layer exists there).

d. Structural discontinuity over the Lombok Island

As discussed in **Sec. 3.2.2**, the decreasing of geomagnetic anomalies in the Lombok Island are up to 100 nT , whereas the maximum magnitude of the seismo-magnetic effects (as calculated above) is less than -15 nT . A specific condition of inhomogeneous magnetization is needed to enhance the piezomagnetic fields. The enhancement due to inhomogeneity of crustal magnetization can be investigated by the volume element method (Stacey, 1964). Applying this method, Oshiman (1990 in Sasai, 1994) showed that a strong enhancement effect is expected near a discontinuity of magnetization close to the Earth's surface.

In this study, a specific feature of P3 profile could be the hint for the existence of such discontinuity. The transition between the negative and positive part of anomaly in this profile opens the possibility that the anomaly is of a longer wavelength, and therefore indicates a deeper source, such as contrasts in the basement rocks due to a structural discontinuity. The present position of the Lombok Island which is about the transitions between the continental Sundaland and the oceanic Flores/Banda Sea (Hamilton, 1979), while it has been added to the continental Sundaland by Early Miocene (Hall and Smyth, 2008), supports this idea. However, the definitive structural margins in this region are for long time and broadband spectrums debatable (Wallace, 1869; Audley-Charles, 1975; Genrich et al., 1996; Audley-Charles, 2004; Müller et al., 2008; Pubellier et al., 2008; Roosmawati and Harris, 2009; Nugroho et al., 2009). **Figure 4.34** summarizes all the proposed structural margin of this region.

A recent study, synthesizing the tectonic events throughout Asia and parts of Eastern Europe, fully supports the idea of structural discontinuity over the Lombok Island. It is published as the Structural map of Eastern Eurasia by Pubellier et al. (2008). Their work proposed two structural strike-slip active Quaternary faults (depicted as red lines of **Fig. 4.34**) which cross the western edge of the LSI (one crosses the Lombok Island and the other crosses the Sumbawa Island), both are in the Southeast-Northwest direction. The one that crosses the Lombok Island is nearly perpendicular to (parallel to the modelled strike of) the P3 profile of this study.

The same research group has conducted a newer and more detailed study on the Sumba Island (southeast of the Lombok Island), and have proposed that the Sumba Island is the “asperity” of this region, where a major fault is stuck or locked. Meanwhile, they concluded that the Lombok Island, together with (the west part of) the Sumbawa Island and the Bali Island, acts as a “backstop” for the recent subductions (Fig. 8 of Fleury et al., 2009). It means that the Lombok Island will be slightly deformed in accommodating the ongoing subductions from both sides. However, instead of two active structural faults, the authors now emphasize only one fault that crosses the Sumbawa Island (Pubellier, *pers. communication*). The other one that crosses the Lombok Island could not be justified so far, and more evidence is certainly needed to do so.

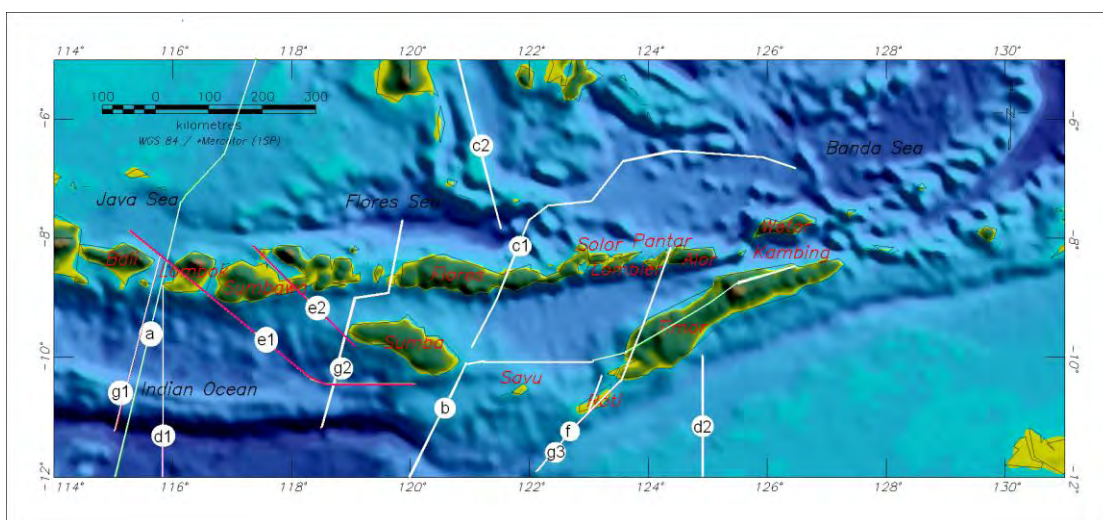


Figure 4.34 The summary of all proposed structural boundaries crossing the LSI region, based on the study of: (a) Wallace (1869), (b) Audley-Charles (1975, 2004), (c1 and c2) Genrich et al. (1996), (d1 and d2) Müller et al. (2008), (e1 and e2) Pubellier et al. (2008), (f) Roosmawati and Harris (2009); and (g1, g2 and g3) Nugroho et al. (2009). Two Quaternary active faults (red lines), one of them crosses the Lombok Island, are proposed by Pubellier et al. (2008).

Chapter 5

Conclusions and outlook

The first new geomagnetic measurements carried out in 2006 and 2007/2008 provided a detailed magnetic anomaly map for a large part of the Lombok Island. The new data have shown that the general pattern of the geomagnetic anomaly over this island is contiguous negative-positive anomalies, revealing an active magmatic arc related subduction region. They agree with earlier results obtained by satellite, aeromagnetic, and marine platforms; and provide a much more detailed picture of the strong anomalies on the Island.

Three profiles were investigated, modelled, and interpreted in detail. They provide the following new insights into the tectonics and geological evolution of the Lombok Island: Geological structure of the Lombok Island can be divided as two main parts with different consecutive ages (the older parts in the South and the younger ones in the North) with two big normal faults in the southern part which could be reactivated due to strong nearby earthquakes. A new subduction in the back arc region (the Flores Thrust zone) is considered mature and active, showing a tendency of progressive subduction during 2005–2008. The extension of the Flores Thrust zone to the West has reached north off the Lombok Island. Geothermal potential in the northern part of this island can be mapped in more detail using these geomagnetic regional survey data. The earlier estimates of reservoir can be confirmed further to a depth of about 800 to 2800 m, providing the reservoir thickness of about 2 km thick.

Changes of the geomagnetic field intensity and anomaly values were also evaluated, with some possible explanations related to a progressive subduction of the back arc region, large stress accumulations over the Lesser Sunda Islands (LSI) regions, a specific electrical characteristic of the crust of the Lombok Island region, and a structural discontinuity over this island.

Considering the achievements obtained via this work, several possible advanced studies involving geomagnetic data and anomaly investigations over the Lombok Island region can be proposed for several future projects:

1. Monitoring the subduction activity of the back arc region (the Flores Thrust zone) and the accumulated stress over the LSI, that could be related to hazard assessment due to volcanism or seismicity of this region, with a special attention to the earthquake occurrence/hazard in this region.
2. Investigating the specific electrical characteristic (high conductivity) of the crust, that is probably related to some aquifer layers or metal mineralization.
3. Determining the existence of an active structural fault over the Lombok Island, that would be reactivated when the Sumba Island “asperity” fails.

To sustain the first objective, it is dramatically needed to get continuous geomagnetic field measurements from a geomagnetic observatory, which can be established in the northern part of the Lombok Island. The data from this observatory can be corroborated with systematic measurements at several repeat stations. Thus, a middle term hazard assessment over the LSI region is aimed for, based on monitoring the geomagnetic changes on this island. This could be possible because the sensitivity of this island to the piezomagnetic fields is supposed to be much higher than in neighbouring/other areas.

The second objective needs other complementary geophysical methods, such as magnetotelluric (MT) or DC resistivity measurements. Although MT measurements are preferable to investigate the electrical conductivity of Earth's rocks and sediments, it would be very difficult to conduct such measurements appropriately over the Lombok Island, because of some topographical constraints and very dense population at some places. DC resistivity measurements are, therefore, expected to provide complementary information.

The last objective needs more efforts, since detailed regional surveys not only over the Lombok Island, but also the neighbouring islands (the Bali Island in the West and the Sumbawa Island in the East; probably also the Sumba and the Flores islands) should be conducted. The aim is a long term hazard assessment over the LSI region, based on the geomagnetic anomaly pattern over the LSI region. This seems possible because the regional magnetic lineations might be used to delineate some structural discontinuities, based on the modelling of contrasts in crustal magnetizations.

Appendix A

Final results of the 2006 and the 2007/2008 survey

Explanations of each column and several remarks are given bellow:

Station	Name of the station; with the colour scheme as follows Black = of good quality, Red = of intermediate or low quality, Blue = not obtained on the magnetic quietest period (in 2006) Green = difference of anomaly value (Diff.) more than 100 nT, while no further relocation of station location in 2007/2008 The <i>italic</i> style means that manual measurements have been conducted using (the ENVI PRO).
Long.	Longitude (geographic, in °E).
Lat.	Latitude (geographic, in °N).
Altitude	Elevation above the sea level (in meter).
Mean	The mean value of instantaneous geomagnetic field intensity (valid over survey time), after preliminary processing and data reduction (in nT).
StDev	Standard deviation value of instantaneous geomagnetic field intensity, after preliminary processing and data reduction (in nT).
IGRF-10	The 10 th IGRF value of the location on the day of survey (in nT).
Anomaly	The geomagnetic anomaly value of the station (valid over survey time; i.e. the Mean subtracted with the IGRF-10 , in nT).
Diff.	The difference between the anomaly value in 2007/2008 and that in 2006 (in nT).
Date	Date of the survey.
Class	The remark of data quality; with the number means as follow 1 = good (StDev < 2 nT), 2 = intermediate (2 nT ≤ StDev < 5 nT), 3 = low (StDev ≥ 5 nT).

Table 3.3 Final results the 2006 survey.

Station	Long. [°E]	Lat. [°N]	Altitude [m]	Mean [nT]	StDev [nT]	IGRF-10 [nT]	Anomaly [nT]	Date	Class
M91	115.95	-8.74437	11.28	45665.9	0.67	45,378.2	287.71		1
M96	115.93	-8.75798	25.60	45340.1	2.36	45,387.3	-47.13	3.11.06	2
M90	115.92	-8.74643	6.10	45378.7	0.73	45,382.6	-3.84		1
M97	115.94	-8.76017	0.00	45368.4	0.45	45,388.2	-19.72		1
M105	115.93	-8.77372	0.00	45284.4	0.77	45,396.0	-111.52		1
M104	115.91	-8.77590	5.49	45332.2	0.49	45,398.7	-66.49	4.11.06	1
M98	115.94	-8.76852	32.31	45452.1	0.46	45,391.4	60.70		1
M92	115.98	-8.73785	17.98	45529.4	0.19	45,372.5	156.97		1
M93	115.99	-8.74133	16.46	45243.4	0.20	45,373.1	-129.61		1
Mxx	115.97	-8.74823	145.39	45300.1	0.38	45,375.6	-75.42		1
M94	116.02	-8.74192	13.41	45258.5	0.27	45,371.0	-112.49		1
M100	116.03	-8.75965	30.48	44872.0	0.73	45,379.4	-507.40	5.11.06	1
M106	116.04	-8.77852	0.00	45171.6	0.62	45,389.6	-217.94		1
M107	116.07	-8.78312	0.00	45039.2	0.45	45,389.8	-350.57		1
M99	116.00	-8.75762	0.00	44805.3	2.05	45,381.6	-576.29		2
M10	116.06	-8.76185	19.20	44929.2	2.87	45,378.3	-449.09		2
M09	116.08	-8.73750	30.78	46145.7	0.81	45,362.8	782.94		1
M11	116.09	-8.75723	27.43	45754.8	0.94	45,373.3	381.57	18.11.06	1
M29	116.11	-8.76888	255.73	45326.9	0.74	45,372.6	-45.70		1
M28	116.07	-8.76055	24.99	45309.6	0.65	45,376.1	-66.48		1
M04	116.09	-8.59408	20.42	45596.3	5.91	45,286.1	310.25	9.11.06	3
M17	116.11	-8.60255	25.60	45517.0	3.34	45,288.7	228.38		2
M23	116.13	-8.60013	34.14	45504.5	2.20	45,285.5	219.04		2
M31	116.15	-8.59058	60.35	45403.5	1.25	45,278.0	125.55		1
M35	116.17	-8.59162	96.62	45776.7	2.78	45,275.9	500.80	10.11.06	2
M36	116.18	-8.61358	94.18	45342.4	2.92	45,287.5	54.98		2
M30	116.15	-8.61825	49.38	45416.1	2.09	45,293.2	122.99		2
M24	116.13	-8.61523	42.06	45244.7	3.06	45,293.6	-48.89		2
M86	116.09	-8.71122	17.07	45664.7	0.39	45,348.7	316.08		1
M82	116.14	-8.68330	27.74	45522.8	1.42	45,329.6	193.26		1
M83	116.19	-8.68448	70.10	45591.4	2.40	45,325.2	266.22	15.11.06	2
M89	116.20	-8.70298	89.31	45416.3	1.02	45,333.5	82.86		1
M80	116.19	-8.66237	68.28	45474.3	2.23	45,312.9	161.46		2
M18	116.11	-8.57533	23.77	45561.1	1.10	45,273.7	287.46		1
M19	116.11	-8.55625	18.59	45641.6	1.01	45,264.0	377.68	16.11.06	1
M03	116.09	-8.55425	20.42	45353.2	0.52	45,264.8	88.49		1
M22	116.13	-8.54763	33.53	45435.4	1.00	45,257.2	178.23		1
M57	116.21	-8.58957	145.08	45397.5	0.92	45,270.9	126.61		1
M41	116.20	-8.55908	146.00	45490.0	0.41	45,254.9	235.19		1
M34	116.16	-8.56798	92.35	45649.8	0.46	45,263.9	385.92	17.11.06	1
M32	116.16	-8.54940	141.73	45374.0	0.78	45,253.3	120.75		1
M21	116.16	-8.52917	288.65	45150.4	1.30	45,238.7	-88.30		1
M33	116.15	-8.56937	71.63	45478.2	0.43	45,266.6	211.65		1
M06	116.09	-8.64570	7.92	45685.3	0.44	45,313.5	371.88		1
M07	116.08	-8.66645	28.96	45290.0	0.48	45,324.9	-34.90	19.11.06	1
M08	116.09	-8.68967	11.89	45201.4	0.87	45,337.4	-135.97		1
M13	116.10	-8.69142	15.85	45325.6	1.77	45,336.7	-11.06		1
M25	116.13	-8.63972	26.52	45634.4	0.78	45,306.5	327.95	22.11.06	1
M26	116.13	-8.66917	29.87	45396.9	0.42	45,322.4	74.54		1
M16	116.10	-8.61983	17.98	45340.3	1.63	45,298.5	41.88		1
M05	116.08	-8.62293	18.29	45444.5	3.03	45,301.4	143.11	24.11.06	2
M14	116.11	-8.66015	9.45	45658.7	3.59	45,319.5	339.21		2
M15	116.10	-8.64228	18.59	45425.5	5.86	45,310.3	115.24		3
M27	116.13	-8.70835	28.35	45630.4	3.59	45,343.2	287.28	25.11.06	2
M59	116.16	-8.68180	39.62	45651.1	2.76	45,325.8	325.37		2
M37	116.17	-8.70843	65.84	45274.0	3.91	45,338.8	-64.79		2
M23	116.13	-8.60013	34.14	45558.1	1.19	45,284.9	273.25		1
M31	116.15	-8.59058	60.35	45409.3	3.33	45,277.4	131.93	26.11.06	2
M35	116.17	-8.59162	96.62	45789.9	2.82	45,275.3	514.66		2
M36	116.18	-8.61358	94.18	45339.3	0.55	45,286.9	52.47		1
M30	116.15	-8.61825	49.38	45431.3	1.07	45,292.5	138.81		1
M24	116.13	-8.61523	42.06	45271.6	1.48	45,293.0	-21.40		1

Table 3.4 Final results of the 2007/2008 survey.

Station	Long. [°E]	Lat. [°N]	Altitude [m]	Mean [nT]	StDev [nT]	IGRF-10 [nT]	Anomaly [nT]	Diff. [nT]	Date	Class
M18	116.118	-8.575	23.9	45538.09	1.68	45259.8	278.29	-9.18	24.11.07	1
M03	116.091	-8.554	16.7	45306.45	0.44	45251.0	55.45	-33.05		1
M22	116.136	-8.548	39.8	45466.60	0.71	45243.0	223.60	45.37	28.11.07	1
M19	116.113	-8.556	17.2	45743.24	0.43	45250.0	493.24	115.56		1
M17	116.115	-8.603	23.4	45950.48	1.03	45274.6	675.88	447.50	29.11.07	1
M04	116.086	-8.594	17.7	45505.17	0.94	45272.2	232.97	-77.28		1
M57	116.210	-8.589	149	45223.54	0.58	45256.2	-32.66	-159.27		1
M41	116.207	-8.559	165	45433.34	0.79	45240.0	193.34	-41.85		1
M34	116.169	-8.568	92.4	45603.46	1.61	45249.5	353.96	-31.96	4.12.07	1
M32	116.164	-8.550	121	45287.67	0.37	45239.5	48.17	-72.58		1
M21	116.168	-8.530	119	45110.16	0.29	45228.7	-118.54	-30.23		1
M23	116.136	-8.600	34.7	45446.84	0.83	45270.7	176.14	-97.11		1
M31	116.157	-8.591	60.4	45341.14	0.78	45263.3	77.84	-47.70		1
M35	116.179	-8.592	93.6	45958.32	0.63	45261.3	697.02	196.22	6.12.07	1
M36	116.181	-8.614	81.8	45289.87	0.43	45273.1	16.77	-35.70		1
M30	116.156	-8.618	50.6	45367.95	0.15	45278.4	89.55	-49.26		1
M24	116.133	-8.615	35.7	45187.20	0.28	45279.1	-91.90	-70.50	7.12.07	1
M16	116.105	-8.619	19.1	45251.81	0.40	45283.8	-31.99	-73.87		1
M06	116.095	-8.645	21	45557.29	1.51	45298.6	258.69	-113.19	8.12.07	1
M15	116.106	-8.642	24.6	45306.81	0.53	45296.0	10.81	-104.43		1
M05	116.089	-8.623	17.2	45402.65	1.66	45287.2	115.45	-27.66		1
M07	116.086	-8.666	21	45259.69	1.71	45310.6	-50.91	-16.01	9.12.07	1
M08	116.090	-8.690	15.3	45176.00	1.34	45322.9	-146.90	-10.93		1
M13	116.109	-8.691	16.9	45280.60	1.00	45322.2	-41.60	-30.54		1
M25	116.134	-8.640	31.1	45578.69	1.07	45292.0	286.69	-41.26		1
M26	116.132	-8.668	27	45326.42	0.86	45307.5	18.92	-55.62	13.12.07	1
M86	116.093	-8.711	13.1	45620.50	0.59	45334.0	286.50	-29.58		1
M27	116.134	-8.708	18.9	45589.34	0.93	45329.0	260.34	-26.95		1
M14	116.114	-8.660	23.7	45622.77	1.26	45304.6	318.17	-21.04		1
M82	116.141	-8.683	24.9	45491.84	1.59	45314.7	177.14	-16.13	14.12.07	1
M59	116.171	-8.682	46	45628.31	1.23	45310.9	317.41	-7.96		1
M37	116.177	-8.708	66.2	45238.62	1.39	45324.2	-85.58	-20.78		1
M83	116.190	-8.685	71.5	45446.03	0.24	45310.3	135.73	-130.49	15.12.07	1
M89	116.202	-8.702	88.6	45367.03	1.06	45317.9	49.13	-33.73	16.12.07	1
M80	116.195	-8.663	80.6	45487.27	1.23	45297.8	189.47	28.02		1
M92	115.983	-8.738	13.6	45465.14	4.85	45357.0	108.14	-48.83		2
Mxx	115.976	-8.748	147	45270.92	1.64	45360.2	-89.28	-13.86	24.12.07	1
M93	115.999	-8.741	23	45198.16	1.19	45357.4	-159.24	-29.63		1
M99	116.009	-8.754	30.9	44926.04	0.80	45363.2	-437.16	139.13		1
M94	116.029	-8.742	15.5	45197.66	0.64	45355.4	-157.74	-45.25		1
M100	116.038	-8.760	14.8	44969.59	1.13	45364.2	-394.61	112.79	25.12.07	1
M106	116.045	-8.781	9.5	45148.17	0.38	45375.1	-226.93	-8.98		1
M91	115.957	-8.747	11.2	45245.73	1.38	45364.2	-118.47	-406.18		1
M97	115.944	-8.758	12.4	45370.92	0.33	45370.9	0.02	19.74	26.12.07	1
M98	115.949	-8.768	32.8	45522.45	1.89	45375.8	146.65	85.95		1
M105	115.936	-8.774	25.8	45136.80	0.56	45380.0	-243.20	-131.68		1
M107	116.071	-8.783	11.4	44997.30	1.69	45374.1	-376.80	-26.23		1
B21	116.056	-8.806	20.6	45258.25	0.65	45387.4	-129.15		27.12.07	1
B22	116.048	-8.835	130	45411.58	1.46	45400.8	10.78			1
B19	116.034	-8.788	34.5	45168.46	0.46	45378.8	-210.34		28.12.07	1
B18	116.031	-8.768	181	44882.98	1.73	45365.2	-482.22		29.12.07	1
M104	115.916	-8.776	5.4	45362.31	1.48	45383.1	-20.79	45.70		1
M96	115.933	-8.758	22.5	45241.64	1.15	45371.6	-129.96	-82.84	31.12.07	1
M90	115.920	-8.746	24.9	45351.46	1.36	45366.4	-14.94	-11.10		1
B08	115.935	-8.805	24.4	44795.04	1.62	45396.4	-601.36			1
B10	115.954	-8.814	34.7	44761.45	1.07	45399.7	-638.25		1.1.08	1
B09	115.930	-8.831	16.2	45871.68	1.10	45411.2	460.48			1
Bxx	115.937	-8.822	127	44885.76	0.63	45403.1	-517.34			1
B11	115.952	-8.828	306	45229.72	1.36	45400.8	-171.08		2.1.08	1
B14	115.985	-8.868	239	45159.16	0.74	45421.2	-262.04			1
B20	116.034	-8.832	292	45342.42	0.34	45396.6	-54.18		3.1.08	1
B17	116.015	-8.858	65.3	45080.35	0.26	45417.4	-337.05			1

Table 3.4 (Cont.)

Station	Long. [°E]	Lat. [°N]	Altitude [m]	Mean [nT]	StDev [nT]	IGRF-10 [nT]	Anomaly [nT]	Diff. [nT]	Date	Class
B12	115.979	-8.770	263	45434.30	1.88	45368.6	65.70			1
B15	116.003	-8.778	280	45210.29	1.72	45370.1	-159.81		4.1.08	1
B04	115.885	-8.779	25.6	45292.51	0.48	45387.0	-94.49			1
B01	115.854	-8.752	47	45576.94	1.16	45374.2	202.74			1
Bxy	115.840	-8.734	14.5	45642.19	1.02	45366.5	275.69		5.1.08	1
Bxz	115.837	-8.752	100	45581.17	1.61	45374.8	206.37			1
M29	116.109	-8.768	250	45338.76	0.80	45354.1	-15.34	30.36	13.3.08	1
M11	116.090	-8.757	21.5	45746.48	1.43	45354.9	391.58	10.01		1
M09	116.087	-8.737	31.6	46083.24	1.30	45344.6	-348.09	-1131.03	15.3.08	1
M10	116.062	-8.762	30.2	44996.51	0.65	45359.6	-99.84	349.24	16.3.08	1
M28	116.080	-8.761	24.2	45259.76	0.59	45358.2	-98.44	-31.97		1
C08	116.124	-8.390	51.6	44880.71	1.05	45158.0	-277.29			1
C09	116.137	-8.403	138	44982.79	1.41	45161.8	-179.01		12.1.08	1
C05	116.109	-8.405	24.9	45024.44	0.41	45168.3	-143.86			1
C04	116.082	-8.466	333	44873.84	1.12	45195.1	-321.26			1
C03	116.086	-8.445	79	45391.19	1.67	45190.1	201.09		16.1.08	1
Cvz	116.066	-8.408	28.7	45196.66	0.88	45173.3	23.36			1
C02	116.043	-8.454	37.1	44313.00	1.43	45199.0	-886.00			1
C01	116.052	-8.428	15.7	45162.05	0.63	45185.3	-23.25			1
Czz	116.043	-8.476	28.2	44711.84	1.96	45211.1	-499.26		17.1.08	1
Cxz	116.050	-8.493	18.6	45181.61	0.45	45219.6	-37.99			1
C12	116.162	-8.363	26.8	44889.66	1.49	45140.8	-251.14			1
C17	116.175	-8.386	50	44722.59	1.32	45151.5	-428.91			1
C13	116.161	-8.381	72.5	44700.89	0.65	45149.4	-448.51		22.1.08	1
C14	116.160	-8.398	56.4	44470.27	1.37	45159.0	-688.73			1
C16	116.180	-8.355	28.2	45860.01	1.80	45135.1	724.91			1
C19	116.205	-8.329	59	45630.37	1.63	45118.3	512.07			1
C22	116.231	-8.333	234	45430.78	0.53	45114.2	316.58		23.1.08	1
C23	116.231	-8.356	373	44927.61	1.44	45123.4	-195.79			1
C21	116.218	-8.310	90	45333.40	1.68	45106.3	227.10			1
C26	116.256	-8.334	338	45272.48	0.46	45110.1	162.38			1
C24	116.244	-8.283	112	45495.20	0.95	45089.3	405.90		24.1.08	1
C25	116.255	-8.304	232	44956.53	1.01	45097.2	-140.67			1
C29	116.281	-8.304	337	45506.74	1.48	45092.4	414.34			1
C34	116.300	-8.331	561	44812.56	1.14	45099.7	-287.14			1
C33	116.306	-8.307	489	45631.79	1.00	45088.4	543.39		25.1.08	1
C28	116.279	-8.280	195	45649.57	1.55	45083.2	566.37			1
C38	116.321	-8.302	434	46233.06	1.41	45085.6	1147.46			1
C32	116.301	-8.284	197	45682.70	1.81	45083.2	599.50			1
C27	116.279	-8.254	63.1	45546.38	1.76	45072.5	473.88		26.1.08	1
C31	116.298	-8.254	66.7	45066.09	1.09	45070.6	-4.51			1
C10	116.123	-8.421	144	44754.30	1.07	45171.8	-417.50			1
C06	116.092	-8.420	26.8	45103.69	0.94	45176.9	-73.21		27.1.08	1
C18	116.185	-8.401	126	44578.57	1.63	45156.6	-578.03			1
CGA	116.081	-8.360	13.3	45107.46	0.37	45146.5	-39.04		28.1.08	1
C40	116.357	-8.255	161.0	45331.36	1.52	45063.4	267.96			1
C41	116.355	-8.280	331.0	45503.91	0.39	45072.8	431.11		16.2.08	1
C37	116.330	-8.273	250.0	45141.05	0.67	45072.8	68.25			1
C46	116.413	-8.247	108.0	45304.22	0.94	45055.6	248.62			1
C47	116.406	-8.273	279.0	45372.31	2.42	45065.9	306.41		17.2.08	2
C49	116.425	-8.283	356.0	45831.87	0.50	45067.8	764.07			1
C50	116.425	-8.306	591.0	45500.95	0.54	45074.5	426.45			1
C53	116.442	-8.300	489.0	45828.42	1.89	45072.0	756.42		18.2.08	1
C52	116.444	-8.280	272.0	45382.17	0.86	45066.6	315.57			1
C48	116.430	-8.255	100.0	45313.49	1.40	45058.3	255.19			1
C57	116.489	-8.306	643.0	45480.05	1.80	45067.7	412.35			1
C56	116.480	-8.280	289.0	44790.10	1.69	45062.8	-272.70		19.2.08	1
C55	116.479	-8.259	120.0	45078.71	1.10	45055.9	22.81			1
C61	116.497	-8.325	865.0	45137.96	1.53	45071.6	66.36			1
C65	116.516	-8.356	1133.0	45229.19	1.82	45079.9	149.29		28.2.08	1

Table 3.4 (Cont.)

Station	Long. [°E]	Lat. [°N]	Altitude [m]	Mean [nT]	StDev [nT]	IGRF-10 [nT]	Anomaly [nT]	Diff. [nT]	Date	Class
C74	116.55	-8.377	1193.0	45471.3	0.48	45086.8	384.58			1
C73	116.54	-8.358	1143.0	46041.2	0.73	45078.2	963.07		29.2.08	1
C66	116.53	-8.379	1208.0	45625.3	0.70	45089.2	536.15			1
C75	116.55	-8.394	1256.0	44444.4	1.60	45094.1	-649.68			1
C67	116.53	-8.407	1475.0	44449.8	0.78	45097.6	-647.71		1.3.08	1
C68	116.53	-8.430	1453.0	43911.0	1.22	45110.3	-1199.24			1
C67x	116.53	-8.409	1487.0	44738.6	1.33	45098.1	-359.45			1
C69	116.53	-8.450	1091.0	44182.2	0.74	45129.5	-947.21			1
C78	116.55	-8.489	697.0	44994.5	0.74	45157.7	-163.17		2.3.08	1
C79	116.55	-8.507	522.0	45029.2	1.30	45170.8	-141.60			1
C88	116.57	-8.485	658.0	44675.8	1.51	45154.4	-478.55			1
C89	116.57	-8.502	503.0	45005.8	1.20	45166.6	-160.79		3.3.08	1
C98	116.61	-8.504	241.0	45014.4	1.48	45171.4	-156.99			1
C60	116.50	-8.304	671.0	45506.2	1.83	45064.3	441.95		4.3.08	1
CAP	116.50	-8.367	1304.0	45395.5	1.10	45083.1	312.46			1
C77	116.53	-8.435	1244.0	44442.1	1.88	45117.5	-675.35		5.3.08	1
C125	116.70	-8.429	30.6	45206.7	0.73	45127.6	79.17		20.3.08	1
C124	116.70	-8.406	24.2	44985.5	0.48	45115.5	-129.96			1
C118	116.68	-8.382	182.0	45020.7	1.96	45101.0	-80.29			1
C117	116.68	-8.352	29.4	45172.8	0.30	45088.0	84.89		21.3.08	1
C123	116.70	-8.386	72.0	44813.6	1.02	45103.8	-290.16			1
C108	116.65	-8.309	23.7	44761.0	0.68	45068.1	-307.06			1
C116	116.68	-8.329	3.3	45124.9	0.29	45077.1	47.89		22.3.08	1
C122	116.70	-8.359	16.9	44875.8	0.53	45090.5	-214.65			1
C62	116.52	-8.266	48.4	44600.1	1.52	45055.3	-455.17			1
C70	116.55	-8.267	27.3	44915.2	1.39	45054.6	-139.38		23.3.08	1
C80	116.59	-8.280	23.2	45242.2	0.80	45058.6	183.60			1
C99	116.62	-8.305	134.0	44884.0	1.42	45065.5	-181.46			1
C97	116.60	-8.485	477.0	44751.6	0.43	45154.9	-403.27			1
C107	116.62	-8.512	99.6	44874.0	0.93	45176.7	-302.64		24.3.08	1
CN11	116.67	-8.331	5.0	45260.2	0.35	45078.2	182.05			1
C115	116.65	-8.485	23.9	44896.6	1.97	45161.2	-264.51		25.3.08	1
C121	116.68	-8.454	37.6	45216.1	1.68	45142.2	73.97			1
C44	116.38	-8.280	307.0	45049.3	1.40	45071.1	-21.78			1
C43	116.37	-8.255	173.0	45182.3	1.96	45060.9	121.46		14.2.08	1
C42	116.38	-8.230	68.9	45028.8	0.77	45050.1	-21.21			1
C45	116.40	-8.225	28.2	45147.9	1.34	45046.2	101.71			1
C39	116.35	-8.229	43.6	45231.8	1.93	45052.5	179.39			1
C35	116.33	-8.232	64.5	45472.7	1.33	45055.2	417.55		15.2.08	1
C36	116.33	-8.255	194.0	45045.2	0.87	45064.5	-19.23			1
C59	116.50	-8.267	79.7	45031.9	1.91	45059.0	-27.01			1
C51	116.45	-8.255	155.0	45253.2	1.96	45054.7	198.57		20.2.08	1
CSN	116.40	-8.304	580.0	44864.3	0.65	45075.2	-210.89			1
PSG	116.53	-8.384	1184.0	45735.5	0.45	45092.1	643.44		28.2.08	1
D10	116.07	-8.854	16.5	44995.8	1.66	45408.2	-412.37		12.3.08	1
D07	116.03	-8.855	14.3	44935.5	1.31	45412.9	-477.35			1
D11	116.10	-8.860	94.1	44953.1	0.99	45407.8	-454.64		15.3.08	1
DAW	116.26	-8.768	106.0	45341.6	1.58	45343.4	-1.78			1
DPJ	116.28	-8.841	138.0	44914.0	0.50	45380.5	-466.50		29.3.08	1
DKT	116.27	-8.884	13.0	45287.9	0.40	45407.4	-119.47			1
DBO	116.22	-8.782	96.0	45238.6	1.21	45354.4	-115.76			1
DSA	116.21	-8.820	109.0	45296.5	1.68	45375.5	-78.99		30.3.08	1
DLA	116.18	-8.849	138.0	45530.1	1.04	45392.9	137.23			1
DMN	116.15	-8.808	260.0	45181.2	1.25	45371.2	-190.00		31.3.08	1
DMS	116.14	-8.830	237.0	45333.2	0.70	45384.0	-50.78			1

Appendix B

The Talwani algorithm for 2D magnetic and gravity modellings

a. Gravity modelling

Gravitational potential obeys the principle of superposition: The gravitational potential of a collection of masses is the sum of the gravitational attractions of the individual masses. A continuous distribution of mass m is simply a collection of a great many, very small masses $dm = \rho(x,y,z) dv$, where $\rho(x,y,z)$ is the density distribution.

Applying the principle of superposition yields

$$U(P) = \gamma \int_V \frac{dm}{r} = \gamma \int_V \frac{\rho(Q)}{r} dv, \quad (\text{B.1})$$

where integration is over V , the volume actually occupied by mass.

As usual, P is the point of observation, Q is the point of integration, and r is the distance between P and Q , and ρ is the density.

The gravitational attraction outside of any distribution of mass then given by

$$g(P) = \nabla U(P) = -\gamma \int_V \rho(Q) \frac{\hat{r}}{r^2} dv \quad (\text{B.2})$$

For 2D modelling, the density does not vary in the direction parallel to its long axis, then $\rho(x,y,z) = \rho(x,y)$

$$U(P) = \gamma \int_S \rho(S) \left(\int_{-a}^a \frac{1}{r} dz' \right) dS,$$

where S in this case represents the cross-sectional area of the two-dimensional source. As $a \rightarrow \infty$, the inner integral becomes the logarithmic potential of a wire with $\gamma\lambda=1$, and the potential of the two dimensional distribution is given by

$$U(P) = 2\gamma \int_S \rho(S) \log \frac{1}{r} dS \quad (\text{B.3})$$

where r is the perpendicular distance to an element of the body, given by $r = \sqrt{(x-x')^2 + (z-z')^2}$

For simplification, we move the observation point to the origin and require the constant density. The vertical attraction of gravity is given by

$$g(P) = \frac{\partial U}{\partial z} = 2\gamma\rho \iint \frac{z'dx'dz'}{x'^2 + z'^2},$$

and integration over x' yields

$$g = 2\gamma\rho \int \left[\arctan \frac{x'_2}{z'} - \arctan \frac{x'_1}{z'} \right] dz',$$

where x'_1 and x'_2 are both functions of z' and, as shown by **Fig. B.1**, represent separate paths around part of the perimeter of the cross-sectional surface. These two paths, when taken together and considering the change in sign, amount to a single clockwise integration around the perimeter, that is

$$g = 2\gamma\rho \int \arctan \frac{x'}{z'} dz'$$

Now we replace the smooth perimeter with an N -sided polygon so the equation becomes

$$g = 2\gamma\rho \sum_{n=1}^N \int_{z_n}^{z_{n+1}} \arctan \frac{x'}{z'} dz' \quad (\text{B.4})$$

where z_n and z_{n+1} are the z coordinates of the two endpoints of side n .

The expression for x' in term of z' is needed, as

$$x' = \alpha_n z' + \beta_n; \quad \alpha_n = \frac{x_{n+1} - x_n}{z_{n+1} - z_n}; \quad \beta_n = x_n - \alpha_n z_n$$

Substituting these equations to **Eqn. B.4** provides

$$\begin{aligned} g &= 2\gamma\rho \sum_{n=1}^N \int_{z_n}^{z_{n+1}} \arctan \left(\frac{\alpha_n z' + \beta_n}{z'} \right) dz' \\ &= 2\gamma\rho \sum_{n=1}^N \left\{ \frac{\pi}{2} (z_{n+1} - z_n) + \left(z_n \arctan \frac{z_n}{x_n} - z_{n+1} \arctan \frac{z_{n+1}}{x_{n+1}} \right) + \right. \\ &\quad \left. \frac{\beta_n}{1 + \alpha_n^2} \left[\log \frac{\sqrt{x_{n+1}^2 + z_{n+1}^2}}{\sqrt{x_n^2 + z_n^2}} - \alpha_n \left(\arctan \frac{z_{n+1}}{x_{n+1}} - \arctan \frac{z_n}{x_n} \right) \right] \right\} \end{aligned}$$

The first two terms in parentheses of the summation add to zero around any closed polygon, so the previous equation simplifies to

$$g = 2\gamma\rho \sum_{n=1}^N \frac{\beta_n}{1 + \alpha_n^2} \left[\log \frac{r_{n+1}}{r_n} - \alpha_n (\theta_{n+1} - \theta_n) \right] \quad (\text{B.5})$$

In such case where r_n and θ_n are defined as shown in **Fig. B.1**.

b. Magnetic modelling

$M(Q)$ is the magnetization as a function of position Q and the magnetic permeability of free space is $C_m = \frac{\mu_0}{4\pi} = 10^{-7}$ henry.m⁻¹ in SI, then the potential of a distribution of magnetization

$$V(P) = C_m \int_R M(Q) \cdot \nabla_Q \frac{1}{r} dv \quad (\text{B.6})$$

Analogous to **Eqn. B.2**, magnetic induction at P is given by

$$B(P) = -\nabla_P V(P) = -C_m \nabla_P \int_R M(Q) \cdot \nabla_Q \frac{1}{r} dv \quad (\text{B.7})$$

If magnetization is assumed constant over a source body, the total field of anomaly is given approximately by

$$\Delta T = -C_m \hat{F} \cdot \nabla_P \int_R M \cdot \nabla_Q \frac{1}{r} dv \quad (\text{B.8})$$

\hat{F} is a unit vector in the direction of the regional field

For 2D modelling, **Eqn. B.7** is simplified to

$$B = C_m \int_S \frac{M \cdot \hat{n}}{r^2} \hat{r} dS$$

This equation has the same form as the gravity field of a hollow shell with identical shape, that is

$$g = -\gamma_m \int_S \frac{\sigma(S)}{r^2} \hat{r} dS,$$

where $\sigma(S)$ is surface density in units of mass per unit area.

Consider a flat, horizontal ribbon of **Fig. B.2**, with a surface density of σ , continuing infinitely far in the $+y$ and $-y$ directions, and extending from (x_1, z) to (x_2, z) . One element dx of the ribbon penetrates the x, z plane at (x', z) and is equivalent to a wire infinitely extended parallel to the y axis and having mass per unit length $\lambda = \sigma dx$.

The wire has gravitational attraction observed at the origin

$$g = -2\gamma\lambda \frac{\hat{r}}{r} = 2\gamma\lambda \frac{x'\hat{i} + z'\hat{k}}{x'^2 + z'^2}$$

By letting $\lambda = \sigma dx$ and integrating over x

$$g_x = 2\gamma\sigma \int_{x_1}^{x_2} \frac{x'}{x'^2 + z'^2} dx' = 2\gamma\sigma \log \frac{r_2}{r_1}$$

and

$$g_z = 2\gamma\sigma \int_{x_1}^{x_2} \frac{z'}{x'^2 + z'^2} dx' = 2\gamma\sigma(\theta_1 - \theta_2),$$

then

$$g = 2\gamma\sigma \left[\hat{i} \log \frac{r_2}{r_1} + \hat{k}(\theta_1 - \theta_2) \right] \quad (\text{B.9})$$

For a general ribbon, the ribbon is rotated to an arbitrary amount, and two unit vectors \hat{n} and \hat{s} are defined as of **Fig. B.2** (b) and (c), that remain normal and parallel to the ribbon, respectively. Note that $\hat{n}_x = \hat{s}_z$ and $\hat{n}_z = -\hat{s}_x$.

Therefore $g_s = 2\gamma\sigma \log \frac{r_2}{r_1}$ and $g_n = -2\gamma\sigma(\theta_1 - \theta_2)$

The x and z components of g are given by

$$g_x = \hat{i} \cdot g = \hat{s}_x g_s + \hat{n}_x g_n = \hat{s}_x g_s + \hat{s}_z g_n = 2\gamma\sigma \left[\hat{s}_x \log \frac{r_2}{r_1} - \hat{s}_z (\theta_1 - \theta_2) \right]$$

and

$$g_z = \hat{k} \cdot g = \hat{s}_z g_s + \hat{n}_z g_n = \hat{s}_z g_s - \hat{s}_x g_n = 2\gamma\sigma \left[\hat{s}_z \log \frac{r_2}{r_1} + \hat{s}_x (\theta_1 - \theta_2) \right]$$

To convert these equations to magnetic case, let $\gamma = C_m$ and $\sigma = -M \cdot \hat{n}$

$$B_x = -2C_m(M \cdot \hat{n}) \left[\hat{s}_x \log \frac{r_2}{r_1} - \hat{s}_z (\theta_1 - \theta_2) \right] \quad (\text{B.10})$$

$$B_z = 2C_m(M \cdot \hat{n}) \left[\hat{s}_z \log \frac{r_2}{r_1} + \hat{s}_x (\theta_1 - \theta_2) \right] \quad (\text{B.11})$$

In such case where r_1, r_2 and θ_1, θ_2 are defined as shown in **Fig. B.2**.

To calculate the magnetic attraction of N -sided prism, these equation can be used N times

$$B = \sum_{l=1}^N (\hat{i}B_{lx} + \hat{k}B_{lz}), \tag{B.12}$$

and the total anomaly can be found as

$$\Delta T = \sum_{l=1}^N (\hat{F}_x B_{lx} + \hat{F}_z B_{lz}), \tag{B.13}$$

where \hat{F}_x and \hat{F}_z are the x and z components of the ambient geomagnetic field.

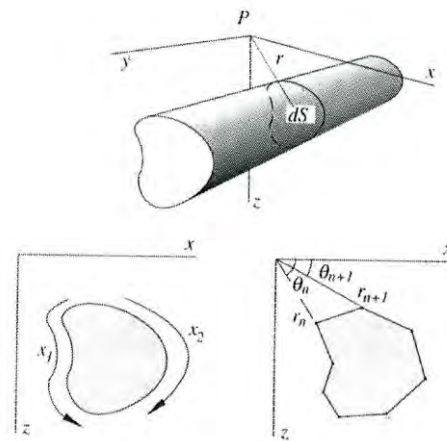


Figure B.1 Approximation of a 2D body by an N -sided polygon for gravity modelling (adopted from Blakely, 1996).

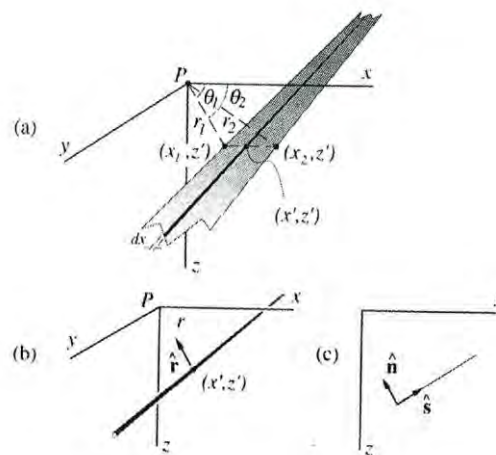


Figure B.2 Approximation of a horizontal ribbon for 2D magnetic modelling (adopted from Blakely, 1996). (a) The horizontal ribbon of mass extending from (x_1, z_1) to (x_2, z_2) and infinitely extended parallel to the y axis. (b) Wire mass infinitely extended parallel to the y axis and piercing the x, z plane at (x', z') . (c) Horizontal ribbon in new coordinate system.

Appendix C

Parameters of geological and tectonic modelling

Table 4.1 Parameters of the P1-06 model

Parameter	Initial value
Earth's magnetic field:	
Magnitude [Am^{-1}]	36.095 (equal to 45358.4 nT)
Inclination [deg]	-34.75
Declination [deg]	1.70
Profile azimuth [deg]	68.2
Relative strike angle [deg]	70

Block's name (<i>label</i>)	Density [kg.m^{-3}]	Susceptibility [10^{-6} SI]	Remanence Magnetization		
			Intensity [Am^{-1}]	Inclination [deg]	Declination [deg]
Intrusive igneous rock (<i>Tmi</i>)	2,740	90,000	0.4	52	1.7
Intrusive igneous rock (<i>Tmi-extR</i>)	2,740	90,000	0.4	52	1.7
Intrusive igneous rock (<i>Tmi-extL</i>)	2,740	90,000	0.4	52	1.7
Volcanic rock (<i>Tomp-R</i>)	2,750	1,000	1.2	17	1.7
Volcanic rock (<i>Tomp-L</i>)	2,750	1,000	1.2	17	1.7
Sedimentary rock (<i>Tomk</i>)	2,700	10,000	1.0	17	1.7
Basement Rocks	2,760	1,000	0.0	-	-
Lithospheric mantle	3,300	1,000	0.0	-	-
Eclogite crust	3,330	0	0.0	-	-
Sea water	1,030	0	0.0	-	-
Air	2,670	0	0.0	-	-

*) when using the Bouguer anomaly data in the GM-SYS modelling, this value has to be set to the same value as the applied Bouguer correction [i.e. 2670 kg.m^{-3} , Sukardi (1979)].

Table 4.2 Parameters of the P1 model

Parameter	Initial value				
Earth's magnetic field:					
Magnitude [Am^{-1}]	36.095 (equal to 45358.4 nT)				
Inclination [deg]	-34.75				
Declination [deg]	1.70				
Profile azimuth [deg]	57.7				
Relative strike angle [deg]	80.7				

Block's name (label)	Density [kg.m^{-3}]	Susceptibility [10^{-6} SI]	Remanence Magnetization		
			Intensity [Am^{-1}]	Inclination [deg]	Declination [deg]
Intrusive igneous rock (<i>Tmi</i>)	2,740	90,000	0.4	52	1.7
Intrusive igneous rock (<i>Tmi-extR</i>)	2,740	90,000	0.4	52	1.7
Intrusive igneous rock (<i>Tmi-extL</i>)	2,740	90,000	0.4	52	1.7
Volcanic rock (<i>Tomp-R</i>)	2,750	1,000	1.2	17	1.7
Volcanic rock (<i>Tomp-LD1</i>)	2,750	1,000	1.2	17	1.7
Volcanic rock (<i>Tomp-LU1</i>)	2,750	1,000	1.2	17	1.7
Volcanic rock (<i>Tomp-LD2</i>)	2,750	1,000	1.2	17	1.7
Volcanic rock (<i>Tomp-LU2</i>)	2,750	1,000	1.2	17	1.7
Sedimentary rock (<i>Tomk</i>)	2,700	10,000	1.0	17	1.7
Alluvium (<i>QaR</i>)	2,500	10	0.0	-	-
Alluvium (<i>QaL</i>)	2,700	1,000	0.0	-	-
Lava (<i>TQp</i>)	2,670	38,000	2.0	28	1.7
Lava (<i>TQb</i>)	2,800	38,000	2.0	0	1.7
Basement Rocks	2,760	1,000	0.0	-	-
Lithospheric mantle	3,300	1,000	0.0	-	-
Eclogite crust	3,330	0	0.0	-	-
Sea water	1,030	0	0.0	-	-
Air	2,670*)	0	0.0	-	-

*) when using the Bouguer anomaly data in the GM-SYS modelling, this value has to be set to the same value as the applied Bouguer correction [i.e. 2670 kg.m^{-3} , Sukardi (1979)].

Table 4.3 Parameters of the P2 model

Parameter	Initial value
Earth's magnetic field:	
Magnitude [Am^{-1}]	35.845 (equal to 45044.2 nT)
Inclination [deg]	-33.75
Declination [deg]	1.70
Profile azimuth [deg]	13.34
Relative strike angle [deg]	44.0

Block's name (<i>label</i>)	Density [kg.m^{-3}]	Susceptibility [10^{-6} SI]	Remanence Magnetization		
			Intensity [Am^{-1}]	Inclination [deg]	Declination [deg]
Magmatic intrusion (#1)	2,740	70,000	0.4	0	1.7
Magmatic intrusion (#2)	2,740	1,000	0.001	-12	1.7
Magmatic intrusion (#3)	2,740	30,000	0.4	-33.75	1.7
Lower sedimentary rocks	2,500; 2,900 ^{*)}	10,000; 1,000 ^{*)}	2.0; 0.001 ^{*)}	52	1.7
Lava (<i>TQp</i>)	2,670; 2,850 ^{*)}	38,000; 1,000 ^{*)}	2.0; 0.001 ^{*)}	28	1.7
Lava (<i>TQb</i>)	2,800	38,000	2.0	0	1.7
Lava (<i>Qvl-R</i>)	750; 2,750 ^{*)}	38,000; 1,000 ^{*)}	1.35; 0.001 ^{*)}	-12	1.7
Lava (<i>Qvl-L</i>)	750; 2,750 ^{*)}	38,000; 30,000 ^{*)}	1.35; 0.001 ^{*)}	-12	1.7
Lava (<i>Qhv</i>)	2,670; 2,400 ^{*)}	50,000; 1,000 ^{*)}	0.8; 0.001 ^{*)}	-33.75	1.7
Partially melted mantle	2,950	0	0.0	-	-
Basement Rocks	2,760	1,000	0.0	-	-
Lithospheric mantle	3,300	1,000	0.0	-	-
Sea water	1,030	0	0.0	-	-
Sedimentary wedge	2,740	0	0.0	-	-
Flores Oceanic crust	2,880	60,000	9.0	90	1.7
Eclogite crust	3,600	0	0.0	-	-
Serpentinized mantle wedge	2,500	150,000	1.5	-90	1.7
Air	2,670 ^{**)}	0	0.0	-	-

*) for the geothermal Reservoir parts

***) when using the Bouguer anomaly data in the GM-SYS modelling, this value has to be set to the same value as the applied Bouguer correction [i.e. 2670 kg.m^{-3} , Sukardi (1979)].

References

- Anand SP, Rajaram M, Majumdar TJ, Bhattacharyya R (2008) Structure and tectonics of 85°E Ridge from analysis of Geopotential data. *Tectonophysics*, doi: 10.1016/j.tecto.2008.09.036.
- Anderson DL (2007) *New theory of the Earth*, Cambridge University Press, New York.
- Audley-Charles MG (1975) The Sumba fracture: A major discontinuity between eastern and western Indonesia. *Tectonophysics*, 26 (3–4): 213–228, doi: 10.1016/0040-1951(75)90091-8.
- Audley-Charles MG (2004) Ocean trench blocked and obliterated by Banda forearc collision with Australian proximal continental slope. *Tectonophysics*, 389: 65–79, doi: 10.1016/j.tecto.2004.07.048.
- Balasis G, Manda M (2007) Can electromagnetic disturbances related to the recent great earthquakes be detected by satellite magnetometers? *Tectonophysics*, 431: 173–195.
- Becker JJ, Sandwell DT, Smith WHF, Braud J, Binder B, Depner J, Fabre D, Factor J, Ingalls S, Kim S-H, Ladner R, Marks K, Nelson S, Pharaoh A, Trimmer R, Von Rosenberg J, Wallace G, Weatherall P (2009) Global Bathymetry and Elevation Data at 30 Arc Seconds Resolution: SRTM30_PLUS. *Marine Geodesy*, 32 (4): 355–371, doi: 10.1080/01490410903297766.
- Bernard P (1992) Plausibility of long distance electrotelluric precursors to earthquakes. *J. Geophys. Res.*, 97: 17531–17536.
- Bird P (2003) An updated digital model of plate boundaries. *Geochem. Geophys. Geosyst.*, 4(3), 1027, doi: 10.1029/2001GC000252.
- Blakely RJ (1996) *Potential theory in gravity and magnetic applications*. Cambridge University Press, Cambridge. ISBN: 0-521-57547-8.
- Blakely RJ, Brocher TM, Wells RE (2005) Subduction-zone magnetic anomalies and implications for hydrated forearc mantle. *Geology*, 33(6): 445–448.
- Bridges DL, Gao SS (2006) Spatial variation of seismic b-values beneath Makushin Volcano, Unalaska Island, Alaska. *Earth and Planetary Sci. Lett.*, 245: 408–415.
- Brye KR, Morris TL, Miller DM, Formica SJ, Van Eps MA (2004) Estimating bulk density in vertically exposed Stoney Alluvium using a modified excavation method. *J. Environ. Qual.*, 33: 1937–1942.
- Campbell WH (2003) *Introduction to geomagnetic fields*, Second edition, Cambridge University Press, Cambridge. ISBN: 0 521 82206 8.
- Eftaxias K, Athanasopoulou L, Balasis G, Kalimeri M, Nikolopoulos S, Contoyiannis Y, Kopanas J, Antonopoulos G, Nomicos C (2009) Unfolding the procedure of characterizing recorded ultra low frequency, kHz and MHz electromagnetic anomalies prior to the L'Aquila earthquake as pre-seismic ones – Part 1. *Nat. Hazards Earth Syst. Sci.*, 9: 1953–1971.
- Engdahl ER, van der Hilst RD, Buland RP (1998) Global teleseismic earthquake relocation with improved travel times and procedures for depth determination. *Bull. Seismol. Soc. Am.*, 88: 722–743.
- Engdahl ER, Villasenor A, DeShon HR, Thurber CH (2007) Teleseismic relocation and assessment of seismicity (1918–2005) in the region of the 2004 Mw 9.0 Sumatra–Andaman and 2005 Mw 8.6 Nias island great earthquakes. *Bull. Seismol. Soc. Am.*, 97: S43–S61.
- Farr TG, Rosen PA, Caro E, Crippen R, Duren R, Hensley S, Kobrick M, Paller M, Rodriguez E, Roth L, Seal D, Shaffer S, Shimada J, Umland J, Werner M, Oskin M, Burbank D, Alsdorf D (2007), The Shuttle Radar Topography Mission. *Rev. Geophys.*, 45, RG2004, doi: 10.1029/2005RG000183.
- Farrell J, Husen S, Smith RB (2009) Earthquake swarm and b-value characterization of the Yellowstone volcano-tectonic system. *J. Volcanol. Geotherm. Res.*, doi: 10.1016/j.jvolgeores.2009.08.008
- Fleury JM, Pubellier M, de Urreiztieta M (2009) Structural expression of forearc crust uplift due to subducting asperity. *LITHOS*, doi: 10.1016/j.lithos.2009.07.007.
- Fowler CMR (2005) *The solid Earth*, Second edition, Cambridge University Press, Cambridge. ISBN: 978-0-521-89307-7.
- GEM System Inc., GSM-19 v7.0 instruction manual, Ontario, Canada.

- Genrich JF, Bock Y, McCaffrey R, Calais E, Stevens CW, Subarya C (1996) Accretion of the southern Banda arc to the Australian plate margin determined by Global Positioning System measurements. *Tectonics*, 15: 288–295.
- Glaßmeier KH, Soffel H, Negendank J (2009) The geomagnetic field *in* Glaßmeier KH, Soffel H, Negendank J (eds.) *Geomagnetic field variations, Advanced in geophysical and environmental mechanics and mathematics*, Springer-Verlag, Berlin Heidelberg. ISBN: 978-3-540-76938-5.
- Gurnis M, Hall C, Lavier L (2004) Evolving force balance during incipient subduction. *Geochem. Geophys. Geosys.*, 5 (7), Q07001, doi:10.1029/2003GC000681.
- Gutenberg B, Richter CF (1945) Seismicity of the Earth. *Bull. Geol. Soc. Am.*, 56: 603–668.
- Hacker BR, Peacock SM, Abers GA, Holloway SD (2003) Subduction factory, 2. Are intermediate-depth earthquakes in subducting slabs linked to metamorphic dehydration reactions? *J. Geophys. Res.*, 108 (B1, 2030), doi: 10.1029/2001JB001129.
- Hadi MN, Yushantarti A, Suhanto E, Sundhoro H (2007a) Survei panas bumi terpadu (geologi, geokimia dan geofisika) daerah Sembalun, Kabupaten Lombok Timur – NTB. *Proc., Pemaparan hasil kegiatan lapangan dan non lapangan tahun 2007*, Pusat Sumber Daya Geologi.
- Hadi MN, Yushantarti A, Suhanto E, Sundhoro H (2007b) Penyelidikan geolistrik dan head-on daerah panas bumi Sembalun, Kabupaten Lombok Timur – NTB. *Proc., Pemaparan hasil kegiatan lapangan dan non lapangan tahun 2007*, Pusat Sumber Daya Geologi.
- Hafkenscheid E, Buitter SJH, Wortel MJR, Spakman W, Bijwaard H (2001) Modelling the seismic velocity structure beneath Indonesia: a comparison with tomography. *Tectonophysics*, 333: 35–46, doi: 10.1016/S0040-1951(00)00265-1.
- Hall R (2002) Cenozoic geological and plate tectonic evolution of SE Asia and the SW Pacific: Computer-based reconstructions, model and animations. *Journal of Asian Earth Sciences*, 20: 353–434, doi: 10.1016/S1367-9120(01)00069-4.
- Hall R, Smyth HR (2008) Cenozoic arc processes in Indonesia: Identification of the key influences on the stratigraphic record in active volcanic arcs, *in* Draut AE, Clift PD, Scholl DW (eds.), *Formation and Applications of the Sedimentary Record in Arc Collision Zones. Geol. Soc. Am., Special Paper*, 436: 27–54, doi: 10.1130/2008.2436(03).
- Hamilton WB (1979) Tectonic of the Indonesian region, Geological survey professional paper 1078, US government printing office, Washington.
- Harijono SWB (2006) Isomagnetic maps of Indonesia for the epoch 2005.0, Geophysical Note No. 11, Badan Meteorologi dan Geofisika (BMG), Jakarta.
- Harris R, Vorkink MW, Prasetyadi C, Zobell E, Roosmawati N, Apthorpe M (2009) Transition from subduction to arc-continent collision: Geologic and neotectonic evolution of Savu Island, Indonesia. *Geosphere*, 5 (3): 152–171, doi: 10.1130/GES00209.1.
- Hattori K, Takahashi I, Yoshino C, Isezaki N, Iwasaki H, Harada M, Kawabata K, Kopytenko E, Kopytenko Y, Maltsev P, Korepanov V, Molchanov O, Hayakawa M, Noda Y, Nagao T, Uyeda S (2004a) ULF geomagnetic field measurements in Japan and some recent results associated with Iwateken Nairiku Hokubu earthquake in 1998. *Physics and Chemistry of the Earth*, 29: 481–494, doi: 10.1016/j.pce.2003.09.019.
- Hattori K (2004b) ULF geomagnetic changes associated with large earthquakes. *TAO*, 15 (3): 329–360.
- Hayakawa M (ed) (2009) *Electromagnetic phenomena associated with earthquakes*. ISBN: 978-81-7895-297-0.
- Hayakawa M, Molchanov OA (eds) (2002) *Seismo-Electromagnetics: Lithosphere-Atmosphere-Ionosphere Coupling*, TERRAPUB, Tokyo, Japan.
- Heidbach O, Tingay M, Barth A, Reinecker J, Kurfeß D, Müller B (2008) The World Stress Map database release 2008. doi:10.1594/GFZ.WSM.Rel2008.
- Heidbach O, Tingay M, Barth A, Reinecker J, Kurfeß D, Müller B (2009) Global crustal stress pattern based on the World Stress Map database release 2008. *Tectonophysics*, doi:10.1016/j.tecto.2009.07.023
- Hinschberger F, Malod JA, Rehault JP, Villeneuve M, Royer JV, Burhanuddin S (2005) Late Cenozoic geodynamic evolution of eastern Indonesia. *Tectonophysics*, 404: 91–118.

- Hunt CP, Moskowitz BM, Banerjee SK (1995) Magnetic properties of rocks and minerals. In: Ahrens TJ (ed) Rock physics & phase relations, Handbook of physical constants, 189–204. American Geophysical Union, Washington.
- IGA WG V-MOD (2005) The 10th-Generation International Geomagnetic Reference Field. *Geophys. J. Int.*, 161: 561–565.
- Ishihara T, Kisimaoto K (2002) Magnetic Anomaly Map of East Asia 1:4,000,000, CD-ROM Version (2nd Edition), Digital Geoscience Map P-3, Geological Survey of Japan (AIST) and Coordinating Committee for Coastal and Offshore Geoscience Programmes in East and Southeast Asia (CCOP).
- Johnstone RD (2005) Contrasting geothermal fields along the magmatic Banda Arc, Nusa Tenggara, Indonesia. *Proc.*, World Geothermal Congress 2005.
- Kim YM, Lee SM, Okino K (2009) Comparison of gravity anomaly between mature and immature intra-oceanic subduction zones in the western Pacific. *Tectonophysics*, 474: 657–673, doi: 10.1016/j.tecto.2009.05.004.
- Kopp H, Flueh ER, Petersen CJ, Weinrebe W, Wittwer A, Meramex Scientists (2006) The Java margin revisited: Evidence for subduction erosion off Java. *Earth Planet Sci. Lett.*, 242: 130–142.
- Kopp H, Flueh ER (2007) Seismic and geoaoustic investigations along the Sunda-Banda Arc transition. FS Sonne Fahrtbericht/Cruise Report SO 190 SINDBAD, Report Nr. 8, IFM-GEOMAR, Leibniz-Institut für Meerewissenschaften an der Universität Kiel.
- Lesur V, Wardinski I, Rother M, Manda M (2008) GRIMM - The GFZ Reference Internal Magnetic Model based on vector satellite and observatory data. *Geophys. J. Int.*, 173: 382–394, doi: 10.1111/j.1365-246X.2008.03724.x.
- Lesur V, Wardinski I, Manda M (2009) GRIMM-2: A core magnetic field model derived under flow constraints. *Proc.*, 11th Scientific Assembly, IAGA 2009, Sopron (Hungary)
- Lin JY, Sibuet JC, Hsu SK (2008) Variations of b-values at the western edge of the Ryukyu subduction zone, north-east Taiwan. *Terra Nova*, 20: 150–153, doi: 10.1111/j.1365-3121.2008.00801.x.
- Lühr H, Korte M, Manda M (2009) The recent geomagnetic field and its variations in Glaßmeier KH, Soffel H, Negendank J (eds.) Geomagnetic field variations, Advanced in geophysical and environmental mechanics and mathematics, Springer-Verlag, Berlin Heidelberg. ISBN: 978-3-540-76938-5.
- Manda M (2006) Magnetic satellite missions: where have we been and where are we going? *C.R. Geoscience*, 338: 1002–1011, doi: 10.1016/j.crte.2006.05.011.
- Manda M, Purucker M (2005) Observing, modeling, and interpreting magnetic fields of the solid Earth. *Survey in Geophysics*, 26: 415–459, doi: 10.1007/s10712-005-3857-x.
- Manda M, Thébaud E (2007) The changing faces of the Earth's magnetic field. CGMW, Paris. ISBN: 978-2-9517181-9-7.
- Mangga SA, Atmawinata S, Hermanto B, Amin TC (1994) Geologi lembar Lombok, Nusatenggara, Lembar 1807, Pusat Penelitian dan Pengembangan Geologi, Indonesia.
- Maus S, Macmillan S, Chernova T, Choi S, Dater D, Golovkov V, Lesur V, Lowes F, Lühr H, Mai W, McLean S, Olsen N, Rother M, Sabaka T, Thomson A, Zvereva T (2005) The 10th generation international geomagnetic reference field. *Phys. Earth Planet Inter.*, 151: 320–322.
- Maus S, Rother M, Hemant K, Stolle C, Lühr H, Kuvshinov A, Olsen N (2006) Earth's lithospheric magnetic field determined to spherical harmonic degree 90 from CHAMP satellite measurements. *Geophys. J. Int.* 164: 319–330, doi: 10.1111/j.1365-246X.2005.02833.x.
- Maus S, Lühr H, Rother M, Hemant K, Balasis G, Ritter P, Stolle C (2007) Fifth-generation lithospheric magnetic field model from CHAMP satellite measurements. *Geochem. Geophys. Geosyst.* 8, Q05013, doi: 10.1029/2006GC001521.
- Maus S, Yin F, Lühr H, Manoj C, Rother M, Rauberg J, Michaelis I, Stolle C, Müller RD (2008) Resolution of direction of oceanic magnetic lineations by the sixth-generation lithospheric magnetic field model from CHAMP satellite magnetic measurements. *Geochem. Geophys. Geosyst.*, Technical Brief 9 (7), Q07021, doi: 10.1029/2008GC001949, ISSN: 1525-2027.
- Maus S (2008) The geomagnetic power spectrum. *Geophys. J. Int.*, 174: 135–142, doi: 10.1111/j.1365-246X.2008.03820.x.

- Mazzini A, Svensen H, Akhmanov GG, Aloisi G, Planke S, Malthe-Sørenssen A, Istadi B (2007) Triggering and dynamic evolution of the LUSI mud volcano, Indonesia. *Earth and Planetary Sci. Lett.*, 261: 375–388, doi: 10.1016/j.epsl.2007.07.001.
- McCaffrey R, Nabelek J (1987) Earthquakes, gravity and the origin of the Bali Basin: An example of a nascent continental fold-and-thrust belt. *J. Geophys. Res.*, 92: 441–460.
- Müller C, Neben S (2006) Research Cruise SO190 Leg 1, Seismic and geoacoustic investigations along the Sunda-Banda Arc transition, with RV Sonne. Cruise report and preliminary results, Bundesanstalt für Geowissenschaften und Rohstoffe (BGR), Hannover.
- Müller C, Kopp H, Djajadihardja YS, Barckhausen U, Ehrhardt A, Engels M, Flueh ER, Gaedicke C, Keppler H, Lutz R, Lüschen E, Neben S, Seeber L, Dzulkarnaen DPS (2008) From Subduction to Collision: The Sunda-Banda Arc Transition. *Eos*, 89 (6): 49–50.
- Murru M, Montuori C, Wyss M, Privitera E (1999) The locations of magma chambers at Mt. Etna, Italy, mapped by *b*-values. *Geophys. Res. Lett.*, 26: 2553–2556.
- Nasution A, Takada A, Mulyana R (2003) Eruptive history during the last 10 ky for the caldera formation of Rinjani volcano, Indonesia. *Proc.*, 2003 IUGG meeting.
- Natawidjaja DH, Triyoso W (2007) The Sumatran fault zone — from source to hazard. *Journal of Earthquake and Tsunami*, 1 (1): 21–47.
- Negro CD, Napoli R (2002) Ground and marine magnetic surveys of the lower eastern flank of Etna volcano (Italy). *J. Volcanol. Geotherm. Res.* 114: 357–372.
- Newitt LR, Barton CE, Bitterly J (1996) IAGA Guide for Magnetic Repeat Station Surveys. ISBN: 0-9650686-1-7.
- Nishida Y, Sugisaki Y, Takahashi K, Utsugi M, Oshima H (2004) Tectonomagnetic study in the eastern part of Hokkaido, NE Japan: Discrepancy between observed and calculated results. *Earth Planets Space*, 56: 1049–1058.
- Nishida Y, Utsugi M, Mogi T (2007) Tectonomagnetic study in the eastern part of Hokkaido, NE Japan (II): magnetic fields related with the 2003 Tokachi-oki earthquake and the 2004 Kushiro-oki earthquake. *Earth Planets Space*, 59: 1181–1186.
- Nugroho H, Harris R, Lestariya AW, Maruf B (2009) Plate boundary reorganization in the active Banda Arc–continent collision: Insights from new GPS measurements. *Tectonophysics*, doi: 10.1016/j.tecto.2009.01.026.
- Olson P (2002) The disappearing dipole. *Nature*, 416: 591–594.
- Price NJ, Audley-Charles MG (1983), Plate rupture by hydraulic fracture resulting in overthrusting. *Nature* 306: 572–575.
- Pubellier M, Chamot-Rooke N, Ego F, Guezou JC, Konstantinoskaya E, Rabaute A, Ali J, Aitchison JC, Aubourg C, Charvet J, Fournier M, Hébert R, Jolivet L, Lepvrier C, Mascle G, Popolov I, Ringenbach JC, Shokalvsky S, Sosson M, Verges J, Wang C (2008) Structural map of Eastern Eurasia: evolution of crustal blocks and orogenic belts through time. Commission for the geological map of the world (CGMW).
- Quesnel Y, Catalan M, Ishihara T (2009) A new global marine magnetic anomaly data set. *J. Geophys. Res.*, doi: 10.1029/2008JB006144.
- Roosmawati N, Harris R (2009) Surface uplift history of the incipient Banda arc-continent collision: Geology and synorogenic foraminifera of Rote and Savu Islands, Indonesia. *Tectonophysics*, 479: 95–110, doi: 10.1016/j.tecto.2009.04.009.
- Sabaka T, Olsen N, Purucker M (2004) Extending comprehensive models of the Earth's magnetic field with Oersted and CHAMP data. *Geophys. J. Int.* 159: 521–547.
- Sanchez JJ, McNutt SR, Wyss M (2004) Spatial variations in the frequency-magnitude distribution of earthquakes at Mount Pinatubo Volcano. *Bull. Seismol. Soc. Am.*, 94: 430–438.
- Sasai Y (1994) Piezomagnetic fields produced by dislocation sources. *Survey of Geophys.*, 15: 363–382.
- Satake K, Atwater BF (2007) Long-term perspectives on giant earthquakes and tsunamis at subduction zones. *Annu. Rev. Earth Planet. Sci.*, 35: 349–74.
- Scintrex Ltd. (1997) ENVI geophysical system operations manual, Concord, Canada.
- Siebert M (1971) Maßzahlen der erdmagnetischen Aktivität, in Hand-buch der Physik Bd. 49/3 (Geophysik 3/3), Ed. S. Flügge, Springer, Berlin, Heidelberg, New York, pp. 206±275.
- Silver EA, Reed D, McCaffrey R, Joyodiwiryo Y (1983) Backarc thrusting in the Eastern Sunda Arc, Indonesia: A consequence of Arc-Continent collision. *J. Geophys. Res.*, 88: 7429–7448.

- Silver EA, Breen NA, Prasetyo H, Hussong DM (1986) Multibeam study of the Flores backarc thrust belt, Indonesia. *J. Geophys. Res.*, 91: 3489–3500.
- Soloviev A, Ismail-Zadeh A (2003) Models of dynamics of block-and-fault systems. In: Keilis-Borok V, Soloviev A (eds) *Nonlinear dynamics of the lithosphere and earthquake prediction*, Springer-Verlag, Berlin-Heidelberg, pp. 71–139.
- Špičák A, Hanuš V, Vaněk J (2007) Earthquake occurrence along the Java trench in front of the onset of the Wadati-Benioff zone: Beginning of a new subduction cycle? *Tectonics*, 26: TC1005.
- Stacey FD (1964) The seismomagnetic effect. *Pageoph.*, 58: 5–22.
- Sukardi S (1979) Peta anomali Bouguer lembur Lombok (Bouguer anomaly map of the Lombok Quadrangle). Pusat Penelitian dan Pengembangan Geologi, Indonesia.
- Sundhoro H, Nasution A, Simanjuntak J (2000) Sembalun Bumbang geothermal area, Lombok Island, West Nusatenggara, Indonesia: an integrated exploration. *Proc.*, World Geothermal Congress 2000.
- Takada A, Nasution A, Mulyana R (2003) Eruptive history during the last 10 ky for the caldera formation of Rinjani volcano, Indonesia. *Proc.*, 2003 Japan Earth and Planetary Science joint Meeting.
- Talwani M, Heirtzler JR (1964) Computation of magnetic anomalies caused by two-dimensional bodies of arbitrary shape. *Geol. Sci.*, 9: 464–480 in Parks GA (ed) *Computers in the mineral industries*, Stanford Univ. Publ.
- Talwani M, Worzel JL, Landisman M (1959) Rapid gravity computations for two-dimensional bodies with application to the Mendocino submarine fracture zone. *J. Geophys. Res.*, 64: 49–59.
- Tapley B, Ries J, Bettadpur S, Chambers D, Cheng M, Condi F, Gunter B, Kang Z, Nagel P, Pastor R, Pekker T, Poole S, Wang F (2005) GGM02 - An improved Earth gravity field model from GRACE. *Journal of Geodesy*, doi: 10.1007/s00190-005-0480-z.
- Toft PB, Hamed JA, Haggerty SE (1990) The effects of serpentinization on density and magnetic susceptibility: a petrophysical model. *Physics of the Earth and Planetary Interiors*, 65: 137–157.
- Uyeda S, Nagao T, Kamogawa M (2009) Short-term earthquake prediction: Current status of seismo-electromagnetics. *Tectonophysics*, 470: 205–213, doi:10.1016/j.tecto.2008.07.019.
- Wallace AR (1869) *The Malay Archipelago*. (Reprinted) Kessinger Publishing, ISBN 1419171380.
- Wandono, Widiyantoro S, Ibrahim G, Soewono E (2004) Analisis Hubungan Frekuensi-Magnitudo Gempa Bumi di Bali dan Sekitarnya. *Jurnal Matematika dan Sains*, 9 (3): 273–277.
- Whitham AG, Sparks RSJ (1986) Pumice. *Bull. Volcanol.*, 48: 209–223.
- Widiyantoro S and van der Hilst R (1996) Structure and Evolution of Lithospheric Slab Beneath the Sunda Arc, Indonesia. *Science*, 271 (5255): 1566 – 1570, doi: 10.1126/science.271.5255.1566.
- Wiemer S, McNutt SR (1997) Variations in the frequency–magnitude distribution with depth in two volcanic areas: Mount St. Helens, Washington, and Mount Spurr, Alaska. *Geophys. Res. Lett.*, 24: 189–192.
- Wyss MF, Klein F, Nagamine K, Wiemer S (2001) Anomalously high *b*-values in the south flank of Kilauea Volcano, Hawaii: evidence for the distribution of magma below Kilauea's east rift zone. *J. Volcanol. Geotherm. Res.*, 106: 23–37.
- Yumoto K, the MAGDAS Group (2006) MAGDAS project and its application for space weather, Solar Influence on the Heliosphere and Earth's Environment: Recent Progress and Prospects, in Gopalswamy N, Bhattacharyya A (eds.), ISBN: 81-87099-40-2, 309–405.
- Zubaidah T, Kanata B, Utama W, Arumdanti N (2005) Pengembangan metodologi elektromagnetik dan aplikasinya untuk evaluasi sumber anomali magnetik bumi: Kajian tentang potensi sumber daya alam di Kota Mataram Pulau Lombok Propinsi Nusa Tenggara Barat. *Laporan akhir kegiatan insentif riset matematika dan ilmu pengetahuan alam*, Jurusan Elektro Fakultas Teknik-Universitas Mataram.
- Zubaidah T, Korte M, Manda M, Quesnel Y, Kanata B (2009) Geomagnetic field anomalies over the Lombok Island region: an attempt to understand the local tectonic changes. *Int. J. Earth Sci. (Geol. Rundsch.)*, published on line, doi: 10.1007/s00531-009-0450-4.

Acknowledgement

1. The reviewers of my thesis (Prof. Michael Weber, Prof. Sri Widiyantoro, Prof. Katsumi Hattori) and the members of the defense committee (Prof. Frank Krueger, Prof. Mioara Manda, Prof. Mohamed Hamoudi, Prof. Patrick O'Brien, Prof. Romain Bousquet, Dr. Makky Sandra Jaya).
2. Dr. Monika Korte for giving her best and full assistances during my PhD time, as well as other members of Sec. 2.3 of the Deutsches GeoForschungsZentrum (GFZ) Potsdam (esp. Martina Krueger and Alexander Jordan) for very good team works and all required supports.
3. The MAGDAS Japan (Prof. Yumoto and Shuji Abe), the BGR Hannover (Dr. Martin Engels and Dr. Udo Barckhausen), and the BMKG Indonesia (Muhammad Husni) for providing the complementary geomagnetic data.
4. The ITS Surabaya (Widya Utama, DD Warnana and the Geophysisc Laboratory team) and the ITB Bandung (Bagus Nurhandoko and the Laboratory Fisika Bumi team) for providing the equipment and giving their best assistances in preparing the field measurements.
5. The big family of H. Basar/Suna'ah, ammah Alma and mbak Joh (Sekotong/Pelangan), mbak Ida (Tanjung), Ust. Abdul Karim and Ummi Halimah (Nurul Bayan Boarding school), H. Abdul Hadi, H. Abdurahim, H. Abdurahman (Sembalun Bumbung), and H. Abdullah (Sambelia) for hosting the survey team during the field measurements.
6. Naila Osman, Yoan Quesnel, Michael Purucker, Ingo Wardinski, Manuel Pubellier, Awang Satyana, Asnawir Nasution and Ade Anggraini for very fruitful technical and theoretical discussions.
7. The Deutsches GeoForschungsZentrum (GFZ) Potsdam, the DAAD, the KNRT, and the DIKTI for giving the financial supports.
8. The KiTa Geolino team of GFZ Potsdam, TKIT Anak Sholeh Mataram and the Rosa-Luxemburg Schule at Freundschaft Insel Potsdam for taking care of and educating my children during whole work days.
9. My colleagues and students at the Electrical Engineering Dept. of Mataram University (Bulkis Kanata, Paniran, Nurul Islamiyah, Niken Arumdati, Sulhaini, Apriliana, Annisa Rachmawati, Lale Diah, Cipta Ramadhani, Suryadi, Adin and other members of EE Laboratory team) as well as om Rio LDK (Driver), ammah Zoh, ammah Yus, ammah Ana, ammah Mustirah and all crews of Titian Hidayah for giving their best commitments to support the field measurements.
10. My best friends at IWKZ Al-Falah Berlin (among other are: Dewi Yuniasih, Indah Kristanti, Mardhiyah binti Mat Husain, Munaya Fauziah and Siti Nurhayati) for giving their uncountable helps and private consultations.
11. Mbak Istiningsih, budhe Yanti, Dr. Qomarul, bu Rosmaliati, bu Tri, mbak Dian Syafitri, ammah Ummu, ammah Cici and all crews of Titian Hidayah for taking care of me and my family during our serious illnesses in Lombok.
12. My lovely family: my husband, my children, and my parents for giving me never ending supports troughout my life.

Curriculum Vitae

Name : **Teti Zubaidah**
Date of birth : 19 November 1974
Place of birth : Wonogiri
Address : Fakultas Teknik
Universitas Mataram
Jl. Majapahit No. 62
Mataram – 83126
INDONESIA
Phone : +62 370 636126
E-mail : tetizubaidah@yahoo.com



Education

Gadjah Mada University, Yogyakarta, Indonesia	Master of Electrical Engineering	2001
University of Indonesia, Depok, Indonesia	Bachelor of Electrical Engineering	1997
SMA Al-Islam 1, Surakarta, Indonesia		1993
Madrasah Tsanawiyah Wonogiri, Indonesia		1990
Madrasah Ibtidaiyah Wonokarto, Indonesia		1987

Research

Observation for the presence of extreme geomagnetic anomaly in Lombok Island West Nusa Tenggara Indonesia: Determination of geomagnetic anomaly pattern for the prediction of tectonic earthquake in subduction zone	2006–2007
Development of electromagnetic method and its application to evaluate geomagnetic anomaly source: Study of natural source potency in Mataram Lombok Island, West Nusa Tenggara Province	2005–2006
Investigation of geomagnetic fields anomaly at Mataram City, Lombok Island, Nusa Tenggara Barat Province	2004
Time Variant Magnetic Fields Measurement with Teslameter	2004
Stationary Magnetic Fields Measurement with Teslameter	2003
Analysis of Electromagnetic Wave Propagation for Locating Slab of Concrete	2003
Software Development for Electromagnetic Compatibility Analysis on Control and Protection Systems at Substations	2001
Electromagnetic Compatibility Analysis on Substation, Case Study of Station Transformer 3 & 4 of Suralaya Power Plant Project	1997

ISSN 1610-0956

Teti Zubaidah, Spatio-temporal characteristics of the geomagnetic field over the Lombok Island

STR10/07